Development of a High Integrity Interlayer Joining Technology for High Temperature Aerospace Applications

Swansea University
Prifysgol Abertawe

Arandeep Singh Johal

(BEng, MSc)

Submitted to Swansea University in fulfilment of the requirements for the Degree of Doctor of Philosophy

Swansea University

2019

SUMMARY

The purpose of this PhD project was the continual development of the powder interlayer bonding technique for high temperature alloys, more specifically Ti-6Al-2Sn-4Zr-6Mo. The application of this technology is for the potential use as a joining and repair technology on BLISKs. The requirement of extended life cycles for aerospace components such as this is important for the viability of technologies which aim to further improve efficiency within the gas turbine engine. The principle of interlayer bonding is on the utilisation of powder based interlayer which is used to improve bond integrity between two surfaces.

Research during this thesis programme has resulted in the development of an interlayer bonding technique that allows for the evaluation of using an inert gas environment, instead of traditional vacuum systems, with a focus on how this technology would eventually be implemented on more complex geometries. The use of argon shielding gas provided the required environment to limit the oxidation of titanium at elevated temperature required for bonding. The results allowed for the mechanical performance of the interlayer bonds to be evaluated, along with the effects of using a post bond heat anneal, with the properties of interlayer bonded Ti-6246 showing only a slight reduction in room temperature properties in comparison to the base material.

Preliminary research was also conducted on evaluating the possibility of joining dissimilar titanium alloys, with a focus on Ti-6246 and Ti-6242. With the right balance of the key bonding parameters it was possible to create low porosity bonds between the alloy systems with the tensile results again showing a small debit in strength.

The final stages of the programme focused on the potential use of alternate interlayers, including different morphology of alloyed titanium powder as well as Commercially Pure powder and foil with potentially further avenues of research available to investigate.

PUBLICATIONS

TITLE:

Powder Interlayer Bonding of Titanium alloys: Ti-6Al-2Sn-4Zr-6Mo and Ti-6Al-4V.

Journal:

The International Journal of Advanced Manufacturing Technology.

July 2019, Volume 103, Issue 1-4, pp441-452.

Authors:

P. Davies [1], A. Johal[1], H. Davies[1], S. Marchisio[2]

[1] Institute of Structural Materials, College of Engineering, Swansea University, Bay Campus, Fabian Way, Swansea SA1 8EN, UK.

[2] Rolls-Royce Plc, PO Box 31, Derby, DE24 8BJ, UK.

Declarations

This work has not previously been accepted in substance for any degree and is not being concurrently submitted in candidature for any degree.

Signed.....  .....

Date.....09/06/2021.....

This thesis is the result of my own investigations, except where otherwise stated. Other sources are acknowledged by footnotes giving explicit references. A bibliography is appended.

Signed.....  .....

Date.....09/06/2021.....

I hereby give my consent for my work, if relevant and accepted, to be available for photocopying and for inter-library loans **after expiry of a bar on access approved by the University.**

Signed.....  .....

Date.....09/06/2021.....

ACKNOWLEDGEMENTS

Without the support and encouragement from the following family and friends none of the work carried out in this project could have been possible:

— Professor Helen Davies who provided invaluable insight, support and continued advice during the course of this project.

— Dr. Silvia Marchisio for supplying the expertise and knowledge required for the development of the repair technology.

— Dr. Peter Davies with whom working to develop the repair technology with most days was a pleasure and without whom would not have been possible to reach this stage.

— Sean John, Jennie Palmer and David Lewis. The daily support and continual enjoyment during the 3 years made it a pleasure to work within the environment of the ISM.

— Dr Robert Lancaster & Dr Spencer Jeffs who provided continual advice and experience on conducting myself in a professional manner within an academic and industrial environment.

— For those within Rolls-Royce plc including Dr Gavin Baxter and Dr Justin Burrows for providing the chance to communicate and share research with experts within the relevant field.

— I greatly acknowledge the funding received towards my PhD from Rolls-Royce plc and EPSRC.

— Finally, to my family including my parents, brother and my wife. You all saw and shared in the experience of the last few years and therefore I hope you share in the pride and joy in the fulfilment of this PhD. Conducting research as a PhD student is known to be tough, both mentally and emotionally, yet with your continued support I enjoyed every moment of it!

Contents

List of Figures

Nomenclature

α	Alpha
α_p	Primary Alpha
α_s	Secondary Alpha
β	Beta
β_T	Beta Transus
BCC	Body Centre Cubic
BLISK	Bladed Disk
BM	Base Material
BSE	Back Scatter Electron
BSE-COMP	Back Scatter Compositional
CP	Commercially Pure
CT	Computed Tomography
DB	Diffusion Bonding
DC	Direct Current
DOE	Design of Experiments
EBM	Electron Beam Melting
EBSD	Electron Backscatter Diffraction
EBW	Electron Beam Welding
ECAS	Electric Current Assisted Sintering
EDS	Energy Dispersive Spectroscopy
EDX	Energy Dispersive X-ray Spectroscopy
ELI	Extra Low Interstitials
FEG	Field Emission Gun
FOD	Foreign Object Damage
FZ	Fusion Zone
GA	Gas Atomised
HAZ	Heat Affected Zone
HCF	High Cycle Fatigue
HCP	Hexagonal Closed Pack
HIP	Hot Isostatic Pressing
HP	High Pressure

HPC	High Pressure Compressor
IFW	Inertia Friction Welding
IP	Intermediate Pressure
IPF	Inverse Pole Figure
LCF	Low Cycle Fatigue
LFW	Linear Friction Welding
LHS	Left Hand Side
LMD	Laser Metal Deposition
LP	Low Pressure
MIM	Metal Injection Moulding
MRO	Maintenance, Repair & Overhaul
NNS	Near Net Shape
PA	Pre-Alloyed
PBHT	Post Bond Heat Treatment
PIB	Powder Interlayer Bonding
PPE	Personal Protective Equipment
PREP	Plasma Rotating Electrode Process
PWHT	Post Weld Heat Treatment
RHS	Right Hand Side
RT	Room Temperature
SE	Secondary Electron
SEM	Scanning Electron Microscopy
SLM	Selective Laser Melting
SS	Stainless Steel
TEM	Transmission Electron Microscopy
TIG	Tungsten Inert Gas
UKAS	United Kingdom Accreditation Service
UTS	Ultimate Tensile Strength
VAR	Vacuum Arc Remelting
WCFB	Wide Chord Fan Blade

1 Introduction

Within the aerospace industry there has been significant focus on the development of joining and repair techniques for high temperature alloys, including titanium alloys. The use of titanium alloys within gas turbines has grown significantly, owing to its elevated mechanical properties, such as tensile strength and crack propagation properties, in relation to its density. With the key drivers for improved performance of gas turbine engines, in the form of reducing weight and increasing combustion temperatures, this has meant lightweight titanium alloys are preferable where temperatures permit their use. Numerous titanium alloys have been developed with each having increased mechanical properties under certain conditions, for example alloys such as Ti-6242 and IMI-834 show enhanced creep performance in comparison to Ti-64 whereas Ti-6246 display very high fracture toughness properties over many other titanium alloys. Therefore, the specific properties of many of these alloys can be utilised within certain sections of gas turbine engines in order to increase the overall performance of the engine. Although using lightweight, high strength alloys is advantageous there are limiting factors which prohibit the extensive use of the alloys throughout all sections, such as the elevated temperatures within the combustion and turbine sections of a gas turbine. Alternate development paths of incorporating increased performance is through the design of specific components, allowing for cooling channels to be used in areas not previously accessible for example. The design challenges along with the material specific limitations have therefore furthered the development of the manufacturing and servicing technologies that are required in order to make the increases in performance and efficiency possible.

The use of joining techniques has increased in numerous industries with applications for many different material types under continuous development. These techniques allow for the fabrication of components and assemblies that would otherwise be difficult to achieve with conventional manufacturing methods for certain gas turbine components. An example of such components include BLISKs which, unlike conventional rotor disks and removable blade assemblies, aims to combine this into a single component. The key benefits of BLISK technology is linked to the overall weight reduction of the component as the design can be optimised with less strengthening of the fixture between the blades and rotor disk required. Other benefits

of this technology over traditional dovetail attachments of blades to disks includes the reduced detrimental effects of fretting fatigue associated with these joints and hence improved life cycle for components. The manufacture of these components has relied heavily on traditional techniques such as machining from billet to joining technologies such as friction welding. Machining from single forgings may allow for a reduced impact on microstructure of the material, and hence reduced impact on mechanical properties, however the challenges arise when machining for low pressure compressor BLISKs for example where the blade forms a large proportion of the overall diameter. In this example the increased amount of machining results in increased lead time and cost meaning other alternatives to manufacture are needed to make it a more viable technology within industry.

As well as developing alternative manufacturing methods for BLISK technology, another challenge is with respect to the servicing of such components. Due to the operational environments of aerospace gas turbines many components, such as compressor blades, require extensive repair or replacement due to foreign object damage (FOD) or general deterioration due to service and therefore repair technologies are another considerable factor with regard to the successful implementation of BLISK technologies. Whereas with traditional blade fixing and disks repairs can be done via removal and replacement of the damaged blade with this process not requiring exhaustive lead time or costs. However, with BLISKs the ability of replacing individual blades is not as straightforward and therefore additional development is required in finding alternative repair technologies. Some of the current methods which show promise as viable technologies include linear friction welding (LFW) as well as processes such as Laser Metal Deposition (LMD) processes which involve the use of metallic powder to form part of the repairs. Extensive research is being conducted in order to further validate these repair technologies as each method brings its own set of challenges in the form mechanical properties of the joins through to the industrial application of the technologies in service where service intervals, lead times and cycle costs are prohibitive factors.

The purpose of this study is to evaluate the possibility of a novel joining and repair method for potential applications on BLISKs as an alternative to the current technologies being developed. The technology under consideration is the Powder Interlayer Bonding (PIB) method which involves the use of a metallic powder

interlayer between two surfaces and electrical resistance heating in order to produce a high integrity bond for titanium alloys. The project is leading on from previous studies by Forsdike [1] which focused on utilising a thermo-mechanical simulator in order to understand the impact of key process variable on mechanical properties and microstructure within the HAZ. This technology aims to produce a cost effective method of creating high integrity joints, between primarily titanium alloys, in order to aid the further implementation of BLISKs with gas turbines. The previous studies have involved the use of a Gleeble thermo-mechanical simulator in order to create Powder Interlayer Bonds, between high temperature titanium and nickel alloys, via electrical resistance heating within the interlayer region, this reducing the HAZ and producing low porosity bonds under certain conditions. The studies showed that under the right conditions of time, temperature and pressure it was possible to create high integrity joins with low levels of porosity and high tensile properties. However, fatigue properties showed to be particularly adversely effected with non-fusion defects contributing towards crack initiation and therefore reducing fatigue performance.

The aim of this study is to further development of the PIB technology, for Ti-6246, by creating an alternative to the Gleeble system used within the previous studies. The key outcome is to understand the possibilities of using argon shielding and induction heating in order to produce high integrity joints between Ti-6246. This would allow for the further implementation of this technology as a possible joining or repair method for complex shapes such as blades within BLISKs. In order to further the development of this technology the effects of the key bonding parameters, temperature, time and pressure need to be understood and further evaluation using mechanical testing and microstructural analysis needs to be performed. The mechanical properties, particularly the High Cycle Fatigue properties, need to be obtained in order understand the possibility of this technology being a viable alternate as a joining and repair methods.

As well as the development of PIB for Ti-6246 another aspect of the study is to investigate alternate interlayers, in terms of alloy type and structure, in order gain a preliminary understanding of their potential applications. The purpose would be to evaluate the use of alternate interlayers that may provide similar high integrity joins as with Ti-6246 powder interlayers but with reduced cost and ease of processing.

2 Literature Review

2.1 The Gas Turbine

2.1.1 A Brief History

With the success of the first powered aircraft from the Wright brothers in 1903 came much research and development into all aspects of flight. Much work centred on understanding the role of aerodynamics and on flight control, as well as this aircraft propulsion became one of the key components for successful powered flight. The early method of aircraft propulsion focused on reciprocating engines with different configurations such as the inline engine built by Charlie Taylor for the Wright flyer or the Manly-Balzer radial engine developed by Stephen Balzer and Charles Manly. It was in this period that the English engineers Charles Rolls and Henry Royce were invited by a mutual friend, Henry Edmunds, to meet with each other and this soon led to both men going into partnership, manufacturing motor cars under the trade name of 'Rolls-Royce Limited'. The company went on to receive high acclaim for the quality and reliability of its motor cars and engines during that period, however the company eventually started work on early aero engines. Charles Rolls was a keen aviator, making numerous balloon ascents and in 1909 proceeded to purchase a Wright flyer aircraft completing many flights, one of which was a non-stop double crossing of the English Channel in 1910, the first man to do so in an aircraft. Unfortunately, not long after this flight Rolls was killed when the tail of his Wright flyer broke off in mid-air during an air display at Hengistbury Airfield in Bournemouth.

With the start of the First World War Henry Royce, who was initially reluctant to enter the aero engine industry, was now fully involved in the war effort when the Royal Aircraft Factory, responsible for supplying military aircraft, approached Rolls-Royce to build Renault engines. Although Henry Royce was suffering with illness and was only able to work away from the unhealthy environment of the factory, he applied the same work ethic as with the previous engines. Seeing that the 80hp, V8 Renault engine was both heavy and low-powered, Henry Royce decided to design an improved engine by using their expertise in water cooled engines rather than air cooled Renault engines. Work soon began on a 200hp V12 engine which became known as the Eagle engine became an instant success with the military exceeding previous engine capabilities,

with smaller variations of the same engine used in smaller aircraft. This engineering excellence continued after the First World War and led to the famous Merlin engine which powered certain models of the Spitfire and the Hurricane which played a crucial role in the defence of the United Kingdom.

Even with the success with these reciprocating engines the drawbacks and limitations were still present when they were used for flight. This led to a range of different engineers, physicists and mathematicians to research possible alternatives to the piston propeller design. In 1926 Dr A.A Griffith, from the Royal Aircraft Establishments Engines Experimental Department, published his work on an engine design that had an axial compressor and a turbine driving a propeller which would form the basis of a turboprop engine. A couple of years later however it was Frank Whittle who submitted a patent for the first turbojet engine, utilising the exhaust gas to provide the propulsion rather than having a propeller. After numerous financial and research setbacks an aircraft was made, known as the Gloster E.29/39, in 1940 to carry Whittle's turbojet designed engine. The first flight took place in May 1941 and lasted 17 minutes achieving a maximum velocity of 350mph at 25,000ft, and with this flight the era of the jet engine began. With this flight Whittle had proven his design in theory but to assure that this could be achieved on a larger scale he soon started work with Rolls-Royce to produce the engine in greater number. The success of the test flight eventually led to the creation of the Gloster Meteor aircraft which was powered by two Rolls-Royce Welland turbojet engines designed in conjunction with Frank Whittle.

With the involvement in the Gloster Meteor, Rolls-Royce had the confidence to fully invest the company's future in jet technology, a decision which was aided by the competitive advantage it already had. Rolls-Royce then entered the civil aviation market in the early 1950's as travelling by aircraft became more viable for the general public. The advancements in the gas turbine technology focused on increasing the thrust of engines in order to allow for larger wide body aircraft to travel further distance. Continuous improvement in material and design technologies have meant current gas turbine engine have far surpassed the thrust to weight ratios of previous designs.

2.1.2 Theory of the Gas turbine

The fundamental principle of aerospace gas turbines is the use of a working fluid, in this case air, to convert chemical energy into mechanical energy and is built on the fundamentals of the Brayton cycle. The four main processes involved in a typical gas turbine engine are as follows:

1. The intake of atmospheric air.
2. Compression of intake air.
3. Combustion of air alongside injected fuel in order to convert stored energy.
4. Expansion of exhaust gas which is utilised to rotate turbine connected to compressor section of engine.

Expanding on the 4 general points, the process involves the compression of intake air to relatively high pressure which results in the conversion from mechanical energy to thermal energy in the process. This increase in pressure can be achieved in either an axial or centrifugal compressor with the difference being in an axial compressor the flows parallel to the axis of rotation and perpendicular in a centrifugal compressor which are typically found in smaller gas turbine derivatives. For Aero derivatives of the gas turbine engine the compressor stages are typically axial compressors with multiple stages. For example, current gas turbines within the civil aviation market will have and intermediate and high pressure compressor stage (IP & HP). Each stage can be made up of a number of rotor and stationary blade stages with the cross sectional area decreasing in order to maintain axial flow velocity. The rotating compressor blades, attached via a disk to a central shaft, act to increase the axial flow velocity with the stationary aerofoils, typically attached to the casing, acting to increase the pressure by converting the kinetic energy and optimise the axial flow for the following rotating stage of the compressor.

After compression the air enters the combustion stage of the process which involves the introduction of fuel for combustion. The combustion chamber is crucial in controlling the maximum working temperature with a typical design split into two segments, primary and secondary zone. The primary zone is important as this zone is designed to control the amount of air that is mixed with the burnt fuel in order to achieve a stoichiometric mixture. The velocities of compressed air into the combustion chamber are so high that flame stabilisation is an important factor in the design of the

combustion chamber, with diffusers used to reduce the velocity and ensure the there is no flame blow out. The second zone involves the introduction of unused intake air in order to cool the combustion products before entering the turbine section of the system.

The expansion and flow through the turbine section of a gas turbine engine is the final stage in the system. The vast majority, over 95%, of gas turbines operate an axial-flow type turbine with flow which enters and leaves in the axial direction and are split into multiple stages [2].The initial stages of the turbine section are designated the High Pressure Turbine (HP) section with the latter stages classified as Low Pressure (LP) turbine section. The overall purpose of the turbine section is to extract the resultant energy from the high temperature, high velocity gas flow which comes from the combustion process. The extracted energy is then utilised, by means of shafts connecting the various stages of compressors and turbines, in order to continuously drive the compressor stages of the engine and hence continue the overall cycle. Although the principles of gas turbine theory are well understood the application of the technology has led to significant advancements in design and materials in order to further improve efficiency of modern gas turbine engines.

2.1.2.1 Materials used in The Gas turbine engine

In the aerospace industry the development of gas turbines has focused on increasing efficiency. One way of doing this by increasing the thrust to weight ratio of engines which is done by increasing thrust or more importantly reducing the overall weight of the engine. With develops also centred around increasing the temperature within the combustion chamber, and hence the turbine section, this has led to the use of materials with increased high temperature performance through heavier alloying elements, for example, or by utilising coatings. Although the highest temperature regions employ the use of nickel superalloys, which typically have high densities, other metals such as titanium alloys are utilised in temperature regions which allow for them such as in the compressor stages of the gas turbine. The reason for this is due to the relatively lowering operating temperatures associated with the compressor stages compared with the combustion and turbine stages.

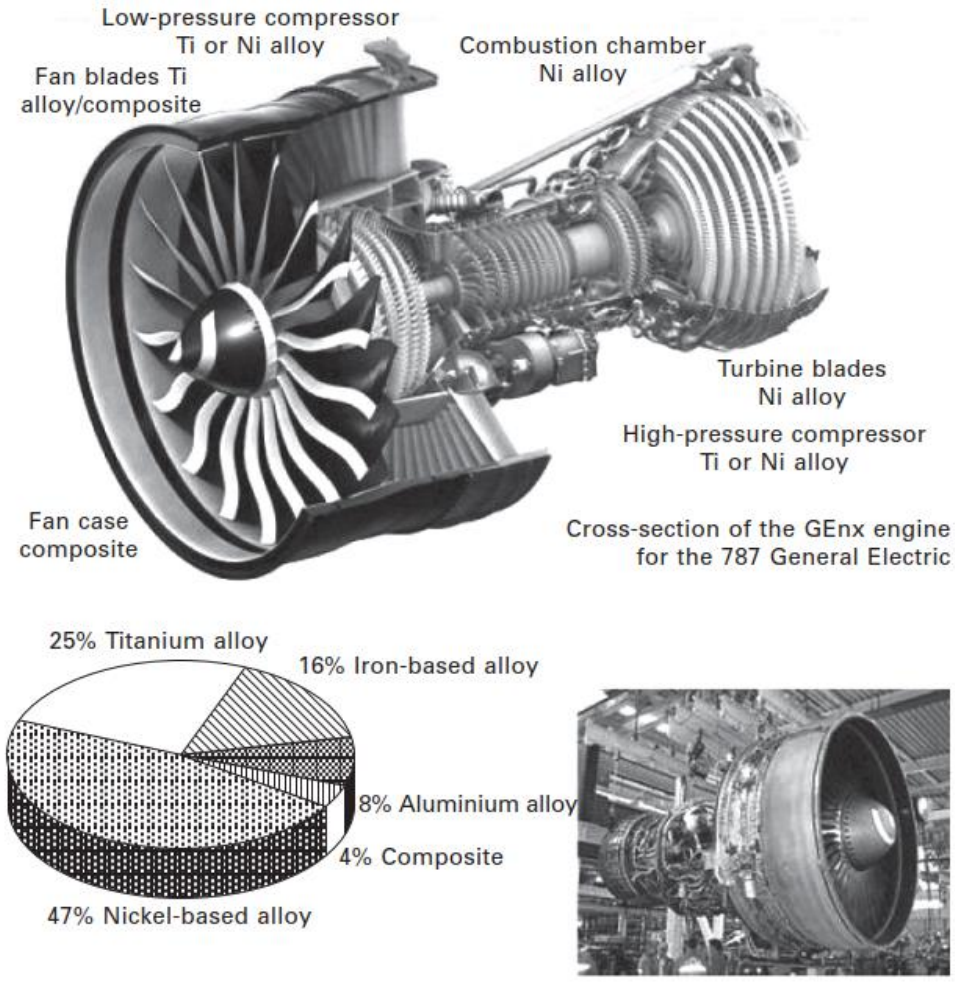

Figure 2.1.2.1 Diagram illustrating the distribution of materials used within a modern gas turbine engine along with the locations for the alloy types [2].

The diagram above, Figure 2.1.2.1 [3], (intro to aero materials, 12) shows the range of materials that are typically used within aero derivatives of the gas turbine and at what stages as well as an example of the distribution of the type of materials.

The initial stage of most commercial aviation gas turbine engine will use a titanium alloy for fan blades on high bypass ratio turbofan engines which are typically the most efficient types of engines in this industry. More recent developments have incorporated composites for the fan blades due their specific strength and lightweight whilst still using a titanium alloy on the leading edge to protect against Foreign Object Damage (FOD). The key considerations for materials used for fan blades is high toughness and good fatigue properties and typical alloys that are used are Ti-64.

The compressor stages are designed to increase pressure with temperature also increasing from the intake onwards. The temperature typically increases up to the maximum temperatures associated for titanium alloys with high strength alloys such as Ti-6246 being utilised for the latter stages. Developments in material technology have allowed for titanium alloys to now be used within the latter compressor stage whereas previous design relied on heavier nickel superalloys in order to meet the high temperature requirements, although with certain design of engines these alloys are still required. Within the combustion and all turbine stages, high and low pressure, relies solely on nickel superalloys due their superior high temperature capabilities in the form of crack growth resistance at elevated temperatures and also enhance creep resistance. Creep deformation is one of the main characteristics that need to be considered due to the length of time the material is exposed to elevated temperatures. As well as elevated temperatures the other factors that need to be considered are resistance against corrosion due to the combustion of fuels resulting in high levels of corrosive elements within the high temperature gas flow out of the combustion chamber.

2.1.3 Recent Gas turbine Developments

Developments in gas turbine engines have seen vast changes in material selection and refinement in order to optimised material properties to the application of the component. As well as this the design of rotating parts, for example, have changed from how blades are attached to discs as well as the overall design moving from turbojet engines to more efficient turbofan engines for commercial aircraft engines. One of the key advancements in designs of compressor and turbine stages is the potential of using Blisks (Blades Discs), which are a single component, as a replacement for the traditional dovetail fixture of blades onto discs, which are assemblies of parts. This development would allow for increased performance of gas turbine engines by firstly, reducing weight as fewer strengthening features are required for the blade fixings resulting in increased material removal. Other improvements include increased aerodynamic efficiency from reduced leakage and removal of features which may cause fatigue damage, and ultimate failure of part.

The manufacture of BLISKS can be complex due to the geometry of aerofoils attached to a large disc resulting in numerous processes in order to achieve a high integrity component. They can be manufactured via machining from solid or by joining the

aerofoil blades onto the central disc. Complexity of BLISKS arises from the increased manufacturing processes and costs compared with traditional methods as well as repair and overhaul. Damage to any one of the blades would require repair to be carried out specialised facilities with the process typically involving the removal of the entire component from the engine in order to allow for sufficient access and overhaul capabilities. This current process of repair is difficult and expensive, decreasing the motivation to implement the technology further into gas turbine engines therefore more robust methods of repair are required in to allow for better life cycle costs. There are technologies that have been investigated as potential repair methods for high temperature alloys used in BLISKS and this is where interlayer bonding may well be suited. There is potential in developing this technology in order to allow for the possibility of repairing damaged blades in a short period of time yet still maintaining high bond integrity that would be required for parts of this nature.

Figure 2.1.3.1: Diagram comparing BLISK technology to conventional method of blade attachment [49].

2.2 Titanium

2.2.1 Introduction to Titanium

Titanium is the 4th most abundant metal and was discovered in 1790 but it was not until early into the 20th Century that a method was developed to extract titanium from its ore. It can be alloyed with a range of elements, such as Aluminium and Vanadium for example which results in increasing the mechanical performance of titanium based alloys. It has long had a presence in a range of industries due to some of its unique collective properties such as having a high strength combined with a relatively low density, as well as having excellent corrosion resistance. With titanium also being biocompatible it has meant that it has been used as a material for surgical implants with the two most prominent uses being in dental implants and joint replacement surgery. Its high specific strength has meant it has a large presence in aircraft components, with greater use in aero engines parts which operate in temperatures of up to approximately 600^{0}C [4]. Titanium, usually alloyed with aluminium, zirconium, molybdenum and tin, to name but a few, are utilised in the gas turbine engine to meet the demands that certain components experience, depending on factors such as application and environment. Depending on the design of the gas turbine engine then up to 30% of the finish weight of the engine can be made from titanium, mainly in the fan and compressor sections.

There has been a certain amount of reluctance from certain industries, such as the automotive, to make more use of titanium primarily because of the high cost of this metal, however in aerospace the costs are offset by the significant advantages it brings when compared with competing engineering materials. The high associated costs arise due to the process that is involved in extracting it from its ore, which is either rutile (TiO_2) or ilmenite ($FeTiO_3$). However, processing improvements have meant that titanium has found more potential applications that can be exploited, for example the understanding and the ability to use diffusion bonding has allowed aero engine manufacturers such as Rolls-Royce to produce the hollow wide chord fan blade (WCFB). Some of the biggest producers of titanium and its ore include Australia, Canada, The United States, South Africa and China among others with an estimated 6500 tonnes produced every year [5].

2.2.2 Processing of Titanium

The high cost of titanium is primarily linked to the extraction and production procedure associated with the metal, as it requires a high energy process to go from its ore to the finished alloy. Even with this high cost of processing titanium the use of its various alloys is ever increasing with more and more applications for various alloys being used, especially within gas turbine engines [6].

The manufacturing process of titanium is done through the Kroll process named after William J. Kroll and was invented in the 1930's. It involves reducing the ore of rutile (TiO_2) or ilmenite ($FeTiO_3$), to a sponge like form, named due to the large pores present at this stage. There are a number of distinct stages for the extraction of titanium from its ore:

- Chlorination of the titanium ore to produce $TiCl_4$.
- Then a distillation stage of the $TiCl_4$ to purify it.
- The kroll process is then used to produce metallic titanium.
- Purification to limit the by-products.
- Then steps involving crushing and shearing in order to allow to for melting and further processing. [7]

The starting point for production of titanium alloys begins with impure rutile or ilmenite. The chlorination occurs in a fluidised bed reactor which also contains Rutile (TiO_2) and carbon (Coke). The process then involves introducing chlorine gas with the rutile and coke to produce metal chlorides and $TiCl_4$ in gaseous form. The resultant metal chlorides include CO_2, CO and MCl_x. These various reaction products are then separated via continuous fractional distillation. This is done to further purify the $TiCl_4$ by using a two step distillation process which removes the lower boiling point impurities first and then the higher boiling point impurities.

The next step involves the use of the Kroll process to allow for the reduction of the $TiCl_4$ by using metallic Magnesium. A reactor with inert gas is used which combines the purified $TiCl_4$ and metallic magnesium and then subsequently heated to 800^0C-850^0C [7]. The resultant metallic Titanium is relatively pure at this stage however, this sponge cake also contains residual $MgCl_2$. In order to separate the two, and further purify the Titanium, there are numerous methods that can be implemented, including vacuum distillation, acid leaching or inert gas sweep. These methods to remove the

$MgCl_2$, apart from acid leaching, can be used within the Kroll reactor vessel and are more used than acid leaching. The resultant Mg and Cl_2 can then be recovered and recycled.

The final stage involves creating granules of metallic Titanium from the Titanium sponge via crushing and sizing. The size of the granules is very much dependant on the end application. Coarser granules, up to 2.5cm, are commonly used for commercially pure Titanium as well as certain standard grades. However, when requiring alloys which are used for high performance parts then smaller granules are needed, typically less than 1cm. The smaller granules reduce the likelihood of interstitial defects occurring for the high performance alloys. Removing these defects also ensures there are no crack initiation sites present after the subsequent melting stages.

2.2.2.1 Vacuum Arc Re-melting (VAR)

In order to get to a cast ingot, the Vacuum Arc Re-melting (VAR) process is used which also provides homogeneity within the ingot, hence improving its quality. It is using this process that Titanium is alloyed with the required alloying elements to produce the required composition. The VAR process alloys for the melting of Titanium whilst avoiding the implications that can arise when handling molten Titanium, which is very reactive, such as reacting with air. The electrode, which is made up of the sponge as well as the alloying elements and typically in the form of a cylinder is placed in a large water cooled crucible under vacuum. The homogeneity of the melt can be improved via electrical coils around the crucible which act to bring about magnetic stirring of the melt. Due to the high cost for the production of Titanium and its alloys significant effort has been put into recycling waste material, commonly referred to as revert by incorporating into the ingots before melting. This is done by only using scrap which has the same alloying content as the electrode and is carefully controlled with regard to its cleanliness. The use revert material in the electrode for the melting process is heavily controlled and only used for certain applications of the produced stock material. During the process a current is used to create and arc between the re-melted material and the electrode. As the process continues the electrode is continuously moved towards the melt to produce the ingot. The water in the crucible allows for a controlled cooling process in order to control the solidification rate of the ingot and produce defect free material. Nominally the solidification rate remains

constant throughout the process however due to the various forms of heat transfer that occur it can be a difficult process to perfect. By performing this process in a vacuum, the amount of oxide inclusions and other elements, such as hydrogen and nitrogen, are significantly reduced. It is normal then for the ingot to go through at least one extra stage of remelting by inverting the ingot and going through the same stage as previously described. The image below, Figure 2.2.2.1, shows a cutaway view of a VAR furnace during the melting stage.

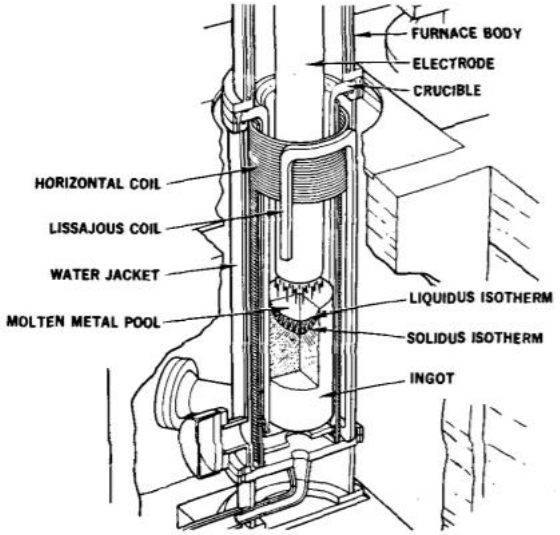

Figure 2.2.2.1 Image of a Vacuum Arc Remelt Furnace [8]

2.2.3 Properties and structure of Titanium

The properties of titanium have proven to be of great use for not only the aerospace industry but also in biomedical devices and chemical processing equipment due to its high specific strength and corrosion resistance. Some of the important properties of

Table 2.2.1 Characteristics of Titanium and other structural metallic materials [4].

	Ti	Fe	Ni	Al
Melting Temperature (°C)	1670	1538	1455	660
Allotropic Transformation (°C)	$\beta \xrightarrow{882} \alpha$	$\gamma \xrightarrow{912} \alpha$	-	-
Crystal Structure	bcc → hex	fcc → bcc	fcc	fcc
Room Temperature E (GPa)	115	215	200	72
Yield Stress Level (MPa)	1000	1000	1000	500
Density (g/cm^3)	4.5	7.9	8.9	2.7
Comparative Corrosion Resistance	Very High	Low	Medium	High
Comparative Reactivity with Oxygen	Very High	Low	Low	High
Comparative Price of Metal	Very High	Low	High	Medium

Titanium are compared with other metals shown in the table below [9]. As well as having a specific strength greater than Fe, Ni, and Al, its elevated temperature properties are also superior to that of Al, which competes against Titanium for its low density, and therefore Titanium alloys have advantages for structural applications at temperature above 150ºC. Although Titanium has favourable properties compared with many metallic materials, its high prices inhibits the extensive use of its alloys due to its high production costs and therefore is in applications where the advantages outweigh the associated costs.

Titanium is made up of two crystal structures, a close packed hexagonal structure, HCP, termed the α phase, and the other a body-centred cubic, BCC, known as the β phase [10]. Commercially pure Titanium undergoes an allotropic transformation at 882^0C, changing from the high temperature β phase to the low temperature α phase [9]. Therefore, the β is stable between the transition temperature up to the melting temperature of 1668^0C whereas the α phase exists at temperatures below 882^0C. The structure of the two types of phases within Titanium are shown, along with the most densely packed planes and directions shown in the Figures below.

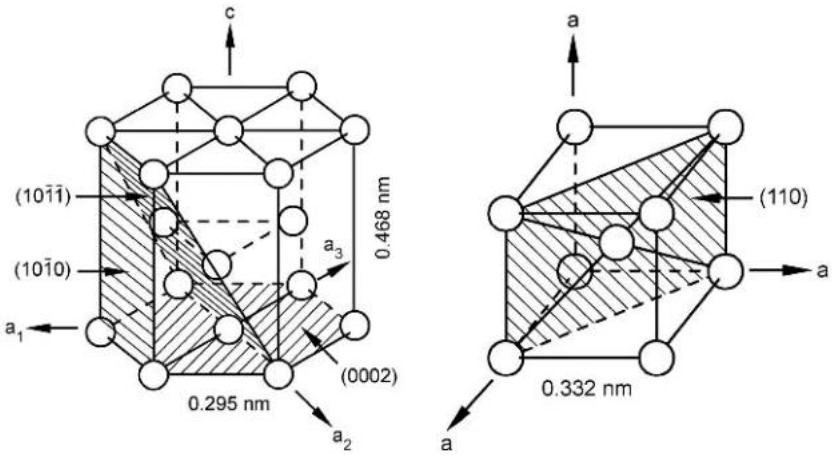

Figure 2.2.3.1 (a) Unit cell of alpha phase, (b) Unit cells of Beta phase. [4]

The hexagonal structure of the alpha phase is shown in Figure 2.2.3.1a showing the room temperature values for the lattice parameters a and c. The Body Centre Cubic (bcc), Beta phase, is shown in Figure 2.2.3.1b indicating the lattice parameter value (a) at 900ºC of 0.332nm. The deformation behaviour of Titanium is closely linked to

the associated crystal structure. For example, there is clear anisotropy of the elastic mechanical performance when considering the α phase at room temperature. The figure below shows the variation of the modulus of elasticity, E, with respect to the

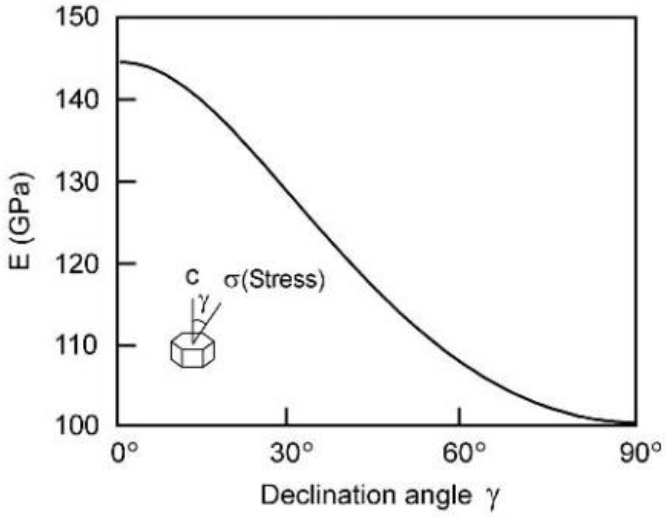

Figure 2.2.3.2 Displaying the Modulus of Elasticity, E, of alpha Titanium single crystal as a function of delcination angle γ [4].

angle, γ, which is the angle between the c-axis of the unit cell and the stress angle [7]. The Young's modulus for the α crystal lattice can range from 145GPa with loading vertical to the basal plane and 100GPa for stress applied perpendicular to the c axis. The shear modulus of single crystals also displays similar trends to that of the elastic modulus with values between 46GPa and 34GPa depending on direction of shear stresses. These ranges of values can vary further depending on the form and strength of the texture.

The ability to measure the elastic modulus of the β is made difficult by this phase not being stable at temperatures below the transus temperature, this is the temperature at which the β phase transforms to the α phase. Only with high concentrations of beta stabilising elements, such as Vanadium, can significant amounts of the β phase be retained at room temperature. When looking at Ti-V alloys with large amounts of the alloying element, Vanadium, the metastable β can be retained to room temperature via rapid cooling from high temperature. When analysing the modulus of elasticity of the beta phase there is a reduction in the modulus for this phase in comparison to the alpha phase, as low as 85GPa for approximately 20% Vanadium.

The hexagonal phase of Titanium is considered to have increased ductility which results from the activation of twinning deformation modes in parallel with slip via dislocations [7]. However, in α+β alloys twinning is reduced due to high solute content and because of the presence of Ti_3Al precipitates but these alloys remain ductile at low temperatures due to small phase dimensions. The β phase also exhibit both twinning and slip but is limited to single phase state as well as decreasing with increasing solute content.

The crystal structures associated with Titanium is of great importance as varying the amounts of the respective phases can greatly impact the resultant mechanical properties. For example the plastic deformation response and diffusion rates of titanium alloys are influenced by the two different crystal structures [11].

2.2.3.1 Nucleation and Diffusional Growth

The diffusion and growth of the α phase is dependent on numerous factors such as alloy type and thermomechanical processing but also cooling rates from the β phase to the α+β phase field. When cooled at relatively low rates the α phase starts to nucleate preferentially at the boundaries of the β phase. This then leads to a continuous layer of α along these boundaries. As the cooling continues the α plates continue to nucleate and grow and either the β grain boundary or the interface between the continuous α. These plates then continue to grow parallel into the β grains and are named α colonies. The α plates that have grown into the β grains are separated by the retained β matrix. For this type of microstructure, shown in Figure 2.2.3.3, the α and β formation leads to this structure being named as a lamellar microstructure.

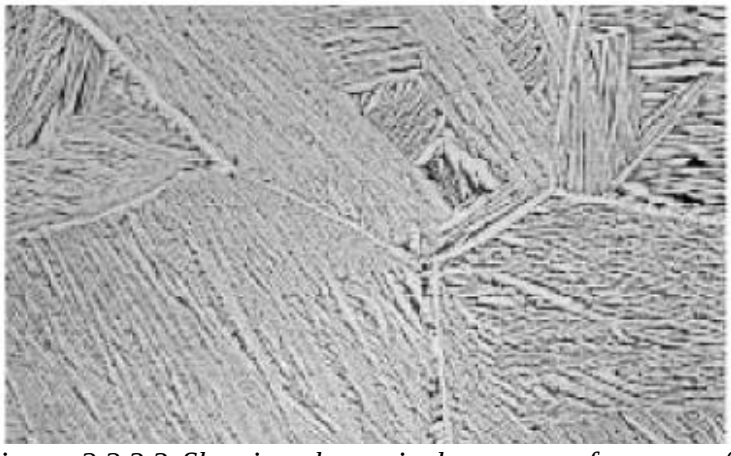

Figure 2.2.3.3 Showing the typical structure for an α+β lamellar microstructure for Ti-64 [8].

The cooling rate has an effect on the size and distribution of the α plates and colonies. With increasing cooling rates, the thickness of the plates and the size of the colonies reduces. With this increased cooling rate, the colonies can no longer grow completely into the β matrix and the α plates grow on the boundaries of previous α colonies. To reduce the elastic strain the new α plates grow perpendicular to the previous plates and result in a different microstructure. This type of growth leads to a microstructure commonly referred to as Basket Weave or Widmanstatten.

2.2.3.2 Strengthening Mechanisms

When evaluating the hardening mechanisms in titanium there are two key mechanisms which have a significant impact on hardening of the two phases within titanium alloys. These are solid solution and precipitation hardening and can be discussed with regard to the two phases, α and β, separately. When analysing the α phase the interstitial element oxygen significantly increases the hardness for this phase. Evidence of this hardening effect can be seen by analysing the yield strength results for a range of CP titanium grades (1-4). The oxygen concentration for these grades increases from 0.18% for grade 1 to 0.4% for grade 4. With this increase in oxygen concentration the yield stress of the grades increases from 170MPa for grade 1 to 480MPa for grade 4. The solid solution hardening of the α phase occurs via substitution from elements such as Al, Sn and Zr which have large atomic size differences to that of titanium. The precipitation hardening of the alpha phase arises from the α_2 particles (Ti_3Al) above certain percentages of Al (5%). These particles have an ordered hexagonal structure which can be ellipsoidal in shape and further stabilise elements such as Sn. The α_2 phase contributes to significantly to the properties of α+β alloys by annealing at specified temperatures depending on the composition of the titanium alloy. This is because at these temperatures, element partitioning takes place with the α phase becomes enriched in elements such as Al, O and Sn, the α stabilising elements [7]. As a result of this a significant amount of the α_2 can be precipitated within the alloy. Typical temperatures to precipitate the α_2 can be from 500^0C for Ti-6Al-4V and 595^0C for Ti-6246 up to 700^0C for IMI834.

For the β phase the hardening mechanisms are not as obvious as the α phase as it is difficult to separate out the effects of the α precipitates, the metastable ω and β' phases

[7]. Although solid solution strengthening effect of the β phase can occur from alloy partitioning during the precipitation of the α phase, the most effect way to harden this phase is by precipitation hardening. Both the ω and β' phase can be sheared by moving dislocations with this leading to poor crack nucleation properties and reduced ductility. Due to the reduced properties these phases are not widely present in β alloys however despite this they are used to aid the precipitation of the α phase. This is done in β alloys by ageing at increased temperatures, when compared with α alloys, and therefore using the ω and β' particles as nucleation sites for the α phase. This then alloys for increased yield strength properties for β alloys due to the small, hard to deform α platelets.

2.2.4 Alloy Classification, Alpha & Beta

In order to classify a titanium alloy then the composition and microstructure need to be known. Therefore, depending on the composition and microstructure titanium alloys can be divided into three main categories: alpha (α), alpha + beta (α+β), or beta (β) alloys, although sometimes alloys can be classed slightly differently, such as near-alpha, near-beta and metastable-beta. Whether an alloy is referred to as and alpha or beta alloy relies heavily on whether the alloying elements stabilise the hexagonal alpha phase or the body centred cubic beta phase. Leading on from this the elements which stabilise the alpha phase are known as α-stabilisers (Al, O, N, C) and the elements which stabilise the beat phase are known as β-stabilisers (V, Mo, Nb, Cr, Fe, Ni). There are also what are known as neutral elements (Sn, Zr) which have a negligible effect on the β-transus temperature as they do not stabilise either the α or β phase however they are highly soluble in the α phase and so are generally perceived to be α strengthening elements [12].

Therefore it can be said that α and near α alloys contain predominantly alpha phase, alpha + beta alloys contain more of a balance between both phases, when compared with alpha alloys, but still usually contain slightly more α depending on the variation in the alloying elements and heat treatment [13]. Beta alloys conversely contain an increased amount of the β phase when compared with the former class of alloys.

The resultant microstructure is greatly affected by the amount of the α/β stabilisers present within the material and therefore by controlling the alloying elements the mechanical properties can be optimised depending on operational requirements of the material.

2.2.4.1 Effect of alloying elements

Titanium's electronic structure is incomplete which allows for the formation of solid solutions with substitutional elements which have a size factor of +/-20%. As well as solid solutions, Titanium can form interstitial with elements such as oxygen and carbon. Which elements stabilise which phase of Titanium is dependent on the number of electrons per atom of the stabilising element. Alloying elements with a ratio of electrons to atom less than 4 stabilise the α phase whereas elements with a ratio greater than 4 stabilise the β phase and finally elements with a ratio of precisely 4 are neutral [14].

The effect of alpha and beta stabilisers in titanium are shown in Figure 2.2.4.1. Both α and β stabilisers have an effect on the β transus temperature, this is the lowest temperature at which the alloy can be transformed completely to the β phase [9], but in different ways. By adding additional amounts of α-stabilising elements to titanium, such as aluminium, then the β transus temperature increases and this then means that the α phase can be stabilised over a greater temperature range. Conversely by increasing the amount of β stabilising elements in the alloy the β transus temperature decreases allowing for an increase in the formation of the β phase. The β stabilising elements can also be separated into two classes, known as β isomorphous stabilisers which continuously suppress the transition temperature, and β eutectoid formers which also lower the transus temperature but compound formation means there is a limit [1]. Common β isomorphous stabilising elements used in industry include V and Mo which can, at certain concentrations, make it possible to stabilise this phase down to room temperature.

There are certain elements which are neutral when it comes to the transformation temperature as they can slightly increase the transformation temperature but also reduce this temperature with increased concentrations. Examples of neutral elements include Zr and Sn with the former being isomorphous with titanium and therefore have

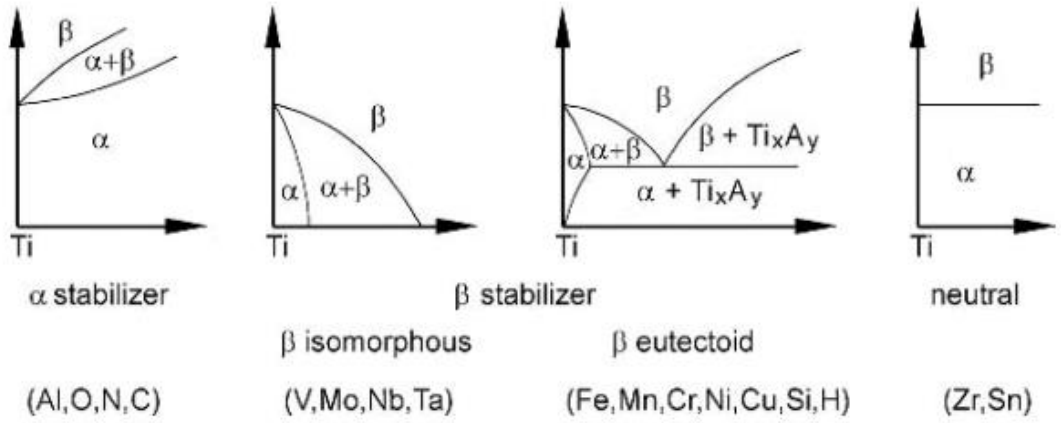

Figure 2.2.4.1 Effect of alloying elements on the phase diagrams of titanium alloys [4].

the same β to α allotropic phase transformation [7]. Although these elements are neutral with regard to the transformation temperature, they are sometimes classed as being α stabilisers for many commercial alloys. The reason for this stems from the chemical similarity between Zr and titanium whereas Sn can replace aluminium in the secondary alpha phase (α_2). The complexity of titanium alloy classification arises from these variances, with regard to the alloying elements, and how they interact with other element within titanium. With regard to multicomponent titanium alloys the effect of the α stabilising elements can be classified by the following equation:

$$[Al]_{eq} = [Al] + 0.17\,[Zr] + 0.33\,[Sn] + 10\,[O] \qquad [7]$$

With the range of effects from alloying elements on different aspects of titanium the classification of alloys is important. The table below, Table 1.2.2, showcases many examples of commonly used alloys of titanium and how they are classed based on the alloying elements. The most common alloy used for Titanium is Ti-6Al-4V, which is classed as an α+β alloy, and has extensive uses in many applications due to the greater understanding from industry with this alloy. This alloy has an excellent balance of strength, fatigue and ductility properties with the ELI version of this alloy have greater fracture toughness and damage tolerance properties. Alloys such as Ti-6Al-2Sn-4Zr-6Mo are commonly referred to as either an α+β or a β alloy. The reason for this arises,

not only from the alloying elements within the alloy, but to how the thermo-mechanical history of the alloy contributes significantly to the distribution of the α and β phases. The processing of for this alloy is discussed further in the following chapters (2.2.5).

Table 2.2.2 List of important commercial titanium alloys and there classifications

Common Name	Alloy Composition (wt%)	T_β (°C)
α Alloys and CP Titanium		
Grade 1	CP-Ti (0.2Fe, 0.18O)	890
Grade 2	CP-Ti (0.3Fe, 0.25O)	915
Grade 3	CP-Ti (0.3Fe, 0.35O)	920
Grade 4	CP-Ti (0.5Fe, 0.40O)	950
Grade 7	Ti-0.2Pd	915
Grade 12	Ti-0.3Mo-0.8Ni	880
Ti-5-2.5	Ti-5Al-2.5Sn	1040
Ti-3-2.5	Ti-3Al-2.5V	935
α+β Alloys		
Ti-811	Ti-8Al-1V-1Mo	1040
IMI 685	Ti-6Al-5Zr-0.5Mo-0.25Si	1020
IMI 834	Ti-5.8Al-4Sn-3.5Zr-0.5Mo-0.7Nb-0.35Si-0.06C	1045
Ti-6242	Ti-6Al-2Sn-4Zr-2Mo-0.1Si	995
Ti-6-4	Ti-6Al-4V (0.20O)	995
Ti-6-4 ELI	Ti-6Al-4V (0.13O)	975
Ti-662	Ti-6Al-6V-2Sn	945
IMI 550	Ti-4Al-2Sn-4Mo-0.5Si	975
β Alloys		
Ti-6246	Ti-6Al-2Sn-4Zr-6Mo	940
Ti-17	Ti-5Al-2Sn-2Zr-4Mo-4Cr	890
SP-700	Ti-4.5Al-3V-2Mo-2Fe	900
Beta-CEZ	Ti-5Al-2Sn-2Cr-4Mo-4Zr-1Fe	890
Ti-10-2-3	Ti-10V-2Fe-3Al	800
Beta 21S	Ti-15Mo-2.7Nb-3Al-0.2Si	810
Ti-LCB	Ti-4.5Fe-6.8Mo-1.5Al	810
Ti-15-3	Ti-15V-3Cr-3Al-3Sn	760
Beta C	Ti-3Al-8V-6Cr-4Mo-4Zr	730
B120VCA	Ti-13V-11Cr-3Al	700

The CP titanium alloys, referred to as Grades 1 to 4 in the table above, are classified based on the oxygen concentration within the alloy. Grade 1 having the lowest amount with 0.18% and Grade 4 containing 0.4%.

The role of alloying elements is key in determining the mechanical properties of alloyed titanium and hence critical when processing these alloys. The presence of certain alloying additions and the makeup of the phases present in the microstructure of Titanium alloys determines how they are classified, as discussed in the following chapter.

2.2.4.2 Alpha alloys

This classification of titanium alloys is made up of various grades of CP Titanium as well as alpha alloys and contain minimal amounts of the β phase. The various grades of CP titanium have differing amounts of oxygen, up to 0.4% with this effecting the yield strength of each of the grades. Alpha alloys are known to have a higher working temperature range and good oxidation resistance than other alloy types of titanium primarily due to the increased aluminium content. The reason for this is due to the strong performance shown, in particular good creep strength, at elevated temperatures. As well as at high temperatures, alpha alloys have also been used extensively for cryogenic purposes with good toughness and ductility at these temperatures derived from the interstitial atoms [10]. As well as this alpha alloys, and also pure titanium, have the highest corrosion resistance. However, unlike alpha/beta and beta alloys, alpha alloys cannot be heat treated, therefore good for welding, to alter the microstructure and hence improve its strength as they are close to single phase alloys. Rather than heat treating, α alloys are generally annealed in order to reduce residual stresses from cold working. There are commercial titanium alloys which are classed as near alpha alloys due to the slight increase in β stabilising that these alloys contain. However, these additions are very low and therefore only contain small amounts of retained β.

Examples of alpha alloys include; Ti-6Al-2Sn-4Zr-2Mo and IMI-685, with Ti-6242 being extensively used in certain gas turbine variants. It is commonly used in rotating components such as blades and disks where the temperatures can reach approximately 550^{o}C, above this temperature nickel alloys are more commonly used due to their improved high temperature strength and also to avoid titanium burn.

2.2.4.3 Alpha + Beta alloys

These alloys have a mix of α and β stabilisers and so therefore the microstructure contains a mix of both the alpha and beta phase. The typical microstructure is made

up of needle-like or acicular α within a prior β grain, also known as a basket weave or Widmanstatten microstructure. They have a good combination of properties owing to the fact they can be strengthened by solution treating and aging to obtain a desired microstructure and hence optimise mechanical and thermal properties [15]. They are quenched in water or oil, from the solution treating temperature, in order to retain the beta phase at room temperature. If cooled rapidly the beta phase may be partly transformed by a martensitic transformation or by diffusion controlled nucleation and growth of the alpha phase [10]. Following this an aging occurs between 480^0C-650^0C in order for the alpha to precipitate and produce a microstructure that has a mixture of both alpha and beta. Processing these alloys via solution and ageing can significantly increase the strength of these alloys and therefore the thermomechanical processes are well controlled in order to produce the optimum combination of mechanical properties.

Typical alpha/beta alloys include the greatly used Ti-6Al-4V and Ti-6Al-2Sn-4Zr-6Mo and are used in air breathing jet engines where the temperatures range from approximately 315-400^0C. These alloys can provide significant weight savings when used over alternate materials within the same operation and can also be cast and forged relatively easily [16].

2.2.4.4 Beta alloys

Beta alloys contain an increased number of β-stabilisers, when compared with alpha and alpha/beta alloys, which acts to suppress the martensitic transformation during quenching to room temperature. The consequence of this is for there to be an increased amount of the BCC beta phase present at room temperature depending on the volume of the alloying elements and also any aging processes. Beta alloys can be split into two categories, metastable β alloys and full stable β alloys with the former being the most commonly used type. However only the metastable beta alloys are heat treatable, to higher strengths of up to 1400MPa, via solution treatment and aging which results in precipitation of the very fine alpha phase, whereas fully stable beta alloys must be annealed [11]. These alloys have very good fracture toughness when compared with alpha/beta alloys which have similar yield strengths. They also have high strength and good forgeability owing to the lower β transus temperature and can have excellent cold formability when in the solution treated condition. However, the disadvantages

associated with beta alloys is that they have a higher density, lower creep strength and can have lower tensile ductility.

Typical beta alloys include; Ti 17 used in engine compressor discs, Ti-15Mo-3Nb-3Al-2Si and Ti-3Al-8V-6Cr-4Mo-4Zr which have excellent fatigue properties and are used in the manufacture of coil springs [17].

2.2.5 Titanium 6-2-4-6

Ti-6Al-2Sn-4Zr-6Mo (Ti-6246) is an alloy developed by Pratt & Whitney designed to combine the elevated temperature capabilities of Ti-6Al-2Sn-4Zr-6Mo-0.08Si (Ti-6246S) with increased strength. Alternate names for Ti-6246 include; AMS 4981, Mil-T-9047 and UNS 56260. It is an alpha/beta alloy and can be heat treated to achieve the higher strength levels required for service. The main use of this alloy is within the compressor regions of an engine for rotating components such as compressor disks and blades due to its high fatigue strength and excellent toughness properties. It operates in temperatures of up to 400^0C for long term load carrying applications, however for short term load carrying applications it can be used in temperatures up to 540^0C [18][19].

As with many titanium alloys Ti-6246 derives its good strength and high temperature properties from the microstructure which is highly dependent on the thermo-mechanical history of the material. When an alloy is forged in a temperature region equal to or below the β transus it is regarded as α+β forging. Forging in this temperature region leads to a dual phase microstructure of both α+β, which includes elongated, equiaxed α grains within transformed β phase Figure 2.2.5.1a [20]. However, this type of microstructure exhibits poor fracture toughness and fatigue crack growth properties when compared with a β-forged material. An example of a β-forged microstructure is shown in Figure 2.2.5.1 and alleviates the poor properties of α+β forging by heating in the β region, showing a fully acicular α microstructure.

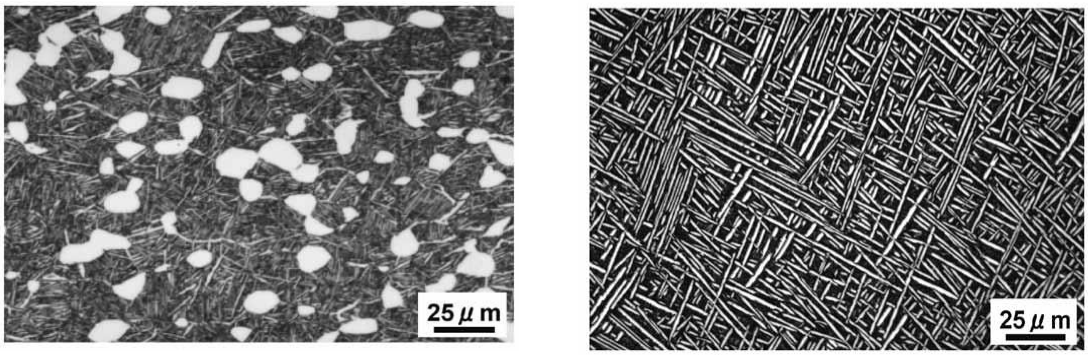

Figure 2.2.5.1(a) Typical microstructure for α+β forging, (b) typical microstructure for β processing [4].

Heating in the β region before forging causes the transformation of the microstructure and therefore removes the effects of any previous processing techniques. As a result of this the microstructure, and hence mechanical properties, are significantly affected by the final forging temperatures. Therefore the β forging process must be highly controlled in order to achieve the correct material properties [20].

Research has shown that microstructural features including continuous α layers at β grain boundaries, volume fraction, α lamellae size and β grain size can significantly impact the mechanical properties of Ti-6246 [21]. In order to fully control the microstructure and hence optimise the mechanical behaviour for this alloy the processing route must be carefully considered.

2.2.5.1 α+β Processing

A typical processing route would involve multiple steps to alleviate the negative impact associated with the microstructural features mentioned previously. Example of a processing route involves homogenisation above the β_T, deformation and recrystallization in the α+β phase field and ageing at lower temperatures or a combination of these steps [15]. With each of these steps the critical parameters centre around time spent at the relevant temperatures and also cooling rates at the end each stage. These factors determine the width of α lamellae, prior β grain size and volume fraction of equiaxed α. For example, the cooling rate from the homogenisation stage would define the size of the equiaxed β as well as the distribution of the grain boundary α. Following the four steps for processing would result in a Bi-modal (duplex) microstructure as displayed in Figure 2.2.5.1a above, leading to equiaxed primary α and recrystallised β.

2.2.5.2 β Processing

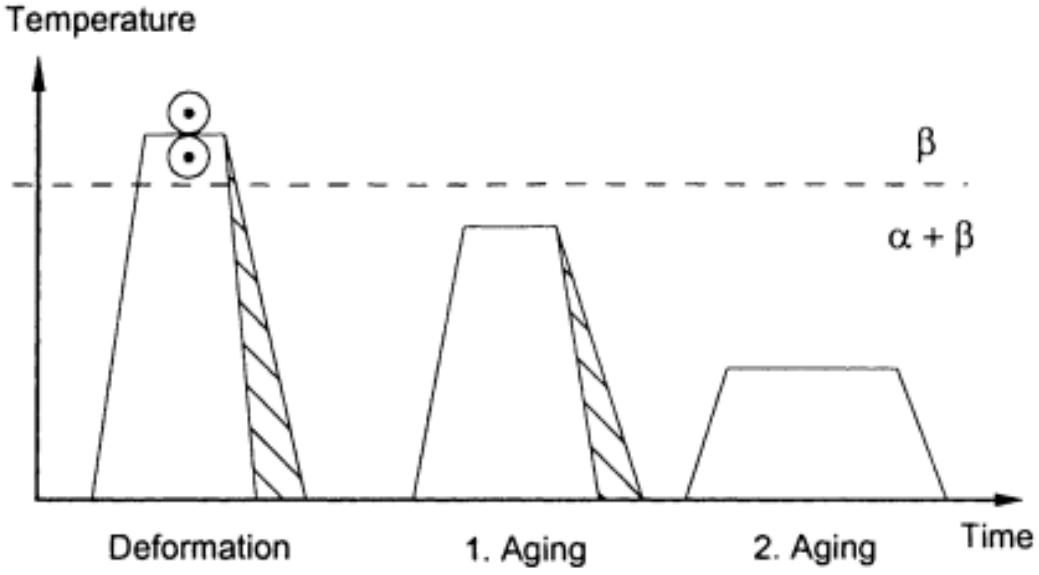

Figure 2.2.5.2 Schematic of β processing for Ti-6246.

This form of processing common for this alloy due to the good combination of processing steps as well as mechanical properties. The processing consists with forging at temperatures above the β_T followed by a fast cooling rate in order to reduce recrystallisation of the β grains. As a result of the deformation at this elevated temperature the β grains exhibit a criss-cross shape. This modulating formation of the β grains limits the formation and growth of grain boundary α to shorter segments. The following stages for this processing route involves a two-step ageing process, shown in the Figure 2.2.5.2 below. The first step takes place towards the upper limit of the α+β phase field in order to produce coarse α plates throughout the matrix [22]. For the second, and lower temperature, ageing step the purpose is to precipitate and increase the volume fraction of the fine secondary alpha (α_s). The volume fraction of the fine α_s is controlled by the difference in temperature of the two ageing steps as well as the cooling rate. The second ageing step needs to closely be defined and controlled as if done at the correct temperature the yield stress of the alloy can be increased however if the temperature is too low it can result in the formation of the brittle ω particles.

However, by only going through a homogenisation and the same ageing steps described above, a vastly different microstructure can be created, shown in the Figure 2.2.5.3. This distinct process would result in a fully lamellar microstructure with α colony size playing a predominant role in the mechanical properties as it defines the

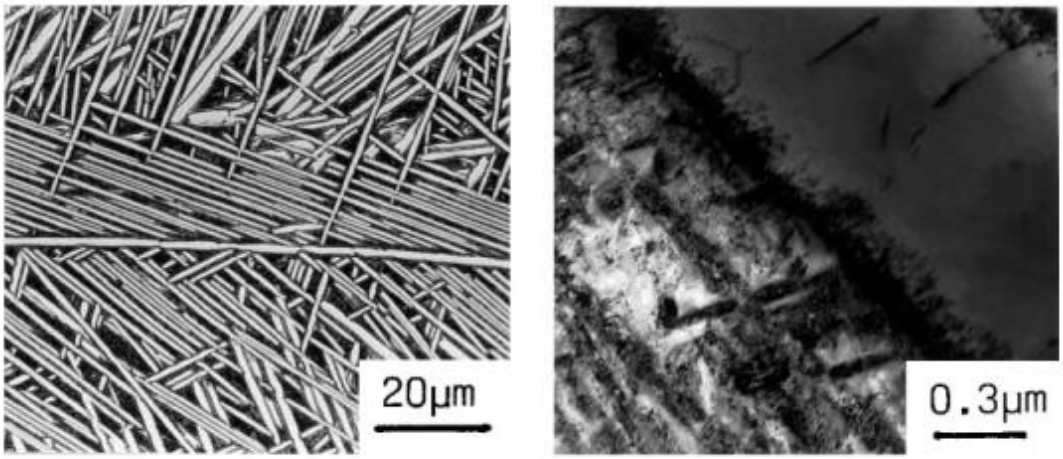

Figure 2.2.5.3 Example of β-annealed microstructure, Ti-6246: (a); (b) TEM [4].

effective slip length [15]. For this scenario a faster cooling rate would result in reduced α colony size and hence an increase in yield stress.

2.2.5.3 Mechanical Properties of Ti-6246

The role of titanium alloys in the gas turbine, such as Ti-6246, stem from their ability to perform well at relatively high temperatures for Titanium. For example, this alloy has a high specific strength property, it has a high tensile strength and yet maintain a relatively low density in comparison to other high temperatures such as nickel superalloys. With the drive for lighter more efficient gas turbines in the aerospace industry titanium alloys play a significant role in reducing weight and increasing performance of modern engines.

Whereas CP titanium has typical Ultimate tensile strength (UTS) values of approximately 550MPa at room temperature for Grade 4, Ti-6246 has peak levels of 1242MPa as shown in Table 1.2.3. This level of strength is similar when looking at the 0.2% Proof Strength of the alloy which can exceed 1100MPa.

Table 2.2.3 Showing variations in tensile properties for Ti-6246 with heat treatment conditions.

TYPICAL VARIATIONS IN TENSILE PROPERTIES WITH HEAT TREAT CONDITION

% Primary α	Condition	Temperature °F (°C)	UTS ksi (MPa)	0.2% YS ksi (MPa)	Elongation %	Reduction in Area %
10-20	STA[a]	68 (20)	176 (1214)	162 (1118)	13	37
10-20	STOA[b]	68 (20)	160 (1100)	150 (1035)	6	12
40-50	STA[a]		180 (1242)	167 (1152)	14	42
40-50	STOA[b]		166 (1145)	155 (1070)	14	41
β forged	STA[c]		174 (1201)	152 (1049)	6.5	13

[a] Solution Treated and Aged at 885°C(1630°F)/1h/AC + 595°C(1100°F)/8h/AC [b] Solution Treated and Aged at 885°C(1630°F)/1h/AC + 705°C(1300°F)/1h/AC
[c] Solution Treated and Aged at 985°C(1810°F)/1h/AC + 595°C(1100°F)/1h/AC

The table shows how the different thermo-mechanical processing can affect the mechanical properties for this alloy, with UTS values as low as 1100MPa and corresponding elongation 6%. The tensile properties for Ti-6246 decrease with temperature with a 50% typically seen at temperatures of approximately 550^0C, obviously this decrease is greatly affected by the processing history of the alloy.

Research has also shown that with the right combination of thermo-mechanical processing it is possible to achieve good fracture toughness and tensile ductility at yield strengths of up to 1241MPa [23]. The corresponding microstructure contains approximately 10% volume fraction of α_p.

For this type of alloy, the key factors that can affect mechanical properties, such as tensile and high fatigue properties, is the primary α volume fraction as well as the distribution and morphology of the α phase [24][25]. It is also accepted that the volume fractions of α_s and transformed β have a beneficial effect in tensile and cyclic behaviour for Ti-6246, irrespective of the type of microstructure.

With respect to repaired or welded Ti-6246 the mechanical properties can vary drastically depending on the conditions of the joining process. Typically for this alloy the temperatures required for the successful joining are near or slightly above the transus temperature of the material. Being at these elevated temperatures leads to microstructural changes as well as affecting residual stresses in the material which

affect mechanical properties. Research has shown that for LFW Ti-6246 the properties and microstructure within the HAZ can vary significantly from the base material after welding. The hardness values within the central weld zone can be as low as 360HV, with a width of approximately 2mm, whereas for the base material this value is 420HV. For the same welds if a post weld heat treatment, 600^0C for 1hr, is applied the hardness can increase by 180HV within the central weld zone [26]. With respect to the microstructure of welded Ti-6246 the weld zone show signs of depleted α_s due to the heating which occurs from the welding process. Also, composition changes can also occur causing a less obvious distinction between the interface of the β and primary α phase.

The mechanical properties of Electron Beam Welded Ti-6246 can improve with a PWHT. Welded samples can have room temperature tensile properties similar to that of the base material with regard to Yield Strength and UTS however there is noticeable decrease in elongation [27].

2.2.6 Applications of titanium alloys in aerospace

The use of titanium has grown rapidly over the previous decades, especially so in the aerospace industry where it now mostly used. Its main use is within the gas turbine, within the compressor disks, blades and vanes as well as in engine cases. Away from the engine titanium has started to be used for landing gear operation, replacing steel in doing so. The predominant reason for using titanium, especially in aerospace, is due to its high strength to weight ratio couple with corrosion resistance. The use of titanium is fuelled by the need to continually reduce weight which leads to an overall increase in engine efficiency and also reduce operational costs.

The Figure below shows the general breakdown of the use of the different type of titanium alloys used in certain parts of a gas turbine engine and also what properties need to be optimised in different areas of the engine [28]. In reality there are an increased number of ‘sister alloys’ of each alloy shown in Figure but for simplicity only one alloy of Titanium is shown for each class of alloy. For example within the Ti-6246 region, alloys such as Ti-17 may also be used but both alloys are aimed at meeting the same, or similar, temperature and cost requirements [28]. The main alloy of choice, if possible, is Ti 6/4 due to its relatively low cost compared to other alloy types and also due to it being a strongly understood alloy with good overall properties

although limited strongly by its temperature capability [29][6]. Where the temperatures within the engine begin to increase, for example within the latter stages of the compressor stage, then Ti-6242 begins to become more relevant due to its enhanced temperature capability. Leading on from the increased temperature requirements, there are components which will be exposed to not only this increased temperature, but also higher loads therefore require increased strength and fatigue properties. This is where alloys such as Ti-6246 and IMI-834 are utilised although these alloys now begin to reach the functional limits of what is possible for titanium when combining strength, temperature and cost together and as a consequence they are not as widely used. Once past a certain temperature of approximately 700K then titanium alloys con no longer be used due to poorer creep properties compared with Nickel superalloys, also titanium burn can become an issue at these temperatures.

The bottom half the figure also shows what the main challenges are that need to be met by future alloys or component design within each region of the engine in order for

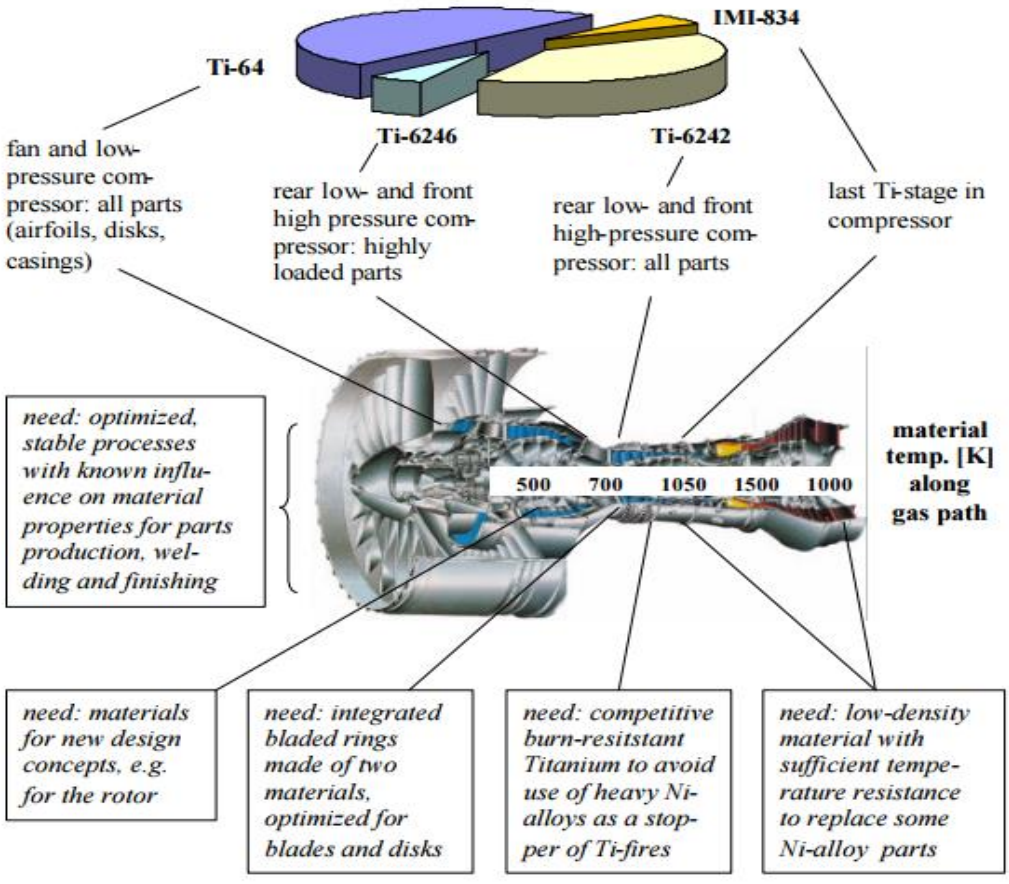

Figure 2.2.6.1 Showing applications of various titanium alloys within a gas turbine engine [28].

future engines to become more efficient overall and continue its growth in performance.

2.2.6.1 α alloys Applications

As discussed previously α alloys exhibit greater temperature capability, including creep properties, than proceeding α/β, and β alloys. The primary alloy for these conditions is Ti-6242S, a variant of Ti-6242 where the 'S' donates an addition of silicon in the range of 0.1-0.25, which further increase the creep resistance of high temperature alloys [30][31]. It can operate in temperatures of up to 540^0C and therefore is used in rotating components such as blades and disks within the high pressure compressor stages of an engine. For static components, such as compressor cases, titanium can be used up to temperatures of 560^0C due to the reduced load.

Although α alloys are the high temperature alloys of titanium they are still unable to meet the higher temperatures experienced in the combustion chamber and also the turbine regions. Nickel superalloys are utilised and although they have a melting temperature slightly below that of titanium, approximately 1450^0C, they have a far greater creep resistance capability. Although Nickel alloys have significantly higher density, the increased creep properties mean that the higher weight is a price worth paying. There is further issue with using titanium above its current limit and this includes the tendency for titanium to ignite and then burn (titanium burn), as well as this titanium oxidises very easily, which encourages the formation of alpha case and can lead to a significant drop in mechanical properties.

2.2.6.2 α/β alloys

The most widely used titanium alloy, Ti 6/4, is an α/β alloy which is relatively low cost alloy with good all round properties with increased strength properties when compared with α alloys. It has a good combination of properties such as; strength, ductility, creep resistance, fracture toughness, weldability and thermal process ability [6]. It is used extensively thorough an aircraft and engine components with the predominant ones being for fan blades, fan casings and intake section where temperature is relatively low [6].

This class of alloys tend to have a wide processing window and therefore the processing of these types of alloy does not need to be as strictly controlled as with

other alloy types. With the increased strength properties comes a reduction in the absolute operating temperature of these alloys which can be used up to approximately 350^0C for Ti 6/4, although some alloys such as Ti-6246 can operate in temperatures of 550^0C [9]. Ti-6246 is primarily used due to its increased fatigue and toughness characteristics at elevated temperatures. For this reason, it is used in the high pressure compressor (HPC) stages for blades and compressor disks, where low cycle fatigue (LCF) and creep properties are required, although the cost of production is an obstacle for further use in the engine.

The strength of these alloys come from their ability to be solution treated and aged which allows the microstructure to be tailored to increase fatigue strength or fractures toughness for example.

2.2.6.3 β alloys

There are a range of β that are or have been in service within the aerospace industry including; Ti-10V-2Fe-3Al (Ti 10-2-3), Ti- 15V-3Cr--3A1-3Sn (Ti-15-3), and Ti-3A1-SV-6Cr-4Mo-4Zr (β-C). Again these alloys can also be heat treated in order to obtain increased strength of up to 1380MPa, in certain cases, or to better fracture toughness [17]. The alloy Ti 10-2-3 can be welded however due to the poor ductility and toughness associated with plasma and tungsten inert gas welding then other forms, such as electron beam welding, are advised [32]. It has found extensive use on the Boeing 777, replacing the maraging steel on the main landing gear leading to a significant weight saving and also alleviated the stress corrosion cracking associated with the steel [33].

The metastable β alloys Ti-15-3 is also used on the Bowing 777 but used for the environmental control system and ducting replacing CP titanium and saving over 60kg in weight in the process [33]. Certain engine manufacturers also use Ti 15-3 for brackets where the lower temperature allows for them.

In general, β alloys have very good fabricability properties and as solution treatment is usually done above the β transus then processing to obtain the correct microstructure does not to be as closely controlled as with α and α/β alloys as a result of this. β alloys are worked to acquire a fine recrystallised microstructure with the exception to this being Ti 10-2-3 which is solution treated below the β transus and therefore retains

some of the microstructural effects of any previous working history [34]. Research on β alloys has shown that the processing steps for the fabrication of component made from these alloys needs to be more carefully controlled than previously thought [35].

Although the aerospace sector is driven by performance of a material rather than its cost, in the long term the expensive production of titanium and its alloys will need to be addressed. As performance starts to reach its peak then cost will soon become a more predominant factor and therefore there remains the risk of competing materials replacing existing titanium components However with more industries now looking to utilise titanium there is a greater possibility of future sustainability succeeding.

2.2.7 Environmental Effects on Titanium

The High reactivity of titanium has been discussed already in regard to the extraction and production of titanium. Although small amounts of oxygen can improve the strength of CP titanium, there is a limit to this, beyond which the mechanical properties are significantly reduced via embrittlement. With oxygen being one of the main alpha stabilisers it can lead to the formation of what is called alpha case, named as such due to it being a continuous layer of alpha, on the outer layers of titanium. The effects of the alpha case lead to the presence of surface cracks which then leads to low ductility or crack nucleation sites. The reactivity that titanium has with oxygen and nitrogen is one of the limiting factors when considering the temperature capabilities for titanium alloys. As a result, the upper temperature range of titanium alloys is approximately 550^0C, alloy dependant. This is because of the diffusion rates are low enough at this temperature that little to no effect is seen on the bulk material. The additions of certain alloying elements, such as Al and Cr, can help reduce the rate of oxidation. This is achieved by forming a more thermally stable Al_2O_3 (alumina) oxide [7]. It is due to the increased volume fraction of Al_2O_3 that titanium aluminides have increased resistivity to oxidation and hence potentially higher temperature capabilities. The increased oxidation resistance from titanium alloys such as γ-TiAl can be used as surface coatings for other titanium alloys in order to increase the temperature capabilities whilst still maintaining high specific strengths and fracture toughness. When processing titanium the alpha case is usually removed prior to service to avoid the detrimental effects described previously. There are a number of ways in which this

can be done by machining or via other mechanical/chemical processes. Typical amounts of material removal required is dependent on the extent of the enriched oxide layer which is linked to the exposure time and temperature. For example, for an exposure time of up to 4 hours at temperatures of between 594^0C – 648^0C then at least 0.008mm (8μm) would need to be removed from the surface. Whereas for exposure times of between 1 and 2 hours at temperatures of 872^0C-898^0C then at least 0.089mm (89μm) would need to be removed [10].

Other elements that can cause detrimental effects include nitrogen which has a much lower diffusion rate than oxygen and therefore does not present as much of a serious contamination risk than oxygen. Other gases such as CO_2, CO and Hydrogen are also cause issues for titanium alloys at elevated temperatures, for example during heat treatment processes. Also, chlorides can significantly impact upon stress corrosion cracking properties and therefore care is required when handling titanium alloys during any form of processing which requires elevated temperatures.

2.3 Metallic Powder

The difficulties in processing and machining titanium are well known and therefore significant work has gone into the development of net shape and near net shape technologies which rely heavily on the use of titanium in the form of fine powder. These technologies allow for the production of parts which require vastly reduced processing and yet still have similar mechanical properties. The key near net shape powder metallurgy techniques include Pre-alloyed (PA), Blended Elemental (BE) and Metal Injection Moulding (MIM). These techniques involve the use of powder or sponge fines with alloying elements in order to produce nearly fully dense volumes of alloyed titanium. Techniques such as MIM have been developed from plastic injection moulding which utilises powder and a polymer binder to produce parts however for titanium these binders need to be removed during a post processing heat treatment stage. The drawback with this is the introduction of Carbon or reactions between the binder and base material. This results in parts which would not have sufficient properties to be used in aerospace application however can be used where certain required properties are not as high. These techniques are sometimes combined with Hot Isostatic Pressing (HIP) in order to allow for full, or nearly full, densification and therefore increase mechanical properties.

2.3.1 Powder Morphology

When considering the morphology of metallic powder, the manufacturing process is vital in determining the key geometrical properties of the powder. With the development of near net shape technologies there is an increased focus on quality and cost of processes and the powder manufacturing process is no different. The elevated costs of metallic powder arise from the low yields that have historically been achievable however with increased demand this cost is slowly decreasing. The critical characteristics associated with powders is size distribution, flowability, powder shape and chemical compositions, which would typically match that of the required alloy however oxygen concentration is also an important consideration. The oxygen concentration for powders is generally to be inversely proportional to powder size, therefore smaller powders have a high concentration of oxygen than larger powders [36]. Near Net Shape (NNS) technologies require high quality of powder to produce parts that meet stringent requirement therefore properties such as flowability, particle size and sphericity. The flowability of metallic powders is affected by features such as powder size and shape as well as environmental effects and friction properties between powders. For good flowability of powder then larger and more spherical powders are more favourable.

There are a number of techniques involved in the production of titanium powders which focus around atomisation or plasma spheroidisation. Although there are numerous methods of manufacture of powders, for this project only the following processes are considered; Gas atomised and Plasma Rotating Electrode Powder. The principles of the two processes rely on solidification of molten metal into powder which is manufactured under an inert atmosphere such as high purity Argon in order to keep oxygen concentrations low, from 100-500ppm.

Surface oxidation is also a key consideration in the use of powders, not just for virgin powder but also for recycled powder. As powder ages and is recycled for reuse the oxygen concentration can increase. Research has shown that for Ti-64 powder the surface of the powders develops a thicker surface oxide with increasing number of recycles [37].

2.3.1.1 Gas Atomised (GA)

For the Gas Atomised process, the feedstock of metal, which is already alloyed to the required composition, is melted, usually under an inert atmosphere, and then forced through a nozzle. This is then broken up using a high velocity inert gas such as argon and then this solidifies in the form of powder. The morphology of the manufactured powder is generally spherical however this process does produce asymmetric and satellite particles of powder. These satellite particles are smaller in size to the powder and are usually attached to the surface of a larger powder particle. They form as a result of extremely fine powder being blown back towards partially solidified formed powder and collide as a result of the circulation of gas within the chamber.

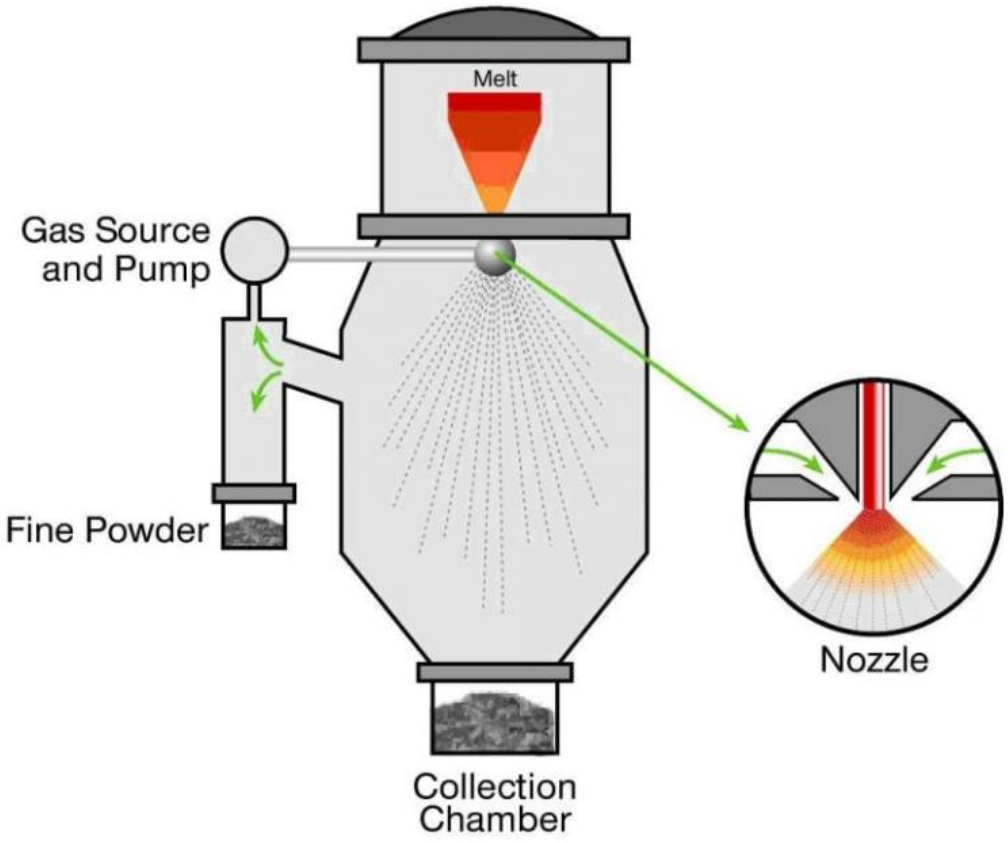

Figure 2.3.1.1 Diagram displaying the method of manufacture for Gas Atomised powder

This type of powder production can create large quantities of powder as well as large powder size distributions, from 20 to 500µm. Due to the large distributions of the powder it is not uncommon for the powder to be sieved in order to create a powder stock of a desired powder size range depending on application. Due to the cost of this

process, in comparison to other methods of powder production, it is extensively used for metals such Nickels and titanium alloys for example. Gas porosity can also be a factor in the production of GA powder due to the use of a high pressure gas during the production process and can therefore significantly affect the resultant properties, especially fatigue, of the powder and/or samples that are created from the powder stock.

2.3.1.2 Plasma Rotating Electrode Powder (PREP)

This form of manufacture for metallic powders relies on a rotating feedstock of alloyed metal. This feedstock acts as the electrode which is then melted from the arc from a tungsten cathode. As with other processes, the molten metal solidifies as a powder during flight and is then collected. This process relies on the spinning of the feedstock which enables the powder to be spun off using centrifugal forces. The advantage of the PREP process, over the of the GA process, is the production of powders that are extremely spherical in nature and have high purity. The presence of satellite particles is drastically reduced as due to centrifugal forces the chances of fine and coarse powder colliding are extremely low. The powder size distribution of the produced powder in PREP is also significantly closer than that of Gas Atomised powder. As well as powder size distribution the purity of PREP powder is higher than that of GA powder as there is no contact with other metals or ceramics prior to melting. As discussed earlier in the chapter the size of the particles also means that the impurity concentration, in the form of oxygen, is reduced owing to the generally larger powder sizes. Another key advantage for PREP powder is the reduced likelihood of gas porosity as this method relies on physical forces rather than high velocity gases.

The PREP process produces powders that are, however, generally coarser than that of GA process with typical powder sizes of between 50-350μm [36]. This does mean that the powder size of the PREP process makes it generally impractical for certain manufacturing technologies such as SLM or EBM applications. Other disadvantages include the rotating speed of the feedstock which directly impacts the resultant powder size as well as the cost of the starting material.

As with stock material alloys, the microstructure of powders is also an important consideration. For example, for Ti-64 PREP powder, the as manufactured powder can typically exhibit a fully martensitic microstructure. This can of course change with

further post processing, in the form of HIP for example. This post process can result in the original changing to an equiaxed regions and lath like microstructure, depending on the HIP conditions [38]. The properties of HIPed Ti-64 powder samples can have the same, if not better, as ingot samples.

2.4 Joining and Repair

2.4.1 Introduction

This chapter will discuss the various methods of joining and repair technologies that are currently being used by the aerospace industry and further afield. The aerospace sector has a desire to manufacture more reliable, lighter, more powerful and hence more efficient engines to continually reduce emissions and offer a more sustainable future. Various technologies and designs from not only within the engine but also from a point of view of logistics have allowed significant progress to be made.

The joining of materials has become one of these technologies that it has seen large growth in terms of perfecting existing methods as well as designing new techniques. Joining methods have meant that manufacturers are no longer limited by the geometries of more conventional processing techniques such as casting and forging. This allows designers the further flexibility to produce components with increased complexity and therefore further exploit any benefits that can be had.

Benefits include optimising the design of components to tailor it to specific loading directions which can mean a reduction in the amount of material needed to provide the strength, therefore reducing weight. Also the engine efficiency is heavily reliant on the airflow through the intake and the rest of the engine, to maximise the energy extraction where needed, and therefore producing blades which have an aerofoil optimised for its interaction with the air flow is crucial [39]. An example of this design optimisation using joining techniques is the use of Wide Chord Fan Blades (WCFB) designed by Rolls-Royce plc. They are manufactured utilising a combination of diffusion bonding as well as superplastic forming to produce a blade that is hollow for weight reduction and yet has the strength properties required for service. The process involves fusing three sheets of titanium using diffusion bonding and in a clean environment. After this argon gas is used to inflate the two outer sheets, in

temperatures of 1000^0C, which causes the middle sheet to stretch and through careful control of this process the middle sheet can be made into the required pattern [40]. When considering that, depending on the engine, the fan blades produce up to 80% of an engines thrust for high bypass turbofan engines then it shows that joining techniques are proving crucial in the quest for improved performance, proven by how Rolls-Royce have over 60 patents just for the diffusion bonding stage for WCFB. Other forms of diffusion bonding for titanium has also involved the joining of different metals. For example, bonding between Ti-64 and a stainless steel (18Cr10Ni) using a nickel interlayer have been investigated [41]. The main purpose of this is to combine the high specific strength and erosion properties of the two metal types. The complications of joining dissimilar metals arises through the formation of complex phases which can significantly impact mechanical properties. In this study the use if a nickel interlayer was used to relieve the hard and brittle phases TiFe, $TiFe_2$, and TiC [41]. As well as nickel interlayers other metals have also been used for diffusion bonding of dissimilar alloys [42][43].

Other examples of joining techniques include the use of friction welding to join dissimilar materials in order to meet the changing properties through a single component using the properties of more than one alloy. The ability to successfully join materials has proven critical during the design phases of a new components, or set of components, however there also relevant field that has benefited greatly. The use of nickel is not the only example of where an interlayer is required in an attempt to alleviate certain phases or properties. With regard to dissimilar metal joining, research has also been trialled with use of a Copper interlayer when welding Titanium with a stainless steel and the results of which showed that the welds with the highest heat input resulted in the best tensile properties [44].

The repair of certain engine parts has become a vital field in the life cycle of an engine. As many materials, and design of components, reach their optimal limit the focus then turns to how to increase the longevity of an engine. After all there is significant cost incurred in replacing a whole engine against a single part and therefore manufacturers are looking into how to implement in-service repairs to avoid scrapping an engine due to damage that can potentially be repaired. This has meant that the maintenance, repair and overhaul segments (MRO) of engine manufacturers have become an ever important part in the life cycle of in service engines. Also, the introduction of new

technologies into an engine rely heavily on whether there is a cost-effective route of salvage and repair in order to try and guarantee a minimum lifespan. An unavoidable consequence of this extra requirement has meant an increase in the amount of time for a new technology to be implemented, however by doing this there is a net benefit in the long term of increased engine life.

As with anything there are always challenges that must be met in order for any joining technique to be considered a useful or reliable method of joining and/or repair. With almost of the techniques that are currently being utilised, or being considered as potential ideas for the future, they must all ensure that a joined or bonded component has near parent properties. This means that a repaired blade for example must have the same, or very similar, mechanical properties as an undamaged designed component. This results in careful control of all aspects of joining methods to alleviate any defects and inherent problems that may be associated with each technique. When considering components fabricated from titanium then it is crucial to take into account its reactivity with nitrogen, hydrogen and oxygen which can result in vastly inferior mechanical properties and therefore must be avoided [45][46]. Therefore, when considering the joining method then isolating the bond to the atmosphere is vital in preventing oxidation from occurring for example. Alongside this any surfaces for joining must be clean of dust, moisture and other particulates that may have an adverse effect on the join by introducing defects and stress concentration features. For some welding techniques the method of cleaning involves acetone degreasing and wire brushing or in some cases the use of alkali clean and acid etching processes.

Although joining techniques such as adhesives and fasteners are successful in other areas it is still the use of welding that the aerospace industry utilises which is because of the success achieved with this type of technique. With the range of titanium alloys available and therefore considerable changes in welding behaviour of each type of alloy, there needs to be a variety of adaptable processes available that can then be used for a range of applications [47]. The following section looks into the range of applications of welding which includes methods which operate both at relatively high and low temperatures, an important factor when joining materials. Within the aerospace sector there has traditionally been two types of joining techniques available. Solid-state joining, where the process occurs below the melting temperature of the

material, and fusion techniques which operate through the melting and re-solidification of the material and therefore is done at elevated temperatures.

2.4.2 Solid State Joining

The previous chapter looked into fusion based welding process that rely on reaching temperatures close to or above the melting temperature of the material being joining. This has meant that most of the techniques sometimes require a post processing heat treatment to reset any microstructural changes that may have occurred during the join. Therefore, the aim of solid state joining is to produce a bond of equal or better properties than fusion based processes and this is done by keeping the temperature during bonding well below the melting temperature of the material and rely on a combination of temperature, time and pressure and this then allows for the diffusion of atoms across the surfaces of two regions of materials to be joined. The effect of joining in the solid state means any metallurgical changes that occur during the melting and solidification stages, seen in fusion based processes, are avoided here, potentially resulting in defect free joints and potentially increased mechanical properties. There is still however a melt zone during solid state welding processes but extrude beyond what is required and therefore can be machined to leave a solid state join.

As with most joining technologies there are still challenges that need to be faced with different technologies and certain criteria that need to be filled in order for the process to be of use. For example, the joining surface for any of the solid state joining techniques need to be extremely clean to avoid the built up of particulates that can have an adverse effect on the properties of any bonded material through increased porosity or defects. Also, as with fusion processes the threat of oxidation still remains and therefore great care must be taken in order to avoid or remove any oxide films/layers.

The following section will detail the main solid state joining techniques currently used within industry. Though they are classed as solid state joining processes, some can show evidence of liquation under certain process parameters.

2.4.2.1 Friction Welding, LFW & IFW.

For aerospace applications friction welding has become an important joining method and has resulted in key technologies being able to go into service on current engines to provide substantial benefits in engine performance. Friction welding involves the

coalescence of material by applying a sliding motion between the two regions of material to provide heat via friction. Throughout the process there is pressure exerted and once the required temperature has been reached the motion of the parts stop. After this the force is increased to ensure coalescence of the material ensure a high quality join is completed. Friction welding can sometimes be referred to as self-cleaning due to the automatic removal of surface contaminations and oxides in the form of flash at the end of a joining cycle [48]. One common use of this technique is the production of BLISKS by friction welding the aerofoils to the disk and in essence producing a single component, removing the need for strengthening structures and hence reducing weight [49].

There are many variants of friction welding, but all apply the same principle. Variants include Linear Friction Welding (LFW), Inertia Friction Welding (IFW), stir welding and friction taper stitch welding, with LFW and IFW being the most widely used types. Both LFW and IFW have enabled the joining of high temperatures alloys hence enabling more complex geometries to be manufactured as well as producing high integrity repairs for damaged components. These techniques have been developed so that the parameters, such as pressure and time, produce welds with optimum properties depending on the welded alloy. As with other joining techniques the stages involve the initial contact of the joined material followed by the creation of further pressure and temperature by various means, for example rotational or linear, resulting in an interface with little to no voids and grain migration across the interface.

However a common problem with friction welding is the development of residual stresses within the joined part and can significantly decrease the overall mechanical properties [48]. Previous work has shown that joints via friction welding of similar material can achieve tensile strength values close to that of as received material [50][51]. Investigations have also been done on the successful joining via friction welding of dissimilar joins using interlayers [52]. The results of these studies show that joins are possible however these joins can produce intermetallic compounds from the use of metallic interlayers at the bond interface which can have a significant impact on hardness within the HAZ [53][54][55].

2.4.2.2 Diffusion Bonding

Diffusion bonding has been used extensively across a wide range of industries from hollow fan blades in the gas turbine engine to electrical and optical components. It involves the diffusion of atoms across the bond interface in the solid state via an applied pressure allowing the interatomic spacing to reduce. The process involves six general stages as shown in Figure 2.4.2.1 [56]. As with most joining techniques the first stage involves bringing the two surfaces into contact. The surface roughness and

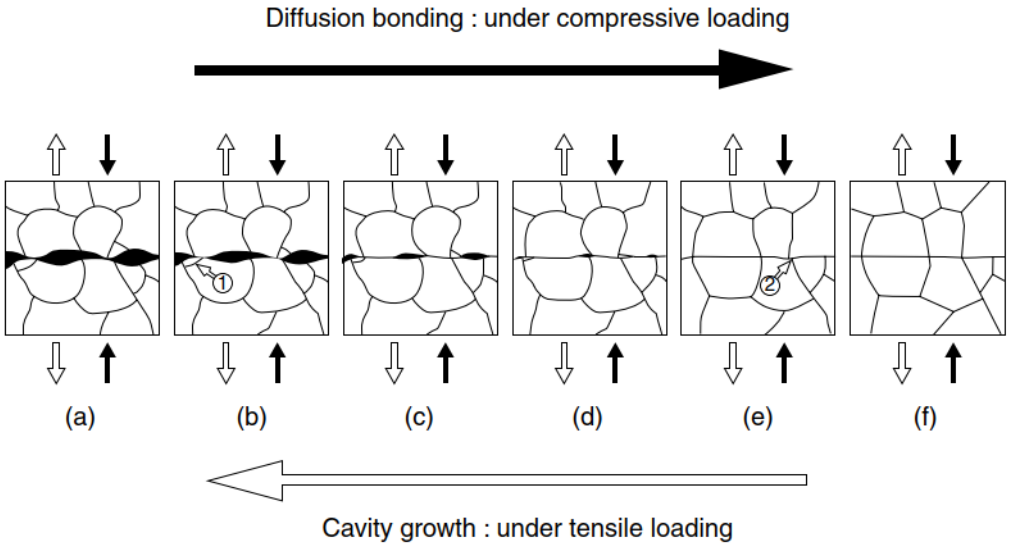

Figure 2.4.2.1 (a-f) Schematic view of the formation mechanism of the diffusion bonding process.

general surface condition of the two surfaces to be joined can impact on the amount of the initial contact. Generally, the higher the surface roughness the longer the bonding time and the higher the pressure that is required in order to form a sufficient bond. Immediately after initial contact the surfaces of the interface regions are plastically deformed without deformation on the macroscopic scale. During this stage the voids form between the two surfaces with any gas from the process trapped in these regions. After this the temperature is increased at which point the surfaces of the voids start to absorb the gases with the oxides present in these regions decomposing above 400^0C and diffused into the bulk. After this the voids begin to shrink as a result of diffusional creep with grain boundary migration starting to occur, Figure 2.4.2.1d. The fifth stage is made up of the final collapse of the remaining smaller voids until finally the process results in an interface which exhibits no clear evidence of the two surfaces and no difference between the grain boundaries [56].

Another important factor is the requirement of elevated temperature which aids the interdiffusion of atoms across the interface and is typically between 50%-70% of the melting temperature of the most fusible metal in the composition and therefore no liquid phase is present [57]. As the process relies on diffusion of atoms in the solid state there is little not metallurgical discontinuity which results in properties at the interface being similar if not the same as the base material [56]. A key aspect of this technique is the joining of material without the use of filler material as in other joining techniques such as brazing and therefore removing the formation of any potential intermetallic compounds.

As with most joining processes for titanium alloys the three key parameters include bonding temperature, holding time and bonding pressure. The importance of temperature is related to the diffusivity of atoms across the bond interface and so therefore crucial in determining the rate at which the porosity at the bond interface collapse.

One of the key advantages of diffusion bonding is the ability to produce a joint with little to no residual stress development, especially when compared with fusion welding techniques. It's success in joining titanium alloys has meant it has been used extensively in the joining of titanium to form lightweight, hollow fan blades via superplastic forming and diffusion bonding in modern gas turbine engines [58][59][60]. As well as reduced residual stresses another advantage compared with other high temperature joining processes is the reduced distortion during bonding. This benefit arises from the typically lower pressures however as a consequence of this the time element of diffusion bonding is extended in order to allow for the reduction in the remaining pores, after the initial collapse. Typical values for diffusion bonding vary depending on alloy type with typical value between 875ºC and 925ºC for Ti-64 although adjusting these temperature is also possible by altering the other key factors of holding time and bonding pressure.

An example of diffusion bonding in industry is through SuperPlastic Forming of Fan blades which involves the joining of thin sheet metal in order to produce a complex structural component. This technology has utilised the effects of diffusion bonding in order to produce larger engine components with increased focus on larger bypass ratio engine designs. The advantages of this process are linked to the ability to produce

relatively complex structures removing the need for additional welds and rivets thereby reducing weight etc. The disadvantages of the process is the relatively high cost and lead time in comparison to certain welding techniques for examples. Also, the downstream post processing in order to remove the alpha case which forms during bonding and this relies on a chemical milling stage as well as tight environmental controls.

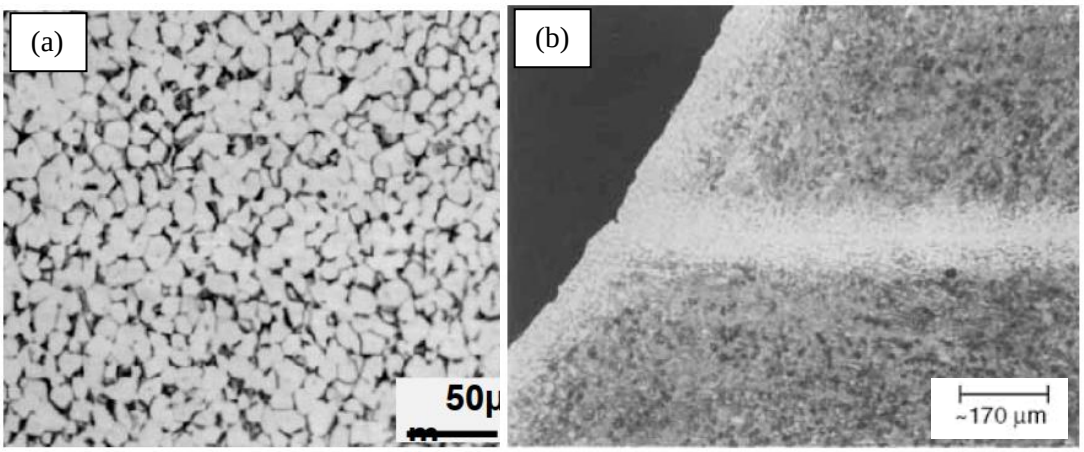

Figure 2.4.2.2 Microstructure of diffusion bonded Ti-6Al-4V (a) via the Superplastic forming (SPF) process [7] (b) Ti-6Al-4V plate diffusion bonded at 925ºC.

Under the correct conditions it is possible to generate high integrity joins for titanium alloys using the SPF method of diffusion bonding. An example of a bond interface for Ti-6Al-4V is shown in Figure 2.4.2.2a which shows that under the correct conditions of Time, Temperature and pressure it is possible to produce bonds which show no sign of the prior bond location. The bondline also shows how the diffusion bonding technique can reduce microstructural changes with the retention of the equiaxed α+β microstructure still visible in Figure 2.4.2.2a. The application of SPF can be used for large components, such as wing boxes for military aircraft, however the surface quality of the joining faces is critical with surface flatness and finish being important factors in order to ensure a high integrity bond.

As with many high temperature joining technologies there have been developments in the potential application of dissimilar alloy joining via diffusion bonding. Typical applications of diffusion bonding dissimilar alloys include CP titanium and austenitic stainless steel as well as titanium to aluminium alloys. Joining dissimilar alloys such as stainless steels and CP titanium finds application within the nuclear industry within vessels and reactors. Complications arise with conventional joining of dissimilar

alloys in terms of the intermetallic that forms at the bond interface which significantly increases the embrittlement and therefore reducing mechanical properties. Diffusion bonding can, under certain conditions, provide high integrity joins and yet avoid the formation of the intermetallic elements within the bond interface. Studies have also shown that atmospheric conditions are considerable factors when producing diffusion bonds, especially for titanium alloys, as shown in Figure 2.4.2.2b which shows that at high temperatures, unless under high vacuum levels or inert environments, high levels of oxidation of the outside and bonding faces can occur. The white band across the microstructure in Figure 2.4.2.2b shows the bond interface contamination in the form of alpha case which has arisen due to the elevated temperature required for bonding.

The reliance on high quality surface finishes and high quality control on bonding environments results in an increase in the cost and complexity of this joining technique.

2.4.2.3 Hot Isostatic Pressing (HIP)

The term Hot Isostatic Pressing refers to the process of densification of, typically, near net shape components produced via alloyed powder, through the application elevated temperature and pressure. The HIP process can accommodate large components, limited by the size of the vessel, schematic shown in Figure 2.4.2.3, and also improve the mechanical performance of parts by reducing the microporosity within parts through diffusion and creep mechanisms. Due to the elevated temperature associated with the process an inert gas is used which is also used to increase the pressure on the material. The pressure is achieved by a combination of compressors and increasing the temperature of the gas and as the HIP vessel acts as a fixed volume then as the temperature increases so too does the pressure in line with the ideal gas law. Typical values for the pressures can be in excess of 100MPa and temperatures typically above solution heating temperatures for nickel superalloys. The term ‘Isostatic’ refers to the pressure being applied by the inert gas and evenly in all directions. The basic method of improving the densification, of parts or partly sintered material, is through the reduction of the surface of the pores and therefore the surface energy [61]. The high pressure enables the hot inert gas, usually argon gas, to collide with the surface of the material at very high velocities in all directions. Densification of components made from partially sintered powder can be done on parts manufactured from Selective Laser Sintering method or from powder that is placed in an envelope in the net shape

required. In this manner the envelope along with the powder will shrink from the initial size due to the isostatic pressure however the shrinkage would be even in all directions due to the reasons mentioned. Potential advantages to the HIP process is the ability to improve the densification of material and thereby improving not only specific mechanical properties but also improving the average result of the mechanical properties through the reduction of scatter [62]. Typically, for high temperature alloys for instance, heat treating the material at high temperatures can result in significant grain growth. The growth of the grains within a material at elevated temperature is due to the diffusion of impurities or precipitates which act to pin dislocations at the higher temperatures.

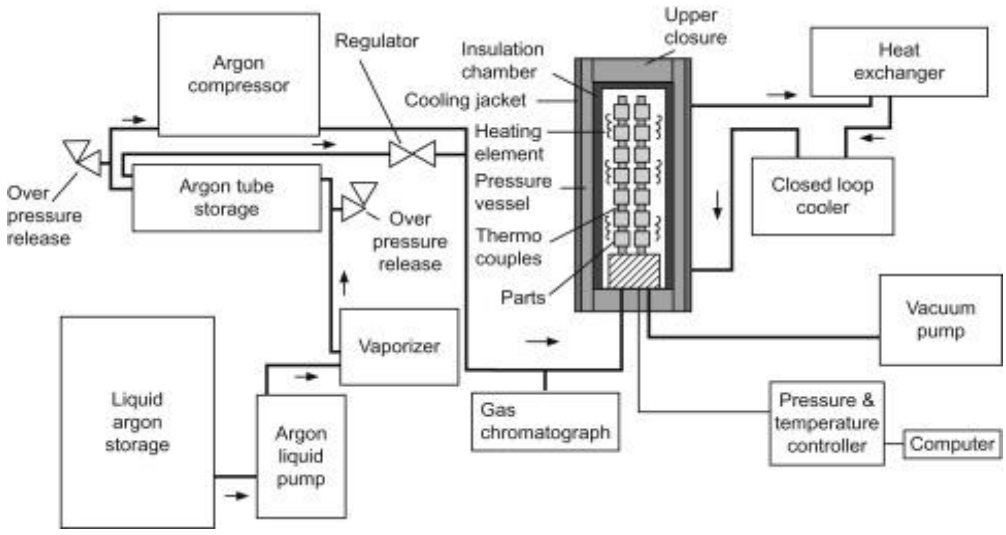

Figure 2.4.2.3 Schematic showing the typical layout of a HIP vessel [62].

The densification during HIP is similar to the sintering mechanisms which rely primarily on only temperature, however with the introduction of pressure the mechanisms are changed slightly. As discussed in diffusion bonding the mechanisms of sintering are split into a number of different stages, with the initial compaction of pores to a point where eventually grain boundary migration occurs leaving spherical pores. With the addition of elevated pressure within the HIP process allows for improved control of the grain growth as a result of the temperature. Typical processes that rely heavily on just the temperature for sintering can find it challenging to avoid excessive grain growth. Within the HIP process the significantly high pressure values

overcome the opposing pressures associated with the gas pores within a body of material and therefore the pore would dissolve into the matrix [61].

The disadvantages of the HIP process mainly stems from the high cost of the process. This is due to the significantly high pressures involved which therefore requires high pressure vessels. The systems therefore require a high safety standard due the various elements involved in the procedure. As well the cost there also technical challenges associate with the HIP process. For example, although the aim of the process is to reduce porosity there is possibility for thermally induced porosity to occur during any subsequent heat treatment phase. Therefore, the parameters of Temperature, Pressure and Time need to be carefully controlled depending on the alloy type to ensure the correct densification and therefore properties are achieved. As well as the technical and safety challenges associated with HIP there is also the practical considerations in industry as it is very difficult to HIP large volumes of parts and therefore it is not practical for high volume production parts. For these reasons the HIP process is mainly utilised within the aerospace and nuclear sector where achieving high mechanical properties for challenging alloys is one of the key considerations.

2.4.2.4 Upset Welding

The terms ‘Upset welding’ relates to a form of welding which utilises pressure and electrical resistance heating in order to bond between two pieces of material. Although it is referred to as a welding process it is a solid state joining process unlike many other typical welding methods. The process involves contacting two pieces of material and then applying an electrical current through the joint area which acts as a resistor and thereby increasing the temperature via the principles of Joule Heat, a schematic

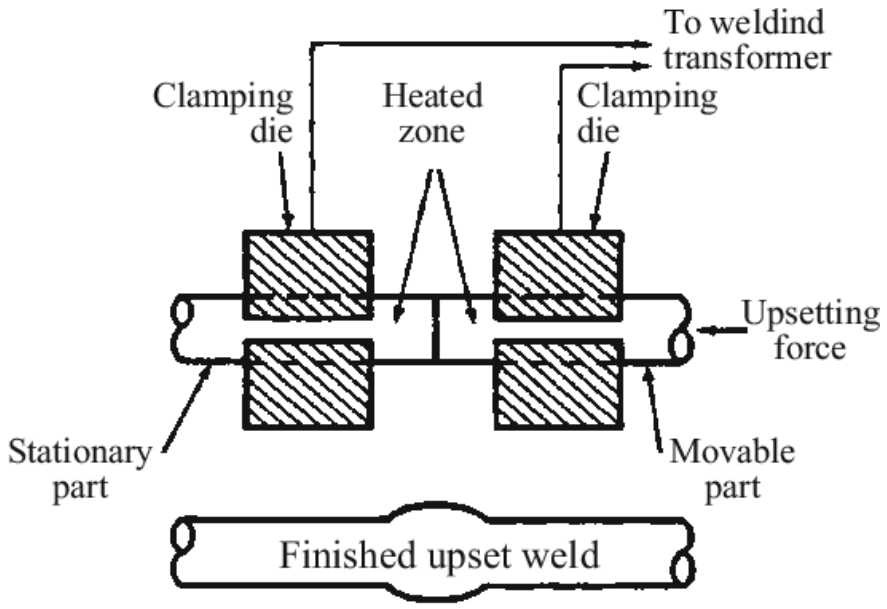

Figure 2.4.2.4 Schematic of a typical layout for an upset welding process.

of a typical setup is shown in Figure 2.4.2.4 [63]. Increasing the current would result in increased resistance at the joint and therefore this would correspond to a rise in the temperature at the interface. The pressure is typically applied before the heating occurs and remains during the bonding process. As with many joining process, including welding diffusion bonding processes, upset welding relies on the elevated temperature and pressure in order to produce coalescence of material. The 'upset' refers to the plastically deformed region at the bond interface which forms due to the elevated temperature and pressure. The key parameters that effect the success of upset welds is the electric current, time and pressure where the electrical current is a factor in determining the temperature at the weld interface. As well as these key parameters there are other variables that can also have a significant impact on the weld success. For example, sample preparation is vital as any surface contaminants can have a significant impact on bondline defects [64].

As discussed with previous joining techniques in order to produce a low porous then elevated temperature is one of the key factors in ensuring this can be achieved. However, this adds a potential drawback of significant microstructural changes within the HAZ and FZ which impacts on the mechanical properties of joined material. With upset welding remaining a solid state joining process then the effects of microstructural changes are reduced. Other advantages of the upset welding process include no weld splatter and relatively simple equipment setup in comparison to some

welding techniques which rely on large rotating components [65]. Some of the other important aspects that need consideration in order to produce a high integrity join is the control of the electrical resistance as with this heating method the heating rates can accelerate rapidly, especially for smaller specimens. Also, part alignment is important as any misalignment can be exaggerated during the bonding process, particularly are high pressures.

Although the process is applicable for a wide range of alloys there are certain alloys that in order to produce the required application specific microstructure and hence mechanical properties then post processing heat treatment stages would be required. Many alloys that have been successfully bonded using the upset welding technique include stainless steels, nickel superalloys and aluminium alloys [65]. As well as similar alloying joining, studies have been conducted on joining dissimilar alloys. For example, a study was conducted which involved the joining of martensitic stainless steel to duplex stainless steel [63]. It showed that by increasing the welding current it resulted in localised 'hotspots' and thereby reducing the tensile properties of the joins with fracture occurring in the HAZ. This showed that carefully monitoring the key parameters is vital in ensuring a high integrity join, with little to no inclusions is created.

Studies have shown that creating resistance butt welds for Ti-6Al-4V can be achieved through the correct combination of Time, Temperature and Pressure. The macro and micro images shown in Figure 2.4.2.5(a)(b) show the possibility of producing low porosity bonds under the given conditions. Despite the reduced pressure in the bond shown in Figure 2.4.2.5(a), plastic deformation is still clearly visible due to the elevated temperature and time. As well as the high integrity join observed in the images above,

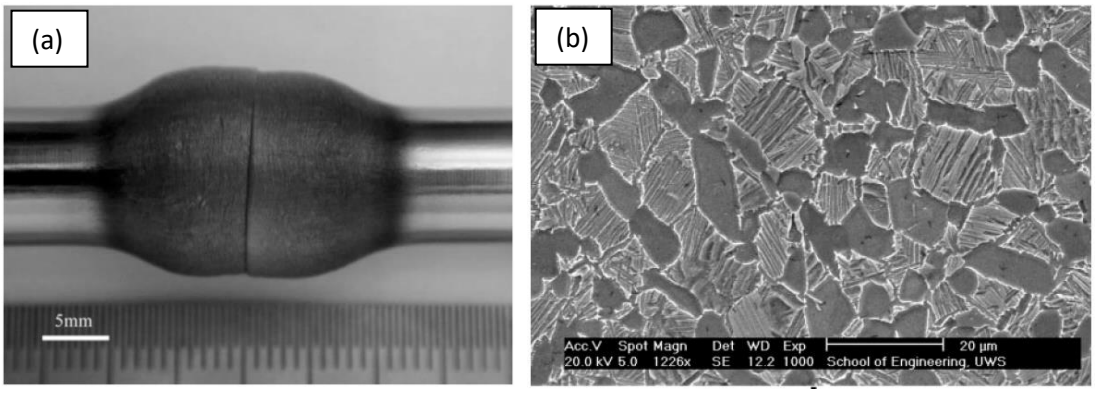

Figure 2.4.2.5 Upset bonded Ti-6Al-4V at 950C, 1800s and 19MPa with (a) showing the macroscopic deformation and (b) showing the bond line microstructure [66].

the importance of the bonding environment is also critical in order to reduce the oxidation and in turn improve bond integrity. The optimised conditions in the study showed that due to the elevated temperature there was an increase in the volume fraction of the transformed β phase, with the bonding temperature being close to the β_T for this alloy [66]. As well as the combination of the bonding parameters being critical in determining the bond integrity, as with other bonding techniques, the welding environment is also important in this case. The image in Figure 2.4.2.6 was done under a vacuum of 7×10^{-2} mbar and even still there was oxidation present on the bond interface, showing the importance of inert or high vacuum environments in order to create high integrity joins for titanium alloys. The process of upset welding is reliant on increasing the temperature via electric resistance heating which is similar to the procedure used for previous Powder Interlayer Bonding studies using a Gleeble thermomechanical simulator. The key difference is the use of the powder interlayer however many of the fundamental aspects are similar. The creation of localised hotspots in temperature could be more common with the use of a powder interlayer with the cavities between the powders having an increased localised resistance and therefore temperature.

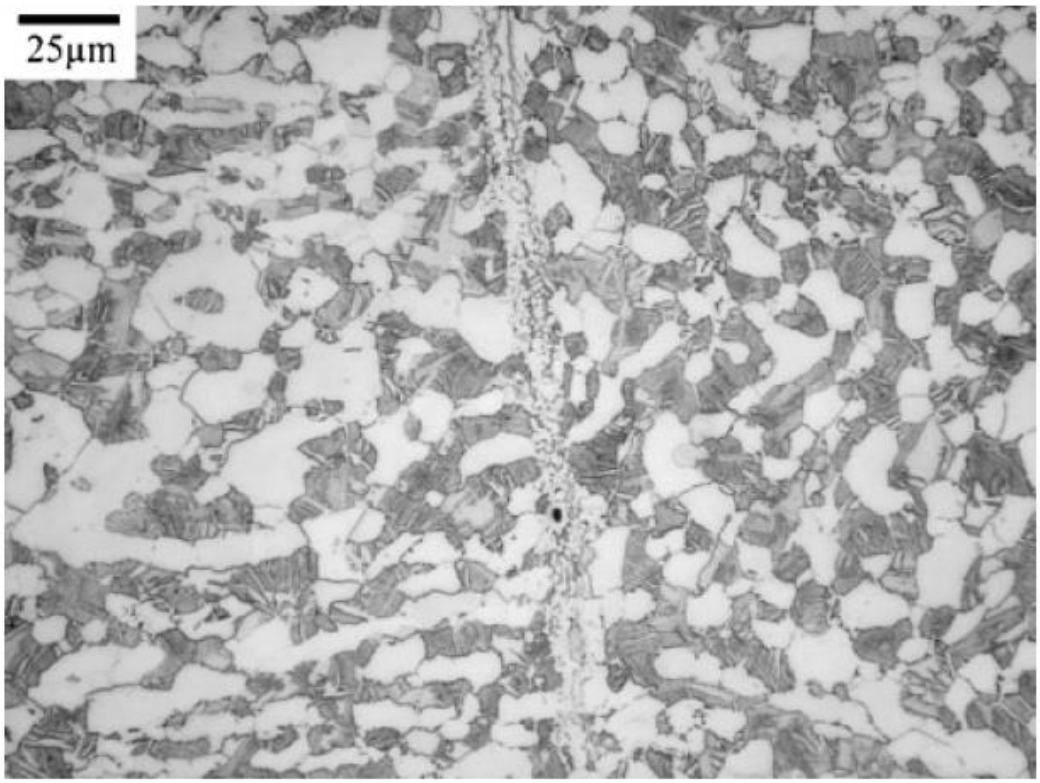

Figure 2.4.2.6 Microstructure of Upset Welded Ti-6Al-4V at 950C, 30s, and 38MPa [66].

2.4.2.5 Powder Interlayer Bonding (PIB)

The case for solid state joining and repair has been made in the previous chapters and details benefits such as reduced residual stresses, lower intermetallic compound formation and reduction in the amount of post process heat treatments required. As a result of combining the high integrity bonds via solid state joining and retaining the flexibility to join complex geometries at a relatively low cost has resulted in early work being done in validating the interlayer bonding technique. More specifically validating the use of a metallic powder based interlayer which is the same as the material to be joined has attracted more attention in recent years due to the potential to produce high integrity bonds with achieved mechanical properties only slightly reduced when compared with as received material [1]. This technique removes the requirement for a smooth surface finish of the faying surfaces as the powder based interlayer acts as a filler material and reduces the asperities between the two surfaces.

The heating method associated with this technique has mainly focused on Electric Current Activated/Assisted Sintering (ECAS) which utilises an electric current passing through the joining specimens, and via the joule effect, provide localised heating to where there is the greatest amount of resistance to this electric current flow [67]. As a consequence of combining a powder interlayer and this heating method the localised heating will occur in the disparities between the powder particles, further aiding the collapse and sintering of the powder interlayer. The conventional method for this process involves applying a constant temperature and force for a fixed period of time, sufficient enough for the powder interlayer to plastically collapse and sinter, resulting in low porous, or pore free, bond region and reduced residual stress development. Previous work for PIB as focused on high temperature metallic alloys such as Nickel Super alloys and Titanium alloys, with previous work focusing on vacuum chambers being used to minimise the oxidation of these alloys at bonding temperatures [1].

Work done by J. Forsdike focused primarily on the joining of Ti-6246 utilising the interlayer bonding method. This project worked through the optimisation of the bonding parameters for Ti-6246 using a Gleeble 1500 thermo-mechanical simulator in order to achieve this. The 5 parameters investigated in this study included Load (kN), Time (mins), Temperature (^{0}C), Interlayer Thickness (μm) and mean powder size (μm). These parameters determine the resultant bond line integrity and strongly

determine the resultant porosity and also microstructural changes throughout the HAZ. The first part of the study involved the use of a Design of Experiments (DOE) test matrix in order to assess the effects of the bonding parameters on sample porosity. The resultant 'optimised bonds' created via the DOE were then mechanically tested to further characterise the bonds. Further work was then conducted on the feasibility of joining IN718 and trialling a join on an aerofoil shaped component.

The results of the study showed the possible success in producing a high integrity bond of Ti-6246 using similarly alloyed powder as an interlayer. Each bond was then characterised by analysing the resultant porosity for each set of parameters with the best performing bond giving a total porosity area of 68.81μm^2 and the worst performing having an area of 29822.44μm^2. The plastic deformation also seen for each join varied depending on the parameters with the greatest upset resulting in an increase of 56% compared with the original diameter of the test specimens. During the analysis of the porosity of the optimised bonds it was found that the distribution of pores was concentrated mainly in the upset regions of the bonds and with the vast majority off the pores having a diameter of less than 4.3μm. Therefore, it can be said that the total porosity is made up of a larger number of smaller pores rather than a small collection of larger pores.

The mechanical testing of the optimised bonding conditions gave varied results when comparing it to the as received material. The low cycle (LCF) fatigue performance of bonded Ti-6246 from Forsdikes work showed that for the higher stress regime tests, greater than 950MPa, the cycles to failure for the bonded samples were the same, and in some cases, exceeded the performance of the as received material. The fatigue tests done on bonded Ti-6246 samples at 950MPa and below showed significantly reduced cycles to failure when compared with the as received material. In some cases, the performance of these lower stress fatigue tests were approximately two orders of magnitude lower than the parent material. The fracture surface analysis on these fatigue tests showed little clear indication as to what caused the sub surface initiations with potential causes for some of the tests being lack of fusion and large pores present within the bond region. The fatigue specimens which fractured in the area of the bond line showed more planar fracture surfaces whereas the tests which failed away from the centre of the gauge exhibited a more undulating fracture surface.

The high cycle fatigue (HCF) tests showed that sub surface features such as large pores and/or inclusions act as crack initiation points and therefore impact fatigue life. Out of the three HCF tests the initiation feature for one of the tests was attributed to a large pore of approximately 26μm with the other two tests showing signs of non-fusion defects as a cause for the crack initiation, with sizes of 32μm and 41μm.

The research done during this time showed that powder interlayer bonding can provide high integrity repairs in a laboratory setting. The mechanical testing of these joins showed potential promise in the interlayer bonding method being used for repairs of highly critical components.

2.4.3 Heat Affect Zones (HAZ)

With the many different technologies available for joining and described in previous chapters there is a common feature related to almost all. The Heat Affected Zone (HAZ) defines the area of material located in the vicinity of a weld or bondline in which the original microstructures, and hence mechanical properties, are altered due to the joining process.

Elevated temperature is a vital parameter for a joining technique however this additional energy results in various forms of changes within a material, microstructurally and/or chemically for example. Leading on from the joining techniques discussed previously the HAZ created as a result of these processes can drastically reduce the mechanical properties of the parts, particularly at the join interface. For nickel based superalloys, various welding techniques can result in the formation of a liquid based film on HAZ grain boundaries. This film is unable to accommodate any large amounts of thermally or mechanically induced stresses, which arise during cooling. As a consequence of this there can be significant decohesion between the solid to liquid grain boundary interfaces leading to what is known as liquation cracking or hot cracking [68]. The formation of liquation cracking is dependent on the parameters during joining and there is still much debate as to whether liquation occurs for many nickel based superalloys and whether certain friction based joining techniques can be classed as solid state joining.

The thickness of HAZ in joined materials can range drastically and is dependent on numerous process parameters such as peak temperature, time at temperature and pressure. As well as process conditions there additional factors that arise from material

properties, for example material type. Nickel based superalloys would have different HAZ as with compared with titanium alloys. The heat input during joining defines the HAZ size with a faster heating process, and therefore faster cooling rates, results in smaller HAZ than for lower heat input processes.

To combat the negative effects from microstructural and phase formations within HAZ there are numerous processes that can be used to alleviate poor performance at the bond interface. This can include pre and post weld heat treatments (PWHT). Preheating prior to welding has shown to improve properties in comparison to as welded material for certain alloys. As well as preheating, post weld heat treatments can also be implemented with a similar purpose of improving properties around the interface region. The parameters for the PWHT depend on the alloy type and the requirements of the joined material, typically the PWHT can involve a solution treatment followed by ageing steps. As discussed previously for titanium alloys such as Ti-6246 the PWHT can significantly improve mechanical properties for welded samples however there can be a trade off with a decrease in other properties, such as elongation for example. The typical HAZ for a titanium sample welded via processes such as LFW or EBW can exhibit similarities with regard to microstructure. For Ti-6246 welds the HAZ can be complex and can exhibit different microstructures at various points as well as being split by a dynamically recrystallized region.

2.5 Induction Heating

Induction heating is a technology that utilises the properties of electrically conductive materials in order to increase the temperature. It is a non-contact method of heating and can be used on ferromagnetic and conductive materials. This form of heating works by producing an alternating electromagnetic field from an alternating current traveling through copper coils. The alternating electromagnetic field penetrates the material to be heated and produces eddy currents as a result. The effect of the eddy current is heating of the material due to material resistivity against the eddy currents and therefore heating via the Joule effect. The induced currents within the workpiece would have the same frequency as the current within the inductor however their direction is opposite to that of the current within the inductor [69]. The theory of

induction heating and alternating magnetic fields is shown in Figure 2.4.3.1 below which displays the distribution of a typical magnetic field for a simple circular inductor design [70].

If a workpiece is then placed within the inductor it would cut through the magnetic fields and create eddy currents within the workpiece. The distribution of the magnetic field for different shape inductors can be complicated and hard to predict, therefore

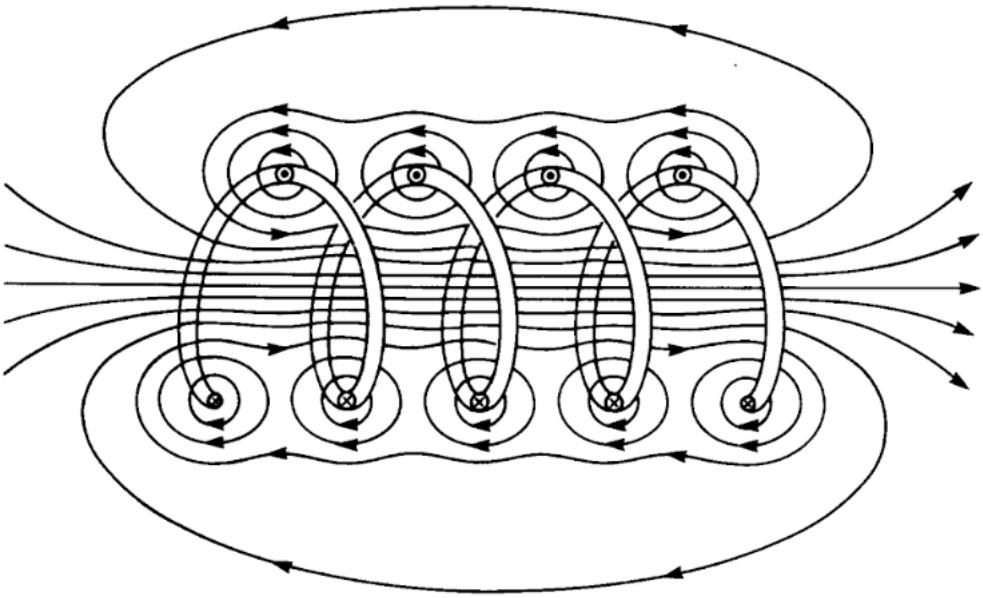

Figure 2.4.3.1 A Schematic showing the distribution of a magnetic field due to an alternating current (ac) passing through an inductor [69].

through continuous research and trials of different designs a greater understanding can be achieved in magnetic field distribution. From the schematic it can be seen how the magnetic field extends beyond that of the inside of the inductor. Therefore, eddy currents would also be induced in any electrically conductive material within close proximity of the inductor and therefore the temperature within these materials would increase. The design of the inductor can therefore have a significant effect on not only temperature capabilities but also uniform heating as well as increased efficiency which is why coil design is one of the key aspects for induction heating. Due to the nature of induction heating it is very difficult to produce uniform heating within a workpiece and this can be for a variety of phenomena which include skin effect, proximity effect, and the ring effect [69].

A typical setup of an induction heating system would include an alternating current power supply, an induction coil, and a workpiece to be heated [70]. The heating can be altered by adjusting the shape and design of the copper coil. For example, increasing the number of turns in a conventional circular coil can increase the heating rate and maximum temperature achievable. Although the workpiece may reach elevated temperatures via the induction heating technique, the induction coil would remain at low temperatures due to continuous water flowing the copper piping. The part to be heated can also be situated in varying environment conditions and still be heated, for example in surrounded by a gaseous environment or within a vacuum.

The difficulties of using induction heating arises from the reliance of the coil design which determines the heating profile on the workpiece. Therefore, for geometries with non-uniform dimensions or features, it can be challenging to create a design of coil that can create a uniform heating profile as well as achieving other common high temperature capabilities such as peak temperature and heating rates.

2.5.1 Application of Induction Heating

The application of induction heating as increased in industries which rely heavily on elevated temperatures and temperature control of materials. Examples of industries would those involved in metalworking, welding, heat treating and melting.

Metalworking of metals such as Steels, Aluminium's, Titanium and Nickel based alloys is a common application for induction heating. It can be used to preheat the materials ready for forging and extrusion which typically are in the shape of round or square bar stock. It is useful in this category of industry due to the high heating rates that can be achieved on high volume bar stock as well as being able to selectively heat certain regions of materials prior to processing. The high heating rates and localised heating can therefore increase productivity with repeatable quality [69].

With the ability of increasing and control temperature in high strength metals the technology is used extensively in heat treating of alloys. A typical use is the surface and through hardening of steels which can lead to increased mechanical properties such as strength and fatigue properties. Further to heat treating induction heating can be used for joining technologies such as welding, soldering and brazing. The reason

Preheating prior to metalworking	Heat treating	Welding	Melting
Forging Gears Shafts Hand tools Ordnance **Extrusion** Structural members Shafts **Heading** Bolts Other fasteners **Rolling** Slab Sheet (can, appliance, and automotive industries)	**Surface Hardening, Tempering** Gears Shafts Valves Machine tools Hand tools **Through Hardening, Tempering** Structural members Spring steel Chain links **Annealing** Aluminum strip Steel strip	**Seam Welding** Oil-country tubular products Refrigeration tubing Line pipe	**Air Melting of Steels** Ingots Billets Castings **Vacuum Induction Melting** Ingots Billets Castings "Clean" steels Nickel-base superalloys Titanium alloys

Table 2.5.1 showing a range of applications for induction heating [69].

for this is due to the controlled and localised heating that can be achieved with induction heating which is crucial for the joining of parts such as welding of pipes products. Typically, these types of industries also rely heavily in increased efficiency and productivity as well as localised heating which is why induction heating can be more useful compared with other forms of heating. Other forms of induction heating being used for joining is in the curing of adhesives used in automotive parts such as clutch plates. This allows for quicker bonding times for these adhesives and also where adhesives are used for the joining dissimilar material types.

Another industry which is starting to see more use of induction heating is in the dairy industry. The non-contact form heating has the advantage in the food industry due to the avoidance of food contamination. It can be used to heat the iron base of cookware

to heat large quantities of food products at uniform and well controlled temperatures [71].

2.5.2 Advantages of Induction Heating

The impact of induction heating has had a considerable impact in improving industries that rely on heating of materials. These advantages have resulted in the technology being applied in some of the examples as detailed in the previous chapter. Although induction heating has its benefits over alternative forms of heating and for certain applications it is not a perfect process and therefore cannot replace other forms of heating for a range of different applications.

One of the key advantages of the technology stems from the high heating rates possible when compared with conventional forms of heating which rely on convection and radiation such as in furnaces. As well as this it is capable of producing uniform, well controlled heating for certain applications.

Aside from the direct benefits with regard to heating materials there are further advantages that can be obtained via induction heating in industry. Examples of this include reduced start up times. Traditional furnaces require the empty chamber to be heated up to the target temperature before material to be heated can be placed inside whereas for induction heating the workpiece and heating system need to be in place and the heating can be started and target temperature achieved much quicker. This also has a knock on effect on productivity of processing parts due to the decreased heating times required.

3 Experimental Procedures

For this study the purpose was to generate a process that would replicate the High Integrity Interlayer Joining process and allow preliminary ideas to be tested for potential application in industry. Once a process had been developed, various parameters of the technology could then be tested to understand their implications on various characteristics from microstructure to mechanical properties. The initial focus was on developing a system that allowed for the use of an inert atmosphere with the samples of material that were available. The development followed the route of utilising an inert atmosphere similar to that used in welding processes whereby a

shielding inert gas, such as argon, is produce an inert atmosphere around the bonding interface.

Various alloys were used in this study, including Ti-6246 and Ti6242. The material was provided in the form of blank cylindrical specimens supplied by Rolls-Royce plc. All specimens were in the form 10mm diameter, and 65mm length, cylindrical specimens with one end threaded, so as to provide a grip surface during testing, and one end finished to a specified surface roughness. As well as blank specimens, powder was also supplied by Rolls-Royce plc in the form of Gas Atomised Ti-6246, Ti-64 and Plasma Rotated Electrode Process powder for Ti-6246. Only a small amount of the PREP was available and therefore only a small number of bonds could be done. This meant the key characteristics that could be analysed were with regard to sectioning the bonded samples and analysed on the SEM.

The research conducted also involved the production of dissimilar bonds between the various titanium alloys however the extent of investigation on this topic was not as extensive as with Ti-6246 bonds due to limited material availability.

3.1 As Received Material

The material used in this study, both forged and powder, was provided by Rolls-Royce plc. The initial focus was on the joining of Ti-6246 with potential applications in BLISK repair viable for this type of titanium alloy. Other titanium alloys were also investigated and these included Ti-6242 and Ti-64. These alloys were used in order to do preliminary research on the study of dissimilar joining of titanium alloys using the High Integrity Interlayer Joining Technique.

3.1.1 Ti-6246

The main alloy used in this study centred on the Ti-6246 variant of this high strength α/β alloy. The as received material was in the form of 10mm cylindrical bars which were taken from a forging that had been β-forged, then solution treated for up to 2h at approximately 870ºC before being aged at approximately 600ºC for 8h. The typical microstructure of the as received material is in shown in Figure 3.1.1.1. The microstructure shown is typical for β forged Ti-6246 composing of prior β grains with an average grain size of ~300μm. Within these β grains are α lamellar with average width of just over 1μm as well as colonies of fine secondary α (α_s) platelets ranging from 50-200nm between the α_p lamellar.

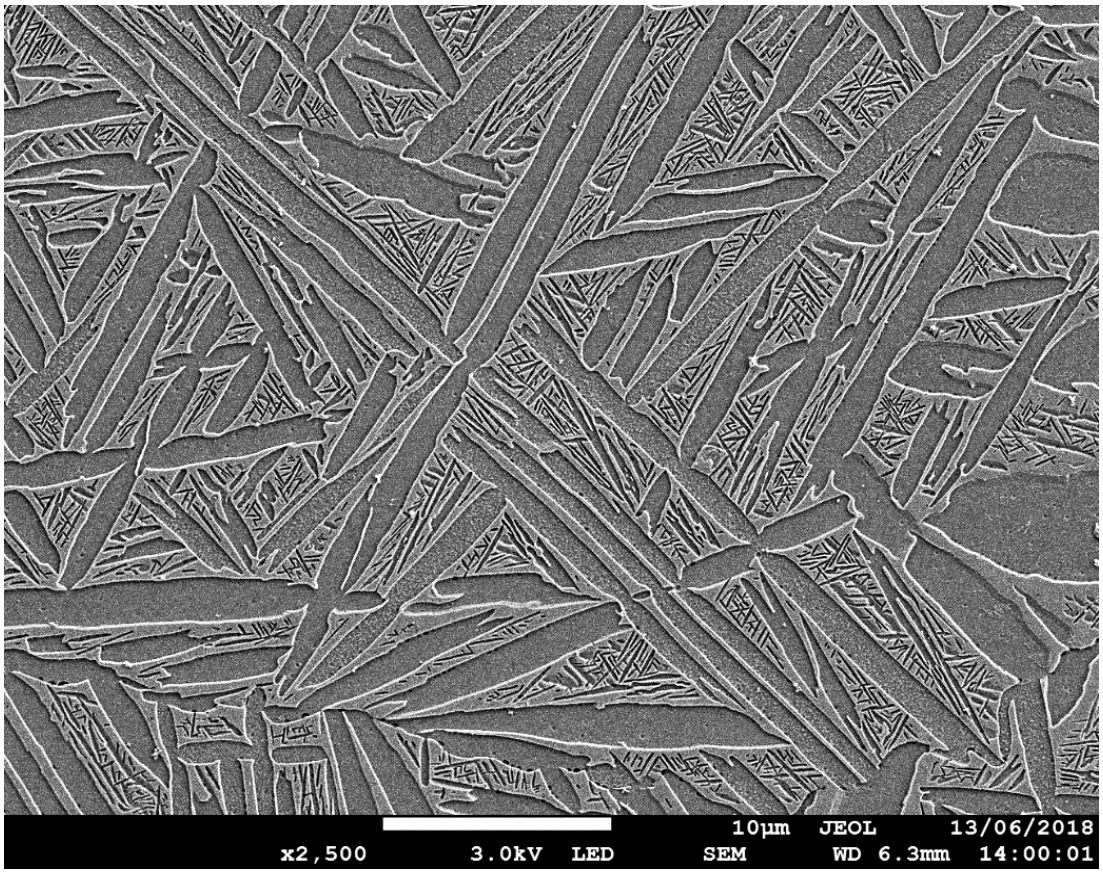

Figure 3.1.1.1 Microstructure of as received Ti-6246 showing both α_p and α_s (dark) and β phase (light)

The bonded samples were then subsequently machined into RLH10004 tensile samples for mechanical testing characterisation or sectioned in order to analyse the HAZ and bondline. High Cycle Fatigue specimens were also produced from bonded trials and machined into RLH8020 samples for testing.

3.1.1.1 Ti-6246 GA Powder

The powder used for the interlayer production was supplied by LPW Technology Ltd with powder particles having a stated diameter of between 15µm and 45µm. Figure 3.1.1.2 shows the size distribution of the powder with a wide range of powder sizes as well as the satellite particles that are common for this type of powder. As described in previous chapters the size and shape of GA powder is heavily reliant on the production process and therefore there's a high presence of elongated powders, with the spherical powders having a large size distribution. The powders were stored in an anti-fire chemical storage cabinet when not being used and were only used in small quantities when required. Care was also taken when handling the powder to ensure that the correct PPE was used and that there were no factors nearby that could ignite the powder.

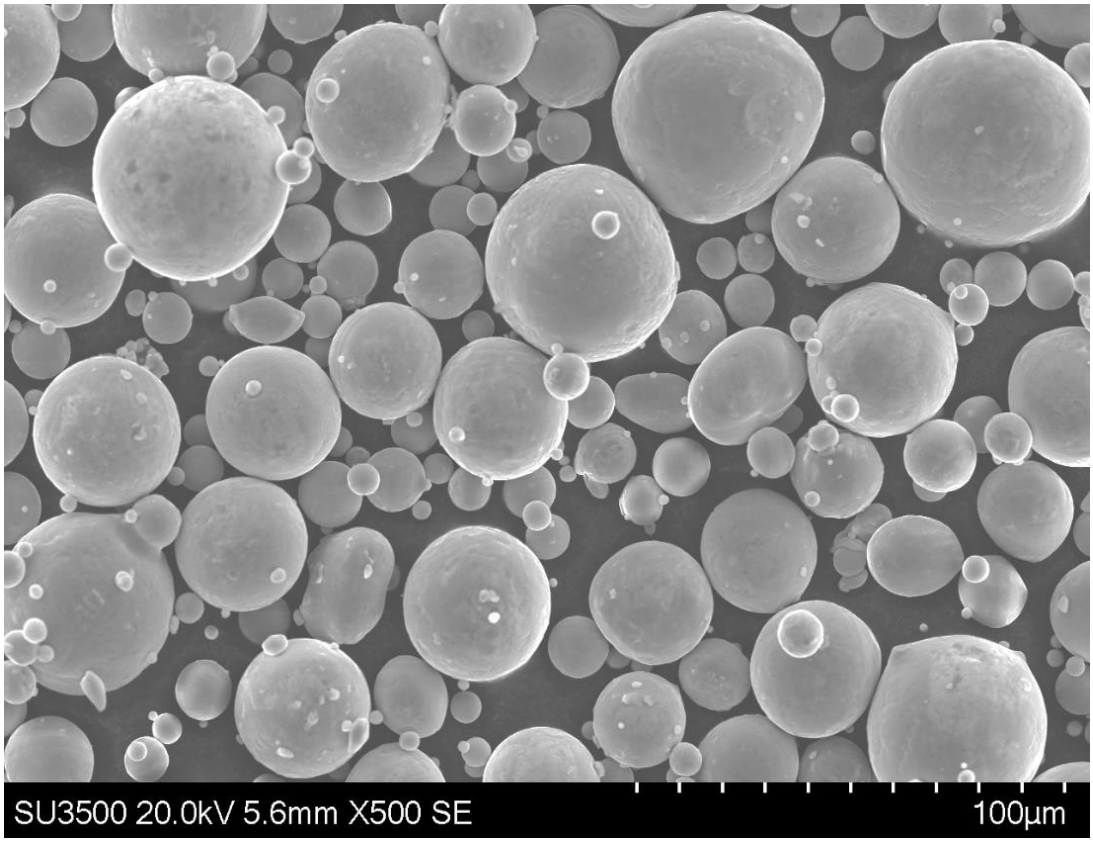

Figure 3.1.1.2 Image showing the GA Ti-6246 Powder

3.1.1.2 Ti-6246 PREP Powder

The second type of powder that was trialled as an interlayer was the PREP powder, shown in Figure 3.1.1.3, supplied by Rolls-Royce plc. The chemistry closely matched that of the forged samples and the powder sizes ranged from 45µm to 60µm. The PREP powders are more spherical and have a narrower size distribution than that of the GA powder with fewer satellite particles also present in the powder batch. The preparation of the interlayer followed the same process regardless of the type of powder, the only variable is the amount of powder used to start.

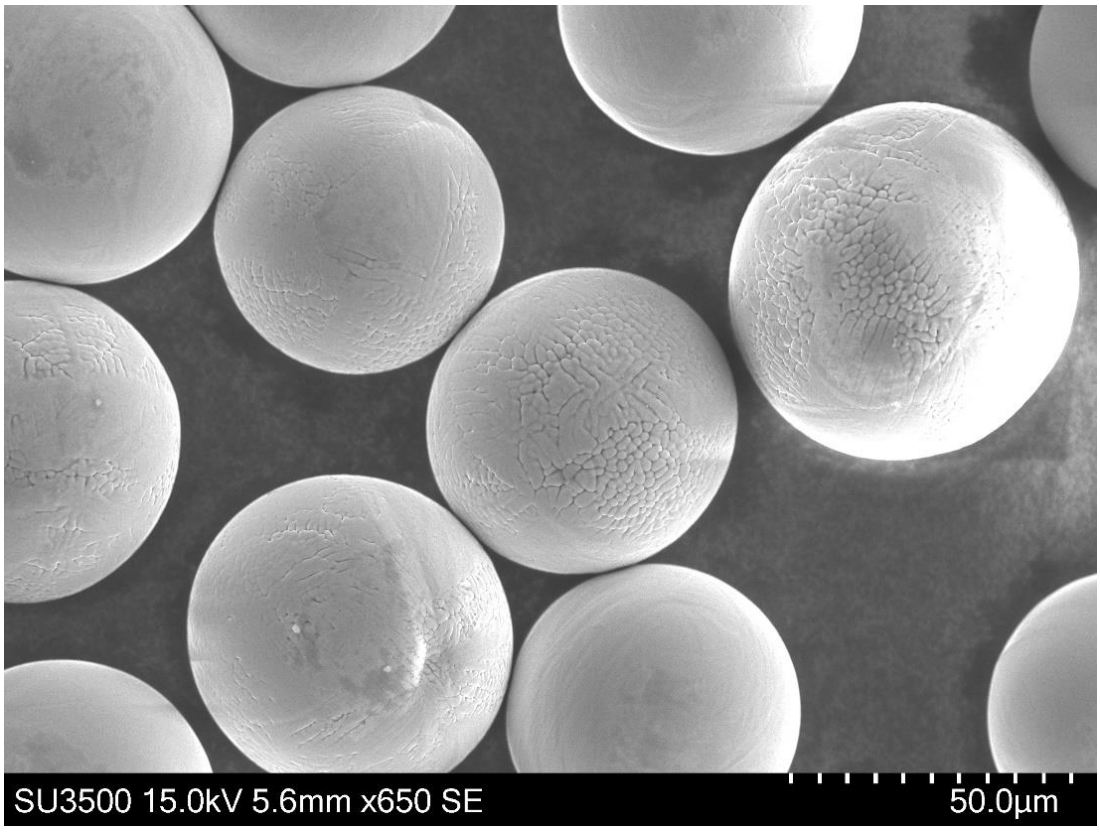

Figure 3.1.1.3: Image showing the Ti-6246 PREP powder

3.1.2 Ti-6242

The second type of Titanium alloy used in this study was a high strength, near alpha alloy, Titanium 6242, offering enhanced creep resistance properties and ductility in comparison to other titanium alloys, such as Ti-6246 and Ti-64. The material was supplied in 10mm cylindrical specimens with one end threaded same as the Ti-6246 samples.

The microstructure of the as received material shows the columnar α grains, shown as the darker phase on Figure 3.1.2.1, surrounded within the transformed β phase which has resulted from it being annealed in the α+β phase field. This α+β type of microstructure for Ti-6242 possesses good high temperature fatigue properties in comparison to the Widmanstatten or basket weave microstructure which can be formed by heat treating above the β transus of this alloy.

At elevated temperatures, approximately 550^0C, this, as well as other α/β alloys, start to oxidise rapidly which results in the formation of an oxide scale as well as an alpha case layer beneath this which significantly reduces mechanical properties. For

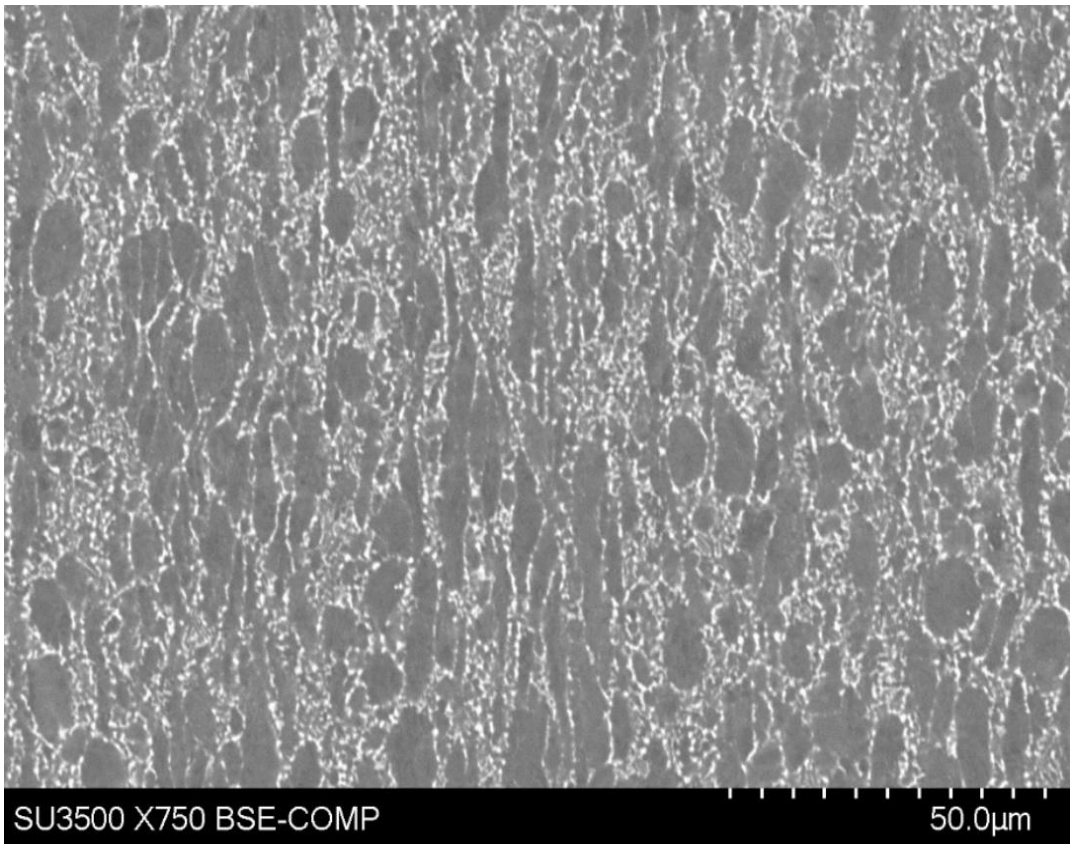

Figure 3.1.2.1 Microstructure of as received Ti-6242 showing the columnar alpha primary alpha phase within beta matrix

Interlayer bonds involving Ti-6242, an interlayer composed of Ti-6246 GA powder was used due to the lack of availability of Ti-6242 powder.

Table 3.1.1 below shows the chemical composition for this alloy in weight percentage. The composition if very similar for that of Ti-6246 however the key difference is the reduction in the amount of Molybdenum, from 6% to approximately 2%.

Table 3.1.1 showing the chemical composition of the near alpha alloy Ti-6242

Element	**Weight%**	
	Min.	Max.
Aluminium	5.5	6.5
Tin	1.8	2.2
Zirconium	3.6	4.4
Molybdenum	1.8	2.2
Silicon	0.06	0.13
Iron	-	0.25
Oxygen	-	0.15
Carbon	-	0.08
Nitrogen	-	0.05
Hydrogen	0.01	0.0125
Titanium	Remainder	

3.2 Powder Interlayer Bonding System

The primary experimental setup used in this study was developed in order to further the progress of Powder Interlayer Joining. The key areas of interest were on how to effectively heat the interlayer region to allow for powder collapse and sintering, and also how to maintain environmental control so as to provide an inert atmosphere for joining.

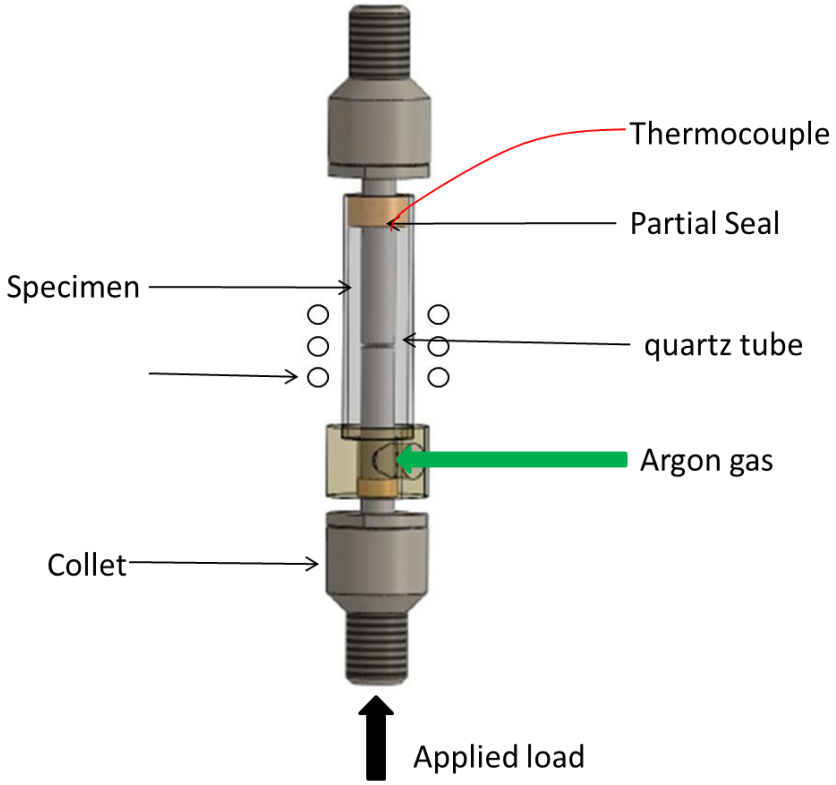

Figure 3.1.2.1 Schematic of the High Integrity Interlayer Joining System

The process that was developed was referred to as the High Integrity Interlayer Joining (PIB) setup and utilised induction heating for the temperature control during the bonding process. For the atmosphere control a continuous flow of argon was used to surround the elevated temperature regions of the bonded specimens in order to reduce the reaction with oxygen and avoid the formation of an extensive oxide layer. A schematic of the developed system is shown in Figure 3.1.2.1.

3.2.1 Induction Heating System

The induction heating system used was an Easyheat Induction heating system with a power of 2.4kW. Trials were conducted in order to determine which type of coil design would give the most consistent temperature readings as well as a design that would hold a region of no more than 1mm at the required bonding temperature. This was done so that only the interlayer and the interface of the specimens would be at elevated temperature to ensure minimal interference with the microstructure of the material. The temperature gradient across the bond region was analysed for a number of different coil designs. The type of coil that produced the narrowest temperature gradient across the bond region whilst still maintaining consistent temperature across the interface was chosen. The different designs of coils are shown in Figure 3.2.1.1a-c. They show the range in coil designs that were tested with some not able to reach the target temperature and some that, although produced the required temperature, showed a large variation in readings when measuring from one side of the specimen to the other. The selected coil, shown in Figure 3.2.1.1c, was chosen as it produced a very narrow temperature region as well as showing a variation of no more than +/-5ºC of the target temperature. The selected coil design could also reach high temperatures with the cylindrical specimens, up to approximately 1200^0C for titanium specimens, as well as achieving sufficiently high heating rates if required.

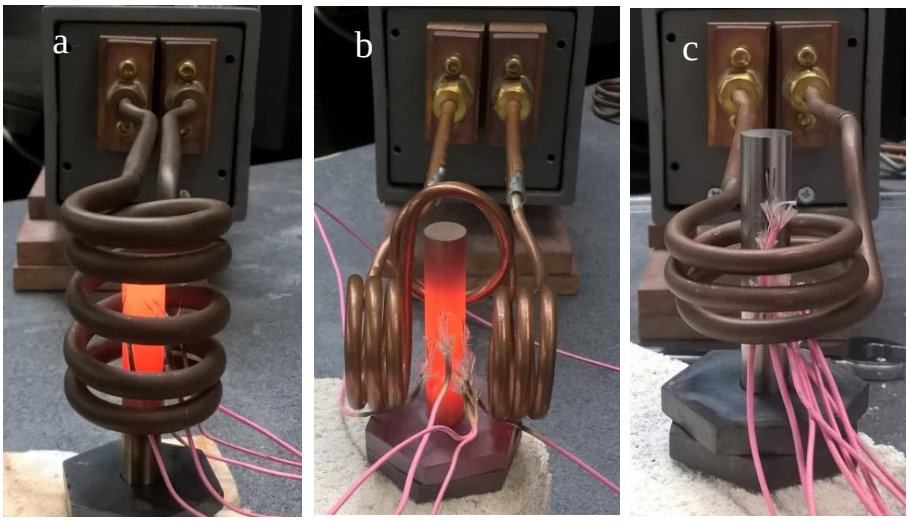

Figure 3.2.1.1(a-c) Images of the trials done with different coil designs.

The graphs below, Figure 3.2.1.2, Figure 3.2.1.3 and Figure 3.2.1.4, indicates the profiles and temperatures observed during a calibration test for different coil designs, shown in Figure 3.2.1.1a-c. It shows how certain designs allowed for a uniform heating profile whereas others might have had increased peak temperature capabilities but were more non-uniform in how they heated the samples. Each coil design was set to a target temperature of 930^0C for 15 minutes in order to establish the temperature variations for each coil design. The minimum, maximum and mean values have been recorded and plotted below.

The first design of induction coil is shown in Figure 3.2.1.2. This design shows to have good temperature capabilities as the power input of the induction heating system was

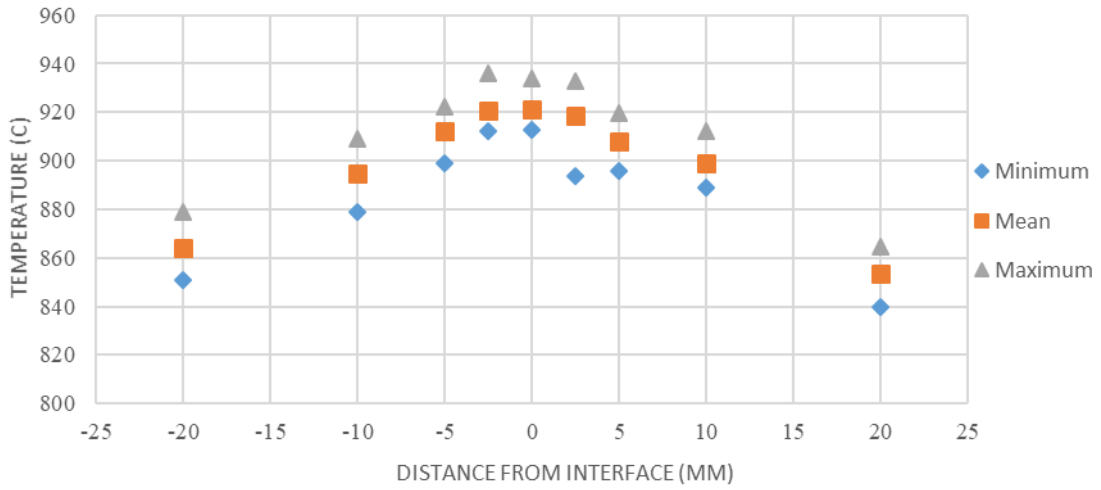

Figure 3.2.1.2 Chart showing the temperature profile for coil design 1

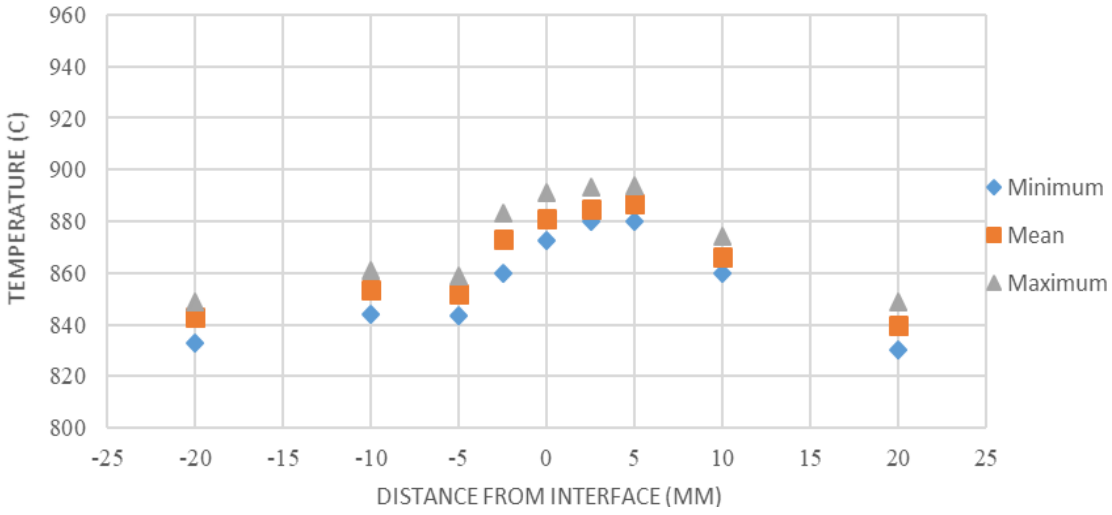

Figure 3.2.1.3 Graph showing the temperature profile for coil design 2

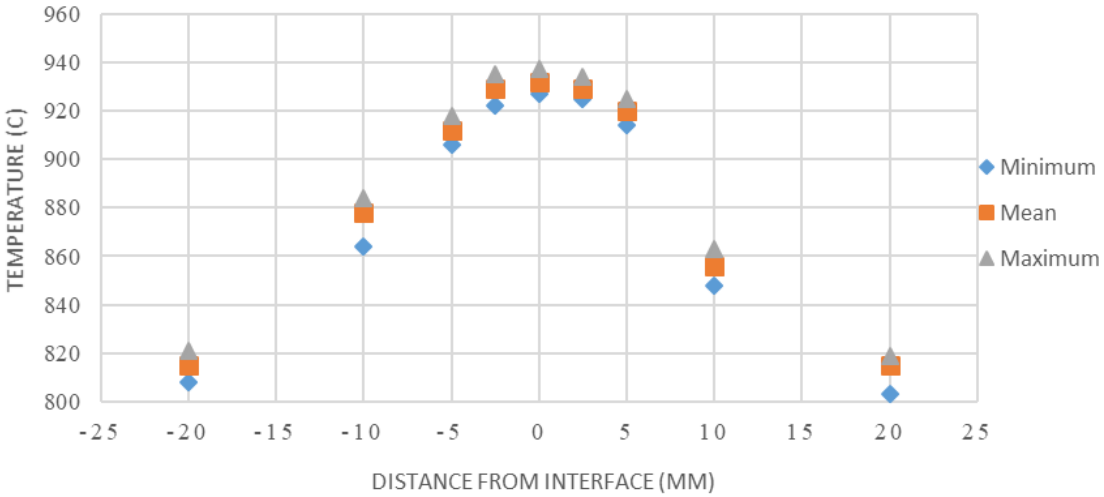

Figure 3.2.1.4 Graph showing the temperature profile for Coil design 3

lower than for any of the other design of coils in order to reach the target temperature of 930^{0}C. For this, as with the other design of coils, the temperature recorded was across a length of 40mm with the middle of the coil being in line with what would be the bond interface. The results shows there is a relatively large temperature spread in comparison to the other coil designs with only a 70^{0}C drop in temperature 20mm from the midpoint. By plotting the minimum, maximum and mean values of the test the temperature variation during the test can be observed. Although the power of the induction heating was kept the same, after the temperature had levelled, there is still temperature fluctuations of up to nearly 30^{0}C at 20mm from the interface for example.

The second coil design was of a different design philosophy which did not encapsulate the specimen to be heated. This type of design would significantly improve the setup of bonding trials as the coil can be removed without first removing the samples from the servohydraulic rig. However, from the graph it can be seen that the temperature capabilities are not sufficient for the bonding of high temperature alloys, with a maximum temperature of 894^{0}C achievable at the high power setting for the induction heating system. As well as not achieving the target temperature the profile is inconsistent across the specimen. There is an initial drop in temperature from the midpoint, however this is not the same on both sides. After the initial trial another test was done to improve the heating profile across the specimen, however it was not possible to achieve this. The profile also shows a large temperature profile with only a small drop in temperature across the 40mm length. At 20mm there is a 7.2% fall in the recorded temperature in comparison to a 10.25% reduction for coil design 1.

The final design of coil that was trialled had a similar design as coil 1 but with reduced number of rings. The profile for this coil was capable of achieving the target temperature with the induction heating system. The results also show a uniform heating profile with a narrow region, approximately 2mm which remains at 930^0C, and drop in temperature of 14.3% from the midpoint to 20mm. The variance from minimum to maximum is also reduced when compared with the previous coil designs. The results from the calibration tests showed that for maximum heating rate achieved for any design of coil was approximately ~10ºC. The results of the heating rate, and the peak temperature capabilities, are determined largely by the number of rings as well as the spacing between these rings. Increasing the number of rings resulted in an increased heating rate but a larger HAZ, whereas reducing the number of rings reduces the heating rate capability but can significantly reduce the HAZ. The location of the induction heating coil rings also effects the heating of the samples. As a result of the trials, coil design 3 was chosen for the optimisation tests for Ti-6246 with it providing a uniform and narrow temperature profile.

The results shown in Figure 3.2.1.5 show the comparison of the selected induction coil design for the PIB bonding trials alongside the temperature profile associated with samples used within the Gleeble Thermomechanical simulator which was used extensively in previous studies. The heating profile of the two heating systems is closely matched within 5mm from the bond interface with approximate decrease in temperatures of ~20ºC from the peak values for both the heating systems. Beyond this point the profiles diverge to a higher degree with the profile for the Gleeble system showing further decrease in temperature in comparison. For example, the temperature

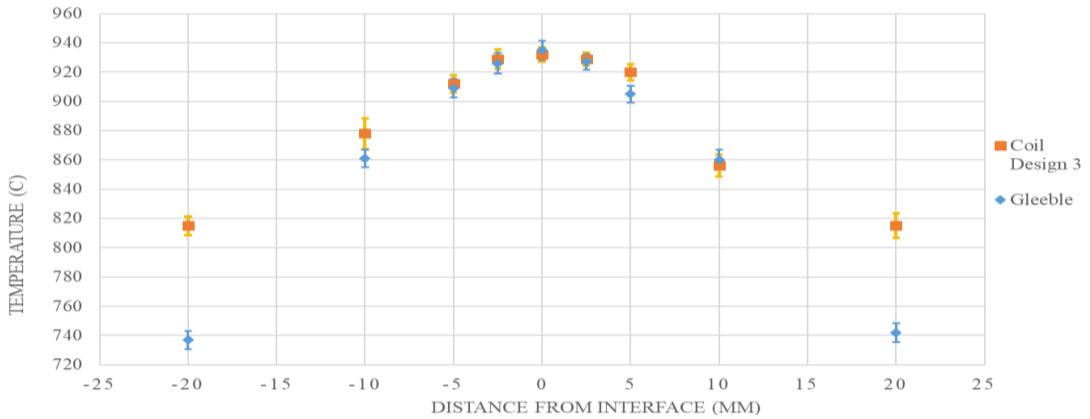

Figure 3.2.1.5 Chart showing the comparison of temperature profile with selected induction coil design as well as the trial done on the Gleeble 1500 system.

difference between the two systems at 10mm is ~20ºC whereas at 20mm this difference increases to ~80ºC. Although there was a significant difference in the profiles further from the bond interface the results showed that within the first 5mm of the HAZ the profiles followed a very similar pattern. The difference further from the bond interface can be explained by the difference in the two heating systems. The key difference being that the Gleeble Simulator makes use of water cooled copper grips which locate the bonding specimens. This acts to draw heat away from the bonding specimens thereby reducing the temperature gradient at a faster rate than with the uncooled samples used within the induction heating system.

3.2.2 Environmental Control

The second area of development for the PIB technique centred on the environmental aspect of the system. The chosen system utilises an argon shielding technique, similar to that seen in certain welding techniques. The aim is to prevent the reaction between the elevated temperature joining samples and, in particular, the oxygen in the surrounding environment. The use of argon allows for the purging of oxygen in the immediate vicinity of the high temperature bond region.

3.2.2.1 Oxidation Comparison

Previous studies have shown that joining Ti-6246 under high vacuum conditions produces strong results in terms of reduced oxidation and high bond integrity. However, in order to consider the evolution of the technology, and a possible alternative to creating a vacuum, then utilising a continuous gas flow to create the inert environment was trialled. Tests were done in order to understand the differences observed on the surface quality of joined parts that had been tested under vacuum and argon gas. A test was done using the PIB system developed as well as under vacuum using a Gleeble 1500 system, used in previous powder interlayer research studies. These tests then provided samples that could be used in order to compare the surface quality and oxidation.

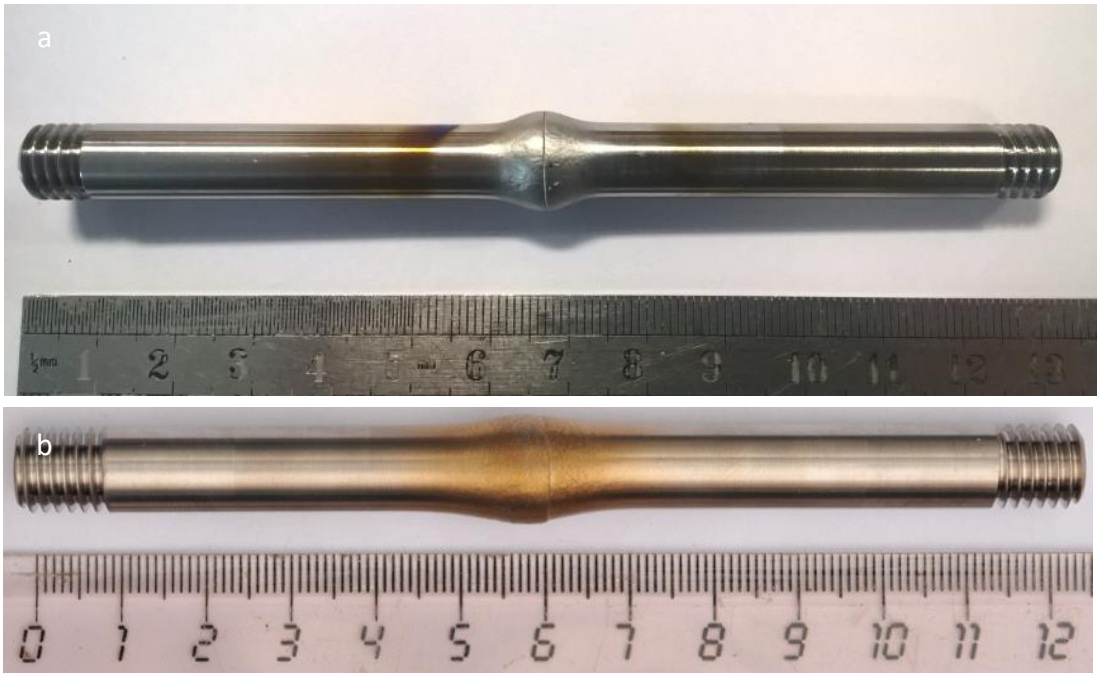

Figure 3.2.2.1: Images of Ti-6246 interlayer bonded under (a) argon shielding and (b) High vacuum

The results of the tests are shown in Figure 3.2.2.1, with Figure 3.2.2.1a showing the test done under argon and the Figure 3.2.2.1b showing the test done under vacuum, with a vacuum level of $1x10^{-5}$ mbar. The results show that from a visual inspection point of view the trials done under the PIB process show very little discolouration compared with those done under vacuum. The surface colour remains a grey/silver colour within the HAZ of the PIB bonds, with more discolouration observed at approximately 20mm from the bonding interface. The vacuum test shows a stronger bronze colour observable around the deformed area with reduced discolour beyond the HAZ.

When looking at the microstructures, at the surface edges, for each of the samples tested under the two different conditions some differences can be observed. For example, the vacuum bonding test sample showed increase surface oxidation when compared with the the traditional sample produced via PIB, seen in Figure 3.2.2.2a-b. The alpha case thickness for the samples bonded under the continuous flow system, within the PIB process, is very minimal and has a thickness of approximately 55µm, Figure 3.2.2.2b. With the vacuum tested sample the α case layer thickness observed within the HAZ had an approximate thickness of nearly 200µm, Figure 3.2.2.2a. For both samples the oxide thickness reduced further from the bondline relating to the reduced temperatures across the length of the specimens. The same trend is seen across

the entire length of the specimen under the same conditions, with the largest differences seen nearest the bond interface of the two samples.

This test was to understand the degrees of difference between the different system ideas and to help down select the chosen type of system that would be developed. The results showed that utilising a continuous flow of inert gas is more beneficial for reducing the thickness of the α case layer, at the elevated temperatures required for bonding, than compared to the vacuum system.

As well as in the bondline region, where the temperature is highest, there was evidence of oxidation on the surface of the as bonded sample under argon with blue and purple colours present. The evidence of the alpha case was not evident other than at the bond interface resulting from the lower temperature within these regions.

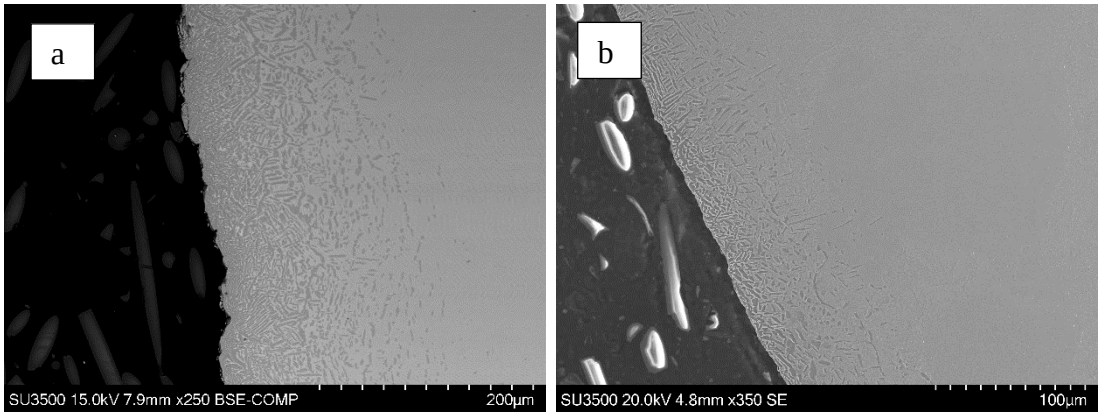

Figure 3.2.2.2 SEM images showing alpha case formation of test sample under (a) vacuum and (b) Argon gas.

3.2.3 Developed PIB System Overview

The completed PIB system was developed to be used alongside a Zwick Roell, servohydraulic mechanical test machine in order to apply the required stress through the samples during a bonding test as shown in Figure 3.2.3.1 below. Each specimen was loaded on the lower and upper platen via a threaded collet. The top specimen would have 2 thermocouples spot welded 1mm away from the bonding surface of the specimen. These would provide the temperature readings during bonding test. The top specimen was then threaded into the test frame until fully tight. The next step was to pass the bottom specimen, which had the prepared interlayer on the bonding surface, through the fixing for the argon intake and threaded to the bottom collet attached to the test frame. The alignment of the specimens was then conducted by loosening the lower platen, bringing the specimens close together, and then placing any spacers in the lower platen in order to provide the correct alignment. Once the alignment had been achieved the platen was tightened and lowered.

The final step was to place the quartz glass tube around the lower specimen and located on top of the argon intake fixing. The specimens were then brought back to together and a small force, 0.2kN, was applied in order to keep the specimens together ready for the start of the test. The lower fixing allowed for the argon to flow from a standard gas cylinder and, as the bottom of the fixing was sealed against the specimen, the argon flow was directed upwards towards the heated region. The flow of argon would then

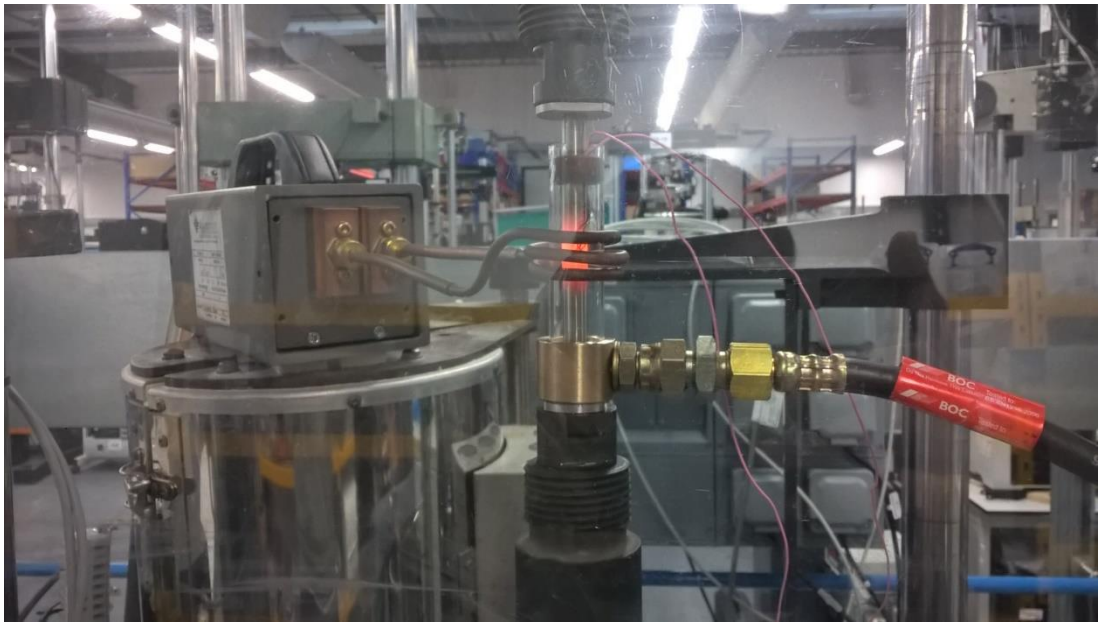

Figure 3.2.3.1 Showing the completed PIB system with the selected coil design

escape out of the top of the top of the glass tube. This meant a continuous flow of argon was used during an interlayer bond at a fixed flow rate in order to achieve the inert atmosphere required for a successful test. The flow rate of argon used in all tests was 20ltr/min as this proved a sufficient amount to create the required inert atmosphere for testing whilst still allowing for a sufficient number of tests to be conducted on a single gas cylinder.

After the gas flow had been started the induction heating system was turned on. The power of the induction heating system was then set so that the required bonding temperature was reached. With the selected coil the highest controllable heating rate that could be achieved was an average of approximately 7.5ºC/sec to reach a bonding temperature of ~910ºC. Once the required temperature was reached the force for that particular trial was applied via the computer of the servo hydraulic test frame. Various trials were done which alternated between continuous force and temperature through to applying larger forces for shorter times in order assess the impact of this variation. However, due to a low volume of material only preliminary tests were done for this type of testing. Table 3.2.1 details the parameters used for the tests conducted in this study for the optimisation of Ti-6246 interlayer bonds. The main variable parameters that were examined were time, temperature, Force and interlayer thickness. The reason for limiting the factors was because in a typical full factorial DOE the number of tests needed would far exceed the number of samples that were available for testing as well as these factors being the predominant parameters on bonding success. By completing a fractional factorial DOE, the number of tests could be reduced whilst still capturing the effects of the main factors. Included in Table 3.2.1 is the test conducted without an interlayer but with the eventual conditions associated with the optimised conditions for Ti-6246.

With previous research having concentrated the interlayer bonding technique on key parameters, this study focused on achieving similar results with only slight variations in these main factors. For example, it was noted that bonding at 930^0C, although below the β_T, still resulted in localised transformation to the β phase and therefore trials with slightly reduced temperatures were conducted in order to prevent this phase transformation. When observing the micrograph images from the HAZ of interlayer bonded Ti-6246 it was clear that although there was a coarsening of α_p phase, which resulted in a reduced V_f, there was no obvious signs of localised heating above the β_T

of the material. Faster heating rates, of above 10^0C/sec, had the potential to go beyond the target bonding temperature of a test and with target temperatures tested being between 5^0C – 45^0C from the β_T any overshooting during the heat up could have an effect on the eventual microstructure of the bonded samples. From Figure 3.2.3.2 below, which shows a test done with a heating rate of ~12^0C and a target temperature of 930^0C, the microstructure across the bond interface shows clear sign of transformation taking place with the V_f of the β phase increased significantly and a reduced amount of the α_p and α_s phase. This test showed that it was possible to fully dissolve the α_p phase within the immediate HAZ if the heating rate and target bonding temperature was too close to the β_T for Ti-6246, which is approximately 935^0C – 940^0C. Although the target temperature would have been slightly below the Beta Transus, the control measurement for the test was taken from welded thermocouples placed on the outside surface of the bonded specimens, no closer than 0.5mm from the bond interface. Therefore, there was potential for increased localised heating within the immediate vicinity of the bonding interface that allowed for the temperature to go beyond the β_T if the target temperature was set at 930^0C

For bonding trials with a target temperature of 890^0C and 910^0C there was still an effect on the V_f of the α_p phase with a slight reduction noticeable. In Figure 3.2.3.2(b) the change in the amount of transformed β from the Figure 3.2.3.2(a) is clearly visible with less of a contrast observable from the interlayer region and the test samples.

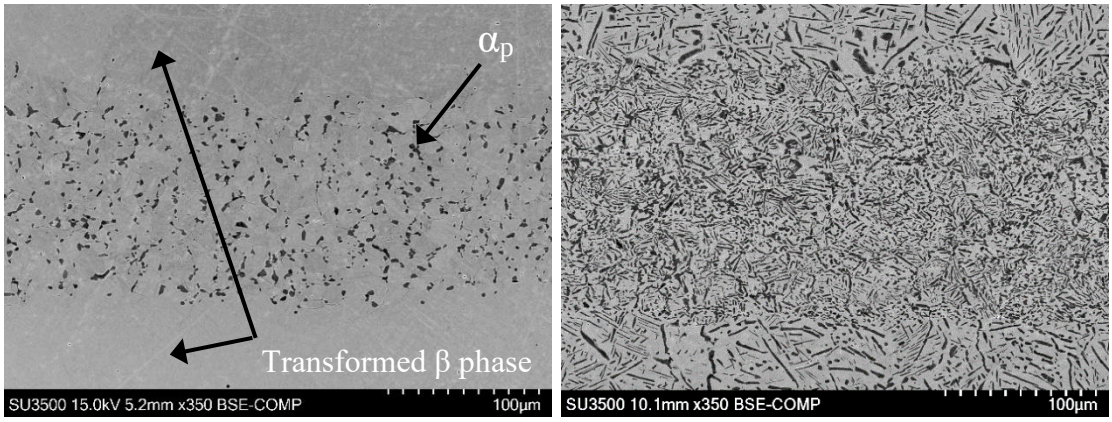

Figure 3.2.3.2: Microstructure of bondline for Ti-6246 PIB bond done at: (a) 930C and (b) 910C

Table 3.2.1 Showing the Bonding parameters for the optimisation of Ti-6246 interlayer bonds

Test No.	Temperature (C)	Time (Mins)	Force (kN)	Interlayer thickness (µm)
1	45	930	2	325
2	30	910	2.5	200
3	30	910	1.5	325
4	30	910	2	325
5	45	910	1.5	325
6	15	930	1.5	200
7	60	890	2	200
8	15	910	2.5	200
9	45	890	2	200
10	45	910	1.5	200
11	15	930	2	325
12	60	910	2.5	200
13	15	930	2.5	200
14	45	890	1.5	200
15	45	910	1.5	-

During a bonding trial the temperature was continuously monitored via the spot welded thermocouples and any deviation from the target temperature could then be corrected for by increasing or decreasing the power of the induction heating system. The flow rate of argon was kept constant as this was controlled via a multi-staged regulator attached to the top of an argon cylinder. A gas hose was then attached to the outlet of the regulator to the specimen collet. This collet allowed for the argon to only travel vertically up and into the quartz glass tube.

At the end of a bonding trial the power of the induction heating system and the load was reduced. This was so that the specimen could cool to room temperature and no stress was applied at the end of the test. The argon was allowed to flow at the set rate until the temperature of the specimen had reached room temperature. This was done

to ensure an inert atmosphere as the bonded specimen cooled through relatively high temperatures. Once cooled the specimen could then be unloaded by unscrewing the bottom collet from the platen and then removing the quartz glass tube. The bonded specimen could then be unscrewed from the collet and taken out of the argon intake sleeve. The bonded sample could then be used for further investigation. For example, metallurgical investigation of the bond line would require the specimen to be section in order to be mounted in Bakelite for investigation in an SEM or machined into a tensile specimen for mechanical testing of the joined specimens.

3.2.4 Interlayer Production

The preparation of the required interlayer was done prior to any bonding trial. This involved the mixing of Gas Atomised Ti-6-2-4-6 powder, cellulose powder, glycerol and deionised water. The quantities of these constituents are show in Table 3.2.2. The percentage weight of each constituent was taken from previous studies in which success was shown in combining these elements in order to produce a powder based paste. This powder paste was then applied to the surface of one of the surfaces to be joined. This was then used in an interlayer applying system that allowed for close control of the interlayer thickness.

Table 3.2.2 Showing the list of ingredients used to create the interlayers

Material	Quantity
Alloy Powder	200g
De-ionised Water	18g
Glycerol	0.5g
Cellulose Ether	1.5g

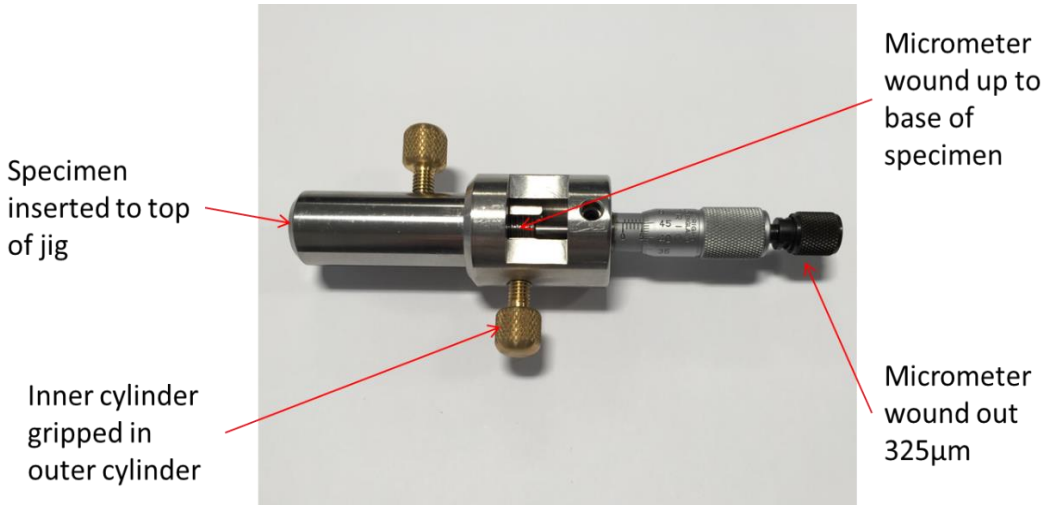

Figure 3.2.4.1 Image of the assemble used for interlayer applications used in this study

In order to produce the specimens with the powder interlayers, the method described in previous studies was initially used. However, although this method produced relatively thin interlayers it did not produce interlayers that were of a consistent thickness across the specimen. Although some variance was to be expected the image shown below shows that this variance was too great, from 404µm to 719µm. As a result of this a new interlayer applier was made in order to improve the application method.

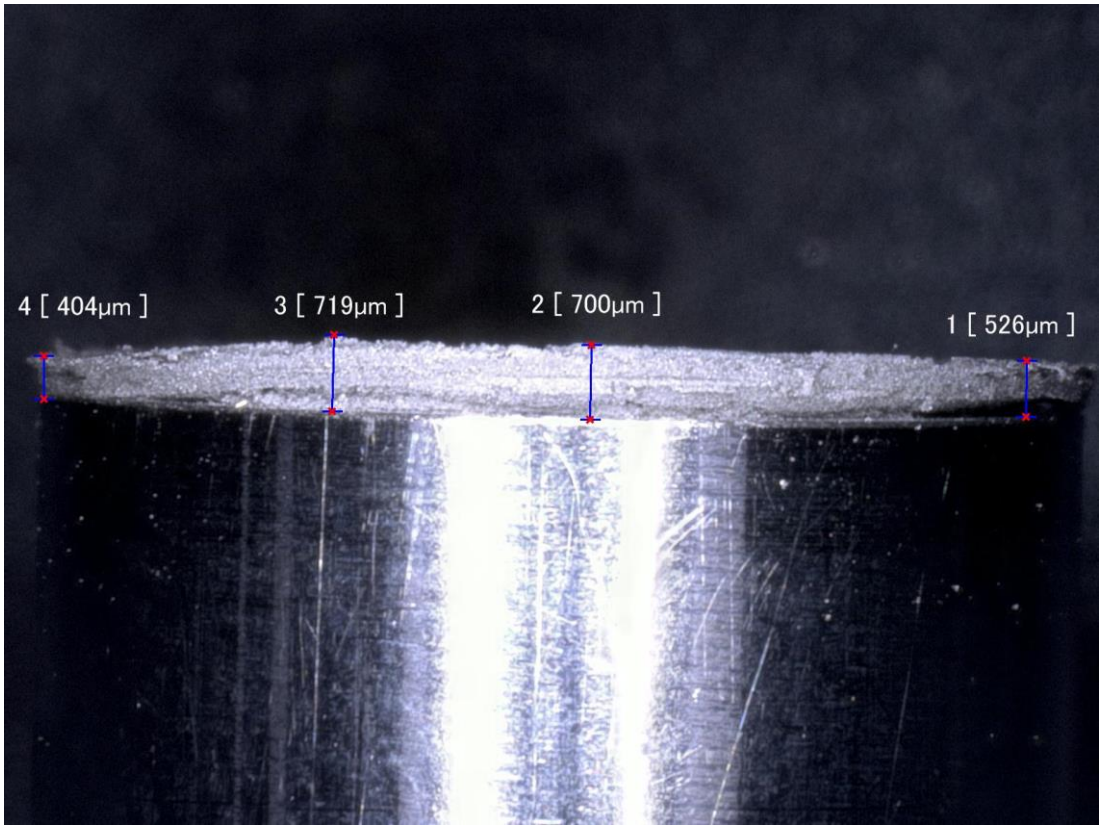

Figure 3.2.4.2 Image showing uneven interlayer thickness using traditional application technique

The system that was used is shown in Figure 3.2.4.1 and shows a specimen holder and a measuring device. This was used by inserting a specimen into the holder and then tightening the screw once the specimen was at its 'zero' position, i.e. in line with the top of the holder. This assembly was then inserted into the interlayer thickness measuring gauge and tightened. The bottom of the specimen would then be in contact with the gauge and once the screw was loosened the gauge could then be lowered by a fixed amount. In this study interlayer thicknesses of 200µm were primarily used with trials conducted at smaller thicknesses such as 100µm and up to 325µm. However, it was found that applying interlayer thicknesses below 200µm was not feasible due to the difficulty in applying the interlayer consistently for all samples. The powder paste could then be spread, using a spatula, in this gap between the top of the specimen and the top of the specimen holder. Care was taken to ensure the powder paste was spread evenly and across the top of whole specimen. Once the interlayer was applied the specimen could then be removed and used for a bonding trial. The lower limit of the interlayer thickness was determined as the smallest interlayer thickness that could be achieved reliably using this method. Attempts were made to create smaller thickness interlayers however it was very difficult to coat the full surface area of the specimen.

Care was taken when handling the specimens which contained the interlayer as they could easily be removed if disturbed in any way. All the individual pieces of equipment were cleaned prior to use in an ultrasonic bath with acetone.

3.2.5 Sample preparation

The evaluation of the High Integrity Joining System meant that mechanical testing and microstructural analysis of joined specimens would be crucial in determining the success of joins and aid in focusing on key parameters for joining. For mechanical testing of interlayer bonds, the different methods of testing included room and elevated tensile testing as well as High Cycle Fatigue (HCF). The test samples used for tensile testing included RLH10004 and for HCF testing the samples used were RLH8020 for HCF. The reasons for this was due to the dimensional constraints that were present from the starting size of the joined specimens. Each mechanical test bar was machined from an interlayer joined specimen and was done so that the joining interface of the 2 specimens was located at the centre of the mechanical test bar. For the purposes of machining the test samples out of the bonded samples it was critical that the alignment of the samples was set to avoid distortion that would make not make it possible to machine out the test specimens.

3.3 Bondline Characterisation

The characterisation of bonded specimens was done in order to determine the success of the parameters used for a particular bond. Using a consistent method of characterisation was important in order to compare and contrast between different parameter sets used for bonding and hence better explain the results that followed. The main focus of characterising the bonds was to analyse the porosity levels and microstructural changes that occurred in the overall HAZ. This acted as a quick way of ranking the bonds created and enabling the study to understand the effects of the different parameters used such as temperature and load.

3.3.1 Porosity Analysis

In order to measure the porosity in the bondline region the bonded specimen had to be sectioned so that it could then be analysed under an SEM. The sectioning of the samples was done on an ATM Brilliant 220 Cut-off machine. The specimens were sectioned so that a section with a total length of no more than 32mm was left remaining

with the bondline located at the centre. The sample was then also sectioned in half so that a cross sectional view was left of the remaining sample. The specimens were then mounted in conductive bakelite using an ATM Opal 410 mounting press and then ground and polished, on a Struers LaboPol-5, using the stages and parameters detailed in Table 3.3.1.

Table 3.3.1 Listing the polishing procedure for Titanium alloys for metallographic analysis

	Step 1	Step 2	Step 3
Base	Piano-220	MD-Plan	MD-Chem
Media	SiC	DiaPro Plan	OP-S
Force (N)	25	30	20
Speed (rpm)	300	150	150
Time (Min)	0.5 - 1	5	10

The SEM was then used in order to obtain relatively high magnification images which could then be used to characterise the porosity within the region of the interlayer. A set magnification and working distance was used on each sample for the porosity characterisation part of the study. Images were then taken on the SEM using the stitch function which allowed for a periodic image to be taken at a set distance across the bondline.

Following on from the capturing the images for porosity analysis, each image taken would then be loaded into an image software tool called ImageJ. This piece of software was then used to highlight the porosity within the image and measure the total area of the pores. This was done by utilising the image process and analysis software within ImageJ. The software allowed for the images taken from the SEM to be analysed for porosity size and distribution. With the images taken at a fixed magnification (x350) from the SEM of the interlayer region each image was analysed in the same way to capture the porosity data. The first step involved setting the scale by using the scale bar on the images and defining the scale bar distance in pixels. This meant that when capturing the size of the pores they would be to scale. In order to determine the pore size and distribution the ‘thresholding’ function could be used which relied on the contrast of the pores in comparison to the surrounding material. Various measurements

can be made using this analysis software and the area could be selected. In order to ensure the thresholding function could distinguish between pores and the typically dark coloured α phase the images that were taken were set with a contrast and brightness level that highlighted the darker pores more than the dark grey coloured α_p.

The results of this could then be exported to Microsoft excel and used to collate the pore size distribution across the entire interlayer region. This was done for all the bonds tested and the results were compiled in order to compare the porosity size distribution for each parameter set. In terms of the images that were analysed the area of each image was approximately 360μm x 250μm which meant that for a typical interlayer bond there were 33 images which would encompass the length of the bondline.

The results from this analysis could then be used to plot the porosity across the bondline, in a single plane, and measure the change in porosity from the middle of the sample to the edge. Although this did not give a figure for the actual porosity across a whole specimen it allowed for trends to be seen between different parameters used for bonding within the interlayer region. This method allowed for the pores to be captured in a 2 dimensional point of view and early work was done in order to determine the possibility of capturing the porosity throughout and entire bond interface using X-ray CT. However, after an initial trial it was decided not to pursue this methodology due to time constraints and material availability.

The results from this stage allowed for a correlation to be made between bonding parameters and the corresponding porosity associated with those parameters. Although porosity is not the only characteristic relevant for good mechanical properties, it is a crucial first indicator.

3.3.2 Microstructure Analysis

After bonded samples were sectioned for analysis in the SEM, they were also used to study the microstructure within the interlayer region as well as the wider HAZ. Certain characteristics for each titanium alloy were captured in order to understand the effects of the bonding process on the microstructure. For each sample that was examined the interlayer and the HAZ was analysed and captured. For typical magnifications, for example up to x5000, and analysis of alpha and beta phases within the samples the Hitachi SU3500 SEM was used. However, for understanding the effect that the

bonding procedure had on smaller phases such as α_s the JEOL 7800F FEG-SEM was utilised. This allowed for clear observations to be made up to approximately x20,000 magnification and beyond. For the analysis of the V_f of the α_p within the HAZ an image was taken at a set magnification starting within the interlayer and the proceeding to capture images at intervals of 2mm in order to quantify the V_f variation. A total of three images were taken at each distance interval from the bondline and then measured using ImageJ. The same technique of measuring the porosity was used, by thresholding the images in order to highlight and quantity the α_p phase. By using the Hitachi SU3500 SEM and capturing using BSE-COMP, it was possible to create high contrast images distinguishing between the α_p and β phase and due to the capture settings and low magnifications, the α_s was not visible and therefore it was possible to measure the α_p in isolation.

As well as image analysis on microstructure of the bonded samples, Energy Dispersive X-ray spectroscopy (EDX) and Electron Backscatter Diffraction (EBSD) was used in order to further understand changes in chemical compositions and microstructure. For EDX analysis a combination of line cans, full chemical composition maps and point scans were used in order to capture the chemical makeup in certain areas of the HAZ. The EBSD analysis was done by further sample preparation. Trials were conducted with differing loads, times and pressures for the final polishing procedure in order to produce the best results for EBSD. The best method involved reducing the load to the 2N and repeating the final stage of the polishing procedure but with a reduced load and significantly increased time. This was found to help during the setup of the EBSD scans which required high spectral patterns in order to produce reliable results.

3.4 Mechanical testing

The mechanical tests done in this study was done to further understand the properties of joining using the High Integrity Interlayer Joining technique. The tests focused around tensile testing and fatigue testing as well as hardness testing within the HAZ of the interlayer bonds. The results from the testing programme allowed for an extensive understanding of the boning process for Ti-6246. All tensile and fatigue tests were conducted within Swansea Materials Research & Testing Ltd (SMaRT) which is a UKAS accredited mechanical testing laboratory.

3.4.1 Tensile Testing

Room temperature tensile tests were done RLH10004 specimens, drawing shown in Figure 3.4.1.1, that had been machined from samples produced via the PIB technique. The best effort was done to ensure the bondline of the joined samples were kept in the middle of the machined samples. The tests were conducted at 20ºC in a temperature controlled laboratory. With the use of a strain gauge extensometer the specimen extension was constantly measured during the tests. An initial strain rate was used and, in accordance with SMaRT guidelines, the strain rate was then increased after passing a total strain value of 5%. This was to ensure the yield stress of the test was captured before any increase in strain rate. The test continued until fracture and the samples kept for analysis and the data compiled using Microsoft Excel.

A small number of elevated temperature tensile tests were also conducted in a similar manner to room temperature tests. However, for the elevated temperature tests a tube furnace was used which was adapted so that it was located around a servo hydraulic test rig designed for tensile testing. The temperature was increased to the testing temperature and held for a fixed amount of time, to ensure temperature uniformity within the specimen, in relation to the SMaRT testing standards. As with previous mechanical testing the samples the fracture surfaces were analysed using SEM and microscopical analysis. Due to the limited availability of material for this study a total of two room temperature tensile tests were completed for the optimised bond conditions with one test being conducted for all other variants.

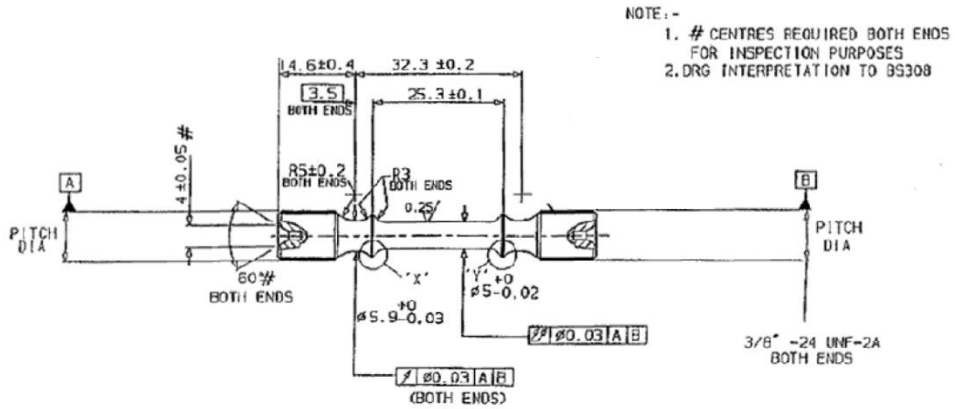

Figure 3.4.1.1 Schematic drawing showing of RLH10004 tensile samples used for testing.

3.4.2 High Cycle Fatigue Testing (HCF)

Fatigue testing was done to further test the capabilities of interlayer joined materials. The tests were conducted on an HCF Amsler vibrophore machine. The tests were load controlled ranging from 550MPa to 750MPa and tests conducted at 50MPa between the stated range values and with an axial load direction. The results from each test were recorded with respect to cycles to failure and an S-N curve plotted, with the runout criteria set at $10x10^6$ cycles. With respect to fatigue testing there are numerous ways to test in order to construct an S-N curve, however with the limited number of specimens that could be generated it was decided to only test with an R ratio of 0, a target frequency of 80Hz and a typical sinusoidal waveform, all conducted at room temperature.

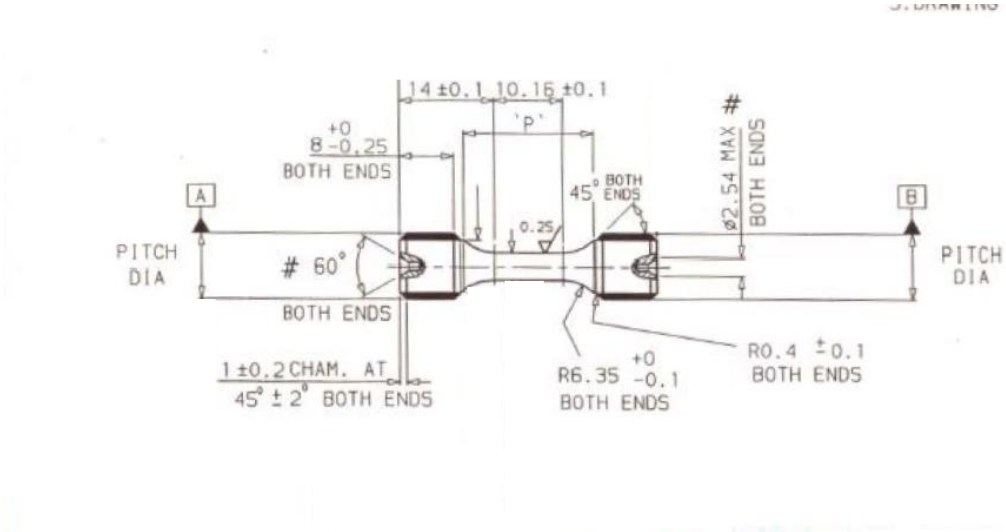

Figure 3.4.2.1 Schematic drawing of RLH8020 used for HCF for PIB Ti-6246.

3.4.3 Vickers Hardness Testing

Hardness testing was conducted on a Zwick Roell Indentec Hardness machine. The samples used were mounted in conductive bakelite and allowed for hardness to be mapped across the HAZ of bonded samples. Hardness indents at HV10 was done at intervals of 0.5mm perpendicular to the bondline, with a 1mm spacing between these rows of indents, in order to map the hardness across the specimen.

Vickers hardness works by holding an indenter at a fixed load for a certain amount of time. This method aims to measure the ability for a material to resist plastic deformation. This then creates a diamond shape, from the indenter, in the surface of

the material which can then be measured in order to produce a hardness value. For this study the dwell time was 10 seconds with a calibration block tested before doing each sample in order to ensure consistency of results. The calibration block has a designed hardness value and so a new indent was done and measured to ensure the result was within the calibrated range of the hardness testing machine. The results of this test were then collated using Microsoft excel and the results plotted showing the hardness profile across the HAZ for the bonded samples. Initial hardness tests were done up to 8mm from the bond interface however the results showed that there was hardness variation beyond this point therefore the hardness maps were increased to 20mm from the bond interface in order to capture the full variations across the HAZ.

4 Results & Discussion

This chapter sets out the results obtained via various tests conducted throughout the course of this study. The main focus of the study was the development and analysis of the PIB process through mechanical testing and microstructural examination. The initial results concentrate around the effectiveness of the induction heating system and argon shielding system being a suitable form of joining for Titanium alloys. Once the feasibility of the system showed it was possible to join high temperature alloys, further testing was done in the form mechanical testing and material characterisation. The core of the study focused on Ti-6246 however in addition to this, early trials of joining dissimilar alloys and alternate interlayers were also investigated.

The system developed in this study arouse from the need of joining high temperature alloys and maintaining, to some extent, the high mechanical properties associated with these alloys. Previous studies have focused on using thermo-mechanical simulators, such as Gleeble welding systems, therefore the initial part of this study focused on evaluating a system that could be used practically for high temperature materials. With the alloys investigated in this study high temperatures are required in order to successfully bond the alloys, even for a solid state joining process. With this need for elevated temperatures the interaction of Titanium and oxygen in the atmosphere becomes an issue that needs to be tackled. These focus areas narrowed the type of system that could be developed. A high temperature, relatively fast heating rate with an inert atmosphere was required. The heating system chosen was an induction heating system as previous work had shown that it was a technology able to heat high temperature alloys to a sufficiently high temperature as well as being a non-contact form of heating which proved useful when considering complex geometries in the future.

4.1 Ti-6246 PIB Trials

The core of the study focuses on the characterisation of the PIB process on Ti-6246, with potential applications for repair within aerospace. Previous studies have shown that utilising the joule effect can produce high integrity bonds for this alloy using thermal-mechanical simulators as a means of producing bonds. Although the induction heating system is different to these simulators it still utilises the joule effect in order to produce the elevated temperatures required. In order to understand the effects of the key parameters for this process, a number of bonding tests had to be completed. This resulted in a test matrix which varied parameters such as force (MPa), Temperature (ºC) and Time (mins). Each parameter set that was tested was then analysed with bondline porosity being one of the main characteristics that was identified. The following chapter outlines the results obtained from the analysis of this test matrix and the tools used to help compare and contrast the effects of changing the key parameters. The porosity and deformation results for the bonded tests are shown in Table 4.2.1 and discussed in the following chapters.

Table 4.1.1: Showing the porosity and deformation for interlayer bonds (#1 - #14) done with various parameters.

Test No.	Time (Mins)	Temperature (C)	Force (kN)	Interlayer thickness (µm)	Total Porosity (µm2)	Porosity Area (%)	Deformation (%)
1	45	930	2	325	1609	0.057	49.2
10	45	910	1.5	200	1919	0.068	28.8
11	15	930	2	325	2229	0.079	39.7
2	30	910	2.5	200	2483	0.088	36.5
12	60	910	2.5	200	2568	0.091	30.2
5	45	910	1.5	325	2766	0.098	29.1
13	15	930	2.5	200	3104	0.11	29
3	30	910	1.5	325	3415	0.121	26.8
4	30	910	2	325	4572	0.162	31.5
6	15	930	1.5	200	6858	0.243	35.8
8	15	910	2.5	200	17553	0.622	22.5
7	60	890	2	200	24580	0.871	17.5
9	45	890	2	200	27967	0.991	14.2
14	45	890	1.5	200	31917	1.131	13.4

The table shows the results of the bonded trials in order of total porosity measured (μm^2). As well as porosity the plastic deformation measured for each test has been displayed showing that there is correlation between the level of measured porosity and the amount of plastic deformation, with there being an inverse linear relationship. With increased plastic deformation the amount of measured porosity decreases. This does not necessarily mean, however, that increasing the plastic deformation results in increased bond integrity as the microstructure of the bonded tests is significant when determining the mechanical properties of bonded Ti-6246. The results from the table show that the tests done at the lowest temperature of 890^0C display the largest amount of porosity regardless of time and force and also the lease amount of plastic deformation. The interlayer test that had the lowest amount of measured porosity, 0.057%, also showed to have the most amount of deformation, 49.2%. Although the results showed that Test #1 had the lowest amount of porosity, the resultant deformation meant these test conditions would prove difficult to repeat with any misalignment of the test samples increasing the chances of a failed test.

As well as the results from the interlayer bonds the results of the test done without an interlayer under the optimised conditions is also shown in Table 4.2.1, test #15. The result for this test showed similar plastic deformation as to interlayer bonds with the same condition. The objective of this test was to understand the impact that the interlayer has on porosity, deformation and mechanical properties under the same bonding parameters.

The following sub chapters will detail the bond integrity from a plastic deformation, microstructural and porosity point of view in order to determine the optimised conditions selected. Although the porosity distribution amongst each interlayer bond was an important factor in determining the optimised conditions, it is accepted that the method of measurements underestimates the actual porosity levels within each test. The key focus therefore was to understand the trends observed in each test and capturing the results in a consistent way in order to establish comparisons between bonding parameters and their effects on the porosity distribution.

4.1.1 Macro Bondline Analysis

Each bondline was analysed as described in the experimental procedures chapter. The results for the bondline analysis were collated in the form of porosity analysis and microstructural characterisation within the HAZ. As well as characterising features associated with the microstructures, the deformation observed was also measured. After a bonding test the diameter was measured at the widest point, normally at or around the bondline region, and compared to the original diameter in order to understand the amount of plastic deformation. The results of this showed that increasing the temperature or force during bonding would result in increased deformation of the samples. When referring back to the table above, the results of the deformation values have been added to understand the effects of the bonding parameters on this characteristic which is shown in Table 4.2.1.

When looking at the deformation observed for Bond 10 there's an increase of nearly 14% for a bonding temperature of 910ºC with a bonding force of 1.5kN. However, when the bonding temperature is increased by 20ºC, to 930ºC, the plastic deformation observed increases rapidly to a value of 58.7% (test #2) even though the bonding time was shorter. It can be said that had the bonding time of the two tests been the same this deformation would further increase, for test #2, and hence a greater difference between the results would be observed than already seen. The images below, Figure 4.1.1.1, show the variance in plastic deformation that can be observed dependant on the process parameters. The plastic deformation is an important factor when considering the bond integrity with an increasing amount of macro plastic deformation being a strong indicator of the deformation of the powder interlayer which is needed in order to allow for the collapse and sintering of the powder during bonding.

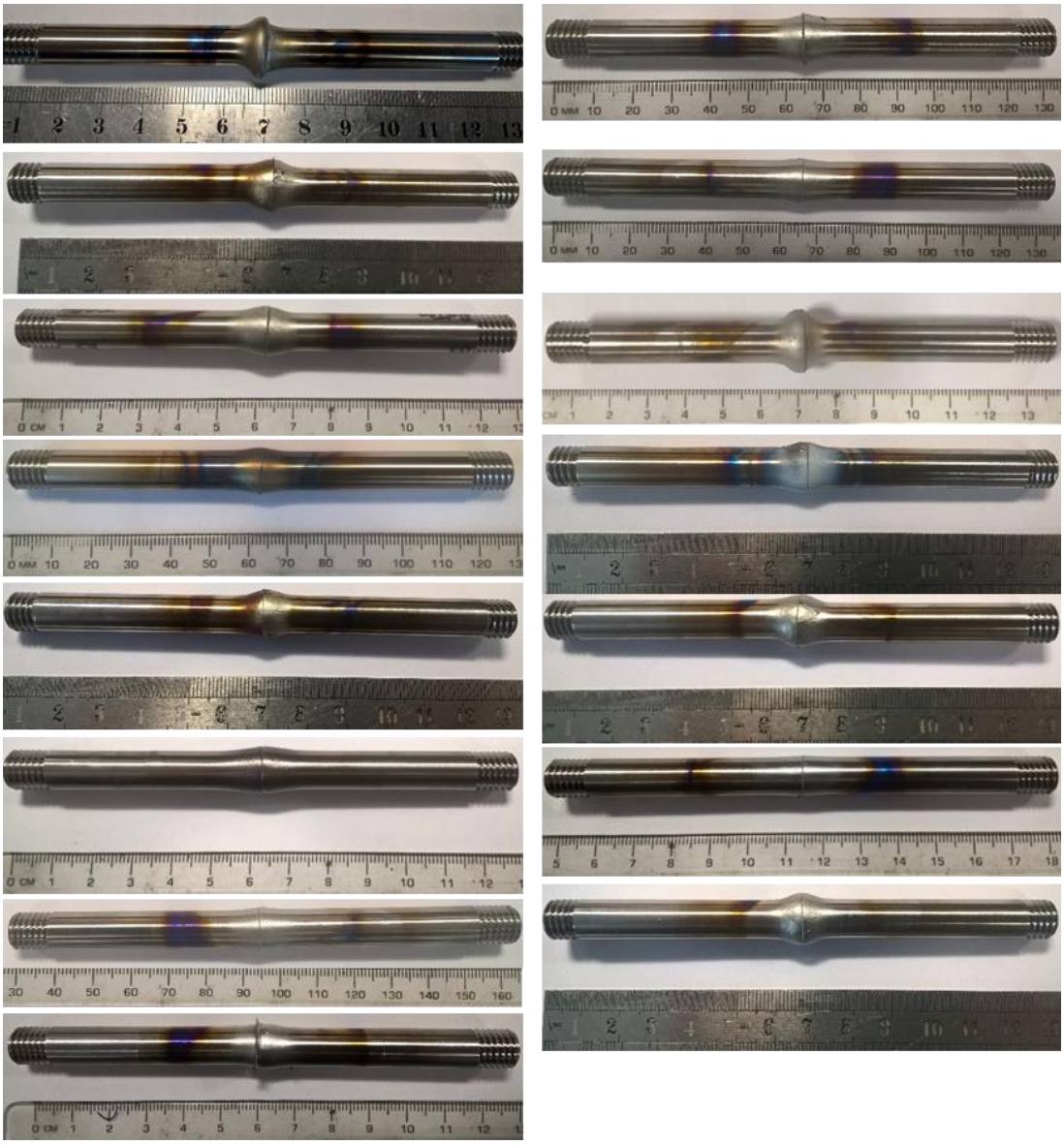

Figure 4.1.1.1 Image of PIB, Left column #1 - #8, Right column #9 - #15

4.1.2 Microstructural Analysis for Ti-6246 PIB

Due the nature of titanium alloys, and more specifically Ti-6246, an important microstructural parameter on overall mechanical properties is the volume fraction of the alpha and beta phases. As described in the experimental chapter of the thesis the volume fraction of the α_p phase was measured at 2mm intervals from the bondline. This was done to understand the effects of the various parameters on the volume fraction within the HAZ. The volume fraction of the α_p is shown in the Figure 4.1.2.1 below and displays the variation in V_f for this phase at the 3 different bonding temperature used in this study. The chart groups the average results of the volume

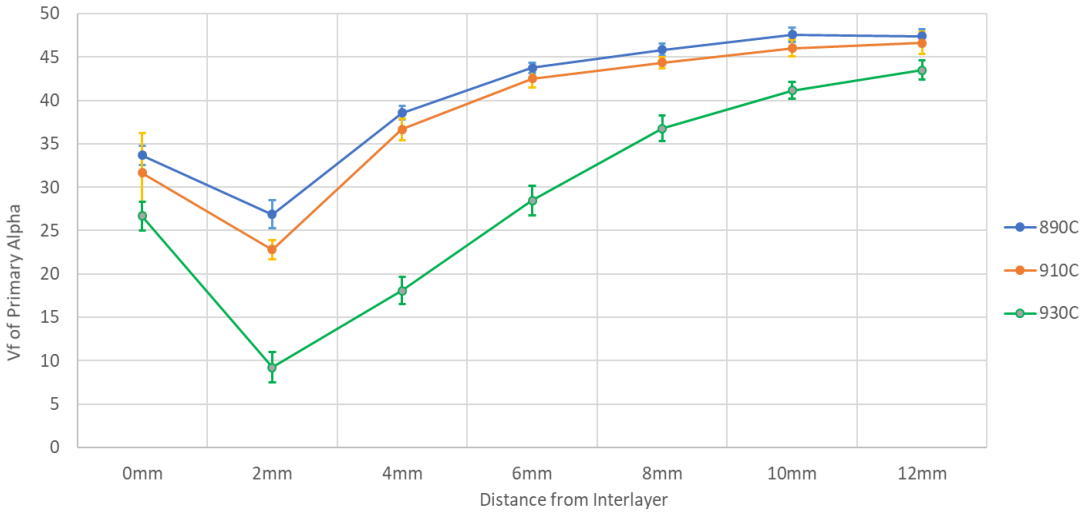

Figure 4.1.2.1 Chart showing the Vf of primary alpha phase within 12mm from the bondline with bonds done at 890C, 910C and 930C.

fraction measurements into the temperatures for the relevant bonds along with the standard deviation related to each point.

The trend for all tests show an initial drop within ~2mm of the interlayer region, with the higher temperatures resulting in a larger drop for the V_f. After this point there is a gradual increase in the V_f across all the bonds reaching close to the nominal amount of ~49% for Ti-6246. The bonds done at 930ºC do however still have a V_f below that of the other bonds at 12mm indicating that due to the slightly increased bonding temperature the HAZ is increased as a result.

The results show, even when considering the variability, the volume fraction for bonds done at higher temperatures results in an overall decrease in the V_f of α_p within the HAZ. This can be seen by comparing the results for the bonds at 930ºC to 890ºC which show that there's approximately a 10% drop on average of the V_f for this phase. Comparing the V_f for bonds done at 890ºC and 910ºC the trends are the same, with the initial drop and then increase, however there is a constant reduction in the V_f for the bonds done at 910ºC.

A factor to observe for the large variance seen for the results within the 910ºC at 0mm is the inclusion of the bond done without an interlayer. The results show that this bond had a V_f for α_p of 20.41%, close to the typical values observed within the HAZ closest

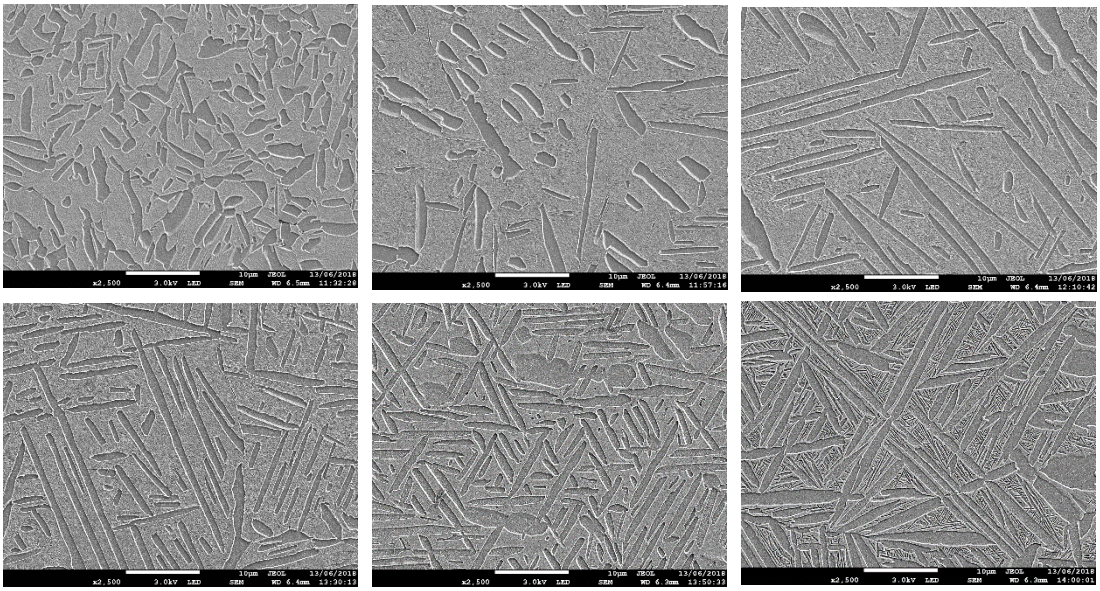

Figure 4.1.2.2(a-f) Microstructure for #10 at 0mm to 10mm from the bondline showing the Vf of the primary alpha phase.

to the interlayer region. The reason for this is explained by the lack of interlayer meaning the measured value is a closer representation of the V_f within the HAZ than within the interlayer region of the other bonds.

The micrographs above show the variation in the microstructure, and more specifically the V_f of the primary alpha phase, across the HAZ for a typical powder interlayer bond for Ti-6246 done at 910ºC. The contrast between partial Bi-modal microstructure within the interlayer region and the needle like laths within the remaining images is clear as well as the coarse microstructure at 2mm from the interlayer in comparison to 10mm.

The larger difference in V_f for bonds done at 930ºC than with bonds done at 890ºC and 910ºC can be explained by the higher temperature bonds being close to the β transus temperature for this alloy and therefore resulting in a signifcant increase in the amount of β transformation within the HAZ. The results also show how the variation in V_f relates to the temperature gradient associated with the induction coil design. When comparing the V_f to the temperature profile for the selected coil, the temperaure is at approxiamtely 840ºC at 12mm from the bond interface.

Another tool that can be used within the SEM is the Energy Dispersive X-ray spectroscopy (EDX or EDS) and is a chemical analysis technique used in conjunction with traditional Scanning Electron Microscopes. It is used to analyse what chemical elements are present within a scanned region and also in what quantity they exist.

When used in relation to the Ti-6246 it shows elements that commonly exist within the alloy, these being Aluminium (Al), Tin (Sn), Zirconium (Zr) and Molybdenum (Mo). The coloured maps clearly show how Aluminium exists in greater quantities within the α phase and vice versa for Molybdenum.

Electron Backscattered Diffraction analysis was done on as received material as well as on Bond #10 of the Ti-6246 interlayer bonds to give the crystallographic information of the microstructure. The results of both the as received material and the interlayer EBSD maps are shown below in Figure 4.1.2.3 and Figure 4.1.2.4 respectively. The EBSD map created for the as received material was done with the largest area possible whilst still obtaining a high indexing rate during the EBSD scan with the map being approximately 3.5mm x 3.5mm. The result of the EBSD can showed the texture associated with the alpha and beta phase for the as received material with crystallographic texture intensities of 5.52 and 3.36 times respectively as illustrated in the EBSD derived IPF//Z pole figures. The map for the as received material shows there is no significant visually observable texture for this alloy in this condition with the range of colours dispersed across the entire map. The generated inverse pole figure (IPF) also showed that there was a slight alignment to the {001} plane for the cubic, β phase however there was a weak overall texture associated with this phase.

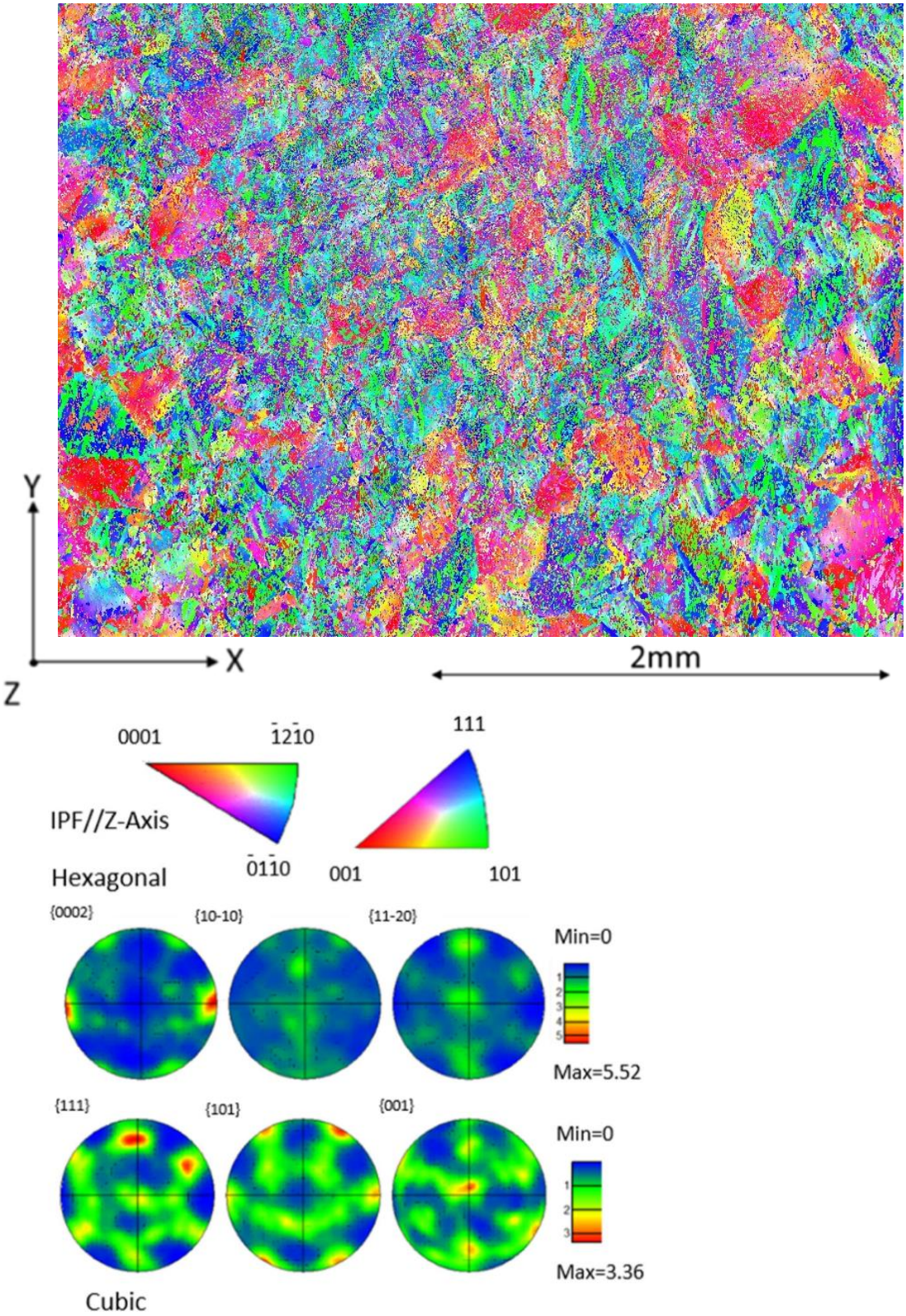

Figure 4.1.2.3: EBSD derived IPF//Z pole figures for as received Ti-6246.

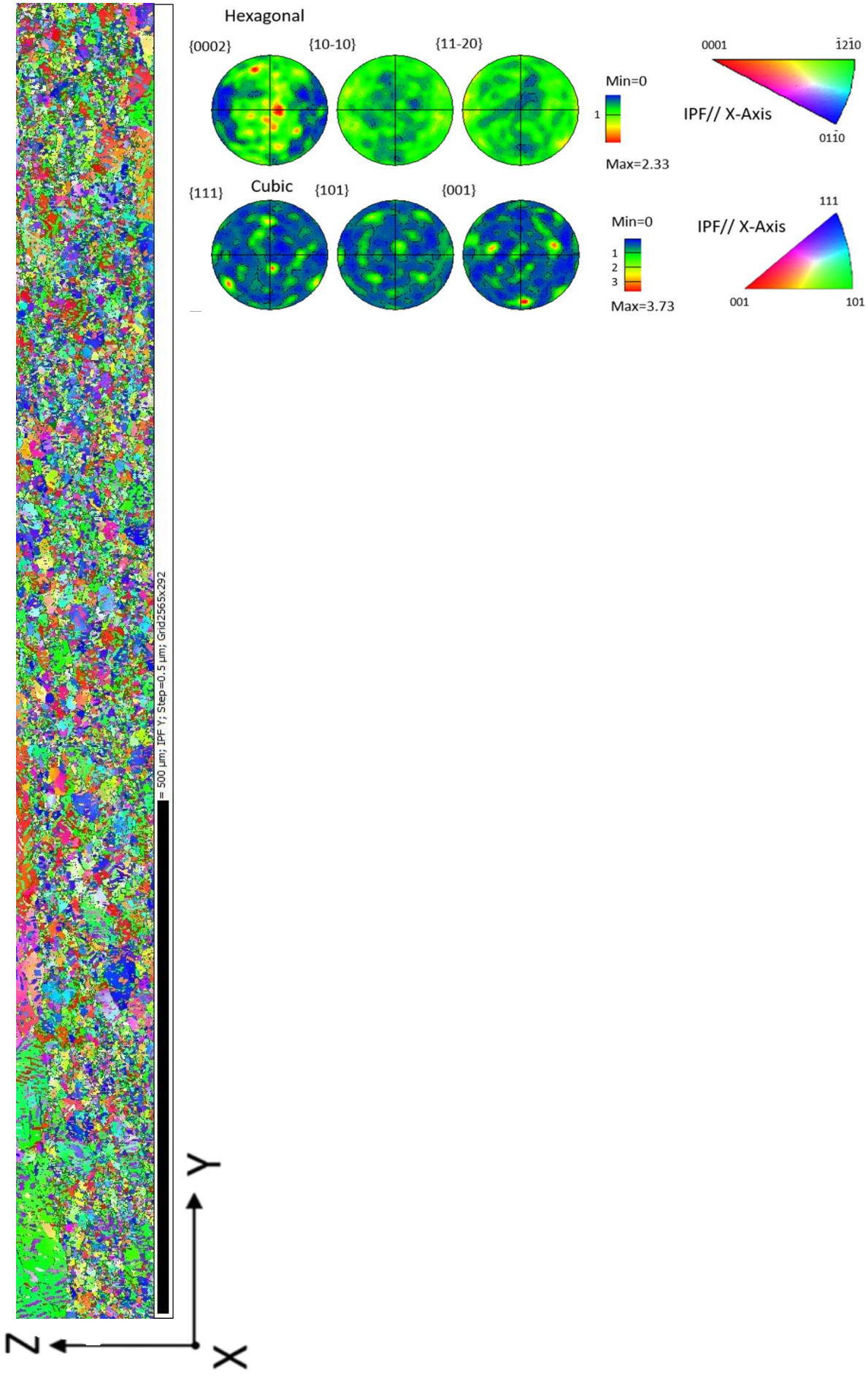

Figure 4.1.2.4: EBSD derived pole figures, IPF//X through interlayer bond region.

With the developed PIB bonding technique one aspect that was hard to control was the cooling rate of the bonded samples at the end of each bonding trial. Due to the constraints of the system the cooling rate could not be sufficiently controlled in order to analyse the effects of differing cooling rates on the final microstructure and mechanical properties. The measured cooling rate of the trial bonds were between 110ºC and 120ºC/min down to 150ºC, at which point the argon feed was turned off and the sample allowed to cool close to room temperature in order to remove from the testing frame. The relatively high cooling rates would ensure that excessive growth of primary alpha phase is avoided with a very fast cooling rate from solution temperatures resulting in more of a fine lamellar structure. With a slow cooling rate, from the solution temperature, would result in increased coarsening of the primary alpha distribution.

An important consideration can be that a slower cooling rate can result in significant impact on the creep and fatigue properties of the alloy. This is due the growth kinetics of the α_p and increased grain boundary α, which is proven to reduce fatigue properties in particular as this is the weakest crack nucleation site.

4.1.3 Porosity Analysis for Ti-6246 PIB's

For the characterisation of the porosity the pore sizes were measured as well as their distribution along the bondline after the bonds were sectioned. This enables the visualisation of the distribution of pores to be seen across a bondline for the different bond parameters. It is worth repeating that these results do not indicate total porosity

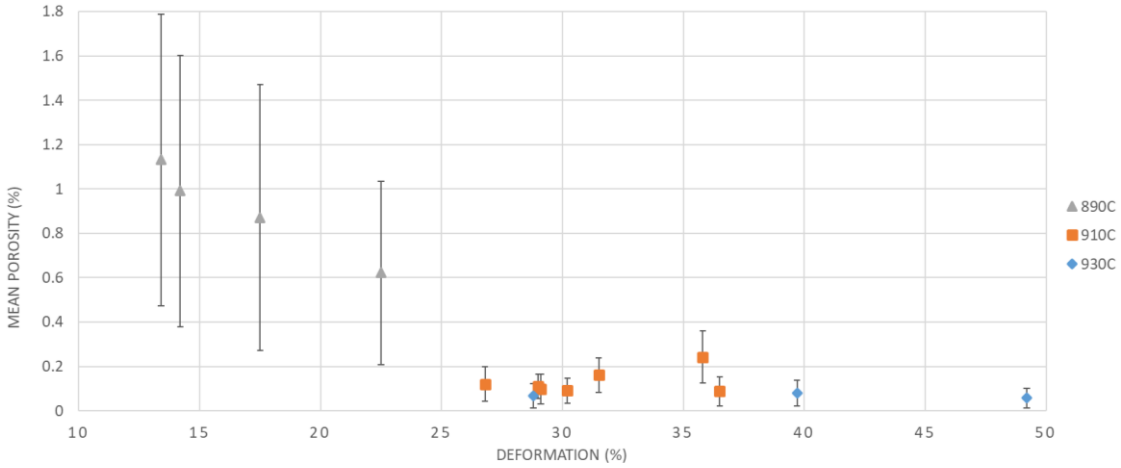

Figure 4.1.3.1 Plot showing the mean porosity, along with the associated standard deviation values, for each Ti-6246 bond related to the deformation.

within a bond and this method was used to compare the trend of porosity distribution. Therefore, when comparing the stated porosity between bonds it is only used for comparison purposes and not for absolute values. The method for measuring the porosity was not comprehensive enough to allow for an indication of the total porosity and for the purposes of this study a comparison of the trends was more applicable.

Measuring the trend of porosity within the interlayer bonds allowed for a comparison to be made between the different parameters and help to establish whether there was a strong link between the parameters and the level of porosity.

When looking back at Table 4.2.1 it is clear there is a large difference between the highest and lowest bonds in terms of porosity across the entire bond interface. In order to help establish whether there is any level of correlation between porosity and other factors such as deformation and/or temperature then using charts can help visualise this. The porosity/deformation chart shows the relationship between the mean porosity level and the relevant deformation as well as highlighting the temperatures at which each bond was done.

The chart above helps to display the relationship between the three parameters of Porosity, deformation and temperature. The results show a negative correlation which dictates that an increase in the amount of deformation, up to ~30%, results in a decrease in the amount of measured porosity. Beyond 30% deformation the level of porosity remains relatively stable with the porosity remaining around ~100μm^2. It is also possible to see a correlation between the temperature of the bonds and the level of porosity. From the chart it is clear that the bonds done at the lower temperatures have resulted in increased porosity levels as with compared with the bonds done at 910ºC and 930ºC.

The plot also indicates the measured standard deviation associated with each bond and the large deviation can be attributed to the large scatter of values measured for the porosity analysis across each bondline. As well as the porosity distribution along the entire bond interface it is also possible to extrapolate the distribution along the same width as the original sample diameter of 10mm. By using the mean porosity distribution along the 10mm region it is possible to plot the same chart as previously in order to understand the, if any, the differences it may have on the porosity distribution comparison between each bond trial.

The chart shows that, as expected, all data points show a reduction in the mean porosity levels for each bond. The trend, in terms of the correlation between temperature/deformation/porosity is the same with higher temperatures resulting in increased deformation and reduced porosity. The key difference between analysing the original diameter and the entire bondline is spread of porosity from the mean values. The standard deviation error bars on the chart show a tighter spread of values particularly for the bonds at 910ºC and 930ºC. When analysing the mean values for the original diameter the order in terms of the lowest and highest porosity bonds doesn't change with the lowest porosity bonds remaining Bonds #1, #10 and #11 respectively

When analysing the results from Table 4.2.1 it is possible to compare the effects of the interlayer thickness of the level of porosity. For example, when looking at the measured porosity for Bond #5 and Bond #10 these have the same parameters in terms of Time, Temperature, Force, whereas the interlayer thicknesses are 325µm and 200µm respectively. Therefore, when comparing the porosity level, it can be seen that increasing the interlayer thickness by 125µm, an increase of 38.46%, the measured porosity increases from 1919µm^2 to 2766µm^2, an increase of 30.6%. These two bond trials help to display that under the same bonding parameters increasing the interlayer thickness results in an increased porosity level throughout the bondline.

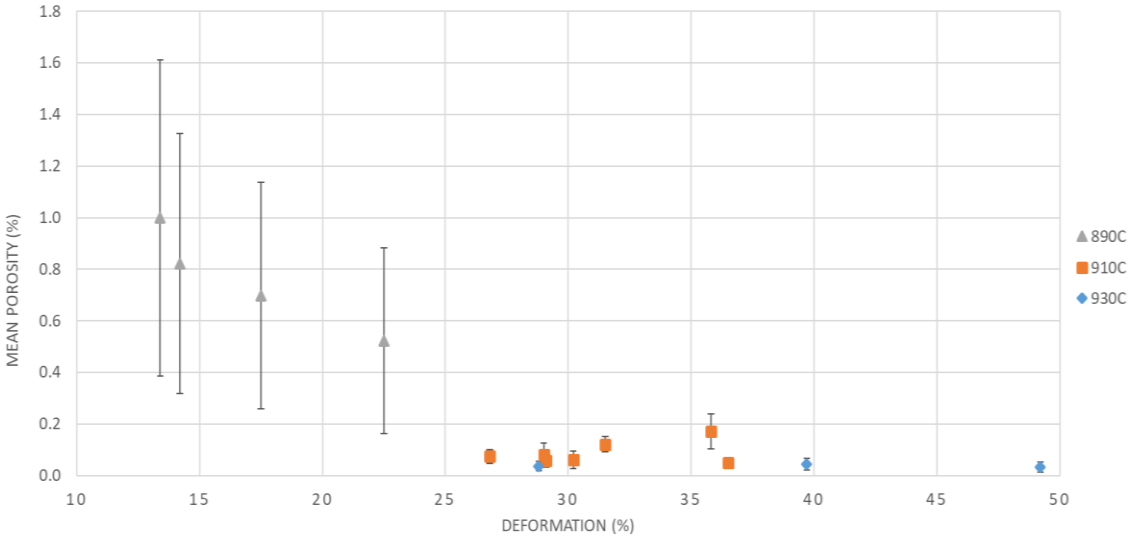

Figure 4.1.3.2 Plot showing the mean porosity value within the original 10mm region for each TI-6246 PIB and the associated standard deviation values.

4.1.3.1 Porosity Distribution Analysis

The chart below, Figure 4.1.3.3, details the distribution of porosity along the bondline for the 3 tests with lowest amount of porosity. They all show a similar trend even though the bonding parameters vary between all the bonds. It can be seen that increased porosity is observed in the plastically deformed areas of the bonds when comparing it to the porosity that is measured in the centre of the samples. For example, bond 10 shows a peak value of 221µm^2 at the edge of the sample whereas the lowest value is 9.2µm^2 at the centre of the sample. The levels of porosity can change for each parameter set, however the trend of the distribution of the porosity remains the same for all the GA Ti-6246 interlayer bonds.

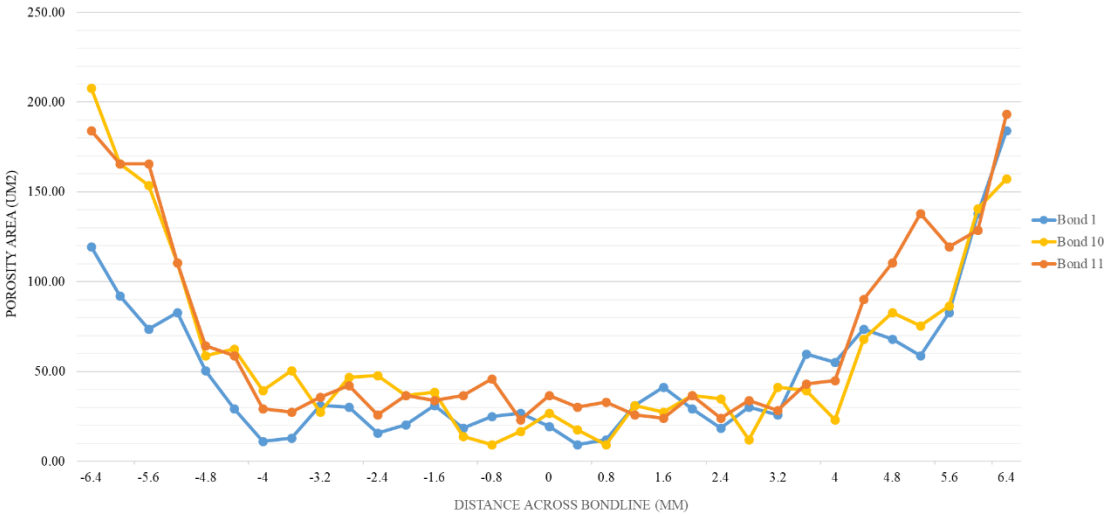

Figure 4.1.3.3: Chart showing the distribution of porosity across the sectioned samples for Bond #1, #10 and #11.

Imaging the bondline also helps to give answers as to where the pores are located and why they remain. For example, the main areas at which the pores are observed is at the boundary between the existing interlayer and the surface of the bonded sample, as seen in Figure 4.1.3.4.

Relating the results on the chart to the results in Figure 4.1.3.1 and Figure 4.1.3.2 shows that by analysing the distribution within the original 10mm diameter relates to the reduction in the standard deviation values observed in Figure 4.1.3.2 for the three bonds. This helps display to show that by removing the porosity values within the plastically deformed regions results in a tighter spread of porosity sizes.

One exception to this trend is the bond that was done without an interlayer, all other parameters being kept the same. This result is more scattered when looking at the distribution of porosity. The peak porosity is no longer seen just within the plastically deformed region as similar pore areas can be observed within the centre of the bondline. Although the trend is dissimilar to the others the total porosity observed is significantly reduced when compared with the powder interlayer bonds. The porosity for this type of bond is also observed only at the interface of the two specimens whereas for the interlayer bonds porosity is present within the powder interlayer region and at the interface between the interlayer and the forged specimens.

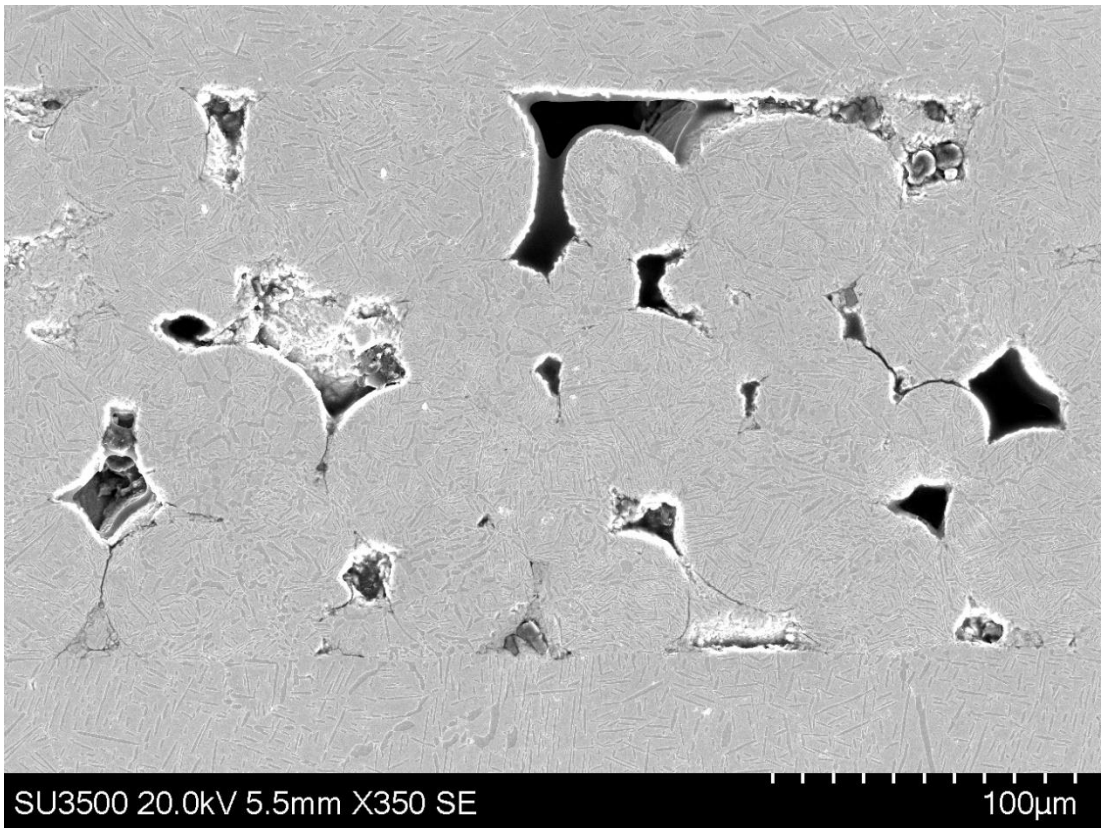

Figure 4.1.3.4: Porosity within interlayer of test conducted with the highest measured porosity.

The findings show that the maximum pore size observed across all the bonds is ~112µm and is for the same bond that has the highest percentage of pore area. When looking at the micrograph, Figure 4.1.3.4, for this particular bond it is clear that the bonding parameters have not resulted in sufficient collapse and sintering of the powder interlayer. This has resulted in significant areas of porosity, especially within the plastically deformed regions. Although some sintering has occurred the existing

powder diameters can still be seen as well as the interlayer thickness, ~200µm, being significantly thicker than with that of the optimised conditions.

Another comparison that can be made is that the amount of deformation observed, the % increase in diameter, is related to the porosity observed within that bond. It can be said that there is an inverse function relationship between the measured porosity and deformation. As the amount of porosity increases the corresponding plastic deformation decreases.

4.1.4 Vickers Hardness Results

As well as evaluating the microstructural and porosity of the interlay bonds another aspect that was analysed was the Vickers hardness across the HAZ of all bonds. The hardness evaluation can give a strong indicator as to the effects of temperature on the microstructure especially for joining technologies such as welding for example. In order to evaluate the hardness variation for the interlayer bonds created in this study the results are plotted in Figure 4.1.4.1. The chart displays the mean hardness values up to 20mm from the bond interface with each data series representing the bonds done at the temperatures of 890ºC, 910ºC, 930ºC.

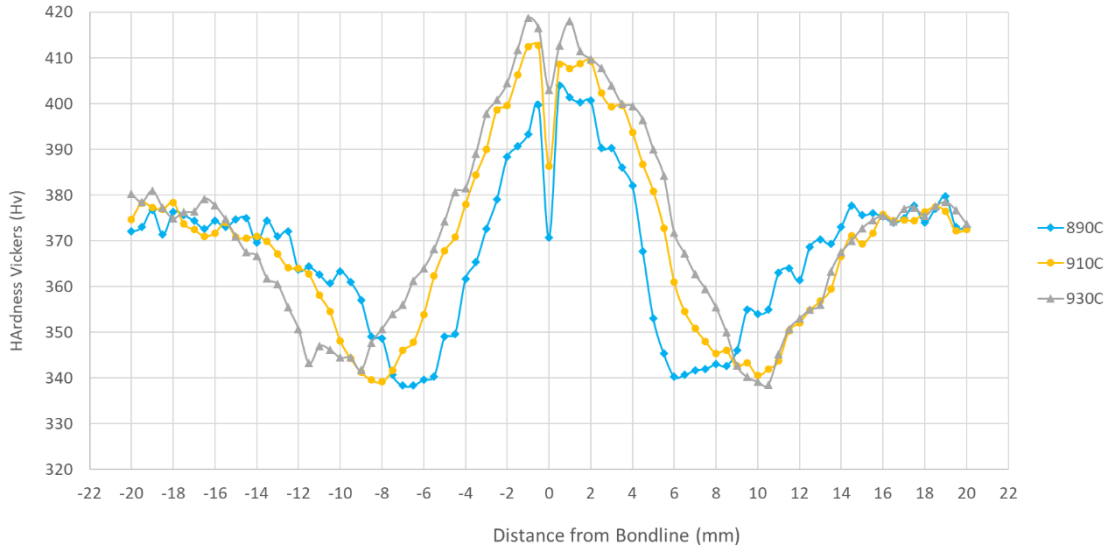

Figure 4.1.4.1 Plot showing the Vickers Hardness value for all Ti-6246 PIB grouped by the three bonding temperature.

The results show a similar trend for all the bonds done across the HAZ. The trend shows that between approximately 12mm and 6mm there is a clear drop in the

hardness with a then gradual rise up to peak values of hardness up to ~405Hv – 420Hv depending on the temperature. As well as the variation across the HAZ there is a similar pattern between all bonds and that is the drop in hardness within the interlayer region compared with the microstructure of the adjacent material.

Although the trend is the same across the 3 temperatures there is a distinguishing feature that can be observed across each temperature. This is the width at which point the hardness drops to its lowest value. When looking at the results for the mean hardness values for bonds done at 890ºC the point at which the hardness drops to its lowest values is at 6mm – 6.5mm either side of the interlayer region. Whereas for the higher temperature bonds done at 930ºC the lowest values are at 9.5mm – 10.5mm either side of the interlayer with the 910ºC bonds being in between these at ~8mm. As well as this the peak values for the three different temperatures bonds show a correlation with an increased bonding resulting in an increased peak hardness value all of which are observed in the material immediately adjacent to the interlayer region. The highest hardness value is observed for bonds done at 930ºC with typical values of ~418Hv whereas bonds done at 890ºC results in peak hardness values of ~405Hv. The hardness results also give a good indicator as to the effect of the HAZ for all bonds. The results show that for the lowest temperature bonds the HAZ extends to at approximately 15mm and the highest temperature bonds up to 16.5mm from the bondline indicating the additional width of the HAZ associated with the high temperatures.

As well as the peak and trough of the hardness values for all the interlayer bonds there is also a significant drop in the hardness within the interlayer in comparison to the peak values associated in the material adjacent to the bondline. From the chart the mean values of hardness within the interlayer for lower bonding temperatures results in lower hardness values.

4.1.5 Ti-6246 Optimised PIB

To be able to effectively determine the correlation between the key bonding parameters then understanding the results in the figures presented above need to be understood. The simplest way of determining the bond integrity would be to compare

the porosity between the bonds. This would show that Bond #1 would produce the highest integrity bond when analysing the total measured porosity with a reduction of nearly 25% from the next lowest porosity bond. When analysing the results shown on Figure 4.1.3.1, the results show a strong correlation between porosity and deformation, with an increased deformation resulting in reduced porosity. By highlighting the temperature of the bonds within the same plot is also possible to draw further correlation between temperature/porosity/deformation. It is clear that increasing temperature of the bonds results in an increase the deformation and hence, as previously stated, a reduction in the porosity. Therefore, by understanding this correlation, as well as the result for the lowest porosity PIB Ti-6246 being at a temperature of 930ºC it is easy to assume that the optimised bond should be selected from this temperature bond. However, when considering the practical effects of bonding at these temperature it is clear that this can introduce other factors that make it impractical to continue with bonds at these temperatures. Among the key challenges with bonding at higher temperatures is the increased deformation that is observed. With the quartz glass tubing of the PIB system the deformation associated to the parameters from bond #1 meant that the bonded specimens may contact the glass tube. As well as the excessive deformation the microstructural analysis showed a drastic decrease in the volume fraction of the α phase due to the target temperature being close to the β_T. The results in the V_f chart help show the increased coarsening effect within the HAZ for the bonds completed at 930ºC when compared with bonding at 910ºC and 890ºC. An advantage of this bonding technology is reliant on the ability to produce high integrity bonds with minimal impact on microstructure in order to reduce downstream post processing steps such as excessively long heat treatments. However, it is clear that bonding at close to the β_T has an exponential impact on microstructure with minimal benefit in terms of porosity levels.

When observing the results seen in Figure 4.1.3.1, although increased temperature clearly results in decreased porosity, the reduction in porosity is negligible when comparing selected bonds done at 910ºC and 930ºC. Even with varying time and pressure values, the porosity levels for select bonds at the two higher temperatures remain within similar levels although the trade-off is the amount of deformation. For example, when comparing the bonds with the lowest levels of porosity at 910ºC and 930ºC the results show that there's only a minor increase in porosity with mean

porosity values of 58μm^2 and 48μm^2 respectively. Despite the porosity increasing by approximately ~20% for the two respective bonds, the deformation increases by ~40%. Combining the effects of increased deformation and significant effects on the microstructure within the HAZ it was clear that bonding at 930ºC didn't necessarily produce repeatable bonds.

The results of the optimisation trials also showed how the interlayer thickness effected the overall porosity measurements with a thicker interlayer resulting in increased porosity for the same set of parameters. For example, when considering the conditions for bond #10, the same parameters were done with an interlayer thickness of 325μm which resulted in an increase in the porosity measurement of nearly 40%. Therefore, this shows that in terms of producing low porosity bonds it is important to utilise thinner interlayers that are practically possible.

As well as the interlayer thickness the bonding temperature also showed to have a significant effect on the resultant porosity. The lowest temperature tests, done at 890^{0}C, showed to have the highest amount of measured porosity in comparison to other tests done at 910^{0}C and 930^{0}C. These low temperature tests showed to have porosity levels more than ten times that of the optimised conditions with clear signs of the GA powder interlayer not collapsing and sintering during the test. Images from bond #14 for example, clearly show how the lack of temperature, time and force has resulted in the powders not collapsing sufficiently to allow for the sintering stage to close of the remaining pores. This lack of collapse and diffusion can also be related to the macro deformation of the sample which was measured to have the lowest percentage increase in diameter, 13.4%. Although in powder form, the interlayer and the test samples behaved in similar ways with regard to deformation, both experiencing very little distortion as a result the associated parameter set.

4.1.5.1 Microstructure and HAZ

With the goal of achieving high integrity bonds for Ti-6246 the optimised conditions needed to obtain the elements that make Ti-6246 a high strength titanium alloy. Therefore, the resultant microstructure within the HAZ was crucial in determining the ultimate strength of the bonds. The microstructure of an as-bonded sample could be broken down to similar stages as a friction weld however in this case there a microstructure associated with the interlayer region as well as the HAZ, as shown in Figure 4.1.5.1. The microstructure associated within the interlayer was distinct from that of the Base Material and HAZ. For the majority of the bonds the interlayer region showed a partial Bi-modal microstructure with the small globular α_p being between 2μm - 8μm. As well as the globular α_p the presence of elongated, needle like α_p still had a relatively high V_f. The α_s was more difficult to image with a standard SEM and therefore a JEOL FEG-SEM was used in order to obtain images of this finer phase. Within the HAZ the microstructure of the materials shows the same key characteristics

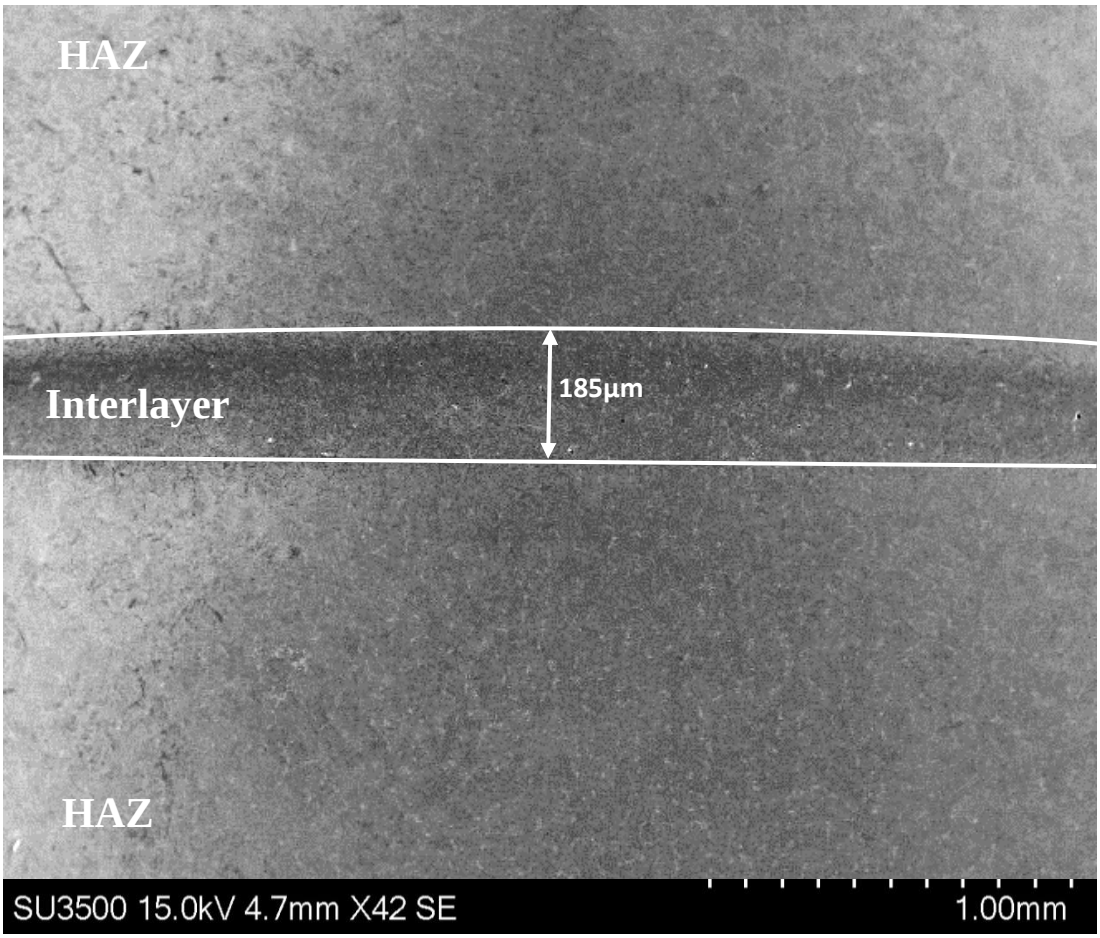

Figure 4.1.5.1: Secondary Electron image showing the microstructure and HAZ for a typical powder interlayer bond of Ti-6246.

as the BM however the α_p laths are more dispersed showing signs of increasing gradual coarsening of the microstructure moving closer to the bond interface. The α_p and transformed β was easier to characterise with clear changes with both phases in comparison to the as received material, however characterising the α_s phase proved more difficult due to the very small lath width. The results showed the there was a trend in the change of the V_f for the α_s across the HAZ. There is a gradual drop in the α_s from the bond interface to approximately 8mm where there is almost no α_s visible in the retained β matrix.

The ability to produce high integrity joints is reliant on compaction and reduction on porosity to level that they can no longer act as crack initiation sites or effect crack growth rates. To do this the process parameters for the bonds need to have a high enough force in order to collapse the powder interlayer as well as a high enough temperature to allow for sintering. The element of time is also relevant in order to allow for the diffusion of atoms to happen and therefore reduce the remaining pore size. The optimised conditions require a balance of these three key factors, time, temperature and force, with an increase in all three decreasing the overall porosity up

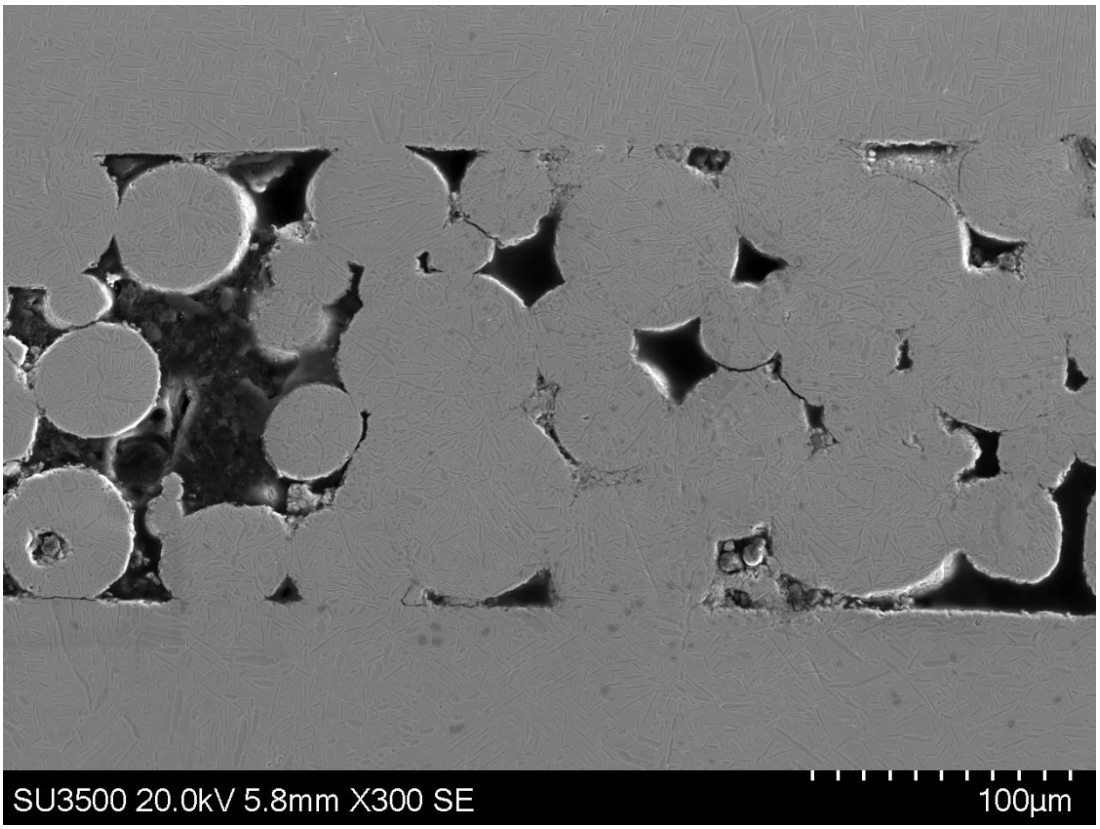

Figure 4.1.5.2: Microstructure showing the lack of collapse and sintering of PIB using lower temperature and force from Bond #14

to a point. Although increasing these parameters allows for reduced porosity, and hence higher bond integrity, this is only true up to a point, past which there are negligible gains to be had. As observed with bond #1, although the porosity was lowest the macro-deformation and change in microstructure meant that the associated parameters yielded little extra benefit when compared with that of the chosen optimised conditions.

The process of collapse and sintering of the powder interlayer is therefore reliant on many factors. The parameters are therefore required in order to reduce the interfacial free energy which would arise from further densification and grain coarsening of the powder interlayer. The process can be illustrated in Figure 4.1.5.3 which describes the stages associated with collapse and sintering. The initial stage focuses on the neck formation of adjacent powders with some plastic deformation occurring. The next step is the referred to as the intermediate stage and requires the transportation of material from the particle to the neck region via diffusion Volume and surface diffusion allow for vacancy diffusion away from the neck region through the bulk or along the surface of the particle [72]. This stage of bonding process is where the majority of the deformation and densification of the powder interlayer occurs. Although the initial stage is controlled by the deformation of the powders the rate of collapse continually reduces as a result of the shrinkage in the surface area of the remaining powders. The final phase of the process is characterised by the eventual densification and elimination

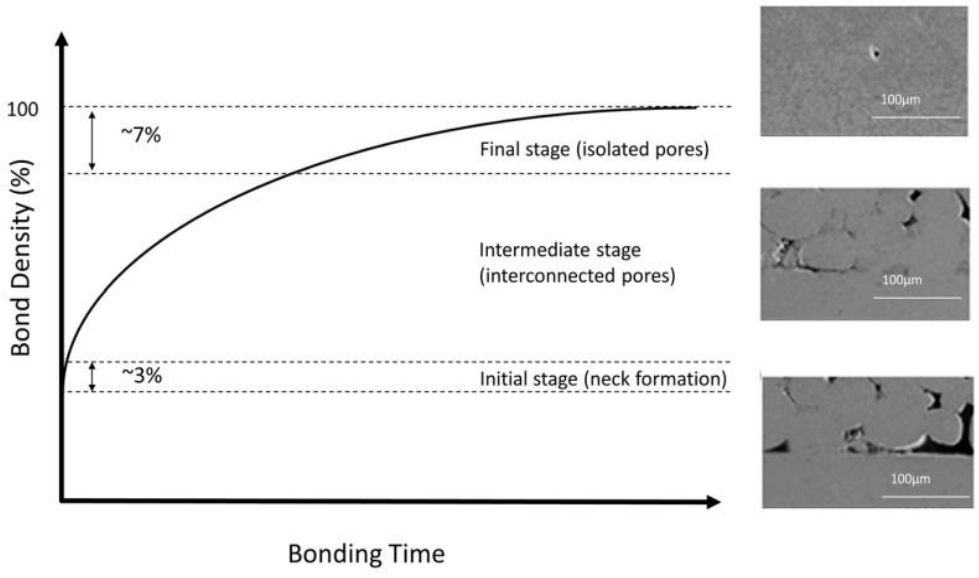

Figure 4.1.5.3: Showing the stages associated with the densification and sintering for Ti-6246 [71].

of the remaining pores via continued pore rounding and general pore shrinkage [73]. This final stage is generally considered to be the longest, with respect to time, as it relies on the diffusion mechanisms to eliminate the remaining pores.

The combination of the there key parameters is therefore what drives the mechanism associated in the stages described in Figure 4.1.5.3. Temperature increase would result in increased densification due to the exponential relationship between temperature and atomic diffusion. The force is related to the compaction of the powders especially during the early stages of the bonding cycle. Too low a force would result in insufficient compaction of powders and therefore decreased diffusion mechanisms and reduced bond integrity and too high a loading force results in excessive macro-deformation which can result in failed tests due to buckling etc. The final parameter of time is key in allowing for the diffusion and closure of the final pores which is the longest stage of the process an essential in producing high integrity bonds. The optimised conditions described in this project allow for the compaction and reduction of pores throughout the interlayer however the results show that there were still small pores remaining. Adjusting one of the parameters would allow for further reduction in the amount of porosity measured however the chosen parameters resulted in high integrity bonds that showed to have mechanical performance comparable to that of as received material as described in the following subchapters.

When considering all of the above factors the chosen optimised bond was #10. This parameter set allowed for significantly lower levels of porosity when compared with bonds done at 890ºC and yet still avoid the increased deformation levels observed with the bonds done at 930ºC. As well as porosity levels the effect of the parameters on the microstructure showed that bonds done at 930ºC showed to significantly impact on the V_f of the α_p as well as increasing the overall width of the HAZ. The volume fraction measurements combined with the results of the Vickers Hardness help to show that increasing the bonding temperature resulted in increased microstructural changes. As well as the effects of the higher bonding temperature the practical effects of this meant that the excessive distortion associated with the 930ºC bonds posed a significant risk with completion of bonds. The main concerns was to do with the bonding specimens deforming excessively and impacting on the quartz glass tube as well as misalignment becoming more of a safety factor at the higher temperatures and pressures.

4.2 Effects of PBHT on Optimised Ti-6246 PIB

In order to understand the effects of the key parameters during the bonding process, such as bonding temperature, analysis of the microstructure was vital. As well as this comparing the microstructure, within the HAZ, to that of the as received material was required in order to understand the changes associated to the bonding temperature and force. In order to characterise the changes in microstructure the samples were analysed in a Scanning Electron Microscope with images and EDX analysis performed at various points across each sample for optimised conditions of interlayer bonded Ti-6246. The micrographs below, Figure 4.1.5.1, show the microstructures seen at various points at the bondline and how it changes moving perpendicular to the bondline (away from the bondline). As well as the typical bond for this alloy a repeat bond was produced but with an additional anneal cycle, similar to a Post Weld Heat Treatment (PWHT) done for different types of welded materials. This was done in order to understand the possibilities of increasing mechanical properties for bonded samples, which will be discussed in the following chapters, by altering the microstructure within the HAZ and reducing residual stresses. The annealing cycle consisted of holding the sample at a temperature of 640ºC for 2hrs. The microstructure across the HAZ for this annealed sample is also shown below. The micrographs for the annealed and unannealed samples have been compiled in order to understand the effects the anneal cycle had on the microstructure.

When looking at the micrographs for the as bonded sample there is a variation across the HAZ. The images show the microstructure at intervals of 2mm, 4mm, 6mm and 8mm from the bondline. At 2mm, Figure 4.1.5.1a, from the bondline the α_p, the darker regions, and the α_s+β phase between the α_p can clearly be observed. The secondary alpha phase in this region has a reduced needle width than that observed in the as received material, with an approximate thickness up to 500nm. When moving further from the bondline the images shown at 4mm and 6mm show a pattern of a decreasing Volume Fraction (V_f) of the α_s phase. At 4mm the α_s phase is starting to decrease whereas at 6mm there is a clear drop in the V_f of this phase with an approximate drop of 67% in area when comparing it with the image from 2mm from the bondline. This trend of the decreasing amount of α_s is observed when looking at the microstructure taken at 8mm from the bondline. This image shows that there is almost no observable α_s remaining within the transformed β and hence between the α_p. With respect to the

α_p the V_f decreases closer to the bond interface within the HAZ with a clear coarsening effect taking place at the highest temperature region of the bonded sample. The change in V_f was observed within 8mm from the bond interface with the same formation and elongated appearance as the base material. Beyond 8mm from the bond interface the reverse trend was observed, with an increasing amount of α_s until the as received microstructure was observed beyond the HAZ which was up to 10mm from the bond interface.

Although plastic deformation has occurred the microstructure close to the bondline has not changed to a great extent. The coarsening of the α plates is present however they have not oriented themselves with the long direction parallel to the bondline as is the case with certain welding techniques.

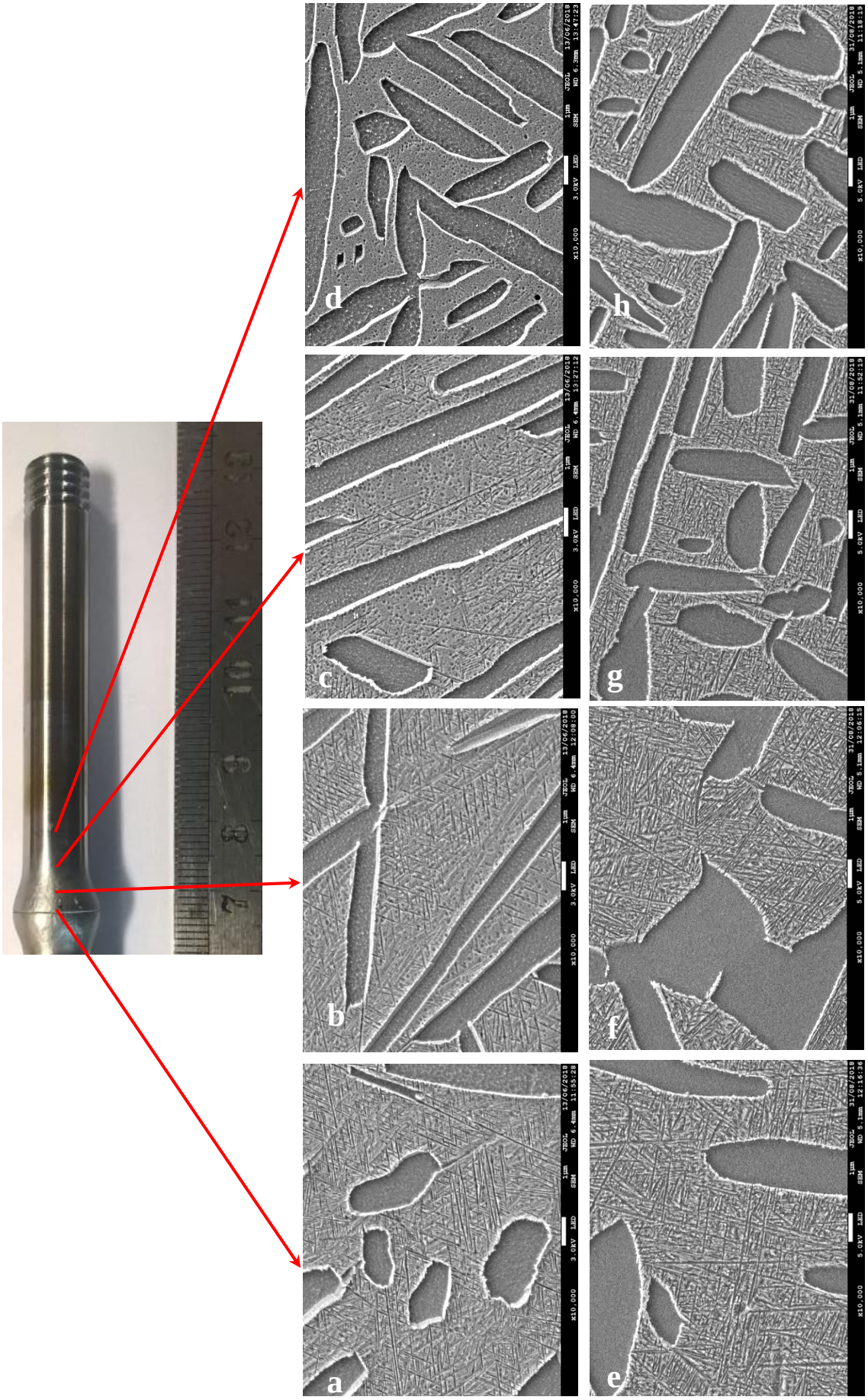

Figure 4.1.5.1 Microstructure within the HAZ of optimised Interlayer bond #10 and (a-d) and annealed (e-h) at 2mm, 4mm, 6mm and 8mm respectively from the bondline.

The same SEM imaging analysis was performed on the Post Bonded Heat Treated samples with the images in the HAZ shown from Figure 4.1.5.1e to Figure 4.1.5.1h. The image in Figure 4.1.5.1e shows the microstructure of the annealed sample at 2mm from the bond interface which shows a similar microstructure shown in the unannealed sample from the same region. The α_s is present between the larger α_p phase particles however there is an increase in the V_f of this phase in comparison to the as bonded sample. The structure of the α_s has a basket weave formation with a lath width also higher than that of the unannealed sample. Unlike the unaged sample, which shows a decreasing V_f of α_s, the α_s has increased in the same regions, shown by the micrographs from 4mm, 6mm and 8mm. The overall V_f of the α_s remains relatively constant throughout the HAZ for the aged sample, with a similar basket weave structure.

The microstructure within the HAZ shows changes with the different phases for this type of alloy. When looking at the microstructure within the interlayer region itself, which has an approximate thickness of 120µm, there is a slightly different change occurring.

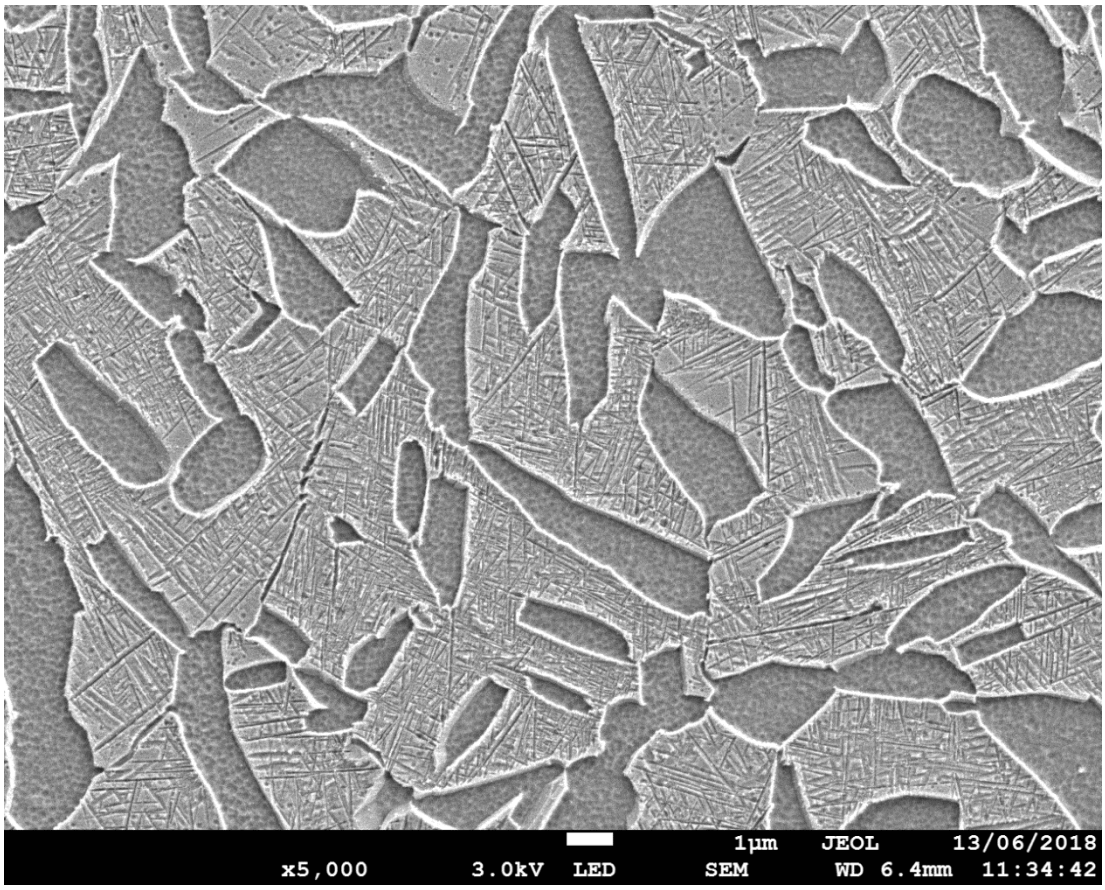

Figure 4.1.5.2 showing the primary and secondary alpha within the interlayer for the unannealed Ti-6246 interlayer bond

The micrograph shown in Figure 4.1.5.2 shows the microstructure observed within the interlayer region of the optimised Ti-6246 bond, which is ~120µm thick. This region of material correlates to the powder interlayer used between the two bonding samples before the test. The same phases are present as with the as received material however the structure of the phases is slightly different. Whereas the as received and material has needle like α_p the interlayer does not contain quite the same formation. The α_p here is more unstructured in shape and exhibits more of a partial bi-modal microstructure due to the globular α_p, with an average grain size of ~6µm, and the α_s laths in the transformed β grains.

This change in microstructure, from the powder interlayer region compared with the Ti-6246 forgings, is clearly evident when looking at the boundary between the two regions, shown in Figure 4.1.5.3. There is a clear divide in microstructure between the top of the image, corresponding to the interlayer region, and the bottom of the image which relates to the original Ti-6246 forging sample. Although the image below does not relate to the optimised bond conditions for Ti-6246 the trend is the same across all successful bonds. In Figure 4.1.5.3 the fine α_s is not visible due to the magnification

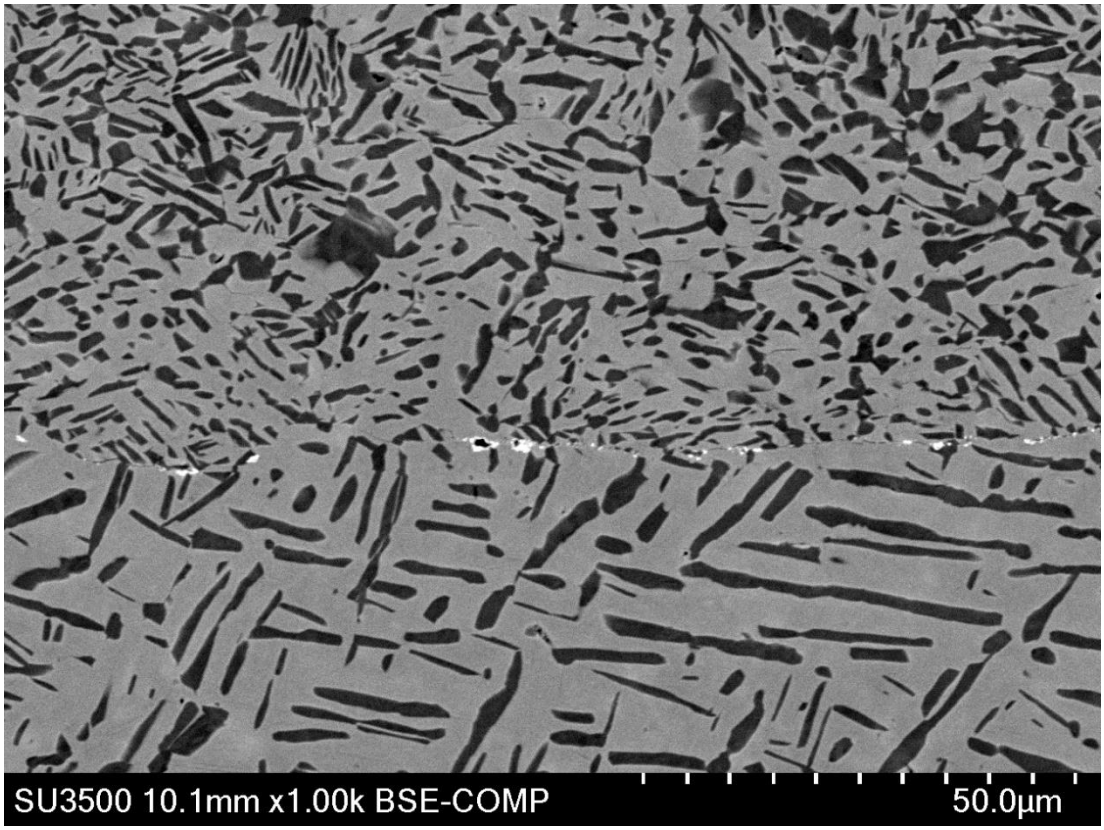

Figure 4.1.5.3 Backscatter Electron image of the microstructure at the interface between the interlayer and forged Ti-6246 sample for Bond #10

but also because of the image being taken using the Back Scatter Electron approach rather than the Secondary Electron method. The micrograph also illustrates the increased V_f of α_p within the interlayer region compared with that in the HAZ. Another key factor that can be obtained from the micrographs taken in around the bond region is the temperature during the bonding cycle. Although the target temperatures were achieved during testing previous work has shown that when heating using electrical resistance heating the internal temperature of the specimens can increase beyond the target temperature and potential above the β_T. However, the micrographs show that the temperature during bonding has not exceeded the β_T for this alloy due to alpha phase still having a relatively high V_f within the interlayer and HAZ.

Although there is a difference in microstructure between the annealed and unannealed samples within the HAZ, the change within the interlayer region is not as drastic. Figure 4.1.5.4 below shows a micrograph of the interlayer region for the Post Bond Heat Treatment (PBHT) sample. The principle features are very similar when compared with the unannealed sample with globular α_p with a very similar grain size

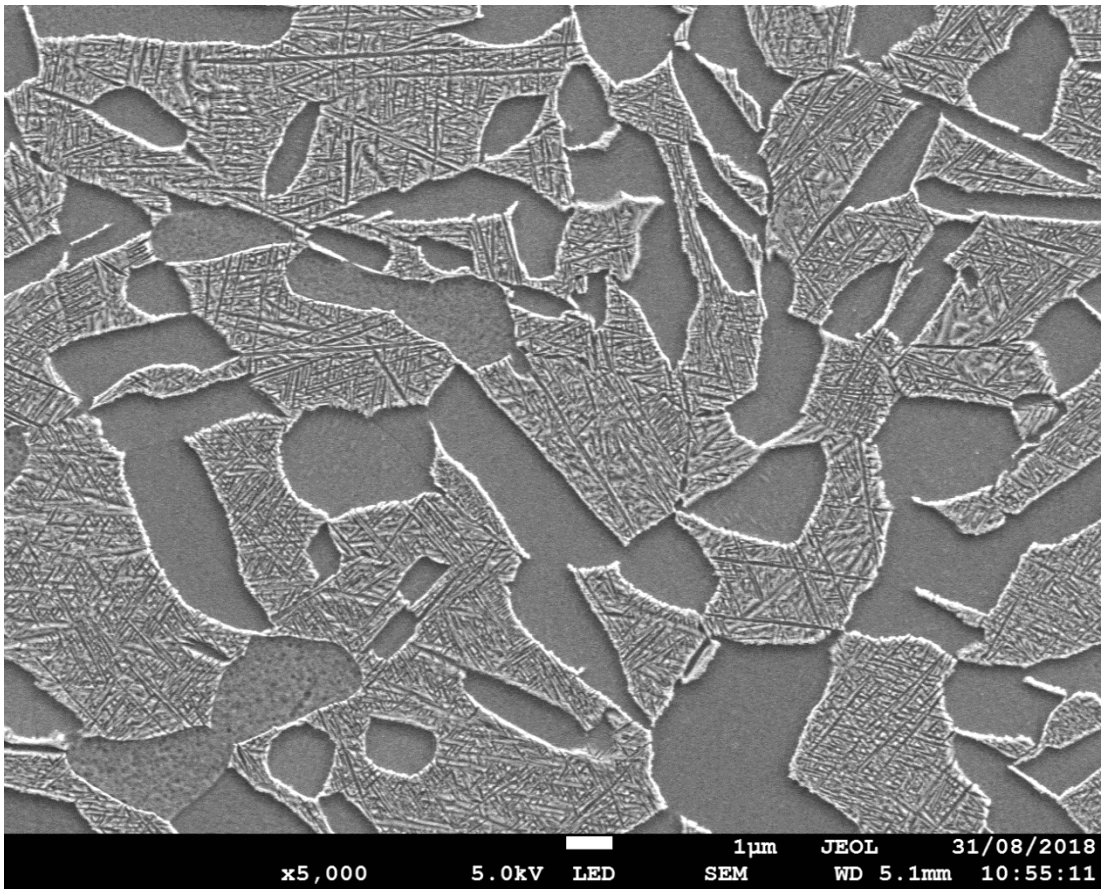

Figure 4.1.5.4 showing the primary and secondary alpha phase within the interlayer for the annealed Ti-6246 interlayer bond.

and fine α_s within the β matrix. The main difference is that the V_f of the α_s has increased slightly although it is not as big an increase as seen within the HAZ. This is primarily due to dissolution of the α_s not occurring within the interlayer region and hence, before the annealing stage, the V_f is already relatively high.

The PBHT does impact the V_f of the α_s more within the HAZ than within the interlayer region. For the unaged sample the amount and size of the α_p increases with increasing distance from the bondline, however the α_s is depleted within the β matrix at ~8mm from the bondline interface. There is a gradual drop in the α_s phase with increasing distance from the bondline starting from approximately 2mm away from the interface. When comparing this with the aged sample however the α_s is no longer depleted within the β matrix at the same point in the unaged sample. The annealing cycle has had a significant impact on the α_s. The greatest effect of the PBHT is the precipitation of the α_s phase within the surrounding β matrix. This precipitation has occurred where in the unannealed sample the volume fraction of the α_s had reduced due to the temperature from the bonding cycle allowing the dissolution of this very fine phase.

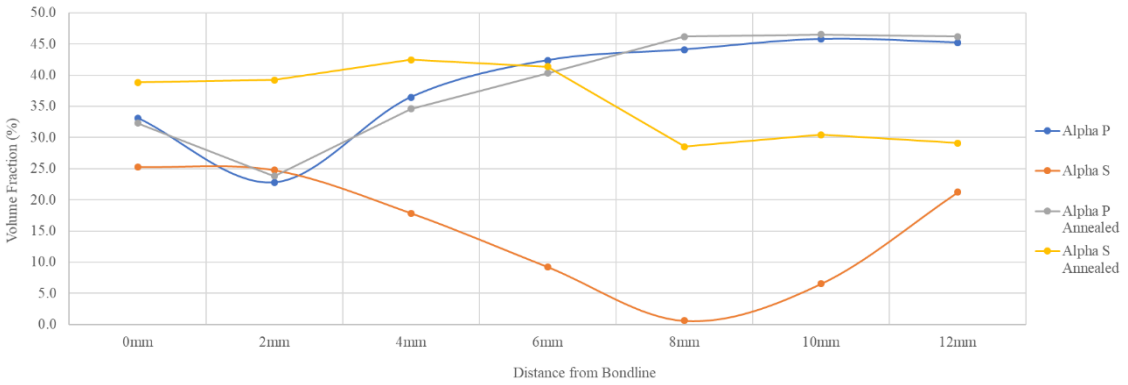

Figure 4.1.5.5 Chart showing the Vf of the two alpha phase for the optimised conditions as well as the PBHT.

The plot above compares the volume fraction of the primary and secondary alpha phases within the HAZ for the optimised bond (#10) as well as the optimised bond + anneal. The results show that the V_f of the α_p as followed the similar trend for both bonds, the main differences is in the V_f of the α_s phase. This chart shows the same trend that was observed through the image analysis detailed above, the V_f has increased significantly with the PBHT stage with a slight reduction in the 8mm region to ~30% whereas the as bonded sample showed an almost complete drop in the V_f of the finer alpha phase. This increase in the α_s phase can be seen to impact on the hardness within the HAZ which is detailed below.

4.2.1 Vickers Hardness Testing

The Vickers Hardness testing allowed for a hardness map to be generate showing the hardness distribution across a sectioned sample which had been bonded using the Interlayer Bonding process described above. The result of the hardness map for the optimised interlayer bond for Ti-6246 is shown in Figure 4.2.1.1. It shows a range of colours which correspond to high or low hardness values. For example, a higher hardness value would show as green and a low value show as red. The Vickers Hardness results shown here are from further investigation of the hardness values shown in the Results chapter for all the interlayer bond trials. The selected optimised bond was further characterised in order understand if there were any further variances parallel to the bond interface.

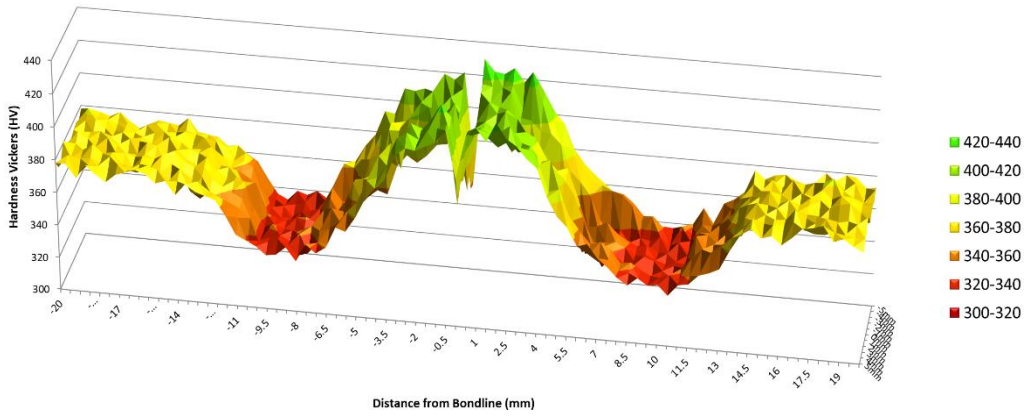

Figure 4.2.1.1: Vickers Hardness profile map for the HAZ of optimised conditions for PIB Ti-6246, Bond #10.

The hardness results for the optimised Ti-6246 bond shows a changing hardness across the HAZ. The chart shows at approximately 16mm away from the bondline the measured hardness values are equal to that of the as received material, ~375Hv. Moving closer to the bondline the hardness begins to drop to around ~310Hv at 10mm from the bondline. This undulating pattern is carried on closer to the bondline with the hardness increasing further beyond the as received material values, up to a peak value of ~418Hv. The results also clearly show the hardness within the interlayer region is considerably lower than the immediately adjacent microstructure of the bonded specimens and more in line with that of the as received material.

The change in the hardness across the bonded specimens displays the HAZ and shows how it is approximately 26mm in length. When relating this back to the results from

the heating profile of the selected induction coil it can be seen that the temperature across the specimen remains above 810^0C within a 20mm band. The temperature profile matches closely with the hardness variations seen in the figure above.

A comparison was done for the Vickers hardness across a bondline that had been annealed in order to understand the difference in mechanical properties before and after the annealing process. The heat treatment step involved holding the entire bonded sample at 640ºC for 2hrs. This temperature and time values are associated with the

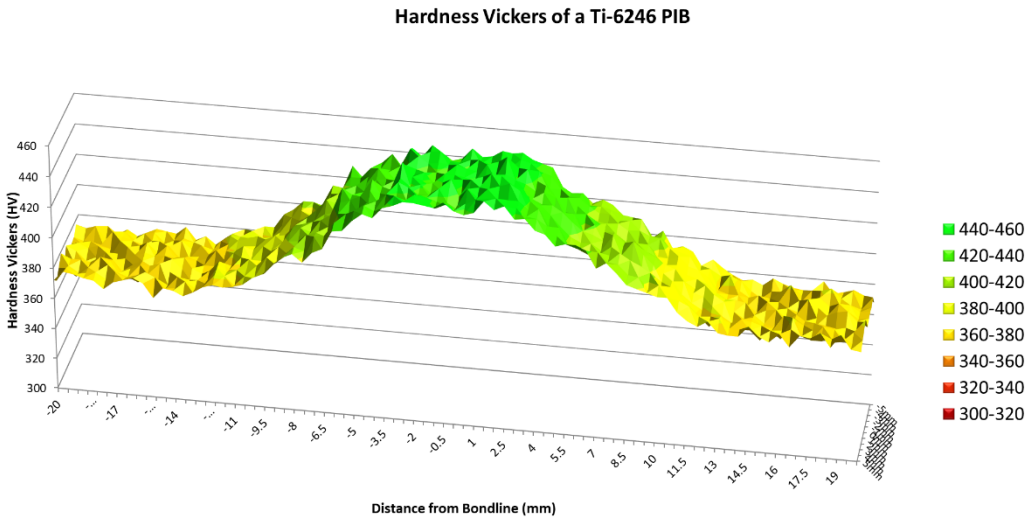

Figure 4.2.1.2: Vickers Hardness profile map for the HAZ of the annealed PIB Ti-6246 using bonding parameters from Bond #10.

heat treatment conditions for this material in order to produce the optimum mechanical properties for its application as a BLISK material. The hardness map below, Figure 4.2.1.2, shows the result from this annealed sample. The result from this map displays the effect the anneal process has had on the bond hardness profile. The overall HAZ zona has remained largely unchanged however the hardness in this region has changed significantly. The aged sample shows a gradual increase in hardness from outside the HAZ towards the centre of the bondline. This increase peaks at a value of ~445Hv which is similar to that seen in the unaged sample. The key difference between the 2 samples is the region between 2mm and 13mm from the bondline. For the aged sample the hardness simply changes at a steady rate, between ~380Hv to 440Hv, and does not decrease to below that of the as received material, as is observed for the unaged sample. Also, the variation from the interlayer and the adjacent microstructure is not as varied, the hardness seemingly drops very little. The results for both the annealed and unannealed sample show a consistent result when looking parallel to the bondline.

4.3 Mechanical Performance of Ti-6246 Interlayer Bonds

In order to characterise the bonds produced via the PIB method a range of factors need to be analysed. Previous chapters have outlined the results obtained from microstructure and porosity analysis of the bonds whereas this chapter will set out the mechanical properties associated with bonds produced via the Interlayer technique. A range of techniques were used during the study in order to gain a broad understanding on how the bonded material would behave under different conditions. The key mechanical tests carried out include Tensile, High Cycle Fatigue (HCF) and Vickers Hardness testing. Each type of testing reveals different properties of Ti-6246 Interlayer bonds and how adding an annealing step can change these properties. The results of the optimisation trials showed that Bond #10 produced the optimised conditions when factoring effects on microstructure, porosity distribution and hardness across the HAZ.

4.3.1 RT Tensile Testing

Although microstructure and porosity analysis can give a good understanding of mechanical properties and bond integrity, one of the best ways of knowing properties such as tensile strength is to complete mechanical tests. The tests that were conducted involved machining the tensile samples from the middle of the bonded samples, as described in the experimental chapter of this study. The initial tests focused on the room temperature tests and were conducted with as received material, Interlayer Bonded Ti-6246, Interlayer Bonded Ti-6246 with an anneal and also a bond done without an interlayer in order to understand the effects of the interlayer on tensile strength. The results of the tests are displayed in Figure 4.3.1.1 as well as summarised in Table 3.2.2. The result for the as received material is in line with what is expected for this alloy that has been β processed. The tensile strength of the alloy is approximately 1210MPa with a Yield Strength of ~1002MPa. The modulus was approximately 125GPa with an elongation of approximately 11.5%. The as received results provided a base line with which to compare the interlayer bonded test results to.

Table 4.3.1: Comparison of room temperature tensile results for various bonds of Ti-6246

	Ti-6246 Base Material	**Ti-6246 PIB**		**Ti-6246 PIB + anneal**	**Ti-6246 (No Interlayer)**	**Ti-6246 (No Interlayer + anneal)**
		Test 1	**Test 2**			
UTS (MPa)	1210	1117	1121	1100	979	1028
Yield Strength (MPa)	1002	968	956	966	922	963
Elastic Modulus (GPa)	125	102	106	102	90	90
Elongation (%)	11.5	6.8	5.7	8.68	0.8	2.5

The tensile test result for the optimised bond for Ti-6246 using GA powder showed good room temperature properties, closely resembling the characteristics of the as received material. The UTS and yield stress of the optimised bond was 1117MPa and 968MPa respectively. With respect to the modulus of elasticity the bonded sample showed a value of 102GPa and an elongation to failure of 6.8%. The results show a decrease in all properties in comparison to the as received material tests, with a drop in UTS of nearly 8%, with a slightly reduced drop in Yield strength observed. For the optimised conditions an additional room temperature tensile test was completed in order to understand the repeatability of the optimised conditions. The results, shown in Table 3.2.2, show that the properties are very similar for both tests with minor increases in UTS and the Elastic Modulus and small drop in Yield strength and Elongation.

The above describes the results obtained from the optimised conditions for Ti-6246 interlayer bonds without a post heat treatment stage. Further tests were done which looked at the effect of utilising the post joining anneal heat treatment on the mechanical performance of the bonds in order to further increase performance. A post

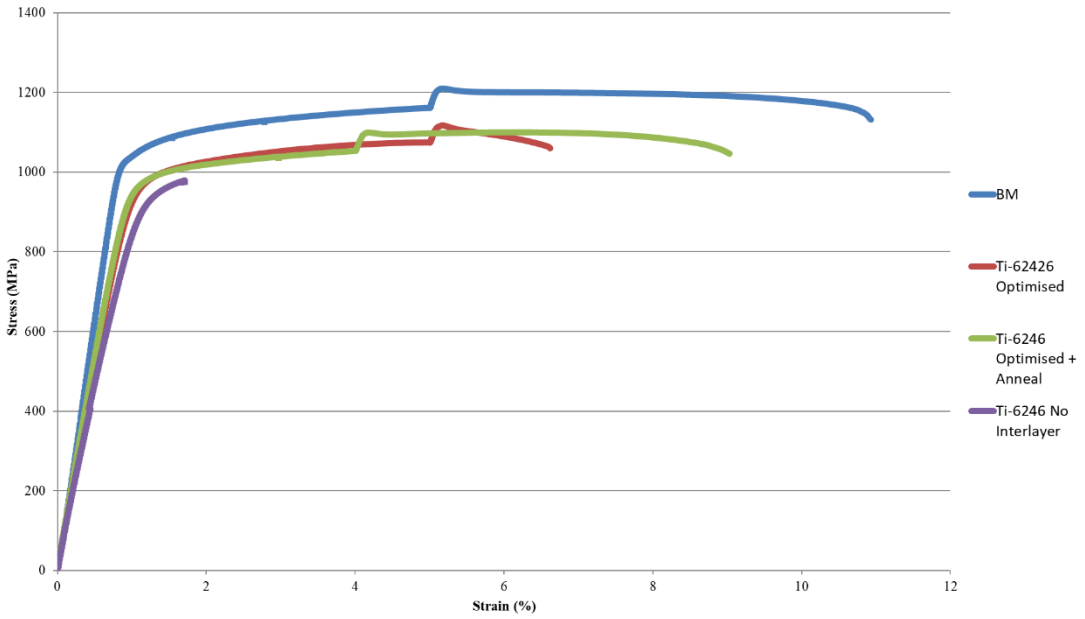

Figure 4.3.1.1: Chart illustrating the Room Temperature tensile properties for various Ti-6246 bonds.

join heat treatment of 640^{0}C for 2 hours was done on a Ti-6246 interlayer bond and subsequently tensile tested at room temperature with the results of the test also shown in Table 3.2.2. The results show that the UTS, Yield strength and Elastic modulus, of the heat treated sample, remained very similar to that of untreated interlayer bond. However, the key difference is with regard to the elongation of the tensile test, which increased from 6.8% to nearly 8.7% and closer to that of the as received material.

As well as the results of the optimised conditions for interlayer bonded Ti-6246, further room temperature tests were done for bonded samples which did not incorporate the powder interlayer but kept the same process parameters as the optimised conditions. The result for this test is also shown in Table 3.2.2 and there are noticeable differences when compared to the interlayer bonded test. The UTS, Yield strength and modulus for the test was 979MPa, 922MPa and 90GPa respectively. The largest difference in properties that was observed was with respect to the elongation of the tested sample which was measured to be 0.8%. This test highlighted the difference of incorporating an interlayer, under the same conditions. The test failed within the bondline region with very little necking, the fracture surface being perpendicular to the bonding direction. By adding a post bond heat treatment cycle the properties increased slightly, however still remained significantly lower than that of the interlayer bonded samples.

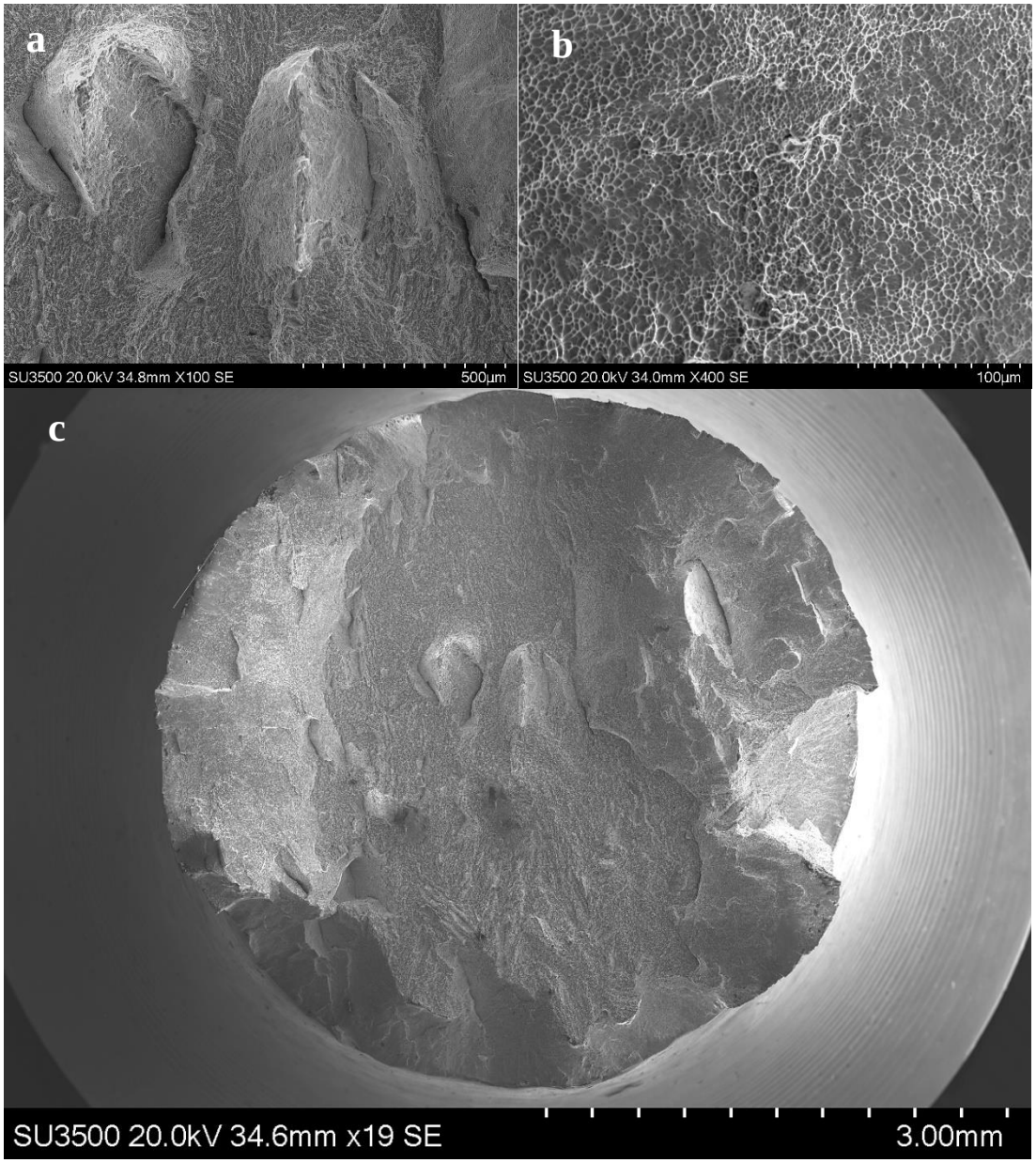

Figure 4.3.1.2(a-c) Fracture surface of as received Ti-6246

The images above show the fracture surfaces associated with the room temperature tensile test for the as received material as described in the experimental section of the study. The fracture surface shows evidence of a moderately ductile failure for this alloy system with dimples observable across the central portion of the surface indicating at least a part ductile failure of the sample. As well as the small dimpleas across the central part of the fracture surface, there are also some cleavage facets visible with smoother faces. As is typical for room temperature tests for this type of alloy which is expected to have a moderate amount of ductility there is evidence of the initial formation of the crack within the central portion of the sample during the test. Final fracture of the specimen occurs via rapid crack propagation around the

perimeter of the sample, the most detailed evidence of this is shown at the left and right sides of the sample which display the fracture surfaces being at approximately 45º to the tensile axis. The failure can be described as moderately ductile as the surface shows ductile features as well as the overall sample showing small amounts of visible plastic deformation.

The fracture surfaces of the powder interlayer bonded Ti-6246 samples are shown in Figure 4.3.1.3. The surfaces shows indications of a medium ductile fracture surface with initial signs of a classic cup and cone observed with moderate ductile failures as well as the final fracture surface, at the edges of the sample, being approximately 45^0

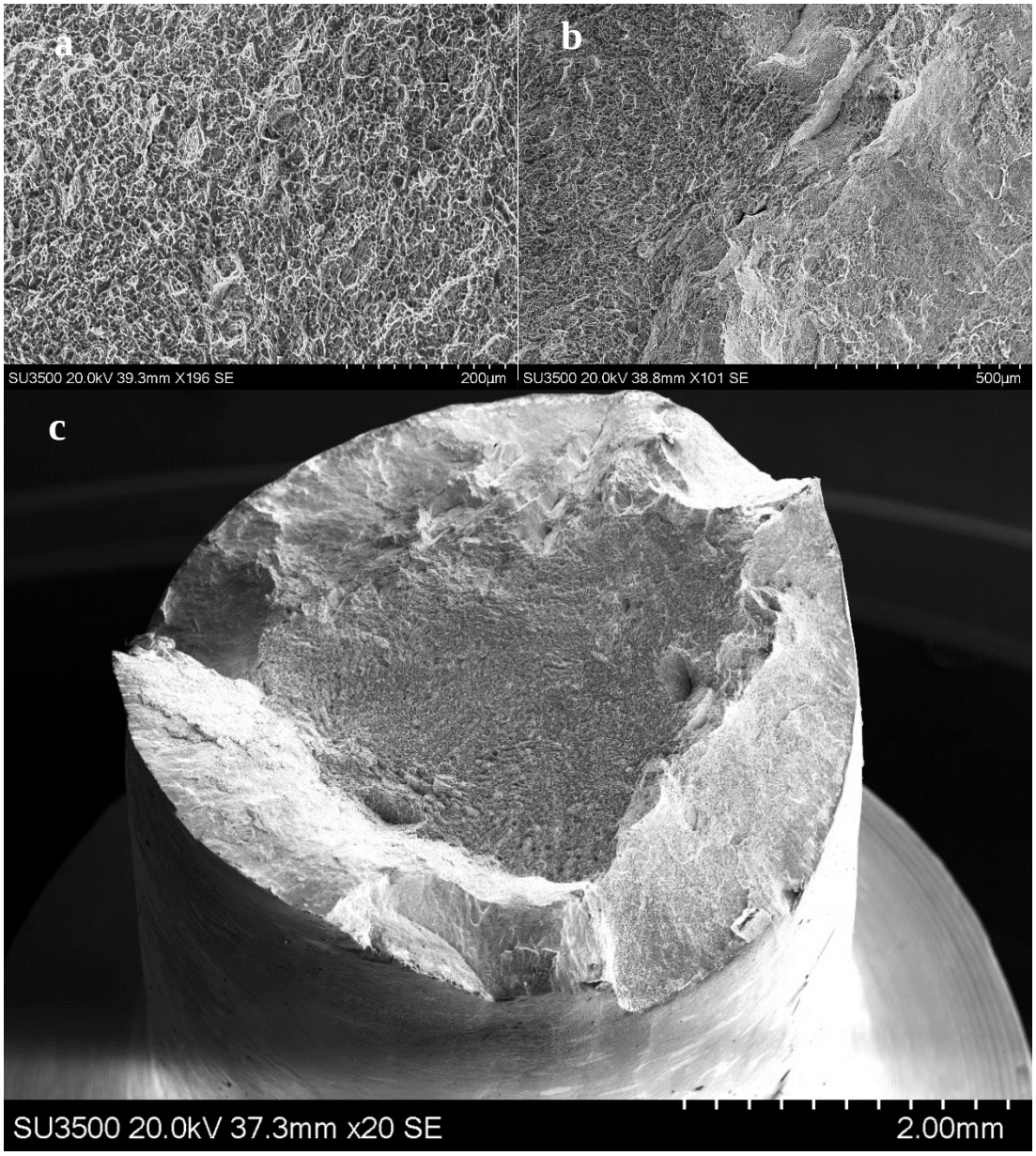

Figure 4.3.1.3: Fracture surface of optimised conditions for Interlayer bonded Ti-6246.

relative to the tensile stress direction. With the failure located away from the bondline and within the bulk material, this type of failure is typical for this alloy system. Higher magnification images shows that some parts of the central portion of the rough fracture surface is made up of dimples and voids. However, the transition from the overload region during final failure to the central portion is made up of a small number of macroscopic cracks with areas of cleavage like facets also observable within the overload areas. This type of fracture surface along with the relevant tensile test results indicate a fracture which is moderately ductile with a combination of brittle and ductile features present on the fracture surfaces.

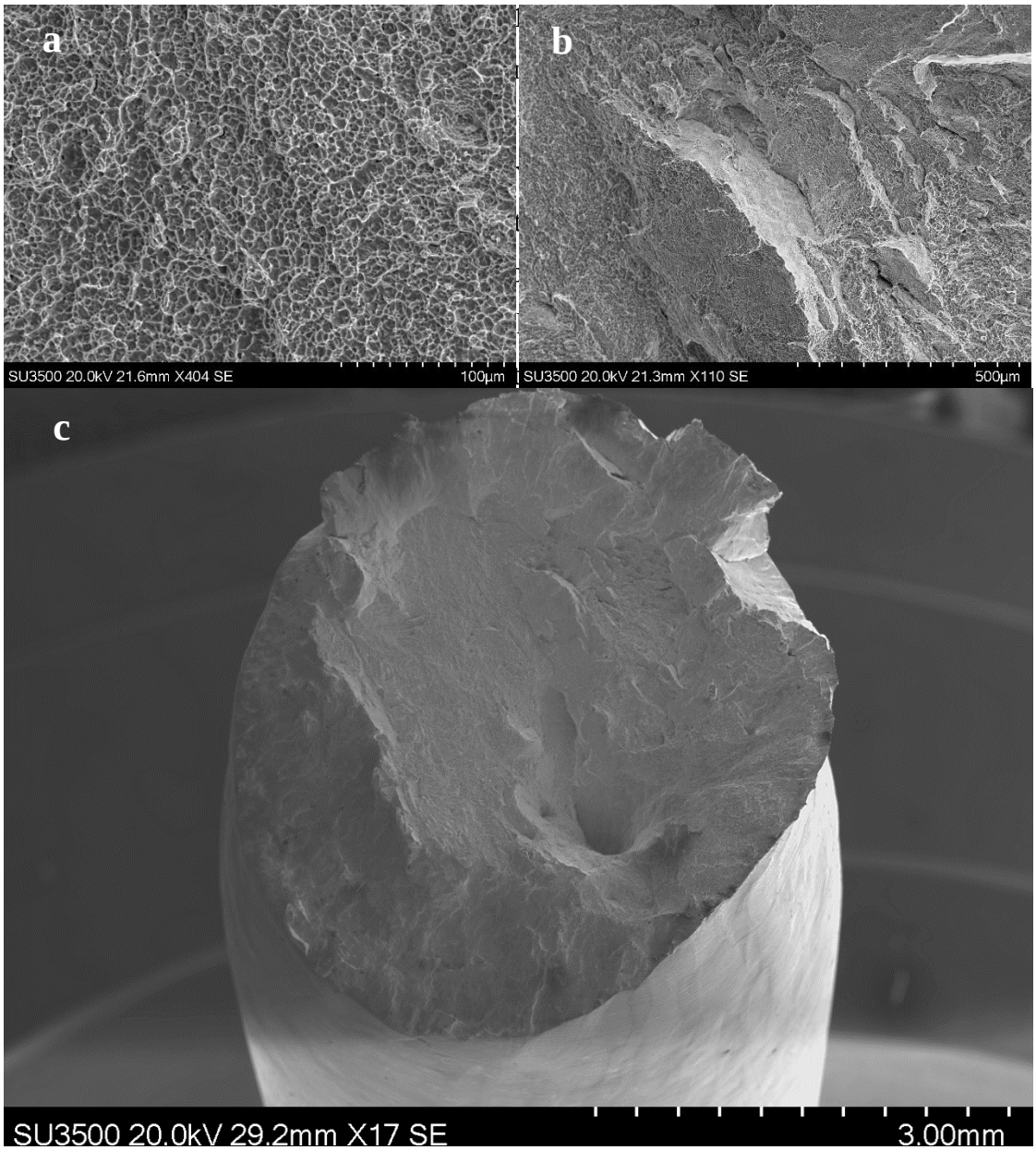

Figure 4.3.1.4(a-c) Room temperature, tensile fracture surface of PBHT PIB Ti-6246 sample

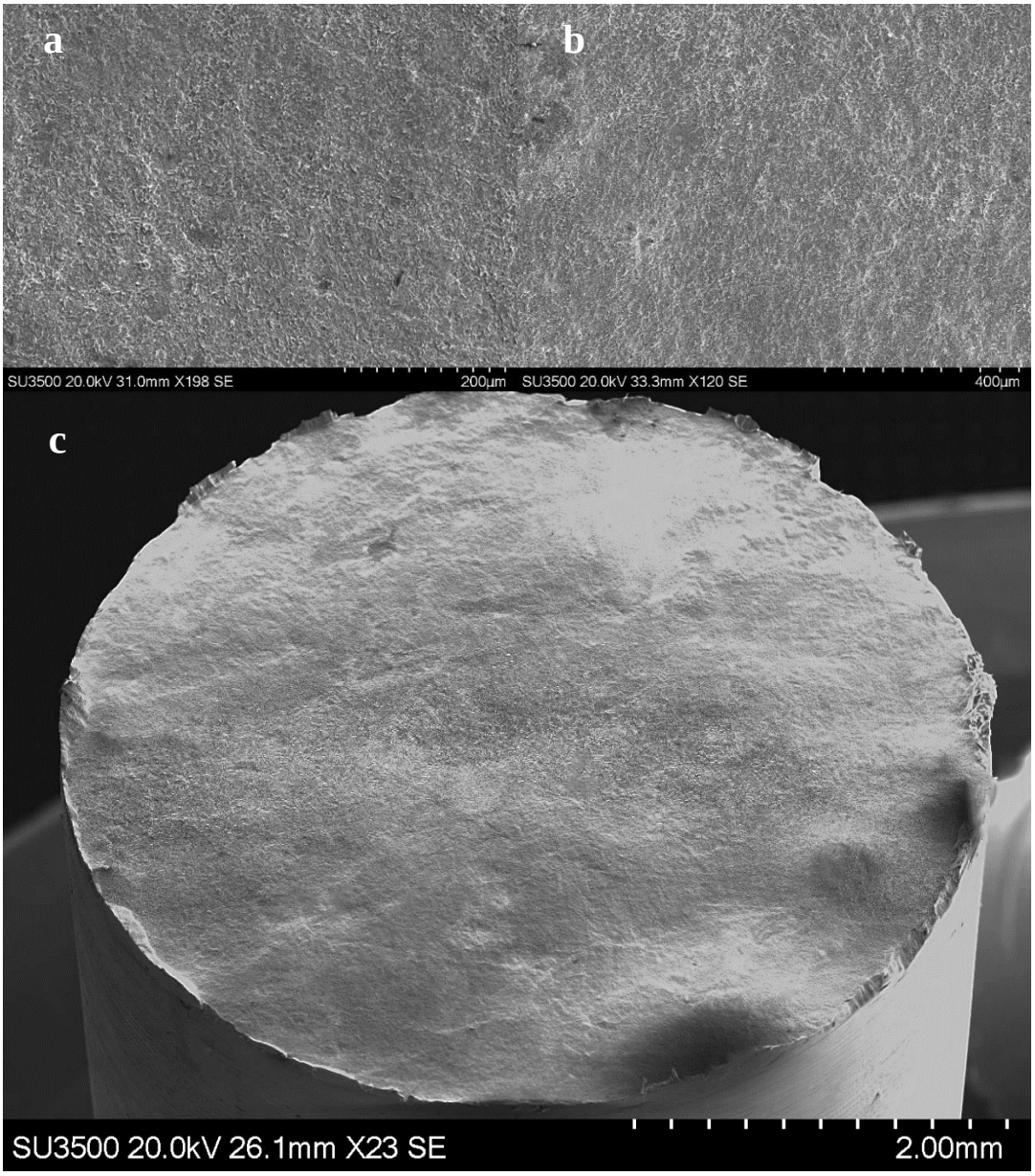

Figure 4.3.1.5: Fracture surface of optimised conditions for Ti-6246 without the use of a powder interlayer.

The fracture surface of the bonded sample which had no interlayer, Figure 4.3.1.5, shows a clearly different fracture surface than that for the optimised Ti-6246 test. This surface shows almost no observable signs plastic deformation of the sample taking place during the test and is expected when looking at the very low elongation value for this test. The fracture surface shows a cleavage across the bond interface with the crack direction perpendicular to the tensile loading direction. The fracture mechanism shows that the early formation of voids, during the tensile test, is accelerated due to the lack of bond integrity as well as them being in the same plane.

4.3.2 High Cycle Fatigue Testing (HCF)

Further mechanical testing was done for the optimised conditions for Ti-6246 under the PIB system. This involved high cycle fatigue testing which was conducted using the settings as described in the experimental chapter of this report. The purpose of the testing was to understand the extended mechanical performance behaviour of room temperature cyclic loading as well the corresponding failure modes under these conditions. The tests that were performed allowed for the creation of a cycles to failure graph detailing the number of cycles to failure under different stresses. The results showed that increasing the stress resulted in the reduced number of cycles to failure as compared to the reduced stress tests performed better with respect to cycles to failure. The longest test had a total of just over $7.5x10^6$ cycles to failure with the shortest lasting 34445 cycles before failure. This variance in cycles to failure is observed from a High Cycle stress loading of 550MPa to 750MPa. The results of the tests are plotted in Figure 4.3.2.1, which show the distribution of the cycles to failure for each of the tests conducted, with the x axis plotted along a logarithmic scale.

Although the results followed a strong trend there were results that showed significant variance away from the trend. The key result was the test, which was done at 650MPa, and showed a slightly reduced number of cycles to failure that was observed for the test done at 700MPa. This test result meant another test was conducted at this stress level which showed an increased life, approximately 900,000 cycles.

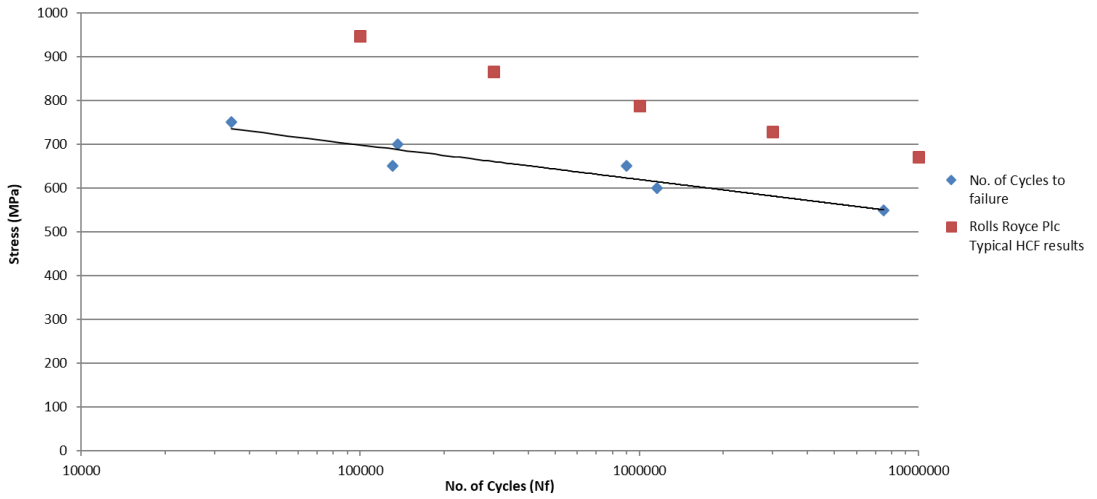

Figure 4.3.2.1: Cycles to failure results for HCF for optimised interlayer bonded Ti-6246

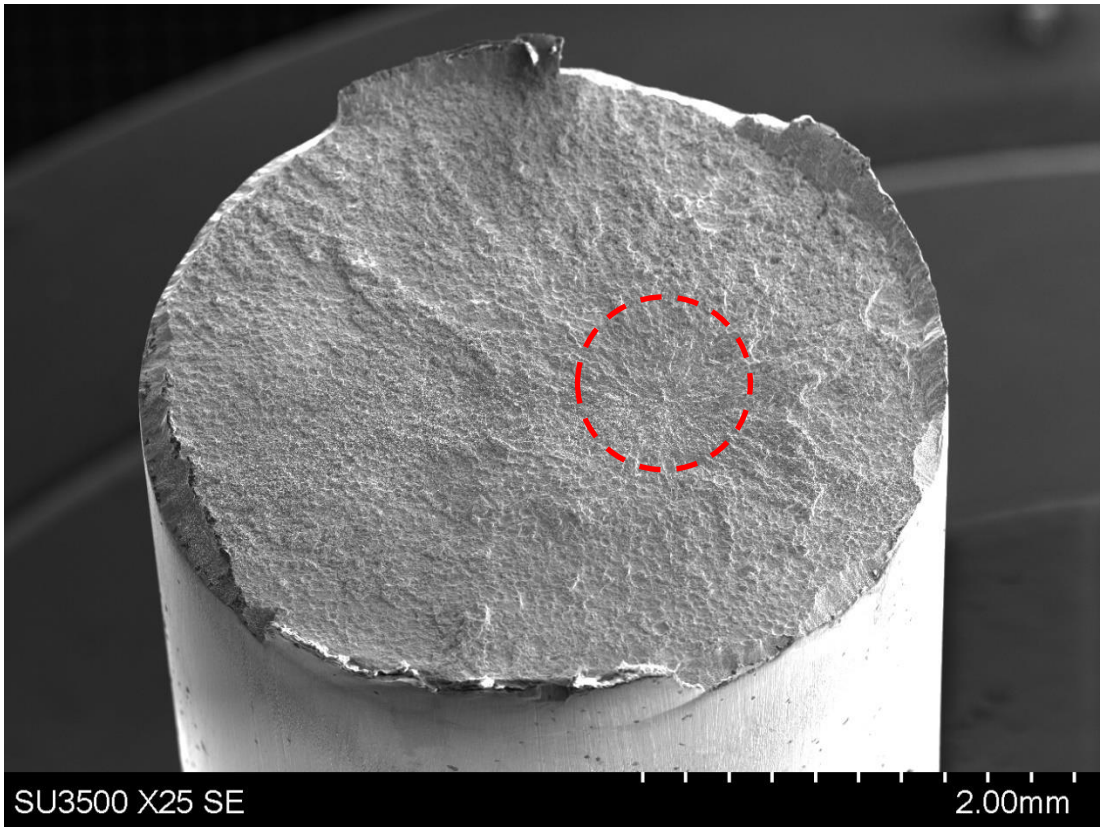

Figure 4.3.2.2: Fracture surface for HCF of interlayer Ti-6246

The results from the tests showed that all the samples fractured at the bondline. The fracture surfaces were then further analysed in order to understand the failure mechanisms taking place. When analysing the samples from the Fatigue tests there were clear subsurface crack initiation sites on each of the samples. Figure 4.3.2.2 shows an example of the initiation site that was observed for all the samples with the image below associated to the test done at 700MPa with the measured defect to be approximately 38μm in length. The initiation sites were investigated further in order to try and understand the causes of the trend seen across all the fatigue specimens whether it be at the low stress levels or the highest stress levels.

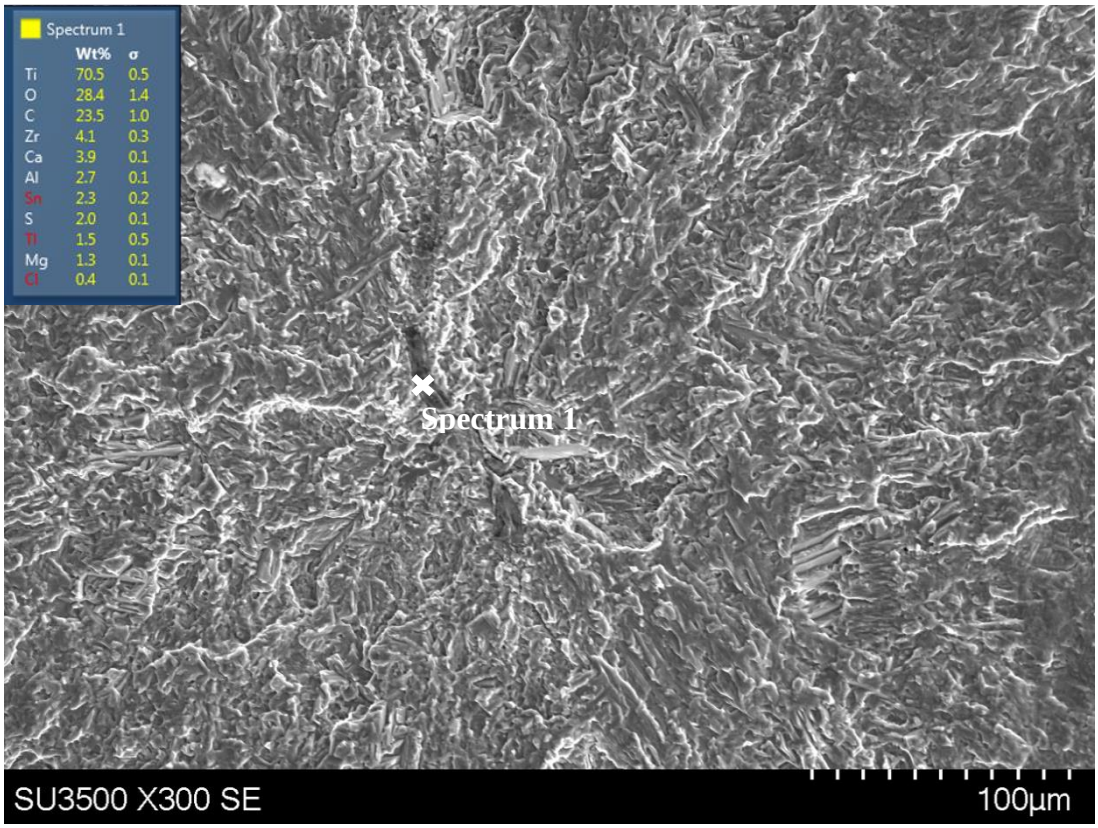

Figure 4.3.2.3: Fracture surface of a HCF specimen showing the crack initiation from contamination.

The fracture surface images, obtained via the SEM, showed that there appeared to be a surface inclusion located at the initiation sites within the surfaces as shown in Figure 4.3.2.3. These sites were further investigated using EDX analysis in order to determine the chemical composition of the inclusion.

The result of using a point EDS scan on one of the inclusions, is shown in the spectral graph in Figure 4.3.2.3 and show that there are a number of elements that were detected which are not included as one of the alloying elements of Ti-6246. For this sample the largest inclusion element detected was Carbon. Other elements that were detected included Oxygen, Silicon and Sulphur as well as other. The high cycle fatigue test conducted at 650MPa and failed after approximately 130,000 cycles showed a clear defect at the initiation site of the fracture surface. The defect, shown in Figure 4.3.2.4, is clearly in the shape of a powder particle with an approximate diameter of 40µm within the surface of the sample.

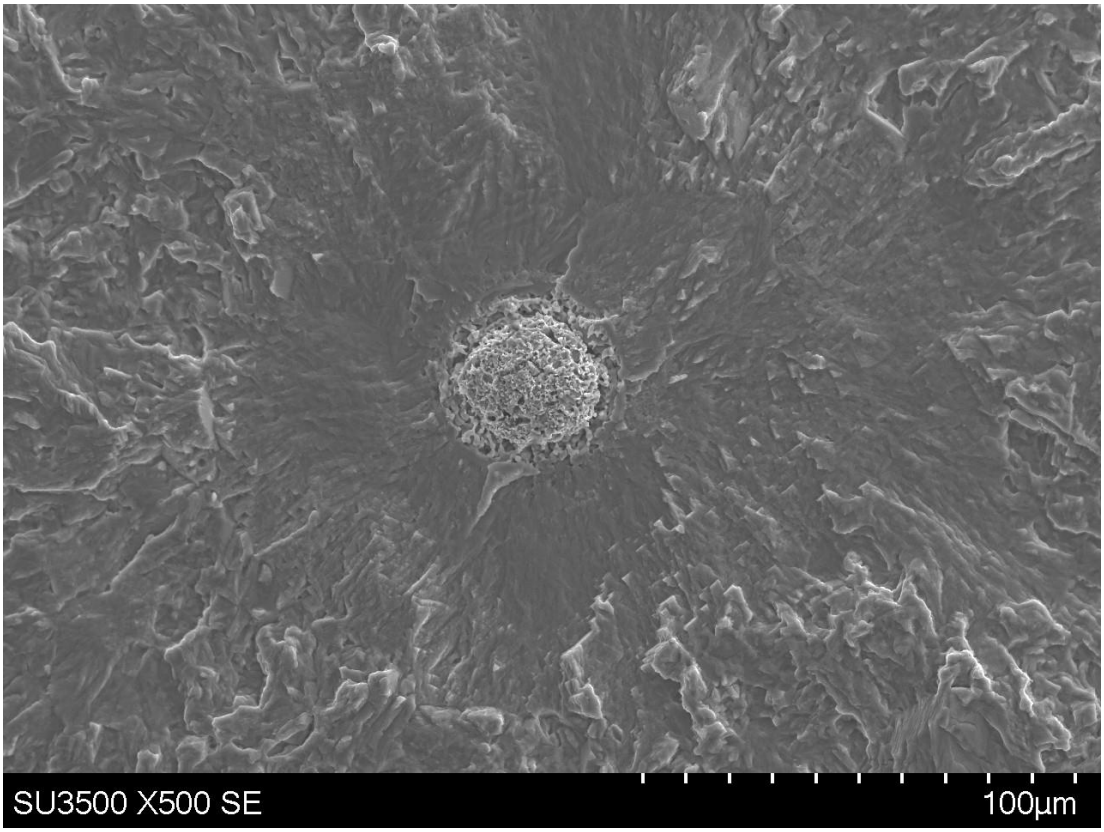

Figure 4.3.2.4: Fracture surface from HCF done on interlayer bonded Ti-6246 with the initiation site containing nickel powder contamination.

The EDS map that was created showed clearly the chemical makeup of the inclusion, shown in Figure 4.3.2.5. The EDS maps of the inclusion clearly show that there an increase in the amount of Nickel observed in this region. The surrounding area is made up of the constituent elements found in Ti-6246 however a point scan on the powder defect showed other elements also were present.

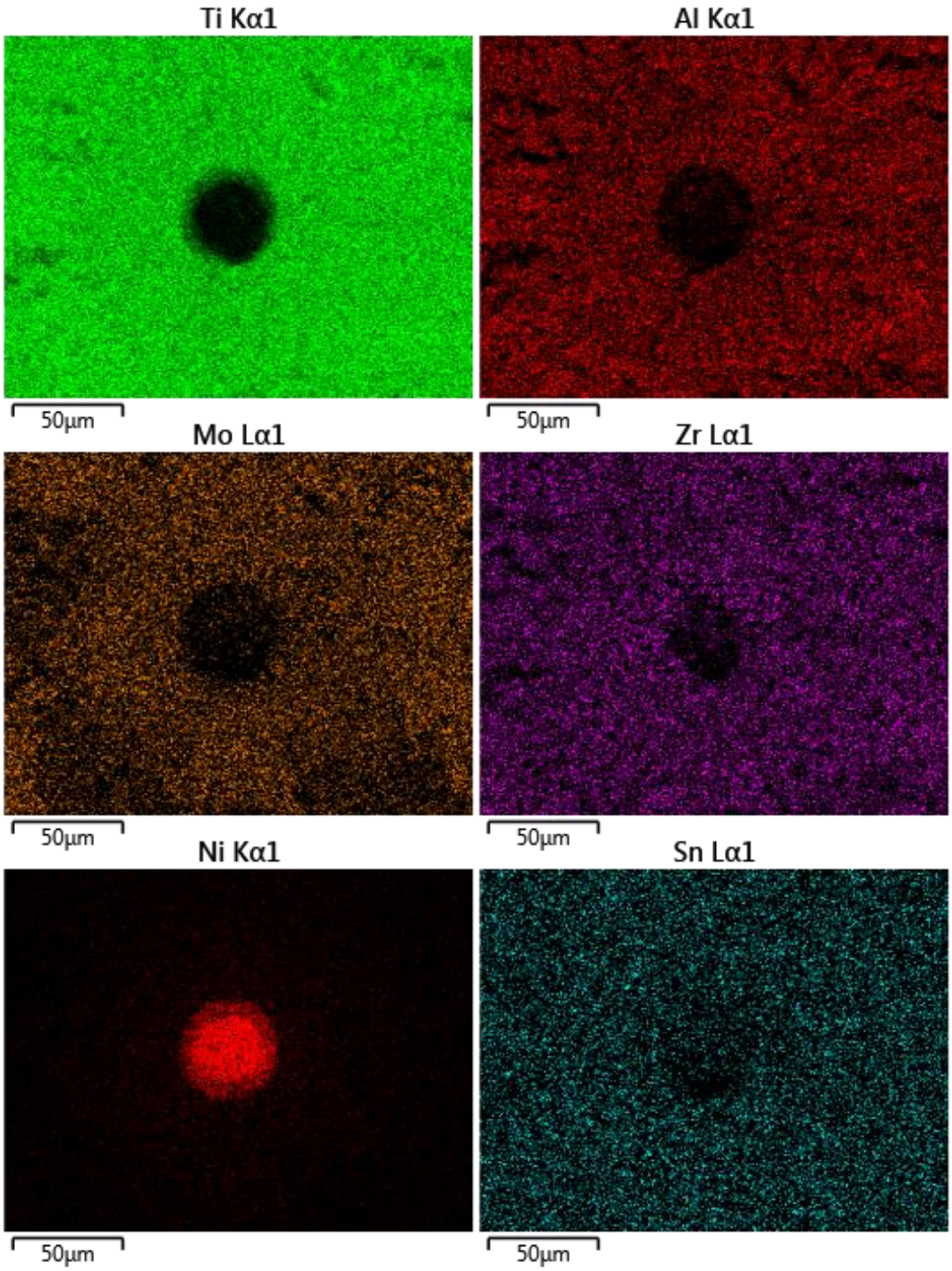

Figure 4.3.2.5: EDS maps of the crack initiation site containing nickel powder contamination.

Beyond the initiation sites of the fatigue samples the fracture surfaces are fairly typical for sample which have undergone cyclic loading at relatively high stresses. The surfaces clearly indicate the direction of the crack propagation away from the initiation site. From the fracture surface images, the initiation site can be observed along with

Figure 4.3.2.6: Macroscopic image of the fracture surface for the interlayer bonded HCF specimen.

the features common in fracture surfaces which can help to show the crack growth rate.

Beyond the crack initiation site, the surface shows signs of the slow and fast crack growth rates, visible by the progression marks. These marks show the transition from where the initial crack growth is slow after initiation however during the overload phase of the test the loading results in fast, instantaneous crack growth.

For the fracture surface shown in Figure 4.3.2.6 the results show that the fatigue crack growth region is a portion of the overall fracture surface, with the majority being the rupture surface from the final phase of the fatigue test. When looking at the fatigue zone at high magnifications the fatigue striations can be observed as shown in Figure 4.3.2.7. Each striation is an artefact of the cyclic loading and can be observed due to the crack growth and the resulting arrest of the crack. The spacing also indicates a relatively equal stress intensity, with increased stress intensity the spacing would increase and vice versa with a lower stress intensity.

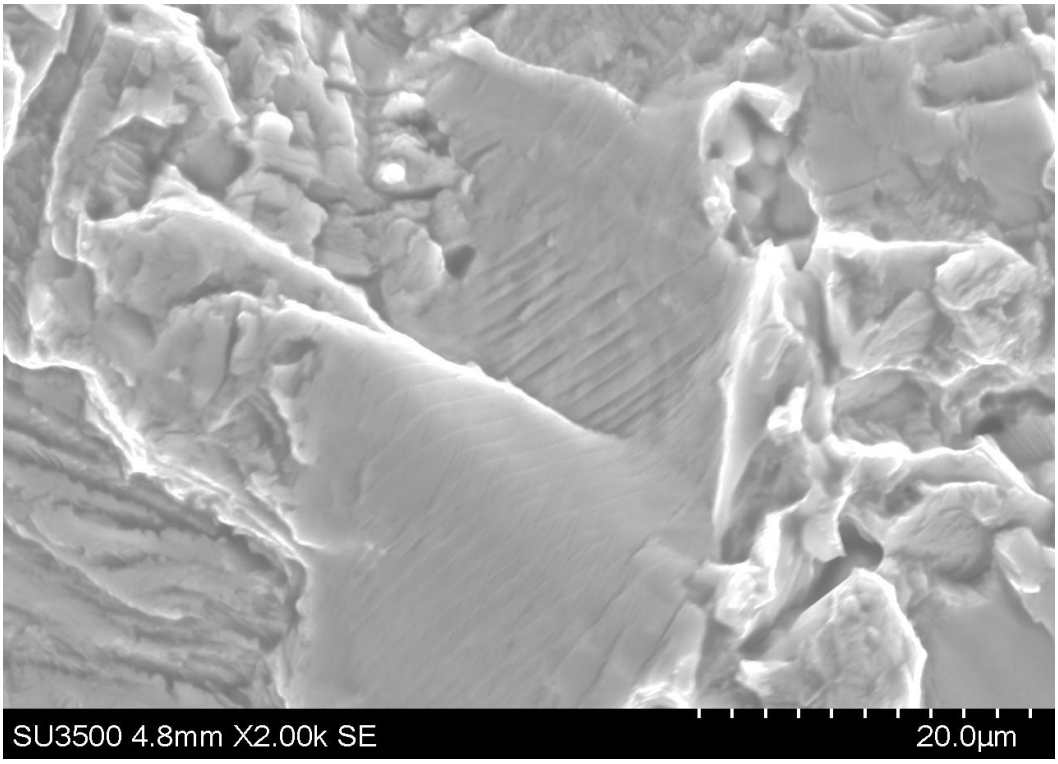

Figure 4.3.2.7: High magnification image showing the striations on the HCF fracture surface.

In order to further understand the HCF results they can be compared against typical cycle values for repaired Ti-6246 that would typically be used in industry. The results showed that there is a significant drop in the cycles to failure for the interlayer bonded Ti-6246 samples when compared with typical repaired values. The comparison is made between HCF test results under the same conditions as the interlayer samples and show that cycles to failure for the bonded samples were reduced for tests under the same stress values. For example, at a stress value of 700MPa the cycles to failure is approximately 10000 for the interlayer bonded samples whereas the typical repaired values is approximately 3,000,000. The reduction in the fatigue properties can be explained via the defects that were identified and therefore had a significant impact on the fatigue crack initiation sites, resulting in reduced fatigue properties.

4.3.3 Performance of Optimised Ti-6246 Interlayer Bond

The mechanical performance of the optimised conditions for Ti-6246 were determined via various mechanical tests such room temperature tensile, high cycle fatigue and further Vickers hardness testing. The results indicated the high integrity that can be achieved via the interlayer bonding process with a debit in strength still present in key mechanical performance characteristics in comparison to the as received material.

4.3.3.1 Tensile & Hardness Properties of Bonded Ti-6246

The optimised parameter sets for Ti-6246 were used to produce sufficient test samples for multiple room temperature tensile tests, hardness evaluation and fatigue testing. When evaluating the properties associated with the interlayer bonded tests the microstructure, fractured tensile samples and results as well as the Vickers hardness results need to be considered together in order to understand the effects of the bonding process.

The tensile results for the optimised conditions showed UTS and yield strength values with only a relatively small drop in values compared with the as received material which was to be expected with the changes that occurred microstructurally within the HAZ. The evaluation of the HAZ for the optimised conditions showed a change in microstructure from the interlayer to the surrounding HAZ. With the selected design of induction heating coil the temperature spread across the specimens dropped to below 850^0C at approximately 8mm from the bond interface. This temperature gradient created a coarsening effect on the microstructure as well as gradually reducing the α_s volume fraction within the HAZ. From ~8mm – 10mm from the bond interface the retained β matrix contained little to no α_s as a result of the bonding cycle. The results indicate that both the temperature and time, in this region, was sufficient in order to dissolve the α_s phase with a slight drop in volume fraction observed elsewhere due to the slight change in temperature experienced in comparison to this region. When comparing the results of the Vickers hardness tests, done within the HAZ, to the micrographs obtained within these regions the drop in hardness is clearly in line with the gradual reduction of the secondary α volume fraction. The lowest hardness values measured, approximately 330HV, are within the regions that are depleted of α_s, shown in Figure 4.3.3.1, with the as received material having a base value of ~375HV. These hardness values within the HAZ are similar to those observed in friction welded samples of Ti-6246 and show the same trends as other friction

welded titanium alloys [74][49]. The result of the hardness values also indicates the overall thickness of the HAZ associated with the optimised conditions with a thickness of just over 12mm either side of the bond interface. This HAZ is significantly larger than that seen for LFW Ti-6246 samples, which have a thickness of approximately 2mm. This is primarily due to the chosen coil design creating a narrow peak temperature band; however, the temperature gradient remains relatively high across the remaining length of the bonded specimens. There is potential in reducing this HAZ by utilising a similar coil design that has reduced spacing between each turn or reducing the overall number of turns in the coil. This thickness in HAZ was similar to that observed in previous done which utilised a thermo-mechanical simulator and focused on electrical resistance as its heating method [1].

With the link between the hardness and depleted α_s observable from the results, the other key effect of the microstructure can also be observed from the room temperature tensile results conducted. The results of these tests showed promising mechanical performance results in the form of UTS, Yield strength and to some extent ductility. However, the fracture surface, and more importantly, the fracture location of the

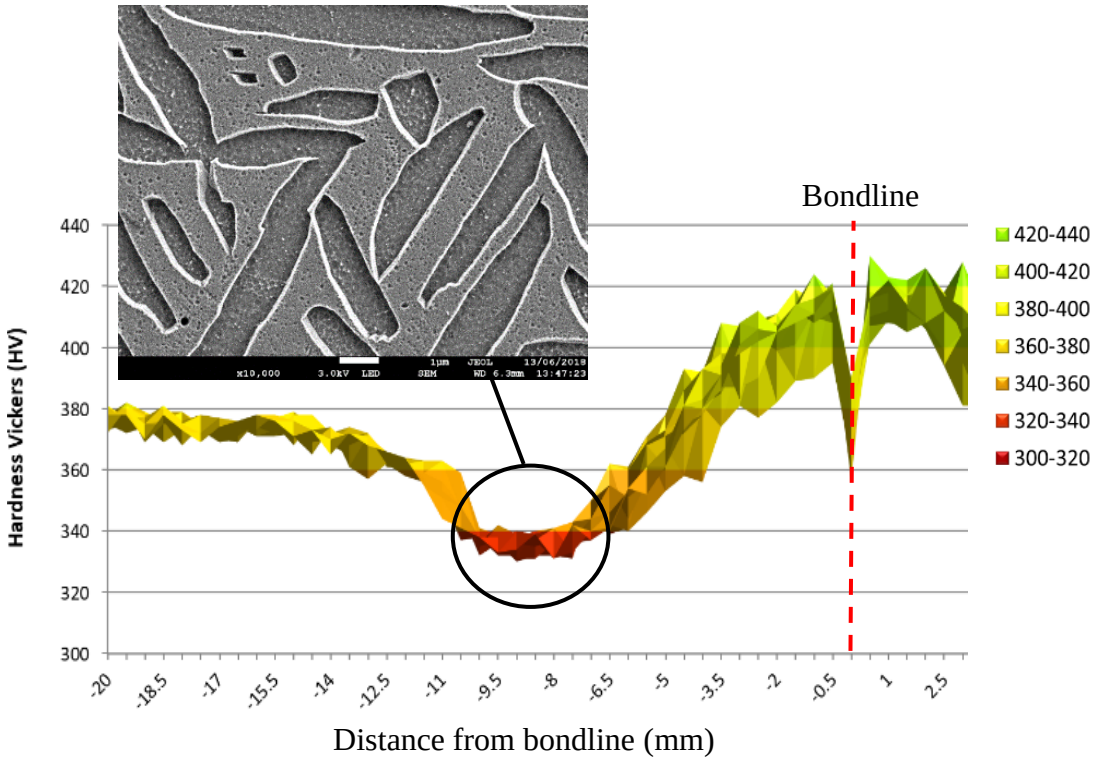

Figure 4.3.3.1: Graph illustrating the drop in Vickers Hardness and the associated microstructure within this region.

bonded samples seemed to show correlation with the hardness and microstructural changes described in the previous part of this chapter. In Figure 4.3.3.2 the fracture location is clearly observed to be away from the bondline by a length of between 8mm and 10mm. The drop in hardness in this region has also transferred to a debit in the tensile strength and therefore causing the fracture to occur in the depleted α_s zone. Studies on titanium alloys have shown the benefits that the precipitation of the fine α_s has on the mechanical properties for these alloys by reducing the effective slip length across the α colonies.

By identifying the root cause of the failures associated with the room temperature tensile tests, a post bond heat treatment could be applied in order to further improve the mechanical performance by introducing microstructural changes and reducing residual stresses. This is similar to a Post Weld Heat Treatment (PWHT) associated with friction welding, or other high temperature joining techniques for high

Figure 4.3.3.2: Image of fractured Tensile sample from Ti-6246 PIB.

temperature alloys. The effect of the anneal that was implemented in this project was shown to have a beneficial effect on the properties of the bonded sample in the form of increased hardness and ductility, with the UTS and Yield strength remaining largely the same. The illustration in Figure 4.3.3.3 displays the increased V_f of secondary α in the once depleted zone and which was the fracture region for the as bonded sample. The post bond heat treatment allowed for sufficient precipitation of the α_s in order to significantly increase the V_f of the fine phase.

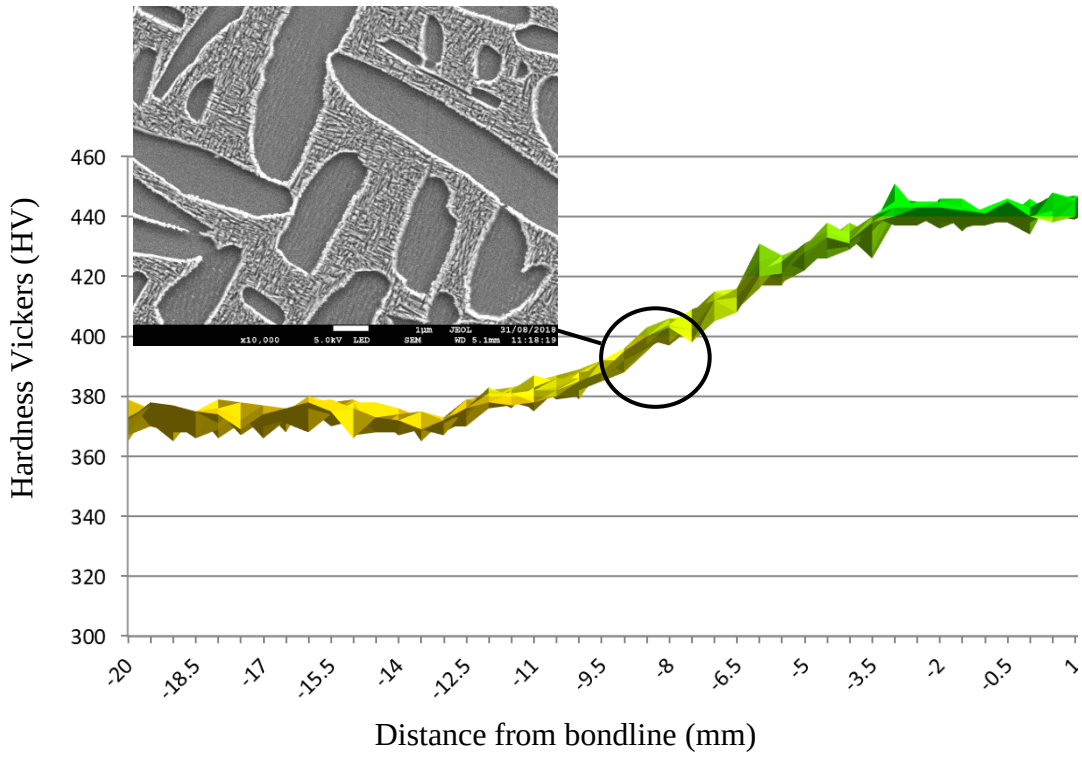

Figure 4.3.3.3: Illustration of the increase in V_f for the secondary alpha phase within the HAZ.

Observing the fracture surface of the post bond heat treated sample showed how the fracture was now located within the proximity of the bondline rather than at the previously weakened zone of depleted α_s. The importance of the α_s has been discussed in literature with the important mechnical propoerties such as fatgiue and strength closely associated to the precipitation of this fine secondary phase [9]. The post bond heat treatment shows the effects that this phase can have on the bonded Ti-6246 mechnical properties and crucial when considering future applicatinos of the interlayer bonding technique which will require high strength and crack grwoth resistance joins for high temperature alloys. The importance of the secondary alpha precipitates within this alloy are further highlighted when considering that the texture before and after the bonding process does not have a significant effect on the tensile properties as shown by the crystallographic texture values shown in the results chapter.

In order to further understand the benefits of the interlayer for the bonding process the room temperature tensile results can be compared with the test done under the same conditions as the optimised conditions but without the use of an interlayer. The results show how the UTS, Yield strength and ductility are significantly reduced in comparison to the optimised interlayer bond. As well as the reduction in properties the

fracture surfaces indicates clear signs of a brittle fracture with little to no necking during fracture. The specimen has clearly fractured across the bond interface of the two specimens resulting from a single plane which has shown reduced diffusion kinteics and therefore, alothugh the measured porosity was significantly reduced, the bond integrity was not sufficient to allow for enhance mechanical properties. Even with the same post bond heat treatment as the interlayer bonds this is not sufficent to greatly increase the properties with only a slight increase in ductility and UTS.

4.3.3.2 High Cycle Fatigue Properties of Bonded Ti-6246

The fatigue life approach in this project focused on the creation of a S/N curve to determine the number of cycles to failure (N) at varying stresses (S). The reason for this approach was due to the relative simplicity of the tests and with it being a simpler approach to achieve fatigue life results. The initial observation that could be made is how the fatigue tests exposed the presence of contamination within the powder interlayer. This was evident from the numerous fracture surface which showed clear signs of contaminants acting as subsurface crack initiation sites for the fatigue tests. Despite the presence of contaminants there was still a clear trend present within the results, with an increasing stress resulting in a reduced number of cycles to failure. The overall cycles to failure was comparable to results for forged Ti-6246 results with a slight reduction in the cycles to failure observable for the interlayer bonded Ti-6246 when compared to previous studies which looked into the high cycle fatigue properties of $\alpha+\beta$ and β processed Ti-6246 [25]. Although Bi-modal microstructures are typically found to possess increased fatigue crack growth resistance than coarse grained β processed microstructures, the presence of contamination severely effects the ability to compare the fatigue cycle results with similar studies. However, the contamination has clearly shown to nucleate and propagate cracks earlier than samples which would ordinarily be free of contaminants. Therefore, if tests were done which would be free of these contaminants then the results of the cycles to failure at specific stress levels would inevitable be closer to studies showing the HCF performance of Ti-6246 forged coupons.

Another consideration that must be observed is the fatigue specimens that were machined from the interlayer bonded samples were significantly shorter in length than the room temperature tensile test bars. Although this would be expected, due to the different test methods, this meant that the result of the depleted α_s could not tested

under cyclic loading as this region was not located within the gauge length of the fatigue specimens. With previous studies stating the importance of the α_s for not only tensile properties but more importantly fatigue properties then it is difficult to obtain the true cycles to failure for the interlayer bonds tested in this study. In order to fully characterise the properties with regard to the fatigue then a test sample which incorporates this depleted region of α_s would need to be used instead in order to establish the degree to which the interlayer bonds have been weakened.

4.4 Joining of Dissimilar Titanium Alloys

Although the main focus of this study was to focus on Interlayer Joining of Ti-6246, another aspect of the study involved the use of investigating the possibility of joining dissimilar titanium alloys. Although there are a vast number of titanium alloys that could have been chosen for this topic it was decided to trial the joining of Ti-6246 with Ti-6242. The reason for selecting these alloys was to do with the relevance that each alloy has in terms of its applications as an alloy. Although the alloying elements in Ti-6246 and Ti-6242 are similar they each have different strengths in terms of mechanical properties, machinability etc. The ability to join dissimilar alloys would open up the possibility for this technology to be used to produce parts which require a range mechanical property characteristic across a part. For example, for BLISK applications the requirements for the disk and the blades differ somewhat due to the mechanical and thermal loading of the two parts. Whereas high strength and strong Low Cycle Fatigue properties are required for disk materials, high creep strength is best for blade materials due to the elevated temperature which the blades are exposed to. Therefore, if a BLISK is machined from a single alloy then the mechanical properties cannot be optimised for disc and blade alike. Being able to produce high strength bonds between dissimilar titanium alloys may allow for this optimisation of mechanical properties to be achieved. In choosing Ti-6242 the increased creep properties associated with this alloy can be combined with the increased tensile strength of Ti-6246.

4.4.1 Joining of Ti-6246 & Ti-6242

The procedure for producing bonds between these two alloys remained the same as with the optimised bond for Ti-6246, explained in the previous Chapter. Although the alloys were different the chemical composition of the interlayer that was used was kept the same as Ti-6246 due to availability and to avoid changing additional parameters. The parameters for the tests, such as temperature, time and force, as well as interlayer thickness, were kept the same as with the optimised conditions for Ti-6246. Although the alloys are similar, they behave differently under mechanical and thermal loading therefore during a bonding trial the first difference observed is the plastic deformation of the two alloys. From the microstructure image below, it can be seen how the Ti-6242 specimen has a significant amount more plastic deformation compared with that of Ti-6246. The diameter of the resultant bond is ~14.6mm which is a 14% increase in deformation compared with that of the optimised bonds for Ti-6246.

The bond between Ti-6246/Ti-6242 were analysed the same by capturing the microstructural changes and evaluating the basic mechanical properties. The results show a similar trend for the Ti-6246 side of the bond compared with the bonds optimised bonds described previously.

4.4.1.1 Microstructure and Porosity Analysis

Microstructural and porosity characterisation was conducted in a similar fashion as with the optimised trial bonds done with only Ti-6246. The results for the Ti-6246 side of the dissimilar bonds behaved in the same way as with the optimised bonds. The effects of the coarsening alpha phase is observed in the immediate vicinity of the bond

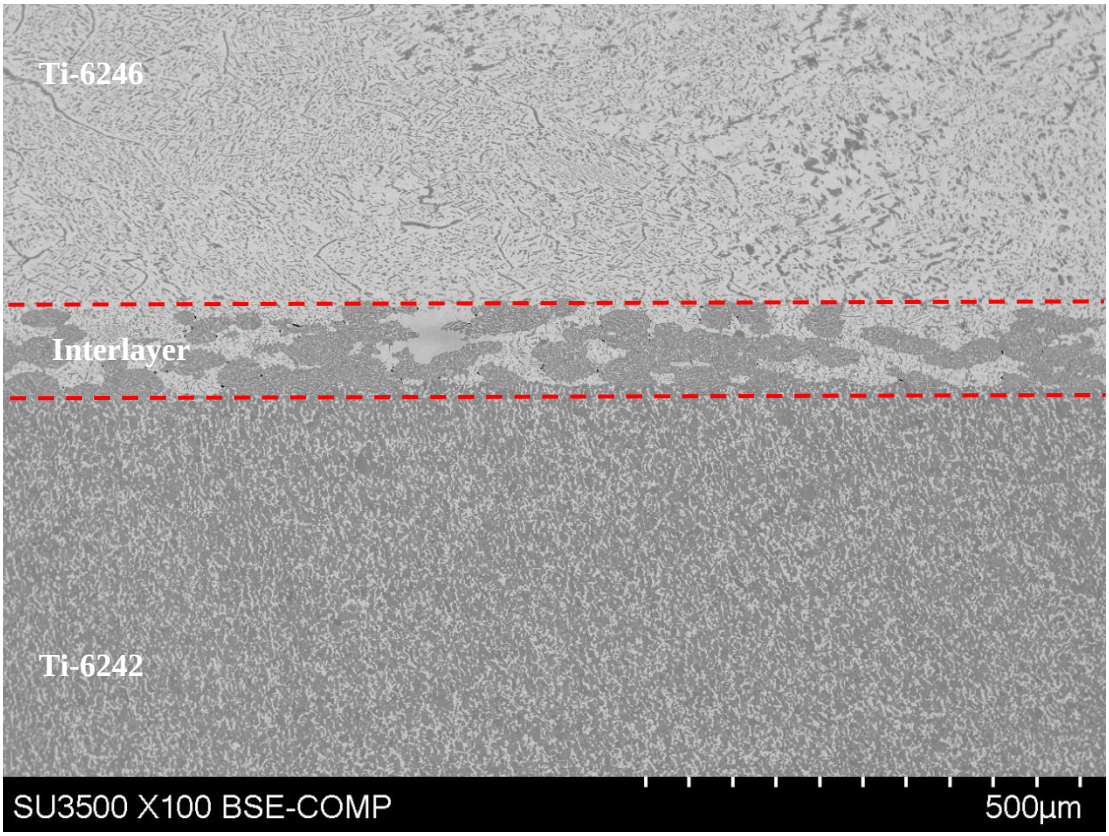

Figure 4.4.1.1: Microstructure of a bond between Ti-6246 and Ti-6242 using GA powder interlayer.

interface, ~2mm. Beyond this the V_f of α_p begins to increase although the V_f of the α_s starts to reduce until at ~8mm from the bond interface the α_s dissolves so that there is a region which is made up of only α_p surrounded by a β matrix and little to no α_s. Moving further from the bondline the α_s is present again between α_p and within the β matrix as is seen in the as received material and beyond the HAZ. This depleted zone of α_s is approximately 3mm in thickness.

The interlayer in the dissimilar bonds also exhibit similar behaviour as in the optimised Ti-6246 bonds. As explained in the previous chapter the interlayer exhibits a partial bi-modal microstructure. The interlayer region can clearly be observed visually due to the change in microstructure when compared with the microstructure of both the Ti-6246 and Ti-6242 samples. In the top of the micrograph in Figure 4.4.1.1 the microstructure of the Ti-6246 can be observed with the Ti-6242 sample microstructure visible in the bottom of the image. The high magnification micrograph shown below clearly shows the α_p and α_s phases present within the interlayer. The distribution and volume fraction of the α_s phase is consistent with what was observed for the optimised bond for Ti-6246.

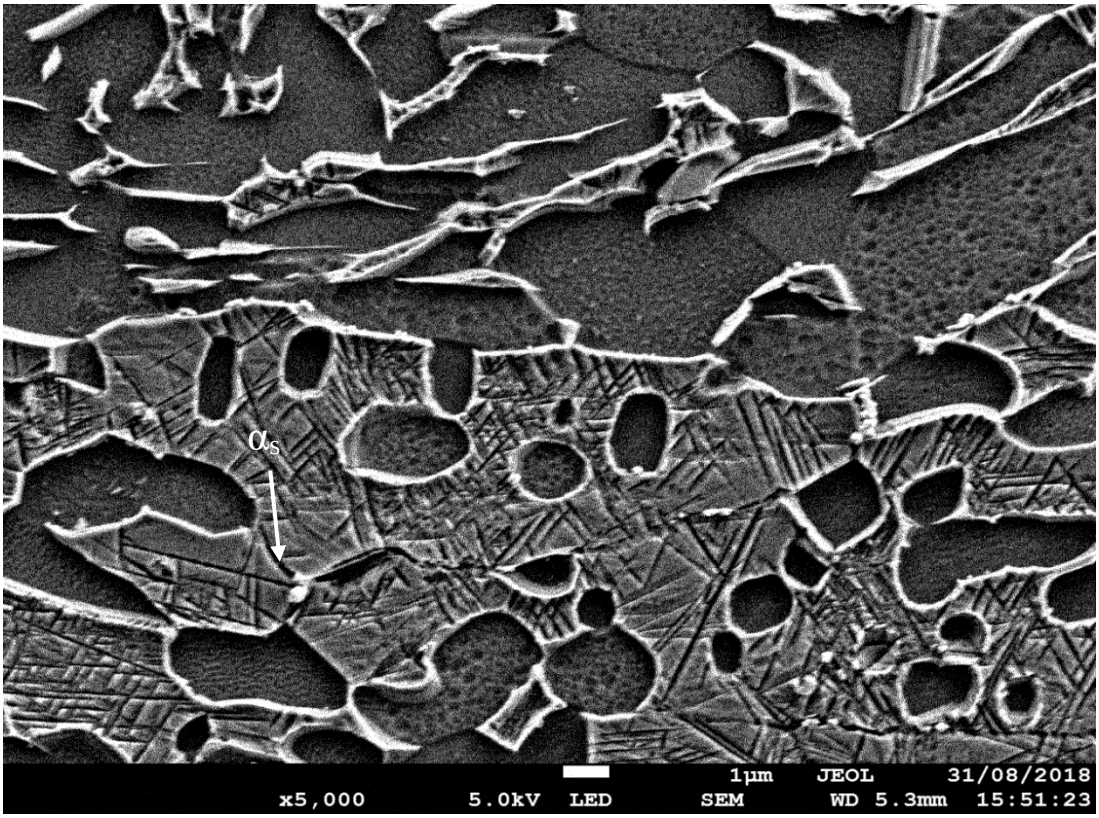

Figure 4.4.1.2: High magnification image showing the primary and secondary alpha phases.

The porosity measured shows a similar trend as with the optimised bonds, with a similar porosity distribution and a percentage of ~0.074% within the measured section. For the graph shown in Figure 4.4.1.3, the behaviour of the distribution shows that there is increased porosity located within the deformed areas of the bond and the lowest porosity shown to be present in the middle of the bonded area. In comparison to the total area of the observed porosity for the dissimilar bond and optimised bond for Ti-6246 there is an increase in the total area of approximately 1200µm2, to give a total value of 3102µm^2, within the measured areas for the two bonds which is more than a 50% increase when comparing the two tests. The distribution, however, remains similar with increased porosity located within the edges of the sample, although higher at each stage for the dissimilar bonded sample.

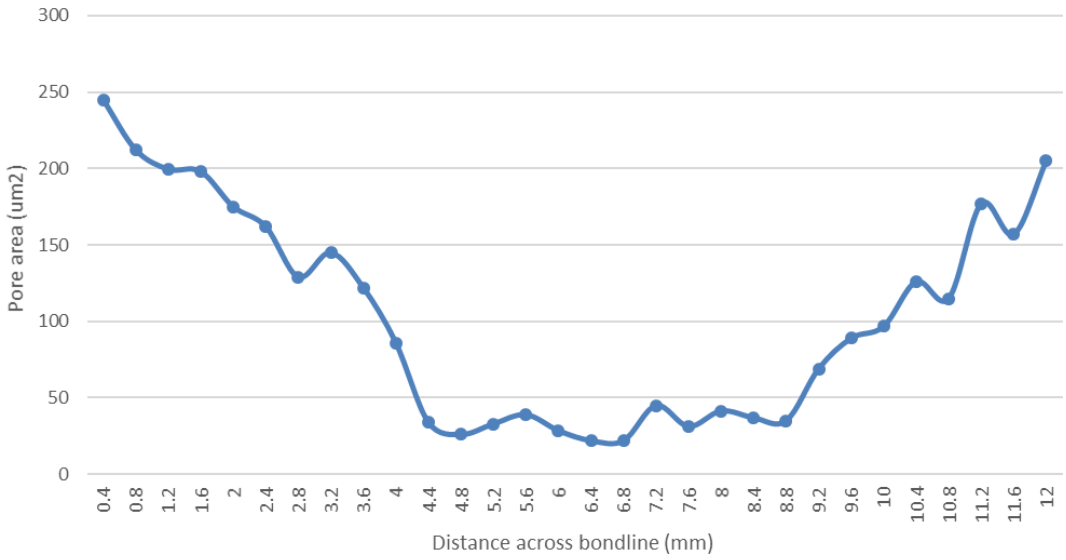

Figure 4.4.1.3: Chart showing the distribution of porosity across the sectioned PIB sample of the dissimilar join between Ti-6246 & Ti-6242.

4.4.1.2 RT Tensile Testing

Bonded samples of Ti-6246 and Ti-6242 were tested under the conditions as described in the experimental section of this report, using an interlayer composed of GA Ti-6246 powder. The results were compiled and shown in Table 3.3.1. The results show that mechanical performance of the bonded sample is lower than that for room temperature properties for both types of titanium alloys and slightly reduced with respect to

Table 4.4.1: Showing the RT tensile results for dissimilar titanium interlayer bonds.

	Ti-6246 & Ti-6242 PIB	Ti-6246 & Ti-6242 (With Post Weld Anneal)
UTS (MPa)	1060	1048
Yield Strength (MPa)	891	985
Youngs Modulus (GPa)	93	104
Elongation (%)	8.2	7.5

interlayer bonded Ti-6246, however the elongation values were increased slightly. The tensile curve results can also be shown in Figure 4.4.1.4 and show a similar curve to that seen for the optimised Ti-6246 curve but with the increased necking evident in the extension beyond the UTS of the dissimilar bond.

The Ultimate Tensile Strength was 1060MPa for the dissimilar bond with a yield strength of 891MPa. Both these values were reduced in comparison to the optimised bond for Ti-6246 with a 5.4% and 6.8% drop in the respective properties. However, the elongation to fracture was increased in comparison with a value of 8.2% and the stiffness measuring approximately 93GPa. The use of a post bond anneal, 640^0C for 2 hours, made little impact on the resultant room temperatures with very similar UTS and elongation values of 1048MPa and 7.5%. There was a significant increase in the yield strength of just over 90MPa. As well as the increase in the yield strength there was also a slight increase in the Young's Modulus, which increased from 93GPa to

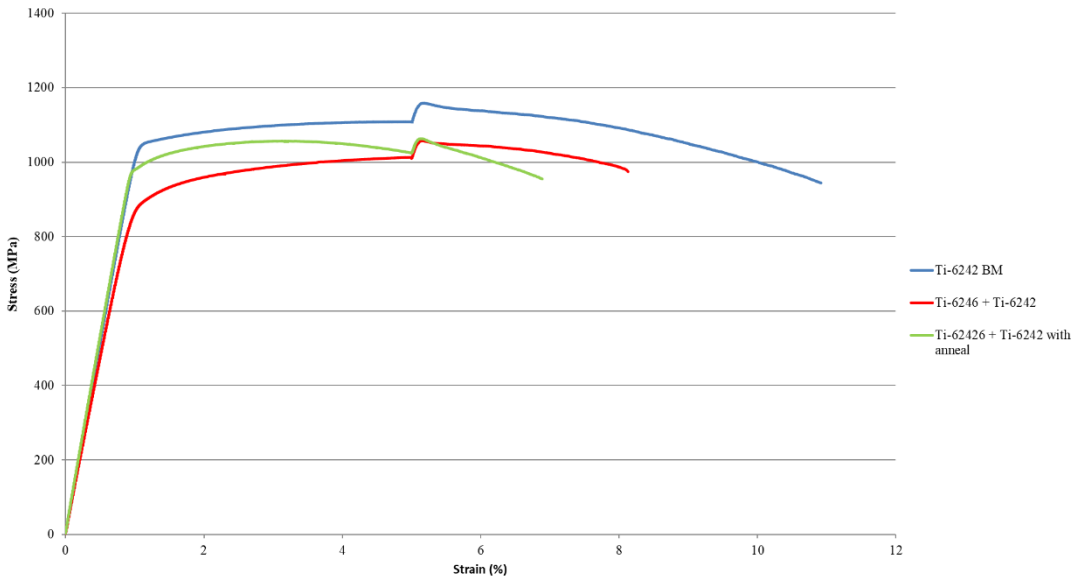

Figure 4.4.1.4: Chart showing the tensile test curves for the dissimilar bonds between Ti-6246 and Ti-6242 using powder interlayer.

104GPa. The location of the fracture was located approximately 6mm from the bondline of the two specimens. The fracture surface was very similar to previous tests done with Ti-6246 with typical features of a ductile failure.

4.4.1.3 Vickers Hardness Testing

Hardness Values were obtained from the dissimilar bonds for both annealed and unannealed samples. The unannealed hardness map, shown in Figure 4.4.1.5 below, shows the hardness profile across this bond.

The profile of the bond shows a distinct difference on either side of the bondline. The left hand side of the chart (Ti-6246) showed the same peak and drop in hardness that is associated with the typical Ti-6246 bond discussed in chapter 3.2.2.4. A similar peak value of 415HV and lowest value of approximately 320HV was observed. As well as having similar values the distance at which these values were observed are very similar to the typical results for Ti-6246 bonds. The pattern of the results of the hardness for the Ti-6242 side of the bond are visibly different. Whereas for the Ti-6246 the hardness oscillates across the HAZ the result for Ti-6242 side of the bondline does not oscillate to the same extent. The result shows that a drop is seen for ~5mm immediately adjacent to the bondline. This drop is relatively constant with an average value of 354Hv and approximately 25Hv below that of the as received material. Beyond 5mm from the bondline the hardness value increases gradually to a level in line with that of the as received material. There is then a relatively small increase in hardness compared with the as received result for Ti-6242 from 9mm to 15mm from the bondline. The interface between the two alloys shows a drastic drop in hardness due to the change

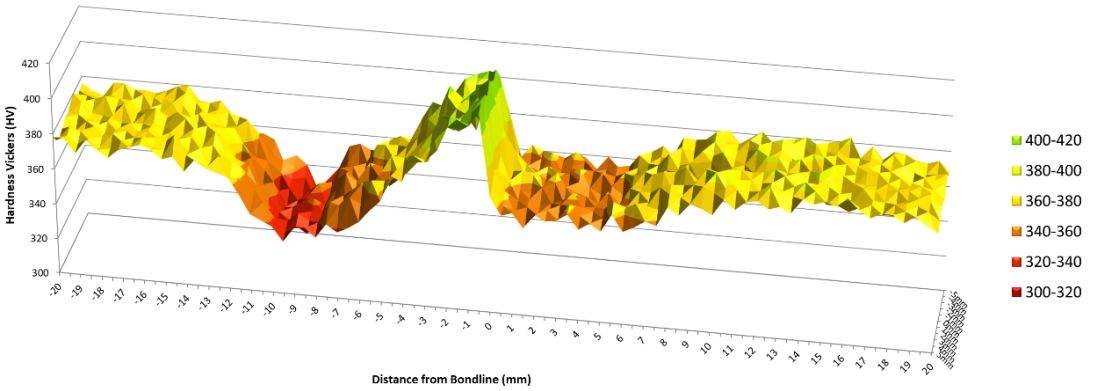

Figure 4.4.1.5: Vickers Hardness map across the HAZ for the dissimilar bond between Ti-6246 (LHS) and Ti-6242 (RHS)

across the bondline from the two alloys. As with the hardness maps for the previous bonds for Ti-6246 there is little to no variation parallel to the bondline for both alloys.

As with the typical Ti-6246 bonds, an annealing trial was conducted on the dissimilar bonds between Ti-6246 and T-6242. This annealing process was kept the same as the previous bonds and the hardness profile for this bond is shown in Figure 4.4.1.6. A similar trend is observed for this bond with regard to the hardness behaviour of the Ti-6246 side of the bond. The typical drop in hardness observed in the unannealed sample is no longer present and instead the results show a gradual increase towards the bondline within the HAZ. The result shows a difference for Ti-6242 side of the bond when compared with the unannealed sample also. The hardness no longer decreases to the same extent as with the previous bond.

The region from the previous bond for Ti-6242 showed a drop of ~25HV whereas for this bond the drop in hardness in the same region it is not obviously present. Due to the standard amount of variation with the hardness results it is difficult to observe if there is a small drop in hardness in this region. Beyond this region there is once again a slight rise in hardness between 10mm and 15mm from the bondline. Although as with the unaged bond this rise in hardness is very minimal with an approximate increase of 10HV present in this region compared with the as received material.

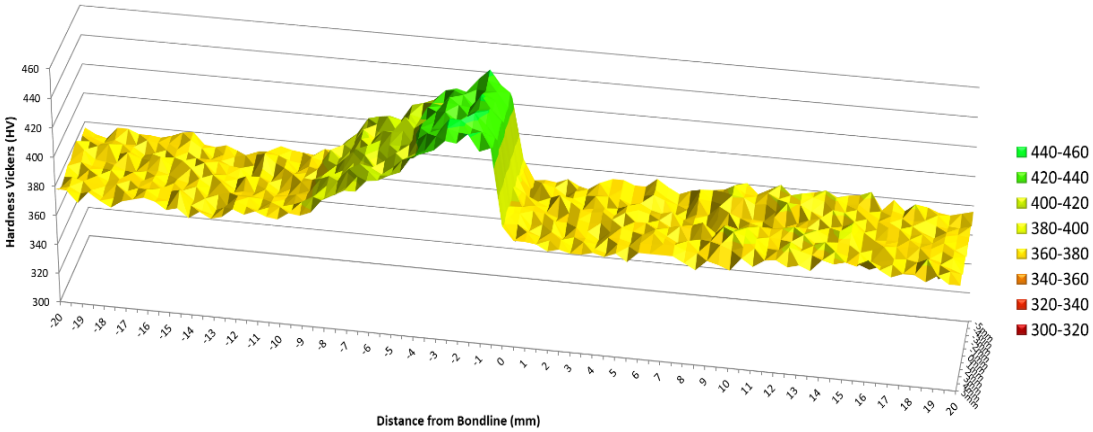

Figure 4.4.1.6: Vickers Hardness across the HAZ for the annealed dissimilar bond.

4.4.2 Dissimilar Alloy Interlayer Bonding

The interlayer bonding technique has been developed with potential repairs for high temperature alloys, such as titanium and nickel superalloys, for turbine components within the compressor and turbine stages for example. Although the preliminary focus of this and previous research topics kept to the joining of similar alloys together. However, with developments in gas turbine engines leading to optimisation of materials for part specific applications. This means that combining different alloys within the same system can provide significant benefits in performance of gas turbine engines by increased efficiency or by extending life cycle times of parts. An example of this would be combining the properties associated with titanium alloys for BLISK manufacture or repair. The possibilities for the disc material would include Ti-6246 due to its high fatigue crack growth resistance and Ti-6242 for the blade material arising from its elevated temperature capabilities.

4.4.2.1 Performance of Ti-6246 and Ti-6242 Bonding

The trials conducted for the dissimilar joining tests used the same optimised conditions for Ti-6246. The low availability of material meant that only a small number of tests could be conducted therefore the parameters, including time, temperature and force, were kept the same. As well as the parameters the interlayer alloy and thickness was kept the same with GA powder and a thickness of 200μm used. The findings of the optimised interlayer bonds for Ti-6246 have shown that high integrity bonds can be achieved with the argon gas flow technique and the mechanical properties showing only a small debit in strength with comparison to forged Ti-6246 as received material in the β processed condition. Therefore, there was a strong motivation to further develop the possibilities of joining dissimilar alloys with relevancy to gas turbine components.

The complexity of joining dissimilar alloys arises from the differing mechanical properties as well as fundamental material properties, such as thermal, chemical and microstructural properties. From the results it is shown that the macro deformation behaviour is different when compared with the Ti-6246 variant of the interlayer bonds for the same parameters. This is to be expected as the properties of Ti-6242 are subtly different to the higher strength variant of this titanium alloy. The deformation shows that due to the difference in properties, at elevated temperature, the Ti-6242 sample shows increased deformation than that of the Ti-6246 sample, resulting in a bondline

that is curved when looking at the sectioned view of the sample. The total deformation that was measured equated to an increase of ~45% in the diameter of the as bonded sample compared with the starting sample diameter of 10mm. Although the properties are different the integrity of the bond was still high with the collapse and sintering of the powder interlayer still similar to that of the optimised conditions for Ti-6246. With the porosity distribution being the same as the optimised Ti-6246 then any variances in mechanical properties can be assumed to be microstructurally related rather than any defect relation.

The mechanical properties of the dissimilar bonds illustrated an interesting picture. With the properties of the two alloy systems varying this translated into how the room temperature tensile tests behaved also. The failure of the bonded sample was controlled by the Ti-6242 sample being the limiting factor in terms of ultimate tensile strength and eventual failure location being within the Ti-6242 side of the bonded sample. This can be attributed to the lower strength associated with this variant of the titanium alloy and hence during the loading initiating and failing before. Although the dissimilar tensile test showed a further reduction, in room temperature mechanical properties, the properties are still comparable with that of the as received material for Ti-6242.

As expected, the variance in hardness for the Ti-6246 side of the bond was the same as previous tests due to the temperature being the same however the hardness associated to the Ti-6242 sample was slightly different, again owing to the alternate microstructure and hence differing mechanical properties. Whereas the optimised Ti-6246 bonds showed a drop in the hardness within the interlayer, due to the partial Bi-modal microstructure, the hardness level of Ti-6242 sample within the HAZ is equal to that observed within the interlayer. This stems from the microstructures associated to the interlayer and HAZ of the Ti-6242 sample being comparable than that of the microstructure within the HAZ of the Ti-6246 sample. With the equiaxed microstructure of the Ti-6242 sample being comparable to that of the interlayer, which had a partial Bi-modal structure, then the hardness of these two regions was not too dissimilar.

By using the same anneal stage during the post bond heat treatment the results show that properties of dissimilar joins can be altered as would be expected based on the

studies that have shown increased properties related to PWHT for friction welding technologies, for example. After the anneal stage the results shows that the bond was more closely aligned to the behaviour of the optimised Ti-6246 bonds with respect to the elastic behaviour of the tensile samples.

Although different heat treatments can be utilised in order to tailor the mechanical properties for better creep or fatigue crack growth properties, for example, certain titanium alloys respond differently depending on their classification as an α, near α, α+β, near β or β alloy. The response to heat treatment is greater for Ti-6246 than for Ti-6242 due to the former being more of a β titanium alloy than Ti-6242 which is a near α alloy. Literature has shown that β titanium alloys can be solution heat treated and aged in order to improve mechanical properties whereas α alloys generally can be stress relieved but higher strength is more difficult to achieve through aging for example. The benefit of the interlayer process arises from the relatively low temperature that it can produce high integrity joins. Although the tests were done at temperatures generally exceeding 900^0C, the process still maintains some form of microstructural homogeneity and hence potential mechanical properties close to that of the as received material for either alloy. When considering the use of alternate titanium alloys, more specifically, alloys that are classified as α and near α then more caution is required to any post joining heat treatment as there is the possibility of forming phases that can severely effect properties, such as Ti_3Al which can enhance stress corrosion cracking for example.

4.5 Alternate Interlayers Characterisation

Although the main focus of the study was on the understanding of using an alloyed powder based interlayer, other types of interlayer were also investigated. This part of the study was not as comprehensive as with the optimisation of Ti-6246 using the GA powder interlayer but it was done in order to start a comparison between alternate interlayers. The types of interlayers used fall into two categories, powder and foil. The powder based interlayers that were used were Ti-6246 PREP powder and CP powder. The foil based interlayer was CP titanium. The reason for choosing these interlayers was mainly due to availability and ease of access. It is understood that for demanding applications such as BLISK repair using CP titanium may not be a viable option due to the significant decrease in thermal and mechanical behaviour for this form of

Titanium. The reason for studying the effects of using foil, for example, instead of powder is to do with the difficulties of handling powder and applying thin layer interlayers as described in previous chapters. The foil used were of a larger diameter than that of the bonding specimens, the foils were 12mm and the specimens were 10mm, and therefore the placement was not as crucial making the setup of the bonds easier.

4.5.1 PREP Ti-6246 Powder

The first alternate interlayer that was investigated was the use of PREP Ti-6246 as the interlayer powder as opposed to the GA powder used for the optimisation trials previously described. The parameters such as time, force and interlayer thickness were kept the same as the optimised conditions in order to understand the effects of changing the interlayer composition. The deformation of the bonded sample was comparable to previous tests with the interlayer having little to no effect on the macroscopic behaviour.

The microstructure across the bond interface is shown in Figure 4.5.1.1 with the boundary of the interlayer highlighted in red. The micrograph shows the change in structure from the coarsened microstructure of the as received material, similar to that of previous tests, with the interlayer region being slightly different to that of the GA powder interlayer microstructure. The equiaxed α_p phase was finer, more globular and coarser than the GA equivalent bond with the test sample microstructure also exhibiting a reduced α_p volume fraction within the HAZ. With respect to the α_s phase there was again a similar trend to the GA optimised bond, with a decreasing V_f with increasing distance from the bondline until eventually there was a depleted region at ~8mm from the bondline.

The contrast between the interlayer and the microstructure of the test samples was not as obvious as with the GA Ti-6246 interlayer bonds and although the parameter resulted in a relatively low amount of porosity, there was sufficiently large pores which gave a strong indication to the existing interlayer region.

The results of the porosity analysis showed that there was a total of 2524μm^2 porosity in the measured area which was an increase of approximately 31% in comparison to the GA optimised bond. Although the overall measured porosity through the bondline was increased from the GA bonded sample, the porosity distribution followed the

same trend with increased porosity located at the edge of the sample than at the centre of the bondline.

A tensile test sample was also produced using the PREP interlayer method along with the optimised conditions for GA Ti-6246. The results of the test are shown in Table 3.4.1 and show comparable room temperature mechanical properties. The UTS, Yield Strength and Modulus all exhibit the same values for the optimised conditions with the key difference observed in the elongation decreasing slightly to 5.53% for the PREP interlayer test. With the similarity in mechanical performance this also translated over to how the specimen fractured at the end of the test. The fracture occurred approximately 8mm away from the bondline with visual observations

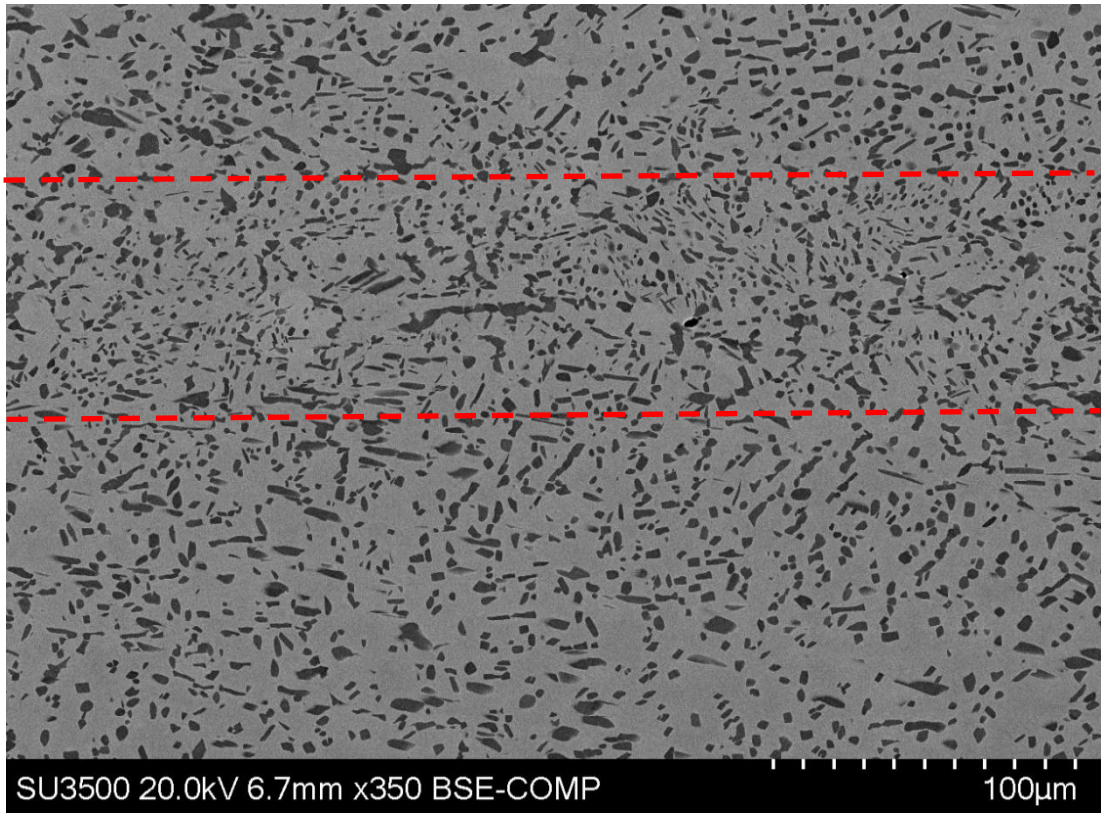

Figure 4.5.1.1: Microstructure of the bondline of a PIB for Ti-6246 using PREP powder.

showing evidence of a cup and cone fracture surface. The test can be characterised as

having a moderate ductile fracture with edges of the sample again having a fracture surface approximately 45^0C to the principal tensile stress during testing.

Table 4.5.1: Comparison of RT tensile results for PIB Ti-6246 using GA and PREP powder interlayer

	GA Ti-6246 PIB	PREP Ti-6246 PIB
UTS (MPa)	1117	1112
Yield Strength (MPa)	968	964
Youngs Modulus (GPa)	102	104
Elongation (%)	6.8	5.53

4.5.2 CP Titanium Powder & Foil

A repeat test was done using Commercial Pure Titanium powder. The parameters were kept the same as the optimised conditions and the sample was sectioned in order to study the HAZ associated with this interlayer. With the introduction of reduced alloying elements in the interlayer region the phase distribution and microstructure was significantly different as compared with previous tests. The micrograph, Figure 4.5.2.1, shows the microstructure in the region located around the bondline. The bondline displayed a clear band across the specimen which represented the CP titanium powder with a resultant thickness of approximately 100µm from a starting interlayer thickness of 200µm. The image shows that α phase associated with the CP titanium powder has remained within the interlayer region with limited diffusion into the test samples of both the titanium and alloying elements with the α phase being the primary constituent within the interlayer.

The use of EDS was utilised in order to view the change in the elements across the bondline from the α+β phase of the Ti-6246 test samples and the α phase within the interlayer, shown in Figure 4.5.2.2. The EDS line scan shows the distribution across

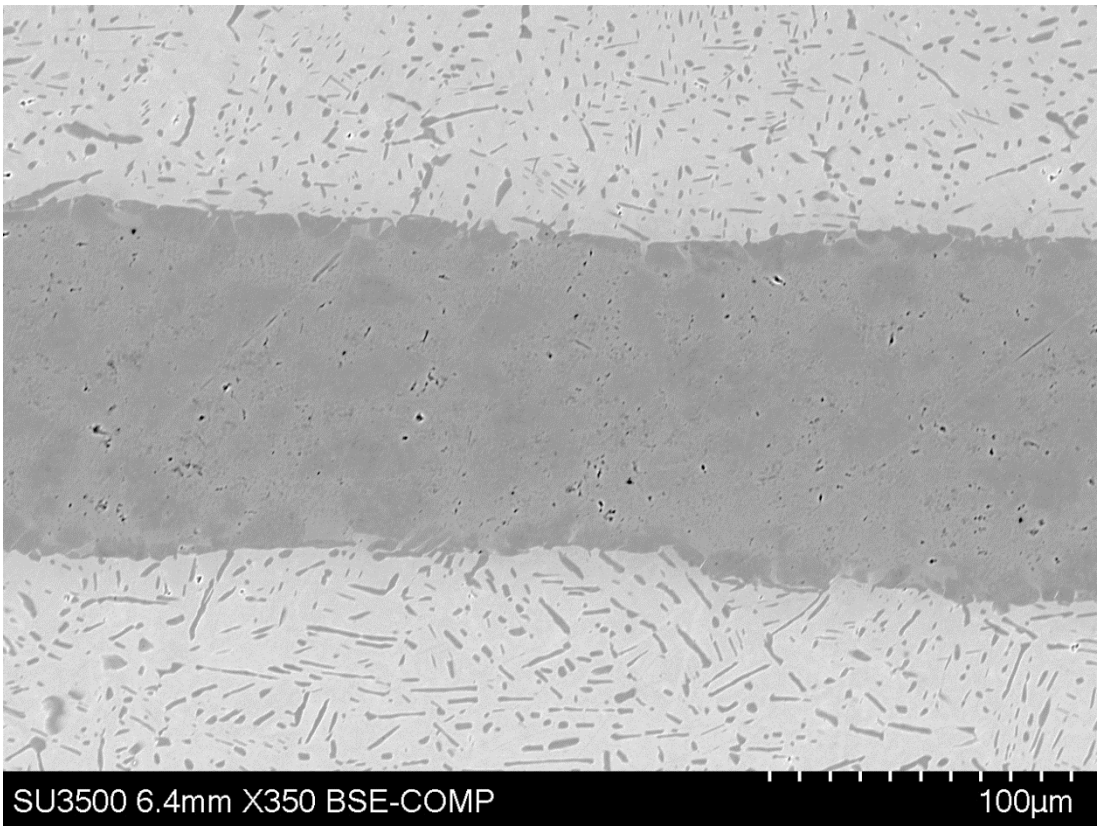

Figure 4.5.2.1: Microstructure across the bondline for PIB using CP Titanium powder interlayer.

the bondline of the base element, titanium, and the relevant alloying elements of Al, Sn, Mo and Zr. The graph shows that the wt% of titanium increases across the interlayer region to nearly 100%, compared with the Ti-6246 samples, and a decrease to zero of the alloying elements in the same region. The graph shows that the transition from Ti-6246 sample to the interlayer region was within 6µm from ~85% to 98% however there was a small continuous increase in titanium approximately 15µm away from the interface between sample and interlayer. This result shows that there was very little diffusion from the interlayer into the bulk material and vice versa.

The measured porosity area for this bond was approximately 8600µm^2 which is significantly higher than that for the optimised conditions using alloyed Ti-6246 GA and PREP powder. The distribution of the porosity was consistent across the bondline with no significant drop in porosity from the edge of the bond to the centre unlike previous tests with alloyed powder. The location of the majority of the porosity was located within the interlayer with a small amount located at the interface between the Ti-6246 samples and the interlayer with an overall average pore size of 5.35µm.

The microstructure within the remaining HAZ of the bonded sample was similar to

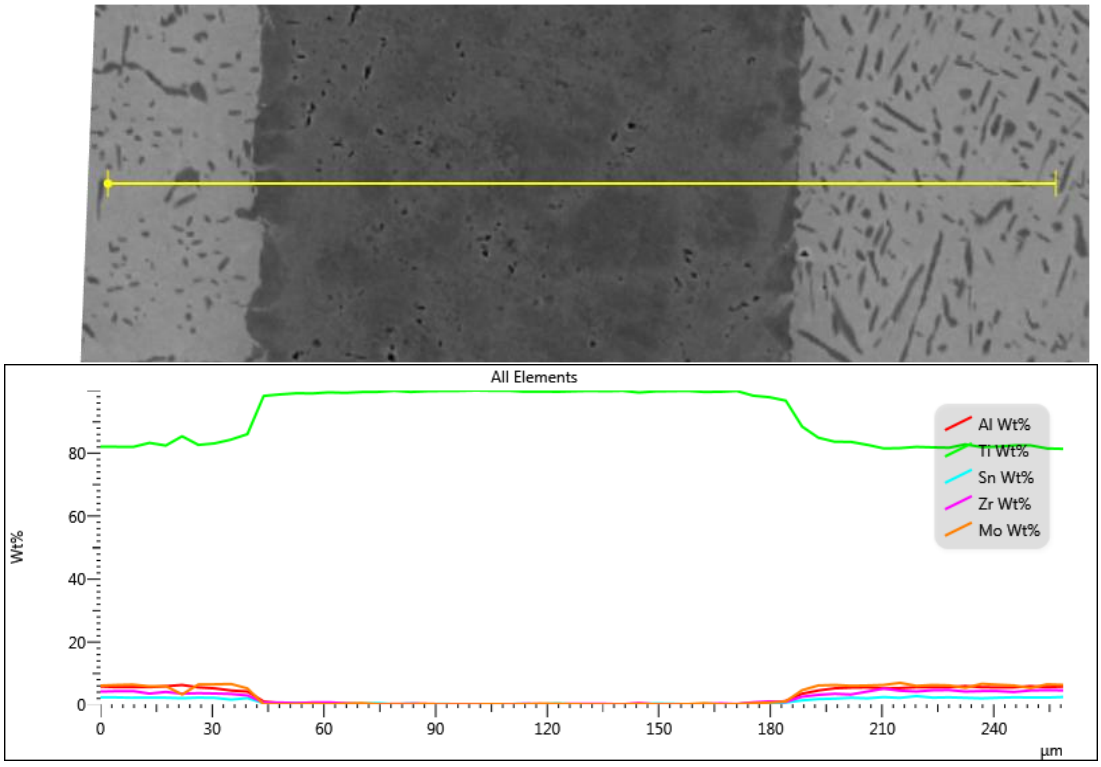

Figure 4.5.2.2: EDS line scan showing the change in chemical composition across the interlayer for PIB using CP powder interlayer.

that observed for the un-annealed Ti-6246 optimised bond conditions with a reducing amount volume fraction of α_s up to approximately 8mm from the bond interface with similar α_p lath width.

A repeat test, with the same parameters, was done using Commercial Pure Titanium foil with a thickness of 200µm and a diameter of 12mm. The advantages associated to using a foil stems from the handling and test setup as handling metallic powder poses increased risks and challenges compared with foil. As previously mentioned, with the alternate interlayers, the macroscopic deformation of the test samples remained

consistent with the main parameters effect deformation being Temperature, force and Time and interlayer type having little to no effect on the overall deformation factor.

The microstructure within the bondline region was observed to be similar to the that of the CP powder interlayer bond with a band of titanium remaining after the bonding cycle, Figure 4.5.2.3. The EDS showed a very similar trend in the increase in titanium within the interlayer and a significant drop in all the alloying elements within the interlayer.

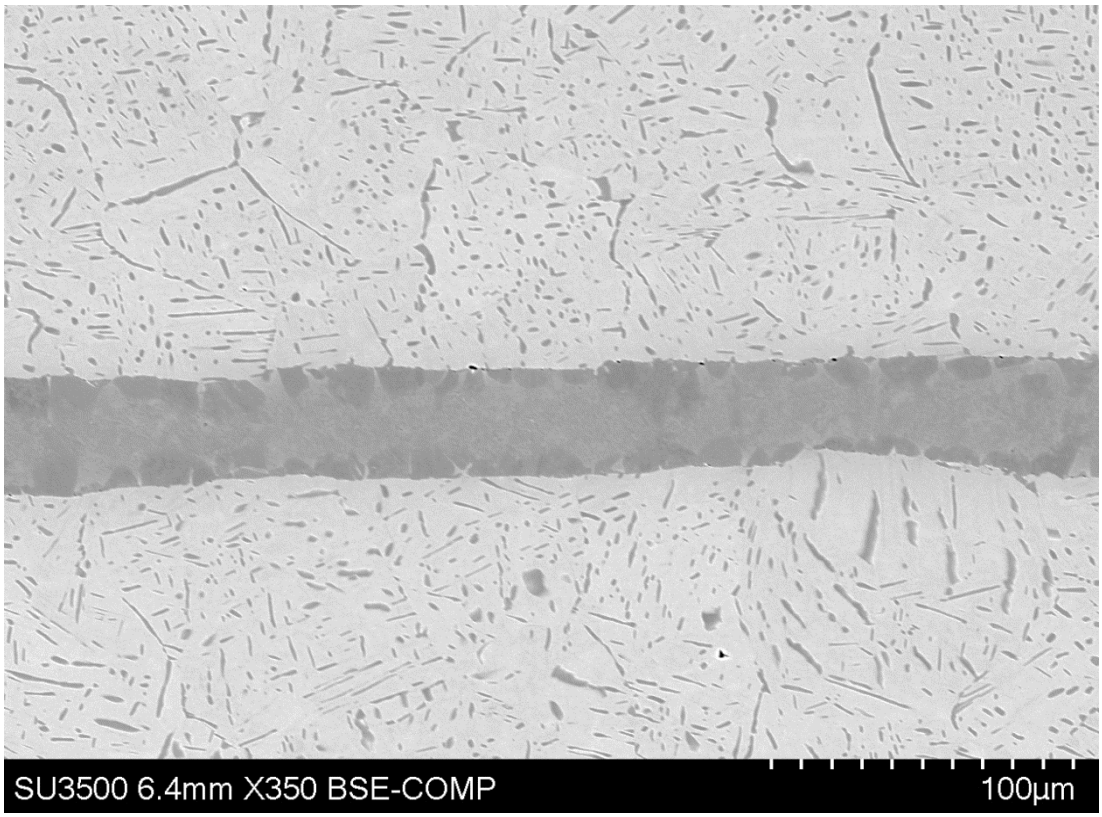

Figure 4.5.2.3: Microstructure of the Interlayer bond using CP Titanium foil.

The porosity distribution along the bond interface was significantly reduced in comparison to both the CP powder and Ti-6246 interlayer bonds with a total measured porosity area of ~628µm^2. The majority of the porosity was measured to be at the interface of the CP Titanium foil and the Ti-6246 test samples, with only a small percentage, ~12%, of the total porosity measured to be within the interlayer itself. The distribution of the porosity was inconsistent across the length of the bondline whereas previous tests with typical powder interlayers showed a similar trend across the bondline with significantly increased porosity at the edges of the test samples than at the centre. The Graph shows the distribution peaks at several points across the bondline with no clear trend observed with respect to increase or decreasing pore area.

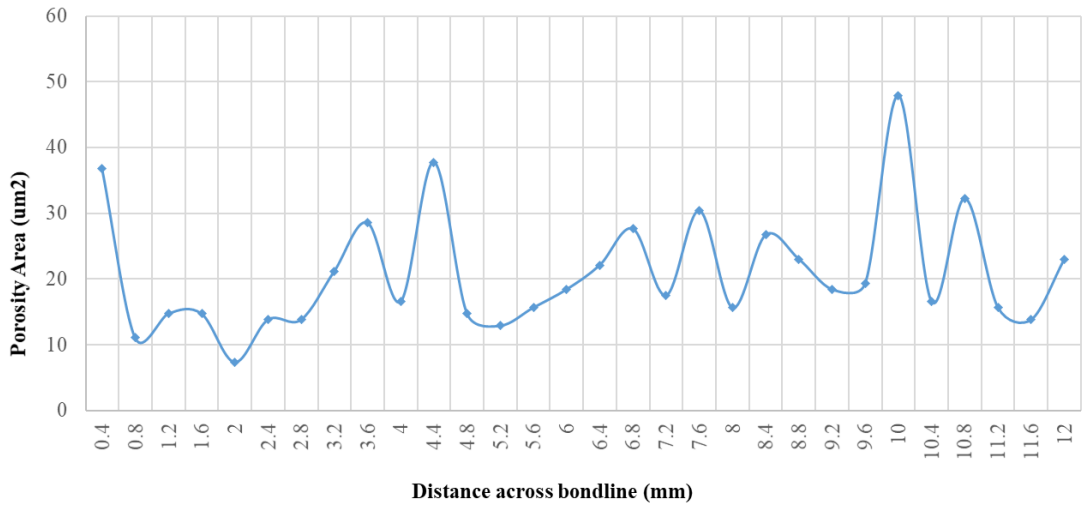

Figure 4.5.2.1: Chart illustrating the porosity distribution across the bond using CP Titanium foil.

4.5.3 Alternate Interlayer Joining

Although the development of interlayer bonding arose from BLISK repair for high strength titanium alloys there are other potential applications for this technology and therefore more avenues that can be explored. Although the focus has been on using an interlayer with the same chemical composition as at least one side of the bonded sample there are possibilities of using alternate alloy with different compositions in order to tailor the bonding process to reduce further reduce porosity or produce a high integrity bond in a shorter time for example. As well as alternate alloys, different forms of interlayer can also be tested, for example rather than using powder there may be the possibility of testing a partially sintered interlayer, one which is easier to handle and therefore reduce test set up times. There are requirements for joining of dissimilar metal alloy systems, not just titanium but steel, nickel and aluminium alloys also, but this creates further complexity not only because of the different mechanical properties of each metallic system but also the potential for creating intermetallic phases that can seriously impact the integrity of the join.

In this study some preliminary work was carried out on alternate interlayers. The interlayers that were used included PREP Ti-6246 interlayer powder as well as Grade 2 Commercial Pure Titanium powder in the form of powder and a thin foil. The purpose for trialling PREP powder as an interlayer centred on understanding the implications of having a powder size distribution that was narrower than that of the GA powder and how this would affect the collapse and sintering kinetics during the

bonding process. Looking back at the theory in how the powder collapses, through reduction in surface energies, the use of PREP powder helped to understand the differences on the neck formation during bonding. The results showed that the bond integrity produced was similar to that of the GA powder interlayer test as well as having room temperature mechanical properties in line with the optimised conditions for GA Ti-6246 interlayer. These preliminary tests for PREP powder interlayer showed that although the powder type is slightly different, the end result on the bond integrity is near enough the same in terms of porosity and room temperature mechanical properties.

The results for the CP powder titanium trial showed that although it was possible to produce a join the porosity levels were higher than expected considering the temperature, time and force applied. In comparison, the CP foil trial produce a very low porosity bond with the majority of pores located at the interface between interlayer and substrate. The performance of a bond with a foil, instead of a powder interlayer, would be expected to behave in line with the trial done without the use of an interlayer. This is because the bondline consists of a two parallel planes which are perpendicular to the loading direction during a tensile test. The tensile result from the bond without an interlayer showed a very brittle failure with little to no plastic deformation before failure. A similar tensile result could be expected for the CP foil trial with a brittle fracture expected for the given bonding parameters. The introduction of CP titanium as an interlayer may not have a significant impact on improving the properties as with mechanical performance of CP titanium is significantly lower, with respect to UTS and yield strength compared with alloyed Titanium, with it being less than half of that for Ti-6246 for example. There are important benefits associated with using a foil interlayer rather than powder which is evident when setting up bonding tests. Great care must be taken when handling any powder, especially titanium powder, whereas using a foil interlayer allows for safer handling and faster setup times. In order for interlayers of this type to be used the diffusion mechanisms associated with this type of bonding need to be optimised in the form of increased time at temperature, similar to that observed for traditional diffusion bonding techniques.

The use of interlayers has developed in recent years, not just within the aerospace industry, but also in industries such as in the nuclear and oil & gas industries with applications looking into the possibility of joining dissimilar metals such as steels to

titanium. The use of interlayers has been trialled with similar goals to that set out in this study, of improving bond integrity and also reducing the negative effects of brittle intermetallic phases [75]. As well as powder interlayers various forms of interlayers can be utilised in order to optimise and tailor the bond integrity to the end application. For example, the use of an electrodeposited nickel coating one of the substrates has been developed in order to increase the bond integrity between a steel and titanium alloy [76][77].

5 Conclusions

The scope of this research involved the further development of the interlayer bonding technique for Ti-6246 with key developments focusing on potential application and use of the technology in industry. The investigation in this body of work focused on developing the technology from research done which utilised the use of electrical resistance assisted sintering by using welding simulators for test trials. The further development focused on how to adapt the conditions required for successful bonding trials in order for potential application on complex parts where creating the high vacuum requirements and high currents within Gleeble systems may not suitable. Potential applications for this technology is for the joining and repair of high temperature titanium and nickel alloys for aerospace components such as blades and vanes. Developments in aerospace gas turbines have included technologies such as BLISK's which provide increased efficiency through weight savings and therefore increasing thrust to weight ratios of modern engines. In order for technologies such as these to become viable then achieving the long cycle times of these components is crucial which is why repair and overhaul of blades, for example, has seen increased research and development. The sustainability of Blisks is centred on the ability to keep the mechanical and microstructural integrity during the lifetime of the component, which can require extensive processes and systems, leading to long lead times and high associated costs for repair of Blisks.

This is where applications for interlayer bonding could generate benefits in achieving high integrity joins for hard to weld alloys, such as Ti-6246 as well as other titanium and nickel alloys and would allow for localised repair rather than complete overhaul of systems, leading to potential savings in reduced cost and process times.

The results of this body of work focused on learning the outcomes of utilising systems and processes that may well be utilised for the application on components within a gas turbine engine. The initial developments focused on creating a system capable of replicating the conditions that could, in time, be tailored to a part specific type of joining system which led to the utilisation of an argon shielding system based from the principles used in TIG welding for example. Leading on from this optimisation trials were conducted using forged Ti-6246 test samples along with Gas Atomised powder of the same alloy. Characterisation of the optimised conditions was then done by various methods of mechanical testing and microstructural analysis, through imaging, elemental and crystallographic texture analysis. Preliminary work was also conducted on dissimilar alloy joining and alternate interlayer characterisation.

The summary of the results and outcomes of this thesis is described in the following points below:

1. The development of an argon shielding for the interlayer bonding of Ti-6246 and other alloys was developed and provided the means for high integrity joins to be created for titanium alloys. The key parameters for creating high integrity bonds are time, temperature and force with a balance of these three parameters allowing for bonds the with very low porosity levels. The atmospheric control on the newly developed system proved to provide an inert atmosphere which allowed for the production of high integrity joins for titanium alloys. Reduced oxidation and presence of α case is achievable with utilisation of argon instead of a high vacuum system as in the Gleeble systems.
2. Mechanical testing has shown high bond integrity is achievable with enhanced properties, with respect to ductility, also possible in the form of a post bond anneal heat treatment. The room temperature tensile properties show a slight debit in UTS and Yield strength in comparison from the as received properties.
3. Post bonding results in a weak region within the HAZ and approximately 8mm from the bond interface with the current system and coil design. This region is depleted of α_s due to the temperature in this area during bonding. Post bond anneal increased the V_f of the fine α_s in this region and increased ductility.
4. The process of preparing the interlayer is vital in ensuring bond cleanliness and ensuring there are no contaminants present. High Cycle fatigue tests

showed that contamination effected the fatigue response of the parts with them initiating and increasing fatigue crack failure.

5. Joining of dissimilar titanium alloys of Ti-6246 and Ti-6242 also produces relatively high integrity bonds with the use of Ti-6246 GA powder interlayer. Porosity distribution remains the same as other tests with the mechanical performance being controlled by the Ti-6242 sample. A similar trend with slightly increased mechanical performance, this time in the form of yield strength, is possible with a post bond anneal heat treatment.
6. The use of alternate interlayers, such as PREP Ti-6246 and CP powder, also create relatively low porosity with the PREP interlayer bond showing very similar mechanical performance compared with the GA powder interlayer bond for the same bonding parameters. With the similarity in behaviour between the GA and PREP powder interlayers then with the increased availability and lower cost associated with GA powder, the use of PREP powder does not seem to create additional benefits.
7. Other interlayer types, such as CP foil, show that very low porosity bonds can be produced with a benefit in test set up and interlayer handling. Continued testing analysis is required in order to further understand the effects on mechanical properties of using a thin foil type interlayer.

In summary the use of an interlayer has shown to bring with it benefits when creating a high integrity bond in a relatively short bonding time. The optimum balance of parameters is required in order to produce low porosity bonds with minimal disruption to microstructure homogeneity. Understanding the effect within the HAZ can lead to further improvements in mechanical properties through post bond processes. Complexity of the system arises from the safe handling of metallic powder as well as maintaining high levels of cleanliness as this can severely effect bond integrity.

Relating the results obtained in this study to the original aims and objectives shows that it was possible to create relatively high integrity bonds using the newly developed system. This provides confidence in upscaling the technology to more complex designs in order to further validate the process. Although room temperature properties showed sufficient tensile properties the fatigue properties weren’t as promising. The aim of creating bonds with relatively high fatigue properties was not met as the effect

of surface contaminants meant it was difficult to compare the properties of the interlayer bonds using the optimised conditions.

6 Future Work

The research carried in this project has answered many questions as well as raising further developments path on which further investigation is required in order to further the understanding of the process. With respect to material and technology development there are numerous projects that can focus on just one aspect arising from the results of another study. The key paths of investigation are discussed below.

Further mechanical testing of the optimised conditions for Ti-6246 is required in order for this technology to be viable for this material. Repeat HCF tests would be needed with assurances of contamination free parts in order to evaluate the true performance of interlayer bonds with respect to fatigue. As well as HCF, elevated temperature testing can be conducted in order to evaluate the properties at the representative temperatures for in service Ti-6246 components.

1. **Upscaling to Complex Geometries.**

The development path for this technology would lead to eventual trials on complex geometries such as aerofoils. Previous studies have shown the challenges that arise from transferring bonding principles10mm diameter cylindrical samples to aerofoil trials. The use of a constrained argon gas system has shown promise in creating the inert environment needed for successful titanium bonding and upscaling this system would be one of the key challenges moving forward. As well as environment control the ability to increase the temperature of a complex part to elevated temperature with a uniform heating profile will also be a challenge. The other key factor to consider is the application of the powder interlayer on complex parts. Although a binder was used to constrain the loose powder future work could investigate the possibility of using a partially sintered interlayer which could take the shape of the substrate surface to be joined, making interlayer application easier and potentially safer handling.

2. **Further Evaluation of Alternate Interlayers.**

Although preliminary work carried out in this study showed potential for using alternate interlayers, further work is required in order to further characterise the effects. For example, using alternate interlayer with a different chemical composition

can create potential problems with regard to intermetallic phases and so further microstructural and chemical analysis would be needed, as well as mechanical performance characterisation. The development of alternate interlayers, and indeed alternate metal systems, would allow for a wider application possibility for the technology with the benefits of this technology more applicable in certain industries than others.

3. HCF Testing of Interlayer Joins.

This study involved the use of mechanical properties characterisation however HCF testing was disrupted through the presence of significant contamination of the interlayers. In order to fully evaluate the fatigue performance of interlayer bonds for Ti-62426 then repeat tests are required in order to fully understand the effects of the bonding process. As well as bonded samples, further tests can be conducted which evaluate the use of a post bond heat treatment in order to further increase the mechanical performance of interlayer bonds. The results in this study illustrated the effects that the bonding process has within the HAZ and therefore post bond heat treatments have the possibility of alleviating many of the knock on effects of bonding at elevated temperature.

7 References

[1] J. Forsdike, “Novel Joining and Repair of Aerospace,” 2009.

[2] M. P. Boyce, *Gas Turbine Engineering Handbook*, Third Edit. Gulf Professional Publsihing, 2006.

[3] A. P. Mouritz, *Introduction to aerospace materials*. Woodhead Publishing Limited, 2012.

[4] A. P. Mouritz, *Titanium alloys for aerospace structures and engines*. 2012.

[5] D. Production and N. T. Relations, “Titanium mineral concentrates 1,” vol. 1, no. September, pp. 2016–2017, 2016.

[6] I. Inagaki, “Application and Features of Titanium for the Aerospace Industry,” no. 106, 2014.

[7] G. Lütjering and J. C. Williams, *Titanium*, 2nd Editio. Engineering Materials And Processes, 2007.

[8] F. J. Zanner, “Metal Transfer During Vacuum Consumable Arc Remelting,” *Metall. Trans. B*, vol. 10B, no. June, pp. 9–10, 1979.

[9] G. Lütjering and J. C. Williams, “Titanium,” *Titanium*, 2007.

[10] M. J. Donachie, “Titanium - A Technical Guide.” p. 469, 1988.

[11] C. Leyens and M. Peters, *Titanium an Titanium Alloys*. 2003.

[12] D. J. Maykuth, H. R. Ogden, and R. I. Jaffee, “The Effect of Alloying Elements in Titanium,” 1961.

[13] F. F. Schmidt and R. A. Wood, “Heat Treatment of Titanium and Titanium Alloys,” *Nasa Tech. Memo.*, 1966.

[14] V. A. Joshi, *Titanium alloys: An atlas of structures and fracture features*, vol. 59, no. 3. 2008.

[15] G. Lütjering, “Influence of processing on microstructure and mechanical properties of (α+β) titanium alloys,” *Mater. Sci. Eng. A*, vol. 243, no. 1–2, pp. 32–45, 1998.

[16] M. J. Donachie, “Introduction to Selection of Titanium Alloys,” ASM International, vol. 180, 2000.

[17] R. R. Boyer, “An overview on the use of titanium in the aerospace industry,” *Mater. Sci. Eng. A*, vol. 213, no. 1–2, pp. 103–114, 1996.

[18] R. Boyer, G. Welsch, and E. . Collings, *Materials Properties Handbook Titanium Alloys*. ASM International, 1994.

[19] A. K. Gogia, “High-temperature Titanium Alloys,” vol. 55, no. 2, 2005.

[20] T. Choda, “Technology for process design of titanium alloy forging,” no. 33, pp. 460–465, 2015.

[21] C. Sauer and G. Lutjering, “Influence of α layers at β grain boundaries on mechanical properties of Ti-alloys,” *Mater. Sci. Eng. A*, vol. 319–321, pp. 393–397, 2001.

[22] C. Sauer and G. Luetjering, “Thermo-mechanical processing of high strength Beta-titanium alloys and effects on microstructure and properties,” *J. Mater. Process. Technol.*, vol. 117, no. 3, 2001.

[23] J. A. Hall, C. M. Pierce, D. L. Ruckle, and R. A. Sprague, “Property-Microstrucure Relationships in the Ti--6AI-2Sn--4Zr--6Mo Alloy,” *Mater. Sci. Eng.*, vol. 9, 1972.

[24] G. Jago and J. Bechet, “Influence of microstructure of (α+β) Ti-6.2.4.6 alloy on high-cycle fatigue and tensile test behaviour,” *Fatigue Fract. Eng. Mater. Struct.*, vol. 86, no. 4, pp. 647–655, 1999.

[25] J. O. Peters, G. Lütjering, R. K. Nalla, I. Altenberger, and R. O. Ritchie, “High cycle fatigue of beta-titanium alloys,” *Fatigue 2002 Stock.*, 2002.

[26] Y. Guo, T. Jung, Y. Lung, H. Li, S. Bray, and P. Bowen, “Microstructure and microhardness of Ti6246 linear friction weld,” *Mater. Sci. Eng. A*, vol. 562, pp. 17–24, 2013.

[27] R. Yang, “Microstructure and Mechanical Properties of Electron Beam Welded Titanium Alloy Ti-6246,” *J. Mater. Sci. Technol.*, 2016.

[28] J. Esslinger, “Titanium in Aero Engines Demands on Titanium Alloys and Processes in Aero Engines,” *Proc. 10thWorld Conf. Titan.*, 2003.

[29] M. T. Whittaker, W. Harrison, P. J. Hurley, and S. Williams, “Modelling the behaviour of titanium alloys at high temperature for gas turbine applications,” *Mater. Sci. Eng. A*, vol. 527, no. 16–17, pp. 4365–4372, 2010.

[30] Y. Li, Y. Chen, J. Liu, Q. Hu, and R. Yang, “Cooperative effect of silicon and other alloying elements on creep resistance of titanium alloys : insight from first-principles calculations,” *Nat. Publ. Gr.*, no. July, pp. 1–8, 2016.

[31] R. . Jaffee and N. . Promisel, *The Science, Technology and Application of Titanium*. Pergamon Press, 1970.

[32] R. W. Messler Jr, “Electron Beam Weldability of Advanced Titanium Alloys,” *Weld. J.*, no. May, p. 79s–84s, 1981.

[33] Y. Momota, A. Shigeomi, S. Ishigai, S. Murakami, Y. Maeda, and T. Choda, “Manufacturing Technologies for Ti-6246 Alloy Aero Engine Disc Forgings,” pp. 881–884, 2007.

[34] C. C. Chen and R. R. Boyer, *Practical Considerations for Manufacturing High-Strength Ti-10V-2Fe-3A1 Alloy Forgings*, vol. 31:7. 1979.

[35] I. Weiss and S. L. Semiatin, “Thermomechanical processing of beta titanium alloys—an overview,” *Mater. Sci. Eng. A*, vol. 243, no. 1–2, pp. 46–65, 1998.

[36] P. E. I. Sun, Z. Z. A. K. Fang, Y. Zhang, and Y. Xia, “Review of the Methods for Production of Spherical Ti and Ti Alloy Powder,” *Miner. Met. Mater. Soc.*, vol. 69, no. 10, pp. 1853–1860, 2017.

[37] S. Axelsson, “Surface Characterization of Titanium Powders with X-ray Photoelectron Spectroscopy,” Chalmers University of Technology, 2012.

[38] K. Zhang, “The Microstruture and Properties of HIPPED Powder Ti Alloys,” 2009.

[39] L. Zhao, P. Wanjara, P. Patnaik, M. Elboujdaini, “Aerospace Materials and Manufacturing: Advances in Materials, Processes and Repair Technologies” *Aircr. Des*, pp. 1–39.

[40] M. Peters, J. Kumpfert, C. H. Ward, and C. Leyens, “Titanium alloys for aerospace applications,” *Adv. Eng. Mater.*, vol. 5, no. 6, pp. 419–427, 2003.

[41] P. He, J. Zhang, R. Zhou, and X. Li, “Diffusion bonding technology of a titanium alloy to a stainless steel web with an Ni interlayer,” *Mater. Charact.*, vol. 43, no. 5, pp. 287–292, 1999.

[42] A. H. M. E. Rahman and M. N. Cavalli, “Strength and microstructure of diffusion bonded titanium using silver and copper interlayers,” *Mater. Sci. Eng. A*, vol. 527, no. 20, pp. 5189–5193, 2010.

[43] S. Kundu, M. Ghosh, A. Laik, K. Bhanumurthy, G. B. Kale, and S. Chatterjee, “Diffusion bonding of commercially pure titanium to 304 stainless steel using copper interlayer,” *Mater. Sci. Eng. A*, vol. 407, no. 1–2, pp. 154–160, 2005.

[44] G. Pardal, S. Ganguly, S. Williams, and J. Vaja, “Dissimilar metal joining of

stainless steel and titanium using copper as transition metal," *Int. J. Adv. Manuf. Technol.*, pp. 1139–1150, 2016.

[45] S. R. Seagle, K. O. Yu, and S. Giangiordano, "Considerations in processing titanium," *Mater. Sci. Eng. A*, vol. 263, no. 2, pp. 237–242, 1999.

[46] H. Lee, J. Yoon, and Y. Yi, "Oxidation behavior of titanium alloy under diffusion bonding," vol. 455, pp. 105–108, 2007.

[47] W. C. for M. J. T. Twi, "Guide to best practice, 'Welding Titanium', A Designers and Users Handbook," p. 5,20,24, 1999.

[48] M. M. Attallah and M. Preuss, *Inertia friction welding (IFW) for aerospace applications*. Woodhead Publishing Limited, 2011.

[49] A. M. M. García, "BLISK Fabrication by Linear Friction Welding," *Adv. Gas Turbine Technol.*, pp. 411–435, 2011.

[50] H. Liu and H. Fujii, "Microstructural and mechanical properties of a beta-type titanium alloy joint fabricated by friction stir welding," *Mater. Sci. Eng. A*, vol. 711, pp. 140–148, 2018.

[51] A. Wisbey, I. C. Wallis, H. Ubhi, P. Sketchley, C. Ward-Close, and P. Threadgill, "Mechanical Properties of Friction Welds in High Strength Titanium Alloys," *9th World Titanium Conference.*, 1999. [Online]. Available: https://www.twi-global.com/technical-knowledge/published-papers/mechanical-properties-of-friction-welds-in-high-strength-titanium-alloys-june-1999/.

[52] A. Mohammad, P. Kalvala, H. K. Rafi, and B. S. Murty, "Friction Welding of Titanium to 304L Stainless Steel Using Interlayers Friction Welding of Titanium to 304L Stainless Steel Using Interlayers," no. April, 2011.

[53] C. Muralimahoan, S. Haribabu, Y. Hariprasada Reddy, V. Muthupandi, and K. Sivaprasad, "Evalution of microstructures and mechanical properties of dissimilar materials by friction welding," vol. 5, pp. 1107–1113, 2014.

[54] J. A. James and R. Sudhish, "Study on Effect of Interlayer in Friction Welding for Dissimilar Steels : SS 304 and AISI 1040," *Procedia Technol.*, vol. 25, pp. 1191–1198, 2016.

[55] Y. Guo, Y. Chiu, M. M. Attallah, H. Li, S. Bray, and P. Bowen, "Characterization of dissimilar linear friction welds of alpha -Beta Titanium alloys," *J. Mater. Eng. Perform.*, vol. 21, no. 5, pp. 770–776, 2012.

[56] H.-S. Lee, *Welding and Joining of Aerospace Materials - 10 - Diffusion bonding of metal alloys in aerospace and other applications*. Woodhead Publishing Limited, 2012.

[57] N. Kazakov, *Diffusion Bonding of Materials*. Mir Publishers; Pergamom Press, 1981.

[58] Y. W. Xun and M. J. Tan, "Applications of superplastic forming and diffusion bonding to hollow engine blades," vol. 99, pp. 80–85, 2000.

[59] M. Reza and N. Zuelli, "Metrology and Microscopy Analysis of Multisheet

Packs Manufactured Via Superplastic Forming to Study Possible Diffusion Bonding," *Procedia Eng.*, vol. 183, no. 0, pp. 251–256, 2017.

[60] D. Leroy, T. A. Siewert, S. Liu, and G. R. Edwards, *Welding Brazing And Soldering*, vol. Vol 6. .

[61] H. V Atkinson and S. Davies, "Fundamental Aspects of Hot Isostatic Pressing : An Overview," vol. m, no. December, 2000.

[62] L. Francis, "Hot Isostatic Pressing." Materials Processing, 2016.

[63] A. Ozlati and M. Movahedi, "Effect of welding heat-input on tensile strength and fracture location in upset resistance weld of martensitic stainless steel to duplex stainless steel rods," *J. Manuf. Process.*, vol. 35, p. Pages 517-525, 2018.

[64] N. G.J.L, "DC upset resistance welding Modelling and control of a weld process," University of Technology Eindhoven, 2005.

[65] W. . Kanne, "Solid State Resistance Upset Welding: A Proccess with Unique Advantages for Advanced Materials," *Adv. Join. Technol. New Mater. II*, 1994.

[66] S. J. Tuppen, M. R. Bache, and W. E. Voice, "Structural integrity of diffusion bonds in Ti–6Al–4V processed via low cost route," *Mater. Sci. Technol.*, vol. 22, no. 12, pp. 1423–1430, 2006.

[67] R. Orru, R. Licheri, A. M. Locci, A. Cincotti, and G. Cao, "Consolidation/synthesis of materials by electric current activated/assisted sintering," *Mater. Sci. Eng. R Reports*, vol. 63, no. 4–6, pp. 127–287, 2009.

[68] O. A. Ojo and N. L. Richards, *Heat-affected zone cracking in welded nickel superalloys*. Woodhead Publishing Limited, 2012.

[69] V. Rudnev, D. Loveless, and R. Cook, *Handbook of Induction Heating, 2nd Edition*. 2017.

[70] S. Zinn and S. L. Semiatin, *Elements of Induction Heating: Design, Control, and Applications*. ASM International, 1988.

[71] S. Kumar and D. B. Puranik, "Induction Heating : Its Applications In Dairy Industry," vol. 3, no. 3, pp. 290–299, 2016.

[72] J. Djohari Hadrian, J. Martinez-Herrera, and J. Derby, "Transport mechanisms and densification during sintering: I. Viscous flow versus vacancy diffusion," *Chem. Eng. Sci.*, vol. 64, no. 17, pp. 3799–3809, 2009.

[73] P. Davies, A. Johal, H. Davies, and S. Marchisio, "Powder interlayer bonding of titanium alloys : Ti-6Al-2Sn-4Zr-6Mo and Ti-6Al-4V," *Int. J. Adv. Manuf. Technol.*, vol. 103, 2019.

[74] S. Bray, M. M. Attallah, and M. Preuss, "Microstructural development during Linear Friction Welding of titanium alloys Microstructural Development during Linear Friction Welding of Titanium Alloys," in *Conference: ASM Proceedings of the International Conference: Trends in Welding Research*, 2009, no. January.

[75] D. Mo, T. Song, Y. Fang, X. Jiang, C. Q. Luo, M. D. Simpson, and Z. Luo, "A Review on Diffusion Bonding between Titanium Alloys and Stainless Steels," vol. 2018, 2018.

[76] M. Cheepu, M. Ashfaq, and V. Muthupandi, "A New Approach for Using Interlayer and Analysis of the Friction Welding of Titanium to Stainless Steel," *Trans. Indian Inst. Met.*, vol. 70, no. 10, pp. 2591–2600, 2017.

[77] M. . Lee, J. . Lee, Y. . Choi, D. . Kim, C. . Rhee, Y. . Lee, and S. . Hong, "Interlayer engineering for dissimilar bonding of titanium to stainless steel," *Mater. Lett.*, vol. 64, no. 9, pp. 1105–1108, 2010.

8 Appendices

High Integrity Interlayer Joining Testing Procedure

A standard operating procedure was developed for the high integrity interlayer bonding system. The following is a step by step guide on how each test was conducted, including the loading and unloading of the bonded specimens.

1. Lower bottom platen of servo-hydraulic system down to lowest position using control panel ensuring sufficient clearance between top and bottom arms for both bonding specimens.
2. Screw first the required collet and then the top specimen into the top arm. Tighten both collet and specimen.
3. Place top seal approximately halfway up the top specimen and tighten grub screw. Connect the welded thermocouples into data logger panel in order to read and capture temperature during bonding test.
4. Slot specimen, with interlayer, through argon copper inlet guide and place bottom seal between inlet and specimen. Continue to screw in the specimen into the bottom platen arm until tight.
5. Bring induction heating system pack, with the relevant coil design attached, into position. Drop the coil if needed to ensure clearance of top specimen. Position coil centrally around the top specimen so that there is an even distance from the outside of the specimen to the inside of the coil.
6. Ensure height of coil is such that the bonding surface of top specimen is situated at the correct height relevant to the coil position. Different coil will

have optimum heating positions relevant to the workpiece and so situate as needed for specific test.

7. Place quartz glass tube within the slot of the copper inlet for the argon taking care to avoid contact with interlayer on bottom specimen.
8. Using control panel of servohydraulic system, bring bottom platen arm up until both specimens make a small initial contact. Take care to guide quartz glass tube through the coil as well as past the top seal located on the top specimen.
9. On PC system of machine, place a small holding load, typically between 0.25kN and 0.5kN in order to hold specimens together during initial part of bonding cycle.
10. Switch on the Easyheat induction heating system via on/off button located on the back of the unit as well as the associated water coolant system.
11. Open initial valve for argon gas cylinder, ensuring the gas flow regulator is closed. Ensure valve is fully open by checking pressure on gauge of the regulator.
12. Open the regulator valve and adjust flowmeter, if applicable, to the required flow rate of argon, typically between 10-25ltr/min.
13. Set estimated power on induction heating depending on initial heating rate required. Once set, start induction heating system and monitor temperature.
14. Adjust the power settings in order to achieve the required heating rate and then change load settings on servohydraulic system to the required load for the test.
15. Adjust power settings to maintain required temperature as well as the load requirement during the test.
16. Once tests is completed reduce or turn off induction heating system and adjust force if needed for the test. Proceed to turn off coolant system after induction heating system is fully off.
17. Allow for bonded specimens to cool before proceeding to unload parts.
18. Turn off argon gas flow via regulator and valve from the gas cylinder.
19. Apply a small tension load, typically between 0.1 and 0.2kN and start to loosen bottom arm. Once arm is it will automatically proceed down to the lowest position due to the small tension load applied.
20. Remove bottom collet from specimen taking care to remove argon inlet and quartz glass tube also.
21. Lower induction heating coil system and position away.

22. Unscrew collet from top arm and once free remove bonded specimen from collet.